Consequences of phase transition dynamics in neutron stars and in inflation

By

Arpan Das

PHYS07201104004

Institute of Physics, Bhubaneswar

A thesis submitted to the

Board of Studies in Physical Sciences

In partial fulfillment of requirements

For the Degree of

DOCTOR OF PHILOSOPHY

of

HOMI BHABHA NATIONAL INSTITUTE

October, 2017

Homi Bhabha National Institute

Recommendations of the Viva Voce Committee

As members of the Viva Voce Committee, we certify that we have read the dissertation prepared by Mr. Arpan Das, entitled "Consequences of phase transition dynamics in neutron stars and in inflation", and recommend that it may be accepted as fulfilling the dissertation requirement for the Degree of Doctor of Philosophy.

A M Jayannavar

Chairman - Prof. A. M. Jayannavar Date: 30.5.18

Ajit M. Srivastava 30-5-18

Guide /Convener - Prof. A.M. Srivastava Date:

Co-guide (if any) Date:

30/5/2018

Examiner - Prof. Rajeev S. Bhalerao Date:

30/5/18

Member 1 - Prof. Pankaj Agrawal Date:

A Virmani 30/05/18

Member 2 - Prof. Amitabh Virmani Date:

Final approval and acceptance of this thesis is contingent upon the candidate's submission of the final copies of the dissertation to HBNI.

I/We hereby certify that I/we have read this thesis prepared under my/our direction and recommend that it may be accepted as fulfilling the thesis requirement.

Date: 30-5-18

Place: IOP, Bhubaneswar

Ajit M. Srivastava

Co-guide (if applicable) **Guide**

STATEMENT BY AUTHOR

This dissertation has been submitted in partial fulfillment of requirements for an advanced degree at Homi Bhabha National Institute (HBNI) and is deposited in the Library to be made available to borrowers under rules of the HBNI.

Brief quotations from this dissertation are allowable without special permission, provided that accurate acknowledgement of source is made. Requests for permission for extended quotation from or reproduction of this manuscript in whole or in part may be granted by the Competent Authority of HBNI when in his or her judgment the proposed use of the material is in the interests of scholarship. In all other instances, however, permission must be obtained from the author.

Date:- 30^{th} May 2018 (Arpan Das)

DECLARATION

I, Arpan Das, hereby declare that the investigations presented in the thesis have been carried out by me. The work is original and has not been submitted earlier as a whole or in part for a degree/diploma at this or any other Institution/University.

Date: 30^{th} May 2018 (Arpan Das)

List of Publications

1. **Published/Accepted for publication/Preprint**

   (a) *Spontaneous CP violating quark scattering from asymmetric Z(3) interfaces in the quark-gluon plasma.*
   Abhishek Atreya, Partha Bagchi, **Arpan Das** and Ajit M. Srivastava.
   Phys.Rev. **D90** (2014), 125016; arXiv:1406.7411

   (b) ***Probing Dynamics of Phase Transitions occurring inside a Pulsar.***
   Partha Bagchi, **Arpan Das**, Biswanath Layek, Ajit M. Srivastava.
   arXiv:1412.4279

   (c) ***Effects of phase transition induced density fluctuations on pulsar dynamics.***
   Partha Bagchi, **Arpan Das**, Biswanath Layek, Ajit M. Srivastava.
   Phys.Lett. **B747** (2015) 120-124; arXiv:1506.03287

   (d) *Reaction-diffusion equation for quark-hadron transition in heavy-ion collisions.*
   Partha Bagchi, **Arpan Das**, Srikumar Sengupta, Ajit M. Srivastava.
   Phys.Rev. **C92** (2015), 034902; arXiv:1507.01015

   (e) *Possibility of formation of a disoriented chiral condensate in pp collisions at energies available at the CERN Large Hadron Collider via the reaction-diffusion equation.*
   Partha Bagchi, **Arpan Das**, Srikumar Sengupta, Ajit M. Srivastava.
   Phys.Rev. **C93** (2016), 024914; arXiv:1508.07752

   (f) *Towards laboratory detection of topological vortices in superfluid phases of QCD.*
   Arpan Das, Shreyansh S. Dave, Somnath De, Ajit M. Srivastava.
   Mod. Phys. Lett. **A 32**, 1750170 (2017); arXiv:1607.00480

   (g) *Effects of magnetic field on the plasma evolution in relativistic heavy-ion collisions.*
   Arpan Das, Shreyansh S. Dave, P.S. Saumia, Ajit M. Srivastava.
   Phys.Rev. **C96** (2017), 034902; arXiv:1703.08162

(h) ***Setting Initial Conditions for Inflation with Reaction-Diffusion Equation.***
Partha Bagchi, **Arpan Das**, Shreyansh S. Dave, Srikumar Sengupta, Ajit M. Srivastava.
Gen.Rel.Grav. **50** (2018) no.3, 27; arXiv:1709.02678

(i) *Pulsars as Weber gravitational wave detectors.*
Arpan Das, Shreyansh S. Dave, Oindrila Ganguly, Ajit M. Srivastava .
arXiv:1804.00453

(*) indicates the papers included in this thesis.

2. **Conference Proceedings**

(a) * *Probing Dynamics of Phase Transitions occurring inside a Pulsar.*
Partha Bagchi, **Arpan Das**, Biswanath Layek, Ajit M. Srivastava.
Springer Proc.Phys. 174 (2016) 415-419

(b) * *Effects of phase transition induced density fluctuations on pulsar dynamics.*
Partha Bagchi, **Arpan Das**, Biswanath Layek, Ajit M. Srivastava.
Presented (Oral presentation) by Arpan Das at CNT QGP Meet 2015, VECC, Kolkata.

(c) *Reaction-Diffusion Equations in ultra-high energy heavy-ion and pp collisions:Effective First order quark-hadron transition and DCC formation.*
Partha Bagchi, Arpan Das, Srikumar Sengupta, Ajit M. Srivastava.
Presented (Oral presentation) by **Arpan Das** at ATHIC 2016, New Delhi.

(d) * *Effects of phase transition induced density fluctuations on pulsar dynamics.*
Partha Bagchi, Arpan Das, Biswanath Layek, Ajit M. Srivastava.
Presented (Poster presentation) by **Arpan Das** at Quark Matter 2015,Kobe, Japan.

(e) *Reaction-diffusion equation for quark-hadron transition in heavy-ion collisions.*
Partha Bagchi, Arpan Das, Srikumar Sengupta, Ajit M. Srivastava.

Presented (Poster presentation) by **Arpan Das** at Quark Matter 2015, 2015, Kobe, Japan.

(f) *Effect of magnetic field on flow fluctuations in ultra-relativistic heavy-ion collisions.*

Arpan Das, Shreyansh S. Dave, P.S. Saumia, Ajit M. Srivastava.

Presented (Poster presentation) by **Arpan Das** at Quark Matter 2017, Chicago, USA.

(*) indicates presentation of the papers included in the thesis.

ARPAN DAS

To My Family, Friends and Colleagues

Acknowledgement

This thesis is the culmination of an extensive research effort. It is, therefore, only natural that the present work owes much to many people. I would like to thank my family for their constant support for my academics. I believe it is only because of their love and blessings that I could make this long and exasperating journey.

I am also grateful to my advisor Prof. Ajit M. Srivastava for his constant inspiration, encouragement and guidance throughout my research period at IoP. I have learned a lot about physics from his innovative and intutive thoughts. I would like to thank all the faculty members for their invaluable help during my stay at IoP.

Special thanks to my collaborators Saumia P.S., Ranjita Mohapatra, Abhishek Atreya, Partha Bagchi, Srikumar Sengupta, Shreyansh S. Dave and Somnath De. It is always a pleasure working with them. Thanks to my office colleagues and my predoc batchmates for informal discussions on physics as well as on nonacademic topics.

I am also thankful to SERC school organization committee for giving me opportunity to attend preparatory school and main schools on high energy physics. SERC schools gave a fantastic platform to learn some basic as well as advance topics in high energy physics. However the best parts of these schools is the opportunity to make friends, some of them will be future collaborators or colleagues. I would also like to express my gratitude to IoP, HBNI and DST-SERB for their financial support to attend conference within and outside India.

My humble regard to all the staff members of the library and the computer section who have maintained the excellent facilities at IoP. My thanks goes to all the administrative and nonacademic staffs for their support, cooperation and help at every stage.

Date: 30^{th} May 2018 **Arpan Das**

Contents

Synopsis

Quantum chromodynamics predicts that at extreme conditions of high baryon density and /or temperature there should be a deconfinement of quarks and gluons, and hadrons should undergo a phase transition to quark-gluon plasma (QGP) [1]. In the hot Big-Bang model of the universe, at very early stages, when the age of the universe was 10^{-5} sec and the temperature was about 10^{12} K, the universe consisted of a hot plasma of elementary particles e.g. quarks, gluons etc [2]. This phase of deconfined QCD matter has been created in heavy ion collision experiments (for reviews on heavy ion collision experiments see [3]. It is important to note that among all the phase transitions which took place in the early universe, only quark-hadron transition can be presently tested in laboratory experiments. These experiments make it possible to explore the interesting phases and phase transitions of QCD.

Apart from the heavy ion collision experiments compact astrophysical objects like neutron stars also provide a great opportunity to explore the properties of QCD matter at extreme conditions. Exotic phases of quantum chromodynamics (QCD) such as quark gluon plasma (QGP), 2 flavour color superconductivity (2SC) phase, color flavour locked (CFL) phase etc [4, 5]. are possible at very high baryon density. Core of an astrophysical compact objects such as neutron star provides physical conditions where transition to these phases may be possible [6]. Superfluid phases of neutrons are also believed to exist inside neutron stars at lower baryon densities. Nucleonic Superfluid phases in the neutron star can explain the phenomena of pulsar glitch [7]. The rotation period of pulsars increases slowly primarily due to magnetic dipole radiation, resulting in the pulsar slowing down. This spin down is gradual and largely predictable. However, there exist timing irregularities such as "glitch" when rotation frequency of pulsar exhibits a sudden increase, followed by a slow exponential relaxation. The relaxation time scale can vary from days to months. The standard theory of pulsar glitch mechanism in intimately related with nuclear superfluidity inside the neutron star. Superfluid vortex pinning and vortex creep model [8] is widely used as the explanation of glitch mechanism. Rotation of the superfluid part in a rotating neutron star is manifested by the presence of superfluid vortices. These superfluid vortices are attached with the crust. Quantized vortices have quantized rotation. Due to radiation energy loss rotational frequency of the crust layer decreases with time

causing differential rotation between the core and the crust. This leads to a magnus force which tries to unpin the vortices from the crust. Superfluid vortices detach when the dipinning force exceeds certain critical value. In this process huge angular momentum is transferred to crust, thus the angular frequency of the crust increases suddenly resulting in a glitch. Thus nucleonic superfluid phase gives a possible explanation of pulsar glitch and the post glitch relaxation. However, few anti-glitches have also been recently observed where, instead of an abrupt spin-up, the star abruptly spins down [9]. Explanation of the observation of such anti-glitches can not be given in the framework of vortex creep model.

In this thesis we have tried to give a unified approach which can explain glitch as well as antiglitch and post glitch/antiglitch relaxation. Our approach is based on the fact that phase transitions are typically associated with density change as well as density fluctuations. Density fluctuation in the core of a star will in general lead to transient changes in its moment of inertia (MI), along with a permanent change in MI due to phase transition. Non zero off diagonal components of MI arising from randomly distributed density fluctuations imply wobbling of rotating neutron star, which leads to modulation of peak intensity of pulses. Wobbling of pulsar is the distinguishable feature of our approach. Density fluctuations also will lead to rapidly changing quadrupole moment which can be a new source for gravitational wave emission [10].

Change in moment of inertia for a spherical neutron star due to a phase transition is [11],

$$\frac{\delta I}{I} \simeq \frac{5}{3}\left(\frac{\rho_2}{\rho_1} - 1\right)\frac{R_0^3}{R^3}, \tag{0.1}$$

where density of the star changes from ρ_1 to a higher density ρ_2 inside the core of radius R_0. R is the radius of the star in the absence of the dense core. For a second order, or a crossover or for a weak first order transition with very large bubble nucleation rate, this change in moment of inertia during phase transition will happen continuously, so no rapid change in MI. However for a strong first order phase transition, for very low nucleation rates, phase transition can be very rapid. This rapid change in MI can give rise to glitch. For a QCD phase transition, density changes can be of order one ($\delta\rho/\rho \sim 1, \rho \sim 100$ MeV/fm^3). If we take density change

$(\delta\rho/\rho)$ by 30%, as an example, and also the observational value of glitch about, 10^{-5}, then $R_0 \leq 0.3$ Km if $R = 10$Km. For superfluid transition we may take the change in density $(\delta\rho)$ to be 0.1MeV /fm^3 [12]. In this case R_0 can be of order 5 Km. We consider a simple case of zero temperature strong first order transition between a nucleonic phase and a QGP phase for a simple bag model equation of state [13]. We have also estimated nucleation rate using the model of quantum tunneling mediated by $O(4)$ symmetric instantons [14] . We have found that the supercritical core can be as large as 300 meters before a single bubble of new phase nucleates. For accretion driven change it will take a long time for the supercritical core size to increase to this size. After nucleation, the bubble will expand fast, sweeping entire supercritical core and converting it to the new phase. This will lead to MI change in a very short time which may be directly observable. QCD transition in a deep interior core of neutron star also has effects on the nucleonic superfluid phase in the outer part of the core. Latent heat released by the QCD transition will heat up the superfluid phase to the normal phase. Latent heat of order few hundred Mev /fm^3 is released in the QCD scale transition. Energy density scale for the superfluid transition being ~ 0.1Mev /fm^3, simple volume ratio tells that latent heat released in a 300 meter core undergoing QCD transition will convert about 3 km radius region from superfluid to the normal phase. Change in MI due to superfluid transition happening in radius of about 3 km will lead to fractional change in MI of order $10^{-5} - 10^{-6}$ [15]. Note that subsequent cooling will again lead to transition to the superfluid phase for all that region.

Change in moment of inertia can also result from random nucleation of bubbles due to statistical non-uniformity of density as well as temperature. Inside the core of radius 300 meters this can give rise to fractional change in MI $\sim 10^{-8}$ [15]. For this estimate we have varied the radius of the bubbles from 20 meters to 5 meters. Due to random nature of bubble nucleation, off-diagonal components of the MI, as well as the quadrupole moment become nonzero and the ratio of both to the initial moment of inertia are found to be of order $10^{-11} - 10^{-10}$ [15].

QCD phase diagram in high baryon density regime shows very rich structure. Apart from the QGP phase, some exotic phases of QCD e.g., CFL phase, 2SC phase, crystalline superconductivity etc. can exist as very high density. Symmetry breaking

pattern associated with the phase transition from hadronic to QGP phase or QGP phase to CFL phase etc are very complex. Symmetry breaking phase transitions naturally give rise to topological defects via Kibble mechanism [16]. These defects can be source of large density fluctuations depending on the relevant energy scales. Defects have initial densities which depend only on the correlation length and on the relevant symmetries. Different topological defects e.g., strings, domain walls etc. all generate different density fluctuations. Detailed simulations can determine the nature of resulting changes in pulsar timings and intensities resulting from these defects. Phase transition from hadronic phase to QGP phase can be characterized by the expectation value of Polyakov loop [17]. The Polyakov loop is defined as

$$L(x) = \frac{1}{N} Tr \left[\mathbf{P} exp \left(ig \int_0^\beta A_0(\vec{x}, \tau) d\tau \right) \right]. \tag{0.2}$$

Its thermal expectation value is related to the free energy of a static test quark in the QCD medium by,

$$l(x) = \langle L(\vec{x}) \rangle = e^{-\beta \Delta F}. \tag{0.3}$$

The two phases of QCD are distinguished as follows:

Confining Phase:- Quarks are confined. Thus, for an isolated static test quark one expects, $\Delta F \to \infty \Rightarrow \langle L(x) \rangle = 0$.

Deconfining Phase:- The color degrees of freedom are liberated, so isolated test quarks can exist. This means, ΔF is finite $\Rightarrow \langle L(x) \rangle \neq 0$.

For the dynamics of the order parameter $l(x)$ which is the expectation value of the Polyakov loop, we use the following effective Lagrangian density [18],

$$\mathcal{L} = \frac{N}{g^2} |\partial_i l|^2 T^2 - V(l), \tag{0.4}$$

where

$$V(l) = \left(-b_2 |l|^2 + b_3 (l^3 + (l^*)^3) + |l|^4 \right) b_4 T^4. \tag{0.5}$$

l has the value zero at low temperatures so the potential has only one minimum at $l = 0$. For $T > T_c$, $l(x)$ has a non-zero vacuum expectation value l_0. For $T > T_c$, $V(l)$ has three degenerate $Z(3)$ vacua. Note that in the presence of dynamical fermions $l(x)$ probably is not a correct order parameter, however we have used $l(x)$

only to estimate the change in the MI due to the presence of topological defects. Spontaneous breaking of $Z(3)$ symmetry gives rise to topological domain wall defects in the QGP phase which interpolate between different $Z(3)$ vacua and also string defects (QGP strings) forming at the junction of these $Z(3)$ walls.We carry out a field theory simulation of the evolution of $l(x)$. Time evolution of $l(x)$ is governed by the field equations obtained from the above Lagrangian. The physical size of the lattice is taken as $(7.5fm)^3$ and $(15fm)^3$ with appropriate lattice spacing. Fractional change in the MI and in the quadrupole moment is calculated for a neutron star core size $R_c = 0.4 \times (lattice size)$. Transient change of diagonal as well as off diagonal components of MI are of the order of $10^{-9}-10^{-10}$. Fractional change in the quadrupole moment is also of the order of $10^{-9} - 10^{-10}$ [15].

In the dense core of a pulsar, at very high density, there is a possibility of phase transition to Color flavour locked phase transition (CFL), due to quark-quark cooper pair formation. In this phase transition QCD symmetry group is broken as:

$$SU(3)_c \times SU(3)_L \times SU(3)_R \times U(1)_B \rightarrow SU(3)_{c+L+R} \times Z_2. \tag{0.6}$$

Breaking of $U(1)_B$ gives rise to superfluid vortices. To roughly estimate resulting change in MI due to superfluid vortices, we have modeled the formation of string defects by replacing $Z(3)$ symmetry breaking to $U(1)$ symmetry breaking (by appropriately changing $(l^3 + l^{*3})$ to $(|l|^2 + |l^\star|^2)^{3/2}$ in the Polyakov Loop effective potential. This modification gives rise to string defect without domain walls. Although the fractional changes in different components of MI are of same order but the magnitude of these changes are slightly larger for $Z(3)$ domain walls and strings.

Dynamical field theory simulations are performed on a small lattice due to limitations of computation. However we have also taken a static approach where we have produced a network of defects inside the core of the pulsar by modeling the correlation domain formation in a cubic lattice with appropriate energy scales of the defects. Results are obtained by varying core size R_c while keeping the correlation length $\xi = 10$fm fixed. We have varied R_c/ξ over a wide range from 5 to 400 and we have taken $R_c = 0.3/10R$. We have considered the fraction change in MI and quadrupole moment due to QCD string and domain wall and also for nucleonic superfluid string defects. Fractional changes in MI and quadrupole moment are of the

order $10^{-10} - 10^{-14}$ [15]. The change due to fluctuations is transient in nature and will dissipate away as star core achieves uniform new phase. Transient change can have either sign, similarly the net change can also have either sign depending on the nature of the transition.

In summary density fluctuations arising during a rapid phase transition lead to transient change in the MI of the star. Such density fluctuations in general lead to non-zero off-diagonal components of moment of inertia tensor which will cause the wobbling of pulsar, thereby modulating the peak intensity of the pulse. We find that moment of inertia can increase or decrease, which gives the possibility of accounting for the phenomenon of glitches and anti-glitches in a unified framework. Development of nonzero value of quadrupole moment (on a very short time scale) gives the possibility of gravitational radiation from the star whose core is undergoing a phase transition. Strain amplitude associated with gravitational radiation is of the order $10^{-24} - 10^{-22}$ [15], for a pulsar at 1Kpc distance. Density fluctuations arising during phase transitions crucially depend on the nature of phase transition. Identification of these density fluctuations via pulsar timings (and gravitational waves) can pin down the specific transition occurring inside the pulsar core. However it is important to point out that, multiple occurrences of glitches may raise concern in this model. For vortex depinning model multiple glitches seem natural. In our model, multiple occurrence of glitches will require multiple phase transitions. Glitches could occur due to multiple reasons, some glitches/anti-glitches could occur due to the model proposed here, that is due to phase transition induced density fluctuations, while other glitches could occur due to the conventional de-pinning of vortex clusters. We emphasize that when a transition happens in the core of a neutron star, it invariably leads to density fluctuations which manifest itself in glitch/anti-glitch like behavior, along with other implications such as wobbling of star, gravitational wave emission etc.

Another case where dynamics of phase transition plays an important role is the cosmological inflation. Historically inflation was proposed to resolve some problems regarding hot big bang cosmology. Hot big bang cosmology has successfully predicted experimentally verified observables, e.g. cosmic microwave background (CMBR), abundance of light elements or big bang nucleosynthesis (BBN) etc [2]. But the hot big bang cosmology has some shortcomings. These are the flatness problem,

the monopole problem and the horizon problem. To resolve these issues inflationary paradigm was introduced (for reviews see [19,20]). Inflation can be characterized as a phase of accelerating expansion. Scalar fields with correct initial conditions can give rise to a early period of accelerating expansion. The main ingredient of the inflation is the accelerating expansion of the universe at a very early stage. If the duration of the inflation $\Delta t \geq 60H^{-1}$, where H is the Hubble parameter during inflation, then one can explain the observed homogeneity and isotropy of the universe, the absence of the magnetic monopoles and the spatial flatness.

First particle physics motivated model of inflation was suggested by A. Guth, which is known as the old inflation model [21]. In this model, the Universe is assumed to be initially in thermal equilibrium and undergoes a strong first order transition (typically at the GUT scale). Inflation occurs when the scalar field (inflaton) gets trapped in the metastable vacuum. In this model inflation ends by quantum tunneling of the field into the true vacuum via bubble nucleation. In his own paper, Guth pointed out the graceful exit problem of this model. In old inflation model, the universe expands at an exponential rate while the bubbles nucleate at a constant rate. Until and unless the nucleation rate is high enough, the bubbles will not collide with each other, which is necessary for the end of the inflation and subsequent reheating. However, if the nucleation rate is large then phase transition will be completed quickly and it will not give enough inflation. Conditions for sufficient inflation and proper reheating can not be satisfied simultaneously. Thus old inflation model suffers graceful exit problem. This problem was addressed in the new inflation model [22, 23], where the shape of the finite temperature effective potential is such that either there is no potential barrier, so the phase transition is second order, or there is a very tiny potential barrier. In this model, the potential must have a very flat portion between the origin and the true minimum. The field starts very close to $\phi = 0$ and slowly rolls to the true minimum. During the slow roll, the energy density is dominated by the potential energy which gives rise to inflation. In new inflation when the classical field reaches the end of the flat part of the potential, it rapidly rolls down to the true vacuum and starts to oscillate. This is the stage of reheating of the universe at the end of inflation. Other inflationary models are also proposed like chaotic inflation [24], stochastic inflation [25], inflation with pseudo Goldstone boson [26], inflation with

modified gravity [27], warm inflation [28] etc.

In the original old inflation model, although the model does not work due to graceful exit problem, $\phi = 0$ is naturally set because of the presence of the metastable vacuum at $\phi = 0$. For new inflation it was hard to justify initial value of field being close to zero when the transition is second order (which requires field always remaining at the minimum of the potential). For this version of new inflation invoked a metastable vacuum with tiny potential barrier, along with a very flat top for the potential. With that, the initial value of ϕ could be set equal to zero due to the false vacuum at $\phi = 0$. The field tunnels through the barrier via nucleation of a bubble which undergoes inflation as the field inside the bubble rolls slowly over the flat top of the potential. The inflation ends when the field reaches the end of flat part of the potential and rolls down to the true vacuum rapidly. Thus the entire observed universe is inside one very large bubble, with other such bubbles constituting different parts of the universe disconnected from our universe by regions which are constantly undergoing inflation. For other models like chaotic inflation and natural inflation, the initial value of the field is not set naturally in this manner. Rather, it is supposed to explore entire allowed (relevant) range of field values. Inflation occurs wherever the field has the correct value.

In this thesis we have discussed the issue of initial condition for inflation in natural inflation model, which is a specific model of inflation. In this model Pseudo Nambu Goldstone bosons, which arise naturally in particle physics models, acts as inflaton field. Nambu- Goldstone bosons naturally arise in particle physics models with a spontaneous breaking of some global symmetry. If there is explicit symmetry breaking in addition to spontaneous symmetry breaking then one gets Pseudo Nambu-Goldstone Bosons (PNGB). In the case of QCD axion model with Pecci-Quinn symmetry breaking two very different scales naturally arises, these are Pecci-Quinn scale f_{PQ} which can be as high as the GUT scale $\sim 10^{15}$GeV, and QCD scale $\Lambda_{QCD} \sim 200$MeV. The same situation arises in low energy QCD theory with chiral sigma model, where pions are PNGB. For natural inflation, potential is of the form $V(\phi) = \Lambda^4(1 \pm cos(\phi/f))$. This potential contains two scales which naturally comes from particle physics model. One can show that if $f \sim m_{pl}$ and $\Lambda \sim m_{GUT} \sim 10^{15}$GeV, then the PNGB field ϕ can drive inflation [26]. This values of f and Λ comes from the constraints from

the requirements of the slow-rolling regime, sufficient inflation and observed magnitude of temperature fluctuations of CMBR. In order to achieve sufficient inflation, the PNGB field has to start very close to $\phi = 0$ in a region of size several Hubble volumes. However it can be shown that if one assumes that the Universe was in thermal equlibrium between the Planck epoch and the GUT scale, then the Hubble volume at the GUT scale contains about 10^9 uncorrelated domains [29]. If we take the probability of required value of ϕ in a single correlation domain is 0.1, then the probability of one single Hubble volume having the required value of ϕ is 10^{-10^9}. Thus the requirement of appropriate value of ϕ over the entire Hubble volume is extremely fine tuned, requiring tuning much stronger than the one inflation was intended to solve.

We have addressed this issue of initial conditions for inflation using specific features of the reaction-diffusion equations [29, 30]. Reaction-diffusion equations are studied typically in the context of biological systems, e.g. population genetics, chemical systems etc. RD equation with appropriate boundary condition gives traveling front with a well-defined profile. This profile mimics the profile of the phase boundary in a first order phase transition. Propagating front solutions of RD equations exist irrespective of the underlying phase transition dynamics. We have applied reaction-diffusion dynamics in relativistic field theory exploiting the fact that classical equation of motion of relativistic field in the presence of thermal bath has a similar form like RD equation except for second order time derivative term in the first case [31, 32]. In the strong dissipation limit, the first order time derivative term in the field equation dominates over the second time derivative term and the resulting field equation of motion directly maps to reaction-diffusion equation. Earlier the existence of propagating front solution in the context of chiral phase transition and confinement-deconfinement (C-D) transition in QCD has been shown even when the underlying transition is a cross-over or a continuous transition [31–33]. The existence of travel front solution of reaction-diffusion equation depends crucially on the shape of the underlying potential. If the potential allows for a non-zero order parameter in the vacuum state, along with a local maximum of the potential, only then traveling front solution exists. The corresponding values of the order parameter provide the required boundary conditions for the propagating front solution. Basic physics of reaction diffusion dynamics

of the transition is as follows. If the underlying potential of a field theory system has a Mexican hat type potential and in the physical space field has an inhomogeneous profile interpolating between the false vacuum at $\phi = 0$ and true vacuum $\phi = v$, then naive expectation tells us that, in a region where field is disoriented from the true vacua, field will quickly roll down to the true vacuum there. However in the presence of reaction-diffusion dynamics field roll down dynamics is different. In this case a travelling front develops between the two vacua and the front moves towards the false vacuum converting regions in false vacuum to true vacuum. Presence of this front is irrespective of the nature of the underlying phase transition dynamics. This front behaves as boundary separating two different phases. Due to this dissipative dynamics, roll down of the field is very slow and in fact the slowly propagating front holds the value of the field near the false vacuum for long time. On top of this if the system is expanding then a region of false vacuum stretches in physical space and eventually one gets large region where the field value if different than the true vacuum.

We have applied this idea of stretching of false vacuum domains in the presence of reaction-diffusion dynamics to resolve the fine tuning of initial conditions in natural inflation [26, 29]. It is important to note that we have taken natural inflation as an example of small field model of inflation. Our model applies to inflationary models if the potential satifies required conditions for RD solution. However we will not discuss the issue of the viability of this model as a correct model of inflation. Any model of inflation has to address the issue of initial conditions for the field. We take the PNGB potential of the form,

$$V(\phi) = \Lambda^4(1 + cos(\phi/f)), \tag{0.7}$$

The potential has a unique minimum at $\phi = \pi f$ and $\phi = 0$ is the local maximum of the potential. The periodicity of ϕ is $2\pi f$. We have taken $f = m_{pl}$ and $\Lambda = 10^{15}$ GeV which satisfies the constraints coming from slow roll condition, the requirement of enough inflation and observational constraint on the density contrast at the surface of the last scattering. Since the potential is symmetric about its minimum, we assume that inflation begins with the value of the field inside a domain, $\phi = \phi_1$, $0 < \phi_1/f < \pi$. For sufficient inflation, ϕ should satisfy the condition $0 \leq \phi_1 \leq \phi_1^{max}$, e.g if one takes

$f = m_{pl}$ then ϕ_1^{max}/f is about 0.2π. We assume that the Hubble volume at the GUT scale is filled with radiation energy (with typical number of degrees of freedom as appropriate for GUT scale, we take it to be 100), in addition to that, Hubble volume contains several field domains where field profile takes non-trivial shape. Inside these domains the field can have high potential energy, while outside the domain the field lies in the true vacuum. Thus typical profile in each field domain will be the field rising up towards the top of the potential inside the domains, while smoothly changing to the true vacuum value outside the domains. We consider a single domain where ϕ_1 is very close to zero inside the domain, and this is the only domain which will survive with nontrivial field profile as the Universe evolves. Now let us concentrate on the evolution of the inflaton field. With the above choice of potential, the equations governing the dynamics of inflaton field become,

$$\ddot{\phi} - \frac{\nabla^2\phi}{a^2} + 3H\dot{\phi} - \frac{\Lambda^4}{f}sin(\phi/f) = 0 \tag{0.8}$$

$$H^2 = \left(\frac{\dot{a}}{a}\right)^2 = \frac{8\pi}{3m_p^2}(\rho_\phi + \rho_{rad}) \tag{0.9}$$

$$\rho_\phi = \frac{1}{2}\dot{\phi}^2 + \frac{(\nabla\phi)^2}{2a^2} + \Lambda^4(1 + cos(\phi/f)) \tag{0.10}$$

$$\rho_{rad} \propto a^{-4} \tag{0.11}$$

We rescale the variables as follows, $\vec{x}\Lambda \to \vec{x}$, $t\Lambda \to t$, $\phi/f \to \phi$, $H/\Lambda \to H$. The resulting equations are,

$$\ddot{\phi} + 3H\dot{\phi} + \frac{\Lambda^2}{f^2}sin(\phi) - \frac{(\nabla^2\phi)}{a^2} = 0 \tag{0.12}$$

$$H^2 = \left(\frac{\dot{a}}{a}\right)^2 = \frac{8\pi}{3}\frac{f^2}{m_{pl}^2}\left(\frac{1}{2}\dot{\phi}^2 + \frac{1}{2}\left(\frac{\nabla\phi}{a}\right)^2 + \frac{\Lambda^2}{f^2}\left(1 + cos(\phi)\right) + \frac{\rho_{rad,0}}{f^2\Lambda^2}\left(\frac{a_0}{a(t)}\right)^4\right) \tag{0.13}$$

where we have taken the value of $\rho_{rad,0} = g^*\Lambda^4$ i.e. radiation energy density at GUT scale with number of degrees of freedom $g^* = 100$. Recall, in our model we have taken $\Lambda = 10^{15}$GeV, and $f = m_{pl}$. If we neglect the $\ddot{\phi}$ term in field evolution equation and

take H to be constant then the inflaton field equation becomes a reaction-diffusion equation (with time dependent diffusion constant). However, the potential term here (the reaction term for the RD equation) is new and we have not seen any standard RD equation with this form of the reaction term. The exact solution of this generalized reaction diffusion equation is not known.

To solve this set of differential equations we need the initial field profile which satisfies proper boundary condition. We have taken *tanh* profile of the field interpolating between minimum of the potential at $\phi = \pi f$ and the maximum of the potential at $\phi = 0$. We have taken this profile for 1-D as well for 3D case. Since the $\dot{\phi}$ term plays crucial role in the propagating front solutions of the RD equations, we have also considered a thermal dissipation term along with the $H\dot{\phi}$ term in the field evolution equation. With this, the equation of motion for ϕ becomes

$$\ddot{\phi} + (3H + \eta)\dot{\phi} + \frac{\Lambda^2}{f^2} sin(\phi) - \frac{(\nabla^2\phi)}{a^2} = 0. \tag{0.14}$$

We have taken thermal dissipation term to be proportional to T [29]. In scaled coordinates η is given by,

$$\eta(T) = \frac{T}{T_{Pl}} 3H_{Pl} = 3\frac{T_{Pl}}{T_{GUT}} \frac{H(T_{GUT})}{a}, \tag{0.15}$$

with the scale factor a taken to be 1 at the GUT scale. We have solved numerically the evolution of the inflaton field coupled with the evolution of the scale factor. We have solved this coupled equations for 1D case with thermal dissipation, 3D case with thermal dissipation and 1D case with out thermal dissipation. For all these cases we have taken the initial field profile of the following form,

$$\phi(z) = \frac{\pi}{2}[1 + tanh((z - z_0)/d)]. \tag{0.16}$$

Here, z_0 characterizes the size of the domain where field is very close to 0, and d gives initial thickness of the region in which field changes to the vacuum value (π). With this type of initial profile we have numerically solved coupled differential equations for 1D as well as 3D case. Note that the form of the initial profile is irrelevant. Even if one starts with a different profile interpolating between correct boundary values, very quickly the profile changes to the appropriate profile corresponding to the RD equation under consideration.

In 1D case with thermal dissipation we have found that initially the energy density is dominated by the sum of kinetic energy and the gradient energy of the field. At the initial stage the radiation energy density is also dominant over the vacuum energy density. But eventually the vacuum energy density becomes dominant. This is the onset of inflation. Beginning of the inflationary era is also evident from the behaviour of the scale factor. Initially the time evolution of the Hubble parameter is non trivial changing as a power law. However when the vacuum energy starts to dominate the Hubble parameter becomes almost constant. Along with this we have also tracked the position of the domain profile and we have found that initially Hubble scale is larger than the domain but due to the onset of inflation the domain becomes larger than the Hubble scale. This is the beginning of proper inflationary phase. In the 3D case as well as in the 1D case without thermal dissipation also we have found similar results [29]. In all these cases the initial domain was taken smaller than the Hubble size at GUT scale and the appropriate initial profile is inhomogeneous. However due to the reaction diffusion dynamics we have found that with inhomogeneous initial condition in domain much smaller than the Hubble scale entered inflation. This happens due to very special nature of propagating front solutions of RD equations which slows down field roll down sufficiently, allowing domain structure to survive for long time. With this, the expansion of the Universe is able to stretch the domain so that the vacuum energy starts dominating over other forms of energy densities signaling beginning of inflation.

It is important to note that we have not accounted for self gravity of these domains which will obviously affect the evolution of these domains. For this one needs to have a more rigorous simulation with full Einsteins equations. Also we have not considered the effect of fluctuations in this case.

Bibliography

[1] C.Y.Wong, "Introduction to High-energy Heavy-ion Collisions", World Scientific Publishing Co. Pte. Ltd, 1984.

[2] E. Kolb and M. Turner, "The Early Universe", Westview Press, 1990.

[3] J.W. Harris and B. Muller, Ann. Rev. Nucl. Part. Sci. **46**, 71 (1996), B. Muller and J.L. Nagle, Ann. Rev. Nucl. Part. Sci. **56**, 93 (2006).

[4] M.G. Alford, A. Schmitt, K. Rajagopal and T. Schafer, Rev. Mod. Phys. **80**, 1455 (2008).

[5] Alford, M. G., and K. Rajagopal, arXiv: hep-ph/0606157, K. Rajagopal and F. Wilczek, hep-ph/0011333; D. H. Rischke and R. D. Pisarski, nucl-th/0004016; M. Buballa, Phys. Rept. **407**, 205 (2005);

[6] K. Fukushima and T. Hatsuda, Rept. Prog. Phys. **74**, 014001 (2011), [arXiv:1005.4814[hep-ph]]

[7] K. W. Lo, "Neutron Star and Superfluidity", Department of Physics, University of Illinois at Urbana-Champaign, 2010.

[8] P. W. Anderson and N. Itoh, Nature **256**, 25 (1975).

[9] R. F. Archibald, V. M. Kaspi, C. Y. Ng, K. N. Gourgouliatos, D. Tsang, P. Scholz, A. P. Beardmore, N. Gehrels and J. A. Kennea, Nature **497**, 591 (2013).

[10] K. Riles, Prog. Part. Nucl. Phys. **68**, 1 (2013); S. Weinberg, Gravitation and cosmology, John Wiley and Sons Inc., 1972, USA.

[11] H. Heiselberg and M. Hjorth-Jensen, Phys. Rev. Lett.**80**, 5485 (1998).

[12] R. W. Richardson, Phys. Rev. **D 5**, 1883 (1972); C.-H. Yang and J.W. Clark, Nucl. Phys. **A 174**, 49 (1971).

[13] J. Cleymans, R.V. Gavai, and E. Suhonen, Phys. Rep. **130**, 217 (1986).

[14] M.B. Voloshin, I.Yu. Kobzarev, and L.B. Okun, Yad. Fiz. **20**, 1229 (1974) [Sov. J. Nucl. Phys. **20**, 644 (1975)]; S. Coleman, Phys. Rev. **D**15, 2929 (1977).

[15] P. Bagchi, A. Das, B. Layek and A. M. Srivastava, Phys.Lett. **B747** (2015) 120-124; P. Bagchi, A. Das, B. Layek and A. M. Srivastava, arXiv:1412.4279.

[16] T.W.B. Kibble, J. Phys. **A 9**, 1387 (1976); Phys. Rept. **67**, 183 (1980).

[17] L. D. McLerran and B. Svetitsky, Phys. Rev. **D** 24, 450 (1981); L. D. McLerran, Rev. Mod. Phys. 58, 1021 (1986).

[18] A. Dumitru and R.D. Pisarksi, Phys. Lett. **B 504**, 282 (2001); Phys. Rev. **D 66**, 096003 (2002); Nucl. Phys. **A 698**, 444 (2002).

[19] A. Riotto, arXiv:hep-ph/0210162.

[20] R. H. Brandenberger, arXiv:hep-ph/9702217.

[21] A. Guth, Phys. Rev.**D 23**, 347 (1981).

[22] A. Linde, Phys. Lett. **B 108**, 389 (1982).

[23] A. Albrecht and P. Steinhardt, Phys. Rev. Lett. **48**, 1220 (1982).

[24] A. D. Linde, Phys.Lett. **B 129**, 177, 1983.

[25] A. A. Starobinsky, in Field Theory, Quantum Gravity and Strings, ed. H. J. de Vega and N. Sanchez (Springer, Berlin 1986); S. J. Rey, Nucl. Phys.**B284**, 706 (1987); J. M. Bardeen and G. J. Bublik, Class. Quan. Grav.**4**, 473 (1987); M. Morikawa, Phys. Rev. **D42**, 1027 (1990); H. E. Kandrup, Phys. Rev. **39**, 2245 (1989).

[26] K. Freese, J. A. Frieman, A. V. Olinto, Phys. Rev. Lett. **65**, 3233 (1990); K. Freese, arXiv:astro-ph/9310012; K. Freese, W. H. Kinney, Phys.Rev. **D70**, 083512 (2004); K. Freese, W. H. Kinney, arXiv:1403.5277.

[27] A. A. Starobinsky, Phys. Lett. **B 91**, 99 (1980).

[28] A. Berera, Phys. Rev. Lett. **75**, 3218 (1995); A. Berera, Contemporary Physics **47**, 33 (2006); A. Berera, I. G. Moss, R. O. Ramos, Rept.Prog.Phys.**72**, 026901 (2009).

[29] P. Bagchi, A. Das, S. S. Dave, S. Sengupta and A. M. Srivastava, arXiv: 1709.02678

[30] J.D.Murray, Mathematical Biology, I : An Introduc- tion, Third Edition, (Springer), 2002; J.D.Murray, Lectures on Nonlinear-Differential-Equation Mod- els in Biology, (Clarendon Press), 1977; B.Bradshaw- Hajek, Reaction-diffusion Equations for Population Genetics, (Ph.D. thesis, School of Mathematics and Applied Statistics, University of Wollongong), 2004, (http://ro.uow.edu.au/thesis/201); B.H.Gilding and R.Kersner, Travelling Waves in Nonlinear Diffusion Convection Reaction, (Springer Basel AG, Switzerland), 2004.

[31] P. Bagchi, A. Das, S. Sengupta, A. M. Srivastava, Phys.Rev. **C92**, 034902 (2015) [arXiv:1507.01015].

[32] P. Bagchi, A. Das, S. Sengupta, A. M. Srivastava, Phys.Rev. **C93**, 024914 (2016) [arXiv:1508.07752].

[33] S. Sengupta, "Aspects of QCD Phase Transition with Reaction-Diffusion Equations", (Ph.D. thesis, Homi Bhabha National Institute, India, 2015).

List of Figures

List of Tables

Chapter 1

Introduction

1.1 Our Universe

It has been a great curiosity for mankind to understand, *"Where do we come from? What are we? Where are we going?"* [1]. These curiosities ultimately boil down to the understanding of our universe. The current understanding of the universe is based on the hot big bang model of modern cosmology. To understand the origin of our universe we need to extrapolate the present universe back in time. According to the big bang Theory of the universe, the early universe was smaller in size and also much hotter with a large energy density in the past. In fact, our observable universe which includes clusters of galaxies having length scales of the order of 100 Mpc (1pc = 3.26 light-years) originated from an infinitesimally small region having a length scale of only slightly bigger than $l_p = 10^{-35}$ meters. To understand our universe scientists have taken two paths, one is by direct observation of the universe using telescopes at different electromagnetic wavelengths and the other is by recreating the early universe scenario in terrestrial laboratories by producing hot and dense medium ("Little Bang"). Apart from the terrestrial laboratories, large compact objects like Neutron stars also help us to understand the properties of matter under extreme conditions.

1.1.1 Observing the early universe

With the advances in observational astronomy in 20th-century, astronomers could measure redshifts of the known spectral lines with optical telescopes. By 1929, enough galaxy redshifts had been measured for the cosmologist Edwin Hubble to make a study of whether a galaxys redshift depends on its distance from us. He found most of the galaxies are receding from us with a velocity proportional to the distance with respect to us [2]. The mathematical form of Hubble's observation or Hubble law is one of the cornerstones of modern cosmology along with cosmic microwave background (CMB) [1, 3] and big bang nucleosynthesis (BBN) [1, 3].

Arno Penzias and Robert Wilson, two radio astronomers from Bell Laboratories found a slightly stronger background in microwave range than they expected when they turned the horn-reflector radio antenna toward the sky. Their observation was in accordance with the prediction of primordial radiation which could be a relic of an early, hot, dense, and opaque state of the universe. This radiation which is known as cosmic microwave background radiation (CMBR) [4, 5] is in strong support of hot big bang model of our universe. Hot big bang cosmology assumes that the universe is in thermal equilibrium for most of the time during its evolution. However some brief out of equilibrium periods occurred during the evolution of the universe. It turns out that, these out of equilibrium phases are really important for our own existence, e.g. photons eventually go out of equilibrium with rest of the cosmic plasma. Observational data from satellites like COBE, WMAP, PLANCK along with various ground-based experiments, galaxy surveys etc and the theoretical foundations of the general theory of relativity, gave us a consistent theoretical framework of the standard model of cosmology.

Apart from the visible sectors, the universe also has mysterious dark sectors, which only interacts with the visible sector by gravitational interaction. The measurement of galaxy rotation curves hinted the presence of dark matter in the universe [6, 7]. Various separate observations like mass to light ratio in the clusters of galaxies, CMB power spectrum, light element abundance etc tell us that the baryonic matter or the

luminous matter is only about 3% of the total matter energy content of the universe and about 25% of the matter is made out of "Cold Dark Matter". Because the gravitational force is attractive in nature it used to be believed that the expansion of the universe will eventually slow down. On the contrary, when luminosity distance of the distant Type Ia supernovae were studied with respect to their redshifts, it was found that universe is accelerating [8]. This acceleration could not be explained by normal matter having attractive gravitational interaction. However contrary to Newtonian gravity, Einstein's gravity (General Theory of Relativity) can accommodates some matter/energy forms which give rise to repulsive gravity. This form of energy which gives rise to accelerating expansion is called "Dark Energy". In Present days the evolution of the universe is dark energy dominated. 72% of the total energy density of the universe is in the form of dark energy. Cosmological constant as introduced by Einstein, in a completely different context, is one of the possible candidates of the dark energy. Hot big bang model along with cold dark matter (CDM) and cosmological constant (Λ) is also known as ΛCDM model of cosmology. Till today ΛCDM model is consistent with all the different experimental observations.

Let us go through the thermal history of our universe briefly [9]. According to the big bang model, the universe started from a singularity where the energy density and temperature of the universe were infinitely large. Around Plank era, the age of the universe is of the order of 10^{-43} sec and the temperature of the universe is of the order of 10^{19} GeV. At this high energy density, corresponding to the Planck scale, it is expected that all four fundamental forces (strong nuclear force, weak nuclear force, electromagnetic force and gravitational force) of nature may be unified. According to the big bang model, the universe has been expanding from the beginning up to now, with the present age of the Universe being about 13.6 billion years. Due to the expansion universe becomes dilute and cooler. As the universe cooled from a very hot early stage, it went through a number of phase transitions e.g. GUT (grand unified theory), electroweak and QCD phase transition etc. The timeline of the early universe which shows important stages of its evolution is presented in Figure 1.1 . Above the GUT scale (temperature $\sim 10^{16}$ GeV) the strong force and the electroweak

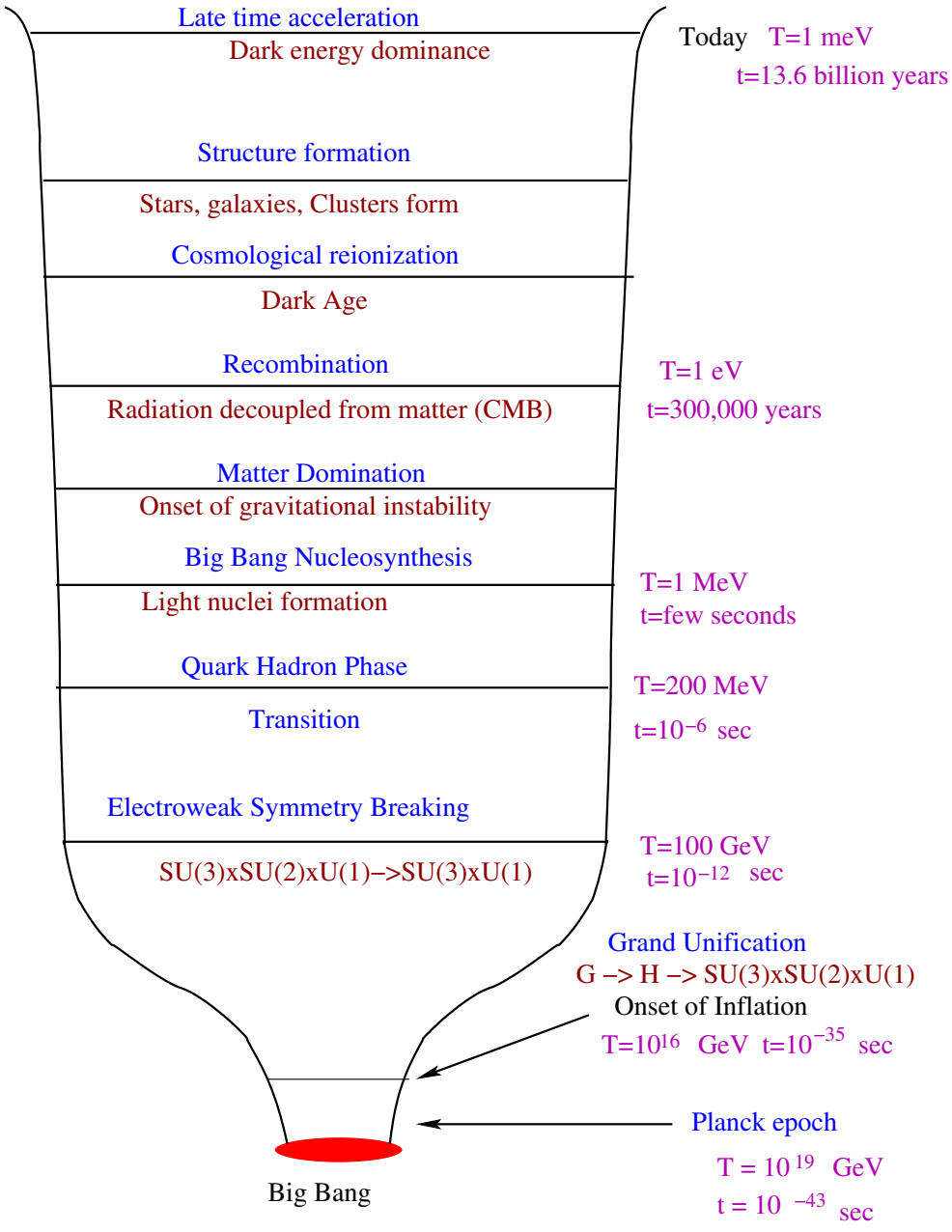

Figure 1.1: Schematic representation of various stages in the thermal history of the universe

.

force were unified. After the GUT phase transition strong force got separated from the electroweak force. Experimentally we cannot probe GUT scale physics directly in present day colliders. However, one of the important aspects of these phase transitions is that they might have left imprints on the universe, which could subsequently have affected the evolution of the universe. During GUT phase transition certain gauge group representing the unified theory (e.g. SU(5) or SO(10)) is spontaneously broken into standard model gauge group i.e. $SU(3)_c \times SU(2)_L \times U(1)_Y$. Here "c" denotes color gauge group (QCD), "L" denotes left chiral fermions and "Y" denotes weak hypercharge. Such spontaneous symmetry breaking phase transition might have lead to the formation of topological defects e.g. monopoles, domain walls, cosmic strings etc, depending upon the structure of the vacuum manifold after symmetry breaking [10]. Study of these topological defects can provide an observational window to test the very high energy scale physics of the early stages of the universe.

When the universe was 10^{-12} sec old, it underwent Electroweak phase transition where the standard model gauge group $SU(3)_c \times SU(2)_L \times U(1)_Y$ spontaneously broke to $SU(3)_c \times U(1)_{em}$ [11]. Due to the spontaneous breaking of gauge symmetry, W and Z gauge bosons got their masses by Higgs mechanism [11, 12] and Yukawa couplings to the Higgs field gave masses to the fermions (quarks and leptons). However, neutrinos remained massless. However we know now that neutrinos have non zero masses, which can be achieve by extension of standard model. It is also believed that during the electroweak phase transition, the baryon-antibaryon asymmetry may have been generated (electroweak baryogenesis or via leptogenesis) leading to the present universe being matter (baryon) dominated [13].

The phase transition which is the most important in our current discussion is the QCD phase transition. Universe undergoes this transition when its temperature was of the order of 200 MeV. The age of the universe was few microseconds at this stage. This happens to be the only phase transition in the very early universe which can be studied in the relativistic heavy ion collision experiments (RHICE), which we will discuss later in section 1.3 . This phase transition occurs as the universe cools from a deconfined state of quarks and gluons, called as the quark-gluon plasma (QGP) phase

at high temperature, to a low temperature confined phase where quarks are confined into color-neutral hadrons.

As the universe cooled, new bound states of elementary particles such as protons and neutrons were formed out of quarks after QCD phase transition. From about one second to a few minutes cosmic time, when the temperature has fallen below 10 billion Kelvin, the conditions are just right for protons and neutrons to combine and form certain species of atomic nuclei. This process is known as big bang nucleosynthesis (BBN) [14, 15]. It turns out that BBN was not efficient enough to produce heavier atomic nuclei such as those necessary to build human bodies or a planet like the earth. Instead, those nuclei were formed in the interior of stars much later during the evolution of the universe (or during supernova explosion). BBN produced about 75% hydrogen, 25% helium and some relatively light elements up to Li^7.

After BBN the universe consisted of electromagnetic plasma consisting mainly of the proton (hydrogen), electron, radiation and few percentage of heavy nuclei (up to Li^7) in thermal equilibrium. When the temperature of the universe was about 1 eV, protons and electrons recombined, and the universe turned neutral. During this epoch because of the reduction in the free electron number density photon's mean free path grew larger and the photons were decoupled from the rest of the plasma. Those decoupled photons started free streaming and we observe these photons as the cosmic microwave background radiation (CMBR). Decoupling of the photons from the rest of the plasma occurred in an era when non relativistic matter dominated the evolution of the universe. Prior to matter domination, energy density of the universe was dominated by radiation. Non-relativistic matter took control of the evolution of the universe when the age of the universe was $\sim 5 \times 10^4$ years. After the radiation matter equality non relativistic matter was the dominant component of the universe, however present day universe is dominated by dark energy. Matter, dark energy equality happened when the age of the universe was ~ 9.5 billion years. Later in section 6.1 we will discuss some of the aspects of the standard model of cosmology in greater details.

1.1.2 Cosmic Microwave Background Radiation

Photons which were decoupled at the time of the last scattering had a temperature of the order 1 eV (for details of the photon decoupling see section 6.2.3). However during free streaming due to the expansion of the universe, those photons were redshifted and cooled down. Thus free streaming photons reaching us today are in the microwave region of the electromagnetic spectrum and carry a temperature of the order of 3K. CMB was discovered by Penzias and Wilson in 1965 [4]. Before this discovery and despite the observation of the expansion of the universe, the steady state model of cosmology had many followers. However, the observation of Penzias and Wilson and its interpretation by Dicke and collaborators clearly demonstrated that the adiabatic expansion and cooling of the universe from a early hot and dense stage. In 1978, Penzias and Wilson were rewarded with the Physics Nobel Prize for their discovery. Gamow and collaborators long time back had predicted the background of cosmic radiation, a relic from the hot early phase [16,17]. Its temperature had been estimated to be of the order of a few degrees Kelvin. The background radiation detected by Penzias and Wilson was highly homogeneous and isotropic having a temperature of 3.5 K at wavelength 7.5 cm. If the early universe was in thermal equilibrium then this background radiation should have a perfect black body spectrum. However Measuring the spectrum of the CMB, and confirming that it is indeed a blackbody, was not a simple task. The current energy per CMB photon is of the order 6×10^{-4} eV, which is much smaller than the binding energy of the atom. However, the mean photon energy is comparable to the vibrational or rotational energy of molecules like H_2O. Earth's atmosphere can strongly absorb microwaves with wavelengths shorter than $\lambda \sim 3$ cm. Thus Penzias and Wilson observed CMB at a wavelength $\lambda = 7.35$ cm, greater than $\lambda \sim 3$cm. However, the predicted peak of the CMB spectrum is around $\lambda \sim 2$ mm. The CMB can be measured at wavelengths shorter than 3 cm by observing from high-altitude balloons. The best way to measure CMB spectrum is to do experiments outside the earth's atmosphere. COsmic Background Explorer(COBE)satellite(1992) which is located 900 km above the earth's surface measured CMB accurately over

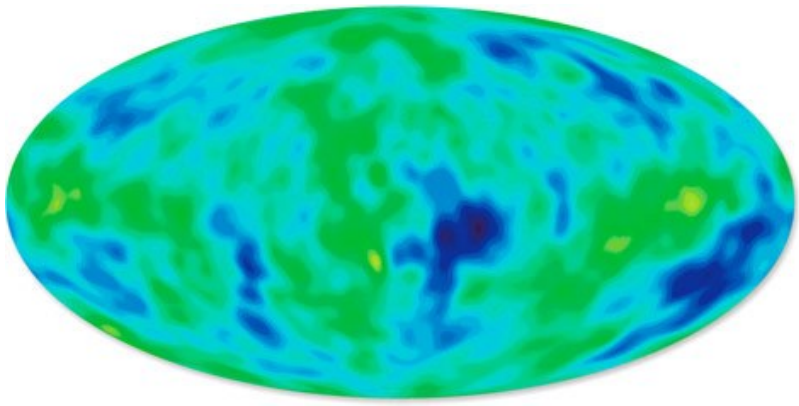

Figure 1.2: CMB sky as measured by COBE (1989-1993) [25].

a wide range of wavelengths. Diffuse InfraRed Background Experiment (DIRBE) and Far InfraRed Absolute Spectrophotometer (FIRAS) measured radiation at the wavelengths 0.001 mm $< \lambda <$ 0.24 mm and 0.1 mm $< \lambda <$ 10 mm respectively [18]. Differential Microwave Radiometer (DMR) measured the full-sky map of the CMB at the following wavelengths $\lambda = 3.3$ mm, $\lambda = 5.7$ mm, $\lambda = 9.6$ mm. Three important results came out of COBE measurements, CMB is very close to that of an ideal blackbody at any point on the sky irrespective of its angular position, CMB has dipolar distortion in temperature due to the fact that COBE satellite has relative motion with respect to the frame of reference in which CMB is isotropic and apart from the dipolar distortion CMB has temperature fluctuation of the order of 10^{-5} [1, 19–21]. Although COBE's discoveries provided important information about the universe, it had a poor angular resolution of $\sim 7^{\circ}$. To improve the accuracy of the measurements new satellites like WMAP and PLANCK were launched in 2001 and 2009 respectively. The angular resolution of WMAP is 33 times higher than that of COBE. PLANCK's resolution is 3 times higher than the angular resolution of WMAP [22–24]. CMB sky as measured by COBE, WMAP and PLANCK satellites are shown in the figures 1.2 , 1.3 , and 1.4 respectively. In these figures different colors denote temperature fluctuation in the CMB sky. These temperature fluctuations also gives the direct indications of the density perturbations at the time of last scattering. These figures are taken from [25]. For detail discussion see [22].

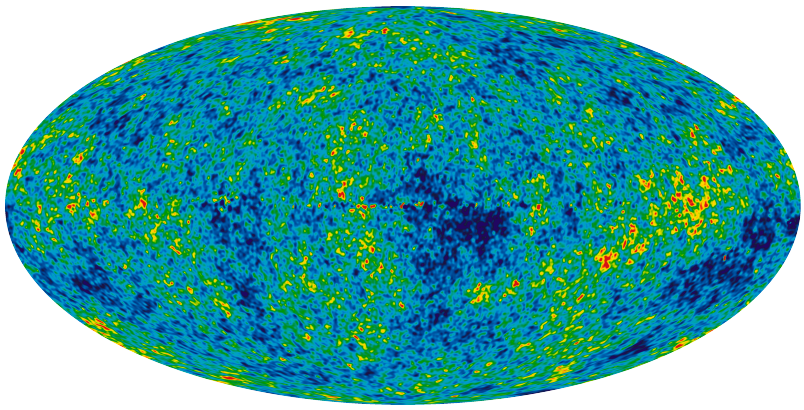

Figure 1.3: CMB sky as measured by WMAP (2003-2012) [25].

.

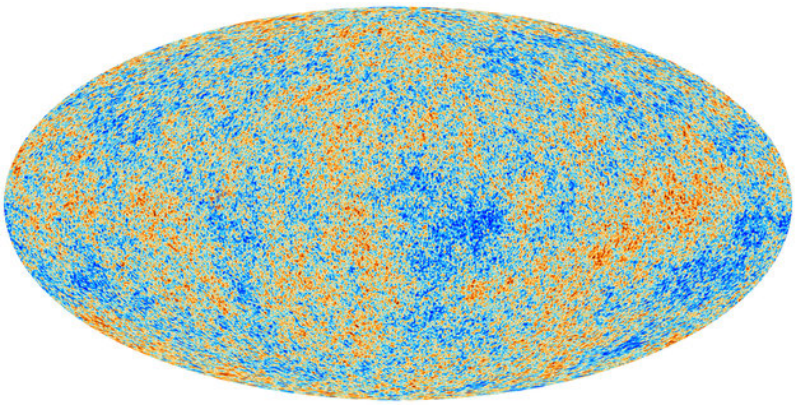

Figure 1.4: CMB sky as measured by PLANCK (2009-2013)(ongoing) [25].

.

1.1.3 Inflation

In this subsection, we will briefly introduce the inflationary paradigm. In chapter 6 , we will discuss the physics of inflation in detail. Despite great success, the big bang model of the Universe suffers from some problems. These are known as horizon problem, flatness problem, and monopole problem [1], [3], [26]. It has been shown that hot big bang model alone cannot explain the large-scale homogeneity of CMB map at the surface of the last scattering. Calculations imply that information would have to travel faster than the speed of light in the early universe in order to achieve the present homogeneity of CMB sky!(for details see section 6.2.3). Flatness problem relates to the observed data showing that our universe is almost spatially flat. It has been shown that for the Universe to have evolved to its present state, the spatial geometry of the early universe must have been precisely flat, to an unbelievable degree of precision and the matter density in the early universe has to be extremely finely tuned, for details see section 6.2.1). We have mentioned earlier that symmetry breaking phase transition gives rise to topological defects. It has been shown that phase transition at GUT scale produces magnetic monopoles as topological defects. One can show that the abundance of monopoles produced during the GUT transition is so large that the energy density would be much larger than the critical energy density of the Universe. So, the presence of monopoles will severely change the evolution of the Universe (for details see section 6.2.2). It has been shown that a brief period of accelerating expansion during the evolution of the early universe can resolve the above-mentioned problems. In short, inflation is an epoch in the evolution of the Universe when the Universe expanded exponentially (by a factor of e^{60} or more) for a very short period of time. Although the concept of inflationary paradigm was understood earlier, the first relatively simple particle physics model where one can achieve inflation was proposed by Guth [27]. This model is known as old inflation model (see section 6.3.1). However, Guth himself pointed out that his model of inflation has some serious problems and later new inflationary models were proposed [28,29]. Details of all these issues we will discuss later in chapter 6. Apart from solving cosmological problems of hot big bang

model, density perturbations generated during inflationary era also give the correct initial conditions for structure formation.

1.2 The Microcosmos

In the early 20th-century particle physics and cosmology developed separately. During 1980's the construction of GUT theories at the very high energy scale of the order 10^{15} GeV finally connected particle physics and cosmology, *"(...)the universe is the only machine we have that can test these GUT ideas. Its the worlds biggest particle accelerator (...). But its hard to use because all the experiments happened only once, (...) a long time ago"* [30]. It is possible today to deduce consequences of particle physics in cosmology and vice versa. The connection between particle physics and cosmology is nicely illustrated in figure 1.5 . Evolution of the Universe at large scales ($\sim$ Mpc) is intimately connected to the physics at small scales ($\sim$ GUT scale). Also, it is important to know that out of all the phase transitions occurred in the early universe only QCD phase transition is accessible in the heavy ion collision experiments. Hence it is really important to understand the QCD sector of the standard model of particle physics. We will discuss QCD phase transitions in details in chapter 2 and QCD phase diagram in section 1.6.

With the understanding developed at the present level of energies and resolution available at colliders, the matter is made up of leptons and quarks, both of which are spin half fermions. The leptons come in three generations and can be listed as: (ν_e, e^-), (ν_μ, μ^-), (ν_τ, τ^-). All the particles have corresponding antiparticles. If neutrinos are not Majorana fermions then neutrinos and antineutrinos are different particles. In that case, we have a total of twelve leptons. Quark comes in six flavors, these are, up (u), down (d), charm (c), strange (s), top(t) and bottom (b). Like leptons quarks are also grouped in three generations, these are (u, d), (c, s), (t, b). Each of the six quarks of different flavors comes in three colors and each quark has its own antiparticle. So we have a total of $(6 \times 3 \times 2 = 36)$ quarks. Thus fermion sector of the standard model of particle physics has 12 leptons and 36 quarks.

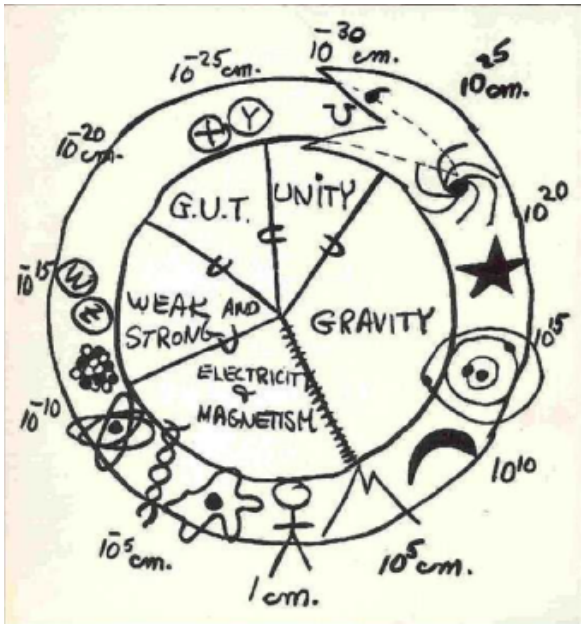

Figure 1.5: Cosmic serpent swallowing its tail, illustrating the interconnection between particle physics and cosmology [31].

These matter particles or fermions interact with each other. Apart from gravity, these interactions are strong interaction, electromagnetic interaction and weak interaction. Principles of quantum field theory suggest that all these forces are mediated by the exchange of "gauge" bosons. Strong interaction is mediated by the gluons, electromagnetic force by the photons and the weak force by $W^{\pm}$, Z^0. Gluons come in eight varieties. Although the quantum theory of gravity is still not well understood, it is known that graviton which is a spin 2 particle is the mediator of gravitational interaction. All the other gauge bosons are spin 1 particles. Graviton, gluons, and photos are all massless. Contrary to that, carriers of weak interactions are massive. They get their masses in a gauge invariant way at electroweak phase transition via Higgs mechanism. Higgs mechanism is also responsible for mass generation of fermions. Higgs boson was elusive for a long time but recently LHC confirmed the existence of Higgs-like boson which has all the properties of Higgs boson. If Higgs is not composite then Higgs boson will be the only elementary spin 0 particle in nature. Graviton is not part of the standard model of particle physics. The standard model thus has

twelve force carriers: eight gluons, $W^{\pm}$, Z^0 and the photon. Gluons and photons are their own antiparticles, whereas W^+ is the antiparticle of W^- and vice-versa. Thus 48 fermions, 13 gauge bosons, and the Higgs boson comprise the standard model of particle physics [11].

1.2.1 QCD: an overview

The fundamental theory of strong interactions between quarks and gluons is known as quantum chromodynamics (QCD). QCD is a non-abelian gauge theory described by SU(3) color gauge group. We will discuss the symmetries of QCD Lagrangian later in chapter 2 . Quarks not only participate in strong interactions but also in weak interaction and elctromagnetic interaction. However weak interaction eigenstate of quarks are different from the mass eigenstates and they are related by CKM matrix. The electric charge of quarks in the units of the positron charge is as follows: u, c, t quarks have charge $\frac{2}{3}$ and the remaining quarks have charge $-\frac{1}{3}$. Quarks have two types of masses:

a) The current quark mass which is the mass of the quark in the absence of confinement and is about 5 MeV for u quark and 10 MeV for d quark. Origin of the current quark mass is the Higgs mechanism. This is the mass that enters in the QCD Lagrangian.

b) Contrary to QED the quantum field theory of electromagnetism, QCD is non-abelian and unlike photons, gluons have self-interaction. This self-interaction of the gauge fields makes QCD very non-trivial in low energy regime. Confinement is an important property of QCD in low energy regime. The constituent quark mass is the effective mass of a quark when it is confined in hadrons. Confinement effect of QCD gives a large contribution to current quark mass. The constituent mass contribution for quarks is of the order of 330 MeV for u, d quarks. For top quark, the notion of constituent mass is superfluous, because no bound state of top quark is discovered.

The color charge was introduced to explain the existence of certain QCD states known as $\triangle^{++}$ baryon. $\triangle^{++}$ is a bound state of three u quarks. Since this is the

ground state, the spatial wave function should be symmetric. The three spins of the quarks are aligned to give the spin $+\frac{3}{2}$. Thus the wave function of the $\triangle^{++}$ does not change if two quarks are interchanged. However, the wave function must be antisymmetric according to the Pauli exclusion principle. This was a great problem for the quark model. To resolve this issue a new quantum number "color" was introduced. Each quark flavor carries three different color charges red, green and blue. Hadrons are color singlets, it is like spin 0 representation of ordinary spin. Like all the other particles quarks also have their own antiparticles known as anti-quarks. Quantum numbers of an anti-quark are opposite to the quantum numbers of corresponding quark, e.g. all the quarks carry baryon number $+\frac{1}{3}$ and the antiquarks carry baryon number $-\frac{1}{3}$, similarly their electric charge is also opposite. The notion of color confinement allows only color singlet objects to be physically observable in an experiment. Color singlet combinations which are allowed are,

a) Mesons: These are $q\bar{q}$ bound states with integral spins (i.e. bosons),

b) Baryons: These are qqq bound states and are fermions.

Now we can briefly discuss the mathematical structure of QCD. Lorentz invariant, renormalizable, UV complete, gauge invariant QCD Lagrangian of interacting quarks and gluons is written as,

$$\mathcal{L} = -\frac{1}{4} G^a_{\alpha\beta} G^{\alpha\beta}_a + \sum_\alpha \bar{\psi}_\alpha \left(i\gamma^\mu D_\mu - m \right) \psi_\alpha, \tag{1.1}$$

where $\alpha = u, d, c, s, t, b$ denotes the flavor index of quarks and D_μ is the covariant derivative which is defined as,

$$D_\mu = \partial_\mu - igT_a A^a_\mu, \tag{1.2}$$

where g is the gauge coupling, T^a are the generators of $SU(3)$ in the fundamental representation and $a = 1, 2....8$. T^a satisfies Lie algebra of $SU(3)$,

$$[T^a, T^b] = if^{abc}T^c \tag{1.3}$$

where f^{abc} are totally antisymmetric structure constants.

$G^{\alpha\beta}$ is the field strength tensor for QCD gauge fields. Contrary to QED field strength tensor, $G^{\alpha\beta}$ is not gauge invariant. $G^{\alpha\beta}$ is defined as,

$$\Big[D_\alpha, D_\beta\Big] = igG_{\alpha\beta} \equiv igT_a G^a_{\alpha\beta}\,, \tag{1.4}$$

where

$$G^a_{\alpha\beta} = \partial_\alpha A^a_\beta - \partial_\beta A^a_\alpha + gf^{abc}A^b_\alpha A^c_\beta\,. \tag{1.5}$$

Under SU(3) gauge transform, fermionic fields transform as,

$$\psi \to \psi' = U\psi, \tag{1.6}$$

where U is a general SU(3) matrix, and

$$T_a A^a_\mu \to T_a A^a_\mu{}' = UT_a A^a_\mu U^{-1} - i\Big(\partial_\mu U\Big)U^{-1}. \tag{1.7}$$

Unlike QED, QCD Lagrangian contains self-interaction terms (three point and four point vertices) of gauge field. Those interaction terms are,

$$g\partial_\nu A^a_\mu f^{abc}A^{\mu b}A^{\nu c} \quad \text{and} \quad g^2 f^{abc}f^{alm}A^b_\mu A^c_\nu A^{\mu l}A^{\nu m}.$$

QCD is a renormalizable theory. An important consequence of renormalizable quantum field theory is the dependence of the parameters of the theory (like coupling constants, mass etc) on the renormalization scale. Energy scale dependence of the strong coupling constant $\alpha_s(\alpha_s = g^2/4\pi)$ is,

$$\alpha_s\left(Q^2\right) = \frac{4\pi}{(11 - 2n_f/3)\ln\left(Q^2/\Lambda^2\right)}, \tag{1.8}$$

where Λ is the QCD scale. Its value is of the order of pion mass. n_f is the number of flavors. Since $n_f = 6$, QCD coupling decreases with the increasing momentum transfer Q^2. So at high energy scale or at a scale where momentum transfer is large, the QCD coupling constant becomes very small, this gives rise to asymptotic freedom [32]. Asymptotic freedom of QCD is well tested in deep inelastic scattering (DIS) experiments. Due to asymptotic freedom perturbative QCD is an important analytic quantum field theory framework for high energy colliders. However in the low energy scales ≤ 200 MeV, strong coupling constant is large and the perturbative framework breaks down. A Large value of the strong coupling constant along with the fact that gluons have self interaction leads to quark confinement or infrared slavery. Because of the confinement, we do not see free quark as a physical observable. Quarks, antiquarks, and gluons are confined within hadrons. There are no isolated particles in nature with non-vanishing color charges.

As we have already mentioned, large numbers of experiments seem to indicate that quarks and gluons do not exist as an isolated state in nature and there is confinement of quarks and gluons in hadrons, which are color singlet objects. In particular, quarks are packaged in colorless packages of two (mesons) and three (baryons). Self-coupling of gluons allows the possibility of the existence of colorless bound states of gluons, known as glueballs, although none has been detected so far yet. If QCD is the correct theory of strongly interacting particles then quark confinement should be achieved

from the first principle calculation. Unfortunately, confinement is a low energy phenomenon where non-perturbative effects of QCD plays a dominant role and there is no rigorous theoretical framework available which can handle this problem. However, string inspired gauge-gravity duality framework, some effective models of low energy QCD, and first principle lattice QCD calculations have helped us to understand QCD in strong coupling regime. In this context, we will recapitulate one of the phenomenological QCD models which takes into account the notion of confinement.

1.2.2 Phenomenological Model of QCD: MIT Bag Model

Among different incarnations of extended models of hadrons, MIT Bag Model is one such phenomenological model of QCD which effectively incorporates both asymptotic freedom and color confinement [33, 34]. In this model, short length scale behavior of QCD i.e. small coupling constant limit is ensured by confining the motion of colored quarks and gluons as almost free particles within the spatial extent of colorless hadron (spherical bag) of radius R, where R is less than 1 fm. Thus the bag incorporates the physics of confinement while the freedom of the constituents inside reflect the spirit of asymptotic freedom.The quarks (light quarks u and d) are treated as massless particles inside the bag due to the small coupling constant (and small current mass of u and d quarks) within the bag and are infinitely massive outside the bag because of confining effects. According to the kinetic theory, the kinetic energy of the quarks gives rise to an internal pressure which is outwards and trying to inflate the bag. In this case to keep the quarks and gluons inside the bag, external bag pressure B was introduced. A balance between outward kinetic pressure and inward bag pressure stabilizes the hadron. The phenomenological quantity B is introduced to take into account the non-perturbative color confining effects of QCD. Interestingly this simple phenomenological model can accommodate glueballs by allowing gluonic fields confined inside the bag.

In this simple model, we can estimate the bag pressure by considering massless

free fermions confined inside a spherical cavity of radius R. The momentum space Dirac equation for a free massless fermion inside the extended region is,

$$\gamma.p\,\psi = 0, \tag{1.9}$$

where the Dirac γ matrices represented in Dirac representation are,

$$\gamma^0 = \begin{pmatrix} I & 0 \\ 0 & -I \end{pmatrix} \tag{1.10}$$

and

$$\gamma^i = \begin{pmatrix} 0 & \sigma^i \\ -\sigma^i & 0 \end{pmatrix}, \tag{1.11}$$

Where I is a 2×2 unit matrix and σ^i are the three Pauli matrices. We express the four component wave function ψ for the massless fermions as

$$\psi = \begin{pmatrix} \psi_+ \\ \psi_- \end{pmatrix}, \tag{1.12}$$

Dirac fermion ψ is a reducible representation of the Lorentz group for the massless case. ψ_+ and ψ_- are two irreducible representations of the Lorentz group also known as the Weyl spinors of opposite chiralities. Plugging the above into equation 1.9 we get

$$\begin{pmatrix} p^0 & -\vec{\sigma}.\vec{p} \\ +\vec{\sigma}.\vec{p} & -p^0 \end{pmatrix} \begin{pmatrix} \psi_+ \\ \psi_- \end{pmatrix} = 0. \tag{1.13}$$

It is important to note that in case of massless Dirac equation ψ_+ and ψ_- completely decouple from each other. This is the manifestation of chiral symmetry which is also a symmetry of QCD Lagrangian in the massless case (see section 2.5 for details). However, in the presence of mass term equations for ψ_+ and ψ_- are not decoupled. Mass term breaks chiral symmetry explicitly. Chiral fermions are very important

in nature, our standard model of particle physics is based on the gauge interactions involving chiral fermions.

On solving the above equations (see [34] for details) one gets the ground state solution as

$$\psi(\vec{r},t) = \begin{pmatrix} \psi_+(\vec{r},t) \\ \psi_-(\vec{r},t) \end{pmatrix} = \begin{pmatrix} \mathcal{N}\, e^{-ip^0 t}\, j_0\,(p^0 r)\, \chi_+ \\ \mathcal{N}\, e^{-ip^0 t}\, (\vec{\sigma}.\hat{r})\, j_1\,(p^0 r)\, \chi_+ \end{pmatrix}$$

where j_0 & j_1 are spherical Bessel functions, $\chi_\pm$ are two component Dirac spinors, and $\mathcal{N}$ is a normalization constant.

Now, the condition for quark confinement is that the normal component of the vector current $j^\mu = \bar{\psi}\gamma^\mu\psi$ must vanish at the surface ($r = R$). This leads to

$$j_0(p^0 R) = j_1(p^0 R). \tag{1.14}$$

Solution of the above equation is,

$$p^0 R = 2.04 \quad \text{or,} \quad \mathrm{p}^0 = \frac{2.04}{\mathrm{R}}. \tag{1.15}$$

One can also get the above result using uncertainty principle, i.e. the kinetic energy of a quark inside a bag is inversely proportional to the radius of the bag. The total energy of a system of N quarks confined to a bag of radius R is

$$E = \frac{2.04N}{R} + \frac{4}{3}\pi R^3 B, \tag{1.16}$$

where the last term originates from the bag pressure. We get the equilibrium radius by minimizing the above equation,

$$B^{\frac{1}{4}} = \left(\frac{2.04N}{4\pi}\right)^{\frac{1}{4}} \frac{1}{R}. \tag{1.17}$$

Using the above equation one can estimate the value of the bag constant. For $R = 0.8fm$ we get,

$$B^{\frac{1}{4}} = 206\text{MeV}. \tag{1.18}$$

However the value of $B^{\frac{1}{4}}$ is, model dependent and it ranges from 145 MeV to 235 MeV. For a more detailed treatment see [35].

In the bag model quarks are confined in the bag as long as the inward pressure is balanced by the outward pressure. If the kinetic pressure exceeds the inward bag pressure, the bag yields and the quarks become deconfined. In this case, we have not considered the presence of gluons when we estimated the bag pressure, but the picture will be similar to the present case. When the bag yields quarks and gluons become deconfined. We then have a new phase of matter containing quarks and gluons. The deconfined quarks and gluons soon reach a state of thermal equilibrium. This phase of deconfined partonic matter is known as Quark Gluon Plasma (QGP).

In nature two different kinds of QGP phases are possible. First is the high-temperature QGP phase and the other is the high baryon density QGP phase. Early universe had QGP phase which is characterized by high temperature and low baryon density or baryon chemical potential. The core of the compact astrophysical objects like neutron stars can have QGP phase which is characterized by high baryon density and low temperature phase of QCD. QCD phase transition is the only phase transition of the early universe which can be probed in laboratory experiment directly. Relativistic heavy ion collision experiments are designed to recreate the phase of the matter similar to the early universe during quark hadron phase transition. In the next section, we will discuss about QGP formation in heavy ion collisions and also QCD at finite temperature and density to understand the QGP phase transition and its phase diagram.

1.3 Heavy Ion Collision Experiments

As already mentioned, apart from the SU(3) color gauge symmetry, classical SU(3) Yung Mills theory has another important global symmetry known as chiral symmetry [36], [37]. This symmetry arises due to smallness of masses of up (u) and down (d) quarks (and to some level strange (s) quark) compared to the QCD scale ($\Lambda_{QCD} \sim 200$ MeV). Due to the chiral symmetry left chiral and right chiral quarks are decoupled from each other. According to the group theory, manifestation of a symmetry in a quantum mechanical system is the presence of group multiplets as physical states. However hadrons, which are the states of QCD, are specific parity states and we do not see any chiral partners of hadrons. The explanation of this is provided by assuming that the chiral symmetry is spontaneously broken in the low temperature hadronic phase where the quarks acquire constituent masses. Chiral symmetry is restored at high temperature. Due to the small masses of u, d, s quarks the chiral symmetry is not an exact symmetry rather it is an approximate symmetry and is explicitly broken by a small amount (softly broken). Lattice QCD results which are applicable for QCD at high temperature and low baryon chemical potential indicate that the deconfinement and chiral phase transition occurs approximately at the same temperature [38], [39], [40], [41]. To understand the phase transition dynamics of QCD, laboratory experiments are being carried out e.g. CERN (SPS, LHC) and at BNL (AGS, RHIC), for some time now. AGS and SPS were both fixed-target experiments which collided Au+Au at up to 11 GeV per nucleon beam energy (AGS) and Pb+Pb at up to 160 A GeV (SPS) respectively. Although these experiments were performed in 1980's with limited technological advances, the results showed the possible existence of a new hot and dense state of matter. In this relatively low energy regime the target and the projectile cannot pass through each other due to the strong coupling constant, giving rise to baryon rich matter in the reaction zone. Thus, these reactions provide a tool to study very highly excited baryon rich matter or baryon rich quark gluon plasma. This baryon rich matter closely resembles the state of the matter inside to the core of compact astrophysical objects like neutron

stars. But to understand QCD phase transition dynamics in the early universe we have to probe QCD at high temperature, hence we have to go beyond the AGS/SPS energy scales. At present, there are two ongoing high energy experiments, one is at RHIC (BNL) with centre of mass energy per nucleon pair up to $\sqrt{S_{NN}} = 200$ GeV and the other one is at LHC (CERN) with centre of mass energy $\sqrt{S_{NN}} = 2.76$ TeV and higher. Contrary to the earlier fixed target experiments these are collider experiments where two heavy ion beams collide at a very high center of mass energy. Because the QCD coupling constant is small at high energy scales the target and projectile nuclei almost pass through each other and the interaction region remains almost baryon free. At relativistic energies when the highly Lorentz contacted nuclei pass through each other, they deposit a large amount of energy at the center of the reaction zone to form secondary partons. These secondary partons redistribute energy within themselves due to enough rescatterings among them and produce a locally thermally equilibrated system which is expected to be in the QGP phase. Thus, the QGP state formed in RHIC and LHC at mid rapidity is almost baryon free with small baryon chemical potential. For a review on heavy ion collision experiments, see [42] .

1.4 QGP at finite temperature

A rigorous and systematic study of QGP at finite temperature demands a statistical description of Yang Mills theory. Using the formalism of finite temperature field theory one can in principle construct the partition function of the system [43]. Once the partition function is known one can compute thermodynamics quantities like energy density, pressure etc. However one can extract lots of information about QCD at high temperature by assuming QGP as a ideal gas of weakly interacting system of quarks and gluons [34].

Number of quarks having momentum between p and $p + dp$, in a volume V and temperature T can be written as,

$$dN_q = g_q\, V\, \frac{4\pi p^2 dp}{(2\pi)^3}\, \frac{1}{1 + e^{(E(p)-\mu_q)/T}}, \tag{1.19}$$

where we have used the Fermi-Dirac statistics for quarks. μ_q is the quark chemical potential, and g_q the quark degeneracy factor. Since quarks are colored spin half particles and also comes in different flavors $g_q = N_c N_s N_f$, where N_c, N_s, N_f are color, spin and flavour degrees of freedom. When $\mu_q = 0$ the number density of quarks is the same as that of antiquarks.

The energy of massless quarks ($E \simeq p$) is given by

$$E_q = \frac{g_q V}{2\pi^2} \int_0^\infty \frac{p^3\, dp}{1 + e^{p/T}}. \tag{1.20}$$

One can perform the above integration using the properties of the Gamma function and the Riemann zeta function. This yields

$$E_q = \frac{7}{8}\, g_q\, V \frac{\pi^2}{30}\, T^4. \tag{1.21}$$

It is known from statistical mechanics that for massless fermions and bosons the pressure P is related to the energy density $\rho = E/V$ as

$$P = \frac{1}{3}\, \rho\,. \tag{1.22}$$

This is nothing but the equation of state for massless relativistic matter. Thus, the pressure of the system of massless relativistic quarks is

$$P_q = \frac{7}{8}\, g_q\, \frac{\pi^2}{90}\, T^4, \tag{1.23}$$

Hence the total pressure exerted by quarks and antiquarks present in the system is

$$P_q \,+\, P_{\bar{q}} = \frac{7}{8}\, (\, g_q \,+\, g_{\bar{q}})\, \frac{\pi^2}{90}\, T^4, \tag{1.24}$$

where $g_{\bar{q}}$ is the degeneracy factor for antiquarks.

The number density of quarks and antiquarks is

$$\begin{aligned} n_q &= n_{\bar{q}} = \frac{g_q}{2\pi^2} \int_0^\infty \frac{p^2\, dp}{1 + e^{p/T}} \\ &= \frac{g_q}{2\pi^2}\, T^3\, \frac{3}{2}\, \zeta(3)\,, \end{aligned} \tag{1.25}$$

where $\zeta(3) = 1.20206$.

Similar procedure can be followed for weakly interacting system of gluons in a volume V and at temperature T. However in the case of gluons we have to use Bose Einstein statistics and correct degeneracy factor for colored massless bosonic field. The energy of such system is

$$E_g = \frac{g_g V}{2\pi^2} \int_0^\infty p^3\, dp \left\{ \frac{1}{e^{p/T} - 1} \right\}, \tag{1.26}$$

where g_q is the gluon degeneracy,

$$g_g = (\text{number of different gluons}, 8) \times (\text{number of polarization}, 2) = 16. \tag{1.27}$$

Hence, we get

$$E_g = g_g\, V \frac{\pi^2}{30}\, T^4. \tag{1.28}$$

Again, using $P = \frac{1}{3}\,\rho$, we get the pressure for the gluon gas as

$$P_g = g_g\, \frac{\pi^2}{90}\, T^4. \tag{1.29}$$

It is important to emphasize that the expressions for E_g and P_g are exactly the same as those for quarks apart from the factor $\frac{7}{8}$, which in the manifestation of Fermi-Dirac distribution.

The number density of gluons is

$$\begin{aligned} n_g &= \frac{g_g}{2\pi^2} \int_0^\infty \frac{p^2\, dp}{e^{p/T} - 1} \\ &= \frac{g_g}{2\pi^2}\, T^3\, \Gamma(3)\, \zeta(3) \simeq 1.202\, \frac{g_g}{\pi^2}\, T^3. \end{aligned} \tag{1.30}$$

The net energy density of a system of quarks and gluons at temperature T is,

$$\begin{aligned} \rho_{QGP} &= \rho_{q\bar{q}} + \rho_g \\ &= \left[\frac{7}{8} \left(g_q + g_{\bar{q}} \right) + g_g \right] \frac{\pi^2}{30}\, T^4, \end{aligned} \tag{1.31}$$

where $g_q = g_{\bar{q}} = N_C\, N_S\, N_F = 3 \times 2 \times 6$ and $g_g = 16$. So,

$$\rho_{QGP} = \left(\frac{7}{8} \times 72 + 16\right) \frac{\pi^2}{30}\, T^4 \tag{1.32}$$

There are two very important assumptions that we have taken in the above derivation. These are, very weakly interacting system of quarks and gluons and that the quarks are massless. However we know that in practical situation quarks are not masslees and the partonic system may not behave as ideal gas. In the ideal gas limit the above derivation is only valid for $T \gg m_{top} \simeq 170$ GeV. At a temperature of the order $T = 200$ GeV (QCD phase transition scale) we can take u and d quarks to be nearly massless. Hence,

$$g_{q+\bar{q}} = 2 \times 3 \times 2 \times 2 = 24, \tag{1.33}$$

and,

$$\begin{aligned} \rho_{QGP} &= \left(\frac{7}{8} \times 24 + 16\right) \frac{\pi^2}{30}\, T^4 \\ &= \frac{37\pi^2}{30}\, T^4. \end{aligned} \tag{1.34}$$

Using the above results of pressure of ideal gas of quarks and gluons and the stability condition of the bag model we can estimate the temperature when deconfinement happens.

By considering only u, d quarks we have,

$$P = \frac{37\pi^2}{30}\, T^4. \tag{1.35}$$

Hence the critical transition to QGP state is,

$$\frac{37\pi^2}{30}\, T_c^4 = B \tag{1.36}$$

$$\Rightarrow T_c = \left[\frac{90B}{37\pi^2}\right]^{\frac{1}{4}} \tag{1.37}$$

If we use the value of $B = (206)^4\text{Mev}^4$, then we get $T_c \sim 144$ MeV. Current estimates of T_c obtained from the lattice calculations is of the order of 154 MeV [44]. For $T = 200$ MeV, we get $\rho_{QGP} \simeq 2.5\,\text{GeV/fm}^3$, where we have used 1fm $= (200\text{MeV})^{-1}$. Therefore, if we are able to create a dense system of quarks and gluons in thermal equilibrium with an energy density greater than the above estimate then we can claim the possibility of QGP formation. Such a scenario is expected to be realized in relativistic heavy-ion collision experiments where central energy density well above 3 GeV/fm^3 can be achieved.

1.5 QGP at high baryon density

In this section we will discuss QGP at high baryon density using Bag model. In this case deconfining pressure develops inside the bag even at $T = 0$ due to high baryon density. Since in this case we are discussing high baryon density at $T = 0$ we can ignore the contribution of antiquarks and gluons to the deconfining pressure. This pressure originates because of the Fermi momentum of the quarks.

The number density of the quarks in a volume V and within a momentum interval p and $p + dp$ is,

$$\frac{g_q\,V}{(2\pi)^3}\,4\pi p^2 dp. \tag{1.38}$$

Because of the Fermi-Dirac distribution at $T = 0$ no states are populated having momentum larger than quark Fermi momentum μ_q. Hence, the total number of quarks is,

$$\begin{aligned} N_q &= \frac{g_q\,V}{(2\pi)^3}\int_0^{\mu_q} 4\pi p^2 dp \\ &= \frac{g_q\,V}{6\pi^2}\,\mu_q^3. \end{aligned} \tag{1.39}$$

The number density of quarks is

$$n_q = \frac{g_q}{6\pi^2}\,\mu_q^3. \tag{1.40}$$

The energy of the quark gas in a volume V is

$$\begin{aligned} E_q &= \frac{g_q V}{(2\pi)^3} \int_0^{\mu_q} 4\pi p^3 dp \\ &= \frac{g_q V}{8\pi^2}\, \mu_q^4. \end{aligned} \tag{1.41}$$

Therefore the energy density is

$$\rho_q = \frac{g_q}{8\pi^2}\, \mu_q^4. \tag{1.42}$$

Again, because of the relativistic equation of state, we have

$$P_q = \frac{1}{3}\, \rho = \frac{g_q}{24\pi^2}\, \mu_q^4. \tag{1.43}$$

Once we have the expression for pressure of the system, now we can estimate the critical value of chemical potential when bag undergoes a transition to QGP state.

$$P_q = B = \frac{g_q}{24\pi^2}\, \mu_q^4, \tag{1.44}$$

leading to

$$\mu_c = \left[\frac{24\,\pi^2 B}{g_q}\right]^{\frac{1}{4}}. \tag{1.45}$$

corresponding value of critical number density quarks is,

$$n_q^{critical} = 4\, \left(\frac{g_q}{24\,\pi^2}\right)^{\frac{1}{4}}\, B^{\frac{3}{4}}, \tag{1.46}$$

and the critical baryon density is

$$n_B^{critical} = \frac{4}{3}\, \left(\frac{g_q}{24\,\pi^2}\right)^{\frac{1}{4}}\, B^{\frac{3}{4}}. \tag{1.47}$$

Considering only the u and d flavors , $g_q = 3 \times 2 \times 2 = 12$ for 3 colors, 2 spins and 2 flavors. Using $B^{\frac{1}{4}} = 206\ MeV$ we get $\mu_c = 434\ MeV$ and the corresponding critical baryon number density is $n_c = 0.72/fm^3$. In comparison the nucleon saturation density in normal nuclear matter in equilibrium is $n_B = 0.16/fm^3$. So the critical baryon density is about 5 times the normal nuclear matter density. This high baryon density is still not accessible in laboratory experiments. However the core of compact astrophysical objects can have deconfined QCD phase. In real situation system will be at finite temperature and finite chemical potential. In this case the critical value of temperature and baryon chemical potential will be in between the values for the two extreme cases we have discussed.

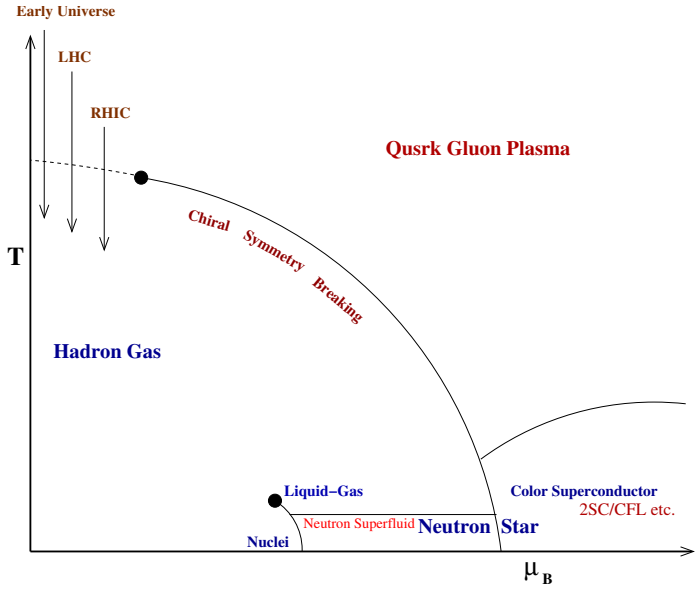

Figure 1.6: QCD phase diagram [45].

1.6 QCD Phase Diagram

In this section, we will briefly discuss our current understanding of the QCD phases. QCD phase diagram as a function of temperature (T) and baryon chemical potential is shown in figure 1.6. Somewhat concrete statements can be made only in the case of finite temperature with a small baryon chemical potential ($\mu_B << T$) and at an asymptotically high baryon chemical potential ($\mu_B >> \Lambda_{QCD}$). This is possible because at finite temperature and low baryon chemical potential lattice QCD calculations, which include non perturbative effects, are predictive and reliable. On the other side for very large chemical potential perturbative QCD is reliable because of asymptotic freedom at large Fermi momentum. In the intermediate ranges of temperature and chemical potential effective models of QCD e.g. NJL, PNJL, PQM etc provide a relatively good description of strongly interacting matter.

The QCD phase transitions at finite temperature and very small chemical potential have been studied extensively in the lattice QCD simulations. However, the dynamics of the phase transition depends on the number of flavors, the mass of the

quarks etc. For three colors, in the pure gauge case (no dynamical fermions), Lattice calculations have shown that the confinement deconfinement transition is of first order with transition temperature $T_c = 270$ MeV [46]. However in the presence of dynamical fermions including realistic u, d, s quark masses confinement deconfinement transition is not a phase transition rather it is a smooth crossover [47, 48]. The crossover temperature is in the range 150-200 MeV.

Along the chemical potential axis and at very low temperature, phase structure of strongly interacting matter is very rich. As we move along the $T = 0$ axis we approach towards the nuclear matter for $\mu_B \sim 940$ MeV. Nuclear matter is separated from the hadronic gas by a first order phase transition line. This first order phase transition line ends at a second order critical point. For larger values of μ_B one expects to find neutron superfluidity. Neutron superfluidity is expected to exists in the interior of neutron stars. At a very large value of baryon chemical potential, one finds some exotic phases of QCD e.g. 2 flavor color superconducting phase, color-flavor locked phase, crystalline color superconducting phase etc. Symmetry breaking pattern in this regime is very complicated. In this case due to the possible attractive channel quark-quark condensate becomes the ground state of the system. This is the analogue of electron superconductivity in condensed matter systems. But QCD color superconductivity [49, 50] is more robust than the electron superconductivity because electron superconductivity is possible because of the relatively weak phonon interaction, but to achieve color superconductivity presence of background lattice is not required. The excitation energy of electron superconductivity is in the electron volt scale, but the characteristic scale of color superconductivity is in MeV scale. At relatively low baryon density with two flavors u and d, 2SC color superconductivity emerges, however, at very high μ_B including the strange quarks in the system it is possible to have color-flavor locked (CFL) phase (for details, see section 3.2.5). In the case of finite chemical potential effective QCD models predicts that the confinement deconfinement transition is of first order. This first order phase transition line, separating nuclear matter and quark matter, ends at a critical point. Finding the exact position of this critical point in $(T - \mu_B)$ plane is one of the main goals of RHIC

beam energy scan program [51]. The core of the neutron star is likely to contain these exotic high μ_B phases. Future experiments on compressed baryonic matter at FAIR and NICA is expected to probe high μ_B region of QCD phase diagram.

With that we come to the end of the brief discussion on the topics which are important for this thesis. The rest of the thesis is organized as follows:

In chapter 2 QCD phase transition will be covered in details. This includes some simple toy models to demonstrate the physics of phase transition in field theory models, phase transitions in QCD and the effective potential etc. In chapter 3 we will discuss neutron star dynamics, pulsar glitches and anti-glitches. The concepts introduced in this chapter will be important for the chapter 4 and 5 , where we will discuss how QCD phase transition can affect the neutron star dynamics. In chapter 6 we will discuss the physics of inflation. In chapter 7 we will take a slight detour and will discuss a key ingredient of our work - the reaction diffusion equation. In the subsequent chapters we will discuss our work on the initial condition of inflation and how reaction diffusion dynamics can resolve the issue. In the end we will conclude the thesis.

Bibliography

[1] B. Rayden, "Introduction to Cosmology", (Cambridge University Press, 2017).

[2] E. Hubble, Proc.Natl. Acad. Sci. **15**, 168 (1929).

[3] D. Baumann, "Cosmology lecture notes", "www.damtp.cam.ac.uk/user/db275/Cosmology/Lectures.pdf".

[4] A.A. Penzias and R.W Wilson, Astrophys. J **142**, 419 (1965).

[5] R.H. Dicke, P.J.E.Peebles, P.G. Roll and D.T. Wilkinson, Astrophys. J **142**, 414 (1965).

[6] F. Zwicky, Helvetica Physica Acta 6, 110127 (1933), See also F. Zwicky, Astrophysical Journal **86**, 217 (1937).

[7] V. Rubin, K. Ford, Astrophys. J **159**, 379 (1970).

[8] S. Perlmutter et al., Bull.Am.Astron.Soc. **29**, 1351 (1997) (arXiv: astro-ph/9812473); S. Perlmutter, Physics Today, April,**53** (2003).

[9] E. Kolb and M. Turner," The Early Universe", (westview Press, 1994)

[10] For a review see, A. Vilenkin and E.P.S. Shellard," Cosmic strings and other topological defects", (Cambridge University Press, Cambridge, 1994).

[11] F.Halzen, A.D Martin," Quarks And Leptons" (John Wiley and Sons); D.Griffiths, " Introduction to Elementary Particles" (John Wiley and Sons), 1987; D.H.Perkins, " Introduction to High Energy Physics" (Addison-Wesley

Publishing Company), 1982; Fayyazuddin, Riazuddin, " A Modern Introduction to Particle Physics" (World Scientific, Singapore), 2000.

[12] P.W. Higgs, Phys. Lett. **12**, 132 (1964); Phys. Rev. L **13**, 508 (1964); Phys. Rev. **145**, 1156 (1966).

[13] M. Trodden, Rev. Mod. Phys. **71**, 1463, (1999).

[14] S. Dodelson, " Modern Cosmology" (academic Press, India, 2006).

[15] For a review see, S. Sarkar, Rept. Prog. Phys. **59**, 1493 (1996).

[16] G.Gamow, Phys. Rev. **70**, 572 (1946); R. A. Alpher, H. A. Bethe and G. Gamow, Phys. Rev. **73**, 803 (1948); G. Gamow, Phys. Rev. **74**, 505 (1948).

[17] R. A. Alpher and R. C. Herman, Rev. Mod. Phys. **22**, 153 (1950).

[18] J. C. Mather et al., Astrophys. J. 512, 511 (1999); G. F. Smoot, in " Proc. 3K Cosmology Conf., eds. A. Melchiorri et al. (1999)" (arXiv: astro-ph/9902027).

[19] P. J. E. Peebles and J. T. Yu, Astrophys. J. **162**, 815 (1970); R. A. Sunyaev and Ya. B. Zel'dovich, Astrophys. Space Sci.**7**, 20 (1970).

[20] J. C. Mather et al., Astrophys. J. **354**, 237 (1990).

[21] G. F. Smoot et al., Astrophys. J. **396**, L1 (1992).

[22] M. A. Malik, International Journal of Astronomy 2(2), 17-22 (2013).

[23] E. Komatsu, C. L. Bennett et al., Prog. Theor. Exp. Phys. **B 6**, 102 (2014) (arXiv:1404.5415).

[24] Planck collaboration, **A & A 594**, A13 (2016) (arXiv:1502.01589).

[25] see "https://dabrownstein.com/tag/cobe/"

[26] A. Riotto, arXiv:hep-ph/0210162.

[27] A. H. Guth, Phys. Rev. **D 23**, 347 (1981).

[28] A. D. Linde, Phys.Lett. **B 129**, 177-181 (1983).

[29] J. Martin, C. Ringeval and V. Vennin, arXiv:1303.3787.

[30] P. Pralavorio, arXiv:1311.1769.

[31] S. L. Glashow, H. Georgi. New York Times Magazine (26-09-1982), 1982.

[32] D. J. Gross and F. Wilczek, Phys. Rev. Lett.**30**, 1343 (1973); H. D. Politzer, Phys. Rev. Lett. **30**, 1346 (1973).

[33] A. Chodos, R. L. Jaffe, K. Johnson, C. B. Thorn and V. F. Weisskopf, Phys. Rev. **D 9**, 3471 (1974); T. Degrand, R. L. Jaffe, K. Johnson and J. E. Kiskis, Phys. Rev. **D 12**, 2060 (1975).

[34] C. Y. Wong, "Introduction to High-Energy Heavy Ion Collisions", (World Scientific, Singapore), 1994.

[35] F. E. Close, "Introduction to Quarks and Partons", (Academic Press, London), 1979.

[36] P. Finelli, "Chiral Symmetry lecture notes", "www.fisicanucleare.it/documents/chiral-symmetry-2012.pdf".

[37] T. Hatsuda and T. Kunihiro, Phys. Rept. **247**, 221 (1994); R. Rapp and J. Wambach, Adv. Nucl. Phys. **25**, 1 (2000).

[38] Y. Aoki, Z. Fodor, S.D. Katz and K.K. Szabo, Phys. Lett. **B 643**, 46 (2006) ; F. Karsch, Lect. Notes Phys. **583**, 209 (2002); F. Karsch, E. Laermann, hep-lat/0305025.

[39] J.B. Kogut et al., Phys. Rev. Lett. **50**, 393 (1983); M. Fukugita and A. Ukawa, Phys. Rev. Lett. **57**, 503 (1986); F. Karsch and E. Laermann, Phys. Rev. **D 50**, 6954 (1994); S. Aoki et al., Phys. Rev. **D 57**, 3910 (1998); C. Gattringer, P.E. Rakow, A. Schafer and W. Soldner, Phys. Rev. **D 66**, 054502 (2002).

[40] F. Karsch, E. Laermann and A. Peikert, Nucl. Phys.**B 605**, 579 (2001).

[41] C.R. Allton et al., Phys. Rev.**D 66**, 074507 (2002).

[42] J.W. Harris and B. Muller, Ann. Rev. Nucl. Part. Sci. **46**, 71 (1996), B. Muller and J.L. Nagle, Ann. Rev. Nucl. Part. Sci. **56**, 93 (2006).

[43] J. I. Kapusta, "Finite Temperature Field Theory", (Cambridge University Press, Cambridge, UK), 1989; A. Das, *Finite Temperature Field Theory*, (World Scientific, Singapore), 1997.

[44] H. T. Ding, F. Karsch and S. Mukherjee, Int. J. Mod. Phys.**E 24**, no.10, 1530007 (2015).

[45] K. Fukushima and T. Hatsuda, Rept. Prog. Phys. **74**, 014001 (20110 [arXiv:1005.4814[hep-ph]]

[46] M. Fukugita, M. Okawa and A. Ukawa, Nucl. Phys. **B 337**, 181(1990).

[47] Y. Aoki, G. Endrodi, Z. Fodor, S. D. Katz and K. K. Szabo, Nature **443**, 675 (2006) (arXiv: hep-lat/0611014)

[48] C. DeTar and U. M. Feller, Eur. Phys. J. **A 41**, 405 (2009) [hep-lat:0905.2949].

[49] M.G. Alford, A. Schmitt, K. Rajagopal and T. Schafer, Rev. Mod. Phys. **80**, 1455 (2008).

[50] K. Rajagopal and F.Wilczek, in Shifman, M. (ed.) : At the Frontier of Particle Physics, vol. 3, 2061-2151 [hep-ph/0011333].

[51] G. Odyniec, Journal of Physics: Conference Series **455**, 012037 (2013).

Chapter 2

QCD Phase Transitions

In this chapter, we will discuss QCD phase transitions. After a general introduction to first order and second order phase transition we will discuss the physics of false vacuum decay. This discussion will be important for subsequent chapters. After this we will introduce QCD phase transitions e.g. confinement-deconfinement phase transition and chiral phase transition. Towards the end of this chapter we will discuss the topological defects which generally appear in symmetry breaking transitions. Effects of these topological defect in the context of QCD phase transition will be important for this thesis.

2.1 Phase Transitions

Phase transitions which we encounter in day to day life are of great importance in every branch of physics, e.g. condensed matter systems, early universe as well as in particle physics. Melting of ice, boiling of water are common examples of phase transitions that we observe almost every day. The other examples of phase transitions are paramagnet to ferromagnet, normal conductor to superconductor, normal fluid to superfluid phase transitions etc.

A thermodynamic system can have different phases e.g. phases of water. A phase of a system in equilibrium is characterized by temperature, volume, pressure, chemical potential etc. A diagram drawn using any appropriately chosen parameters of a

system give us what is known as a phase diagram, e.g. phase diagram of water, where water can have distinct thermodynamics phases. We are familiar with the phase diagram of water as a two-dimensional plot in the pressure-temperature plane, however in general phase diagram can be multidimensional. If a given phase of a system is in equilibrium, then partition function is analytic as a function of these parameters over the relevant part of the phase diagram. Non-analyticity in the parameters of the phase diagram arises due to the presence of a phase boundary separating two different phases. According to the laws of thermodynamics, a dynamical system always tries to minimize its free energy or maximize its entropy and this can drive a system to pass over to a new phase across the phase boundary, leading to phase transition.

Often phase transitions are accompanied by a change in the symmetry properties of the system. From particle physics point of view phase transitions associated with spontaneous symmetry breaking are of great importance. In the early universe various types of symmetry breaking transition happened at different times during the evolution of the universe. The topological defects associated with these symmetry breaking phase transitions were earlier considered a possible candidate for structure formation. In such theories, the ground state does not share the original symmetry of the Hamiltonian and becomes degenerate after the phase transition. In the symmetric phase, the system has a unique ground state but when the symmetry breaks spontaneously, more than one degenerate ground states are available for the system and it has to choose one ground state out of many. For a dynamical system this choice of the vacuum is very important, as perturbative series is developed about a specific vacuum. Once a choice of vacuum is made the system no more remains invariant under the symmetry transformations pertaining to its original unique (symmetric) ground state. The symmetry of the system is therefore said to be broken spontaneously during the transition. The symmetric phase of a system is the disordered phase and the symmetry breaking transition makes it more ordered. But it needs to be emphasized that 'ordering' is not a necessary requirement for all transitions. For example, liquid-vapor transition does not involve any symmetry breaking or ordering since both phases are isotropic.

A suitable order parameter (OP) can be chosen to distinguish different thermodynamics phases. Typically it is zero in more symmetric disordered phase and it takes non zero value for less symmetric ordered phase. The unique values of the order parameter field which minimize the free energy in a particular phase constitute the order parameter space. During electroweak symmetry breaking $G \equiv SU(3)_c \times SU(2)_L \times U(1)_Y$ symmetry group spontaneously breaks down to $H \equiv SU(3)_c \times U(1)_{em}$ via Higgs mechanism. In this case vacuum expectation value of the Higgs field serves as the order parameter field and the vacuum manifold is given as G/H. It is important to note that the order parameter is symmetric under $H \equiv SU(3)_c \times U(1)_{em}$. This is a common feature of symmetry breaking transitions. It is also important to mention that a system can have different kinds of underlying symmetries, e.g. gauge symmetry, global symmetry, discrete symmetry or even space-time symmetries like supersymmetry. Thus the system can have more than one order parameter depending upon the symmetry and the corresponding symmetry breaking transitions can in principle be different from each other.

Order of the phase transition is defined in terms of the nature of the variation of the order parameter as a function of controlling parameters e.g. temperature. If the order parameter changes discontinuously with the control parameter then it is a first order phase transition; otherwise, it is second order or a continuous transition. An everyday example of first order phase transition is the transition between water and ice or water and vapor, where density serves as order parameter. Let us assume that T_c is the transition temperature. Because of the discontinuity, the state of the system at T_c depends on which side the critical temperature was approached from. For first order phase transition coexistence of the phases is possible at T_c. This is exactly what happens when we put ice into a glass of water. A first order transition occurs by nucleation of bubbles. Local fluctuations of the order parameter field drive certain regions of one phase to the other phase because of a lower free energy of the latter. Because of the local fluctuation or due to the presence of impurities bubbles of the phase having lower free energy nucleate in the background of the other

phase having relatively higher free energy. If the nucleated bubble size is larger than a critical size (where critical size is determined by the parameters of the system), then the supercritical bubbles expand, meet, and coalesce until the entire region gets converted to the phase having smaller free energy. Such moving interfaces of bubble walls lead to interesting physical effects. For example, Witten has shown that if the quark-hadron transition in the early universe was a first order transition then moving bubble walls can lead to concentration of baryon number and can lead to the formation of quark nuggets [1]. (Though, now lattice calculations have shown that it is a cross-over). An example of second order transition is para to ferromagnetic transition where magnetization (M) is the order parameter.

2.2 Toy Models

In this section, we will briefly study the dynamics of phase transition in quantum field theory system. Taking two simple Lagrangians [2] we will obtain the effective potential as a function of the order parameter. The behavior of the effective potential dictates the type of the phase transition. These toy models also offer us the opportunity to describe features of the phase transitions that make them relevant in cosmology. For detailed derivations and discussions see [3].

2.2.1 Second Order Phase Transition

To understand the second order phase transition let us consider the following simple real scalar field Lagrangian,

$$\mathcal{L} = \frac{1}{2}\partial_\mu\phi\partial^\mu\phi - V, \qquad V = \frac{\lambda}{4}\left(\phi^2 - v^2\right)^2, \tag{2.1}$$

where ϕ is the real scalar field, V is the potential, and λ, v are constants. $\phi \to -\phi$ is a global symmetry of the above Lagrangian. Vacuum expectation values of ϕ are $\pm v$. However, once the system chooses one of the vacuum states, $\phi \to -\phi$ symmetry is spontaneously broken.

The ground state of the system is determined by minimizing the potential, $\frac{\partial V}{\partial \phi} = 0$,

$$\lambda\left(\phi^3 - v^2\phi\right) = 0 \tag{2.2}$$

Equation 2.2 shows that apart from $\phi = 0$ there are other two non zero solutions, these are $\phi = \pm v$. Note that $\phi = 0$ is symmetric under $\phi \to -\phi$. However, $\phi = \pm v$ is not symmetric under $\phi \to -\phi$. That implies that the symmetry of the Lagrangian is broken by the choice of the vacuum. At a nonzero temperature (T), the value of ϕ fluctuates from point to point. If these thermal fluctuations are small, we can write the field as the sum of the homogeneous background contribution ϕ_0 and the fluctuation $\delta\phi$ on top of ϕ_0.

$$\phi(x) = \phi_0 + \delta\phi(x) \tag{2.3}$$

If we consider only gaussian, symmetric thermal fluctuations then we can eliminate those terms which are averages over odd powers of $\delta\phi$. Using equation 2.2 and averaging over the gaussian fluctuations and eliminating terms averages of odd powers of $\delta\phi$ gives:

$$\lambda\left(\phi_0^3 + 3\langle\delta\phi^2\rangle\phi_0 - v^2\phi_0\right) = 0 \tag{2.4}$$

Once we quantize these scalar field fluctuations $\delta\phi$ interms of creation and annihilation operators, then the thermal vacuum expectation value of $\delta\phi^2$ can be given as [4]:

$$\langle\delta\phi^2\rangle = \int \frac{d^3\mathbf{p}}{(2\pi)^3}\frac{1}{\omega}\frac{1}{e^{\beta\omega} - 1}, \tag{2.5}$$

where $\beta = 1/T$, $\omega = \sqrt{\mathbf{p}^2 + m^2}$. Equation 2.5 does not include the zero point energy term. This term can be absorbed during renormalization of the coupling constant of the theory. Equation 2.5 can be solved in high temperature limit. For the details

of this derivation see [3] and references therein. In conclusion, the leading thermal contribution to $\langle \delta\phi^2 \rangle$ is:

$$\langle \delta\phi^2 \rangle \simeq \frac{T^2}{12} - \frac{mT}{4\pi}. \tag{2.6}$$

After substituting the value of $\langle \delta\phi^2 \rangle$ from equation 2.6 into the equation 2.4 and using a crude approximation by neglecting $\mathcal{O}(T)$ term with respect to $\mathcal{O}(T^2)$ term, we get:

$$\lambda \left(\phi_0^2 + \frac{T^2}{4} - v^2 \right) \phi_0 = 0. \tag{2.7}$$

Effective potential which describes the variation of ϕ_0 as a function of temperature can be obtained by integrating equation 2.7. Hence we get,

$$V_{eff}(\phi_0) = \lambda \left[\frac{\phi_0^4}{4} + \frac{\phi_0^2}{2} \left(\frac{T^2}{4} - v^2 \right) \right]. \tag{2.8}$$

Once we have the effective potential of ϕ_0, we can understand the evolution of ϕ_0 as a function of temperature. Note that ϕ_0 is the vacuum expectation value of the field ϕ and it can also be treated as the order parameter of the theory. From equation 2.7 we can obtain the critical temperature of the system $T_c = 2v$. If $T > T_c$ then from equation 2.7 we can see that $\phi_0 = 0$ is the only solution, however for $T < T_c$ equation 2.7 has two nonzero solutions. This implies that as the temperature decreases from a higher value to a lower value through T_c, we have a phase transition at T_c. For completeness, we have shown the effective potential and its temperature variations in the figure 2.1 . For this simple model, we found that the symmetry of the Lagrangian is broken by the ground state below T_c, where ϕ_0 has nonzero value and the symmetry is restored at a temperature greater than T_c. In the symmetry restored phase $\phi_0 = 0$. As soon as the temperature drops below T_c, $\phi_0 \neq 0$ vacuum becomes energetically favorable for the system and the phase transition takes place. In this type of phase transition, the order parameter ϕ_0 changes continuously. The above

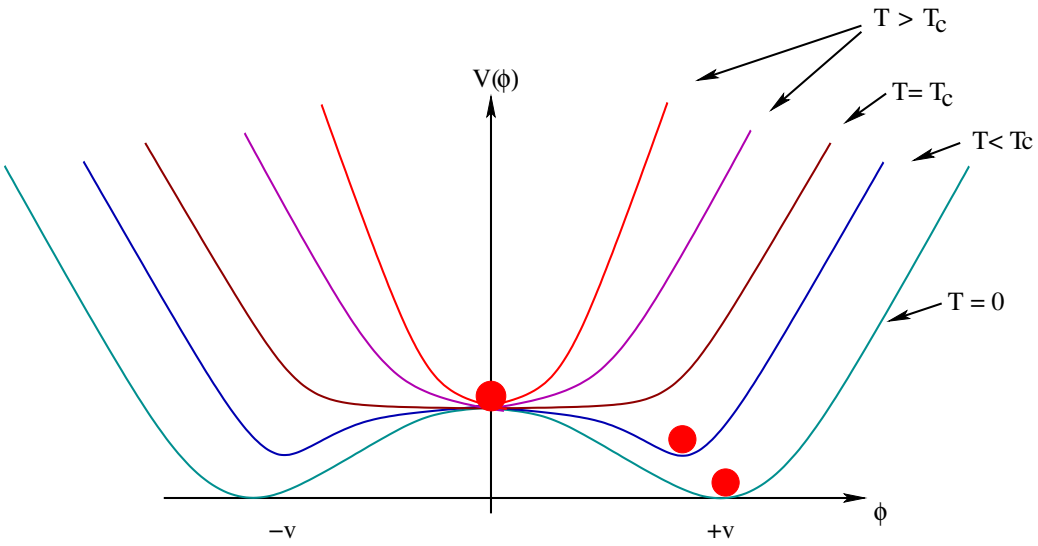

Figure 2.1: Toy model potential for a real scalar field with two degenerate local minima used to illustrate a second order phase transition.

.

mentioned features are the characteristics of second order phase transition. Although in this case, we have obtained second order phase transition in a simple toy model but the conclusions which we have derived in this simple model will be applicable to realistic more complicated cases, e.g. QCD phase transition etc.

2.2.2 First Order Phase Transition

Let us consider a more complicated Lagrangian which can give rise to a first order phase transition [2].

$$\mathcal{L} = D_\mu \phi^* D^\mu \phi - \frac{\lambda}{4}\left(\phi^*\phi - v^2\right)^2 - \frac{1}{4}F_{\mu\nu}F^{\mu\nu}, \tag{2.9}$$

where ϕ is a complex scalar field. The above Lagrangian can be obtained by imposing local $U(1)$ gauge symmetry in the complex scalar field Lagrangian 2.1 . Lagrangian given in equation 2.9 also can be taken as the Lagrangian of the scalar QED [5]. The covariant derivative is defined as $D_\mu = \partial_\mu + igA_\mu$ and the gauge invariant field strength tensor of the $U(1)$ gauge field is $F_{\mu\nu} = \partial_\mu A_\nu - \partial_\nu A_\mu$. Under

local $U(1)$ gauge transformation the complex scalar field changes as,

$$\phi \to e^{i\theta(x)}\phi, \tag{2.10}$$

corresponding transformation of the $U(1)$ gauge field is,

$$A_\mu \to A_\mu - \frac{1}{g}\partial_\mu\theta. \tag{2.11}$$

Following the earlier procedure of decomposing the scalar field into a homogeneous background part and a thermal fluctuation on top of it, we can also decompose the complex scalar field. Since in this case there is a $U(1)$ symmetry associated with the Lagrangian we can split the complex scalar field in the following way,

$$\phi_1 = \phi_0 + \delta\phi_1, \qquad \phi_2 = \delta\phi_2. \tag{2.12}$$

Minimizing the potential with respect to ϕ_1 gives the ground state of the system (including the terms coming from the $D_\mu\phi^* D^\mu\phi$),

$$\lambda\left(\phi_1^2 + \phi_2^2 - v^2\right)\phi_1 + g^2A^2\phi_1 = 0. \tag{2.13}$$

After using the values of ϕ_1 and ϕ_2 from equation 2.12, taking average of gaussian symmetric fluctuations and dropping the terms having odd powers of $\delta\phi_1$ and $\delta\phi_2$, we get,

$$\lambda\left[\phi_0^2 + 3\langle\delta\phi_1^2\rangle + \langle\delta\phi_2^2\rangle + \frac{g^2}{\lambda}\langle A_\mu A^\mu\rangle - v^2\right]\phi_0 = 0 \tag{2.14}$$

Note that once we decompose the scalar field with respect to the homogeneous background, gauge field A_μ picks up an effective mass term because of the interaction term between the scalar field and the gauge field in the covariant kinetic term. The presence of ϕ_0 gives it a mass $m_\gamma^2 = g^2\phi_0^2$. Unlike the massless gauge field which

has only two transverse degrees of freedom, a massive gauge field has an additional longitudinal degree of freedom. Because of the three degrees of freedom it has three times the thermal contribution of the scalar boson field $\delta\phi$ from equation 2.6:

$$\langle A_\mu A^\mu \rangle \simeq \frac{T^2}{4} - \frac{3m_\gamma T}{4\pi}. \tag{2.15}$$

Plugging the expressions of $\delta\phi_{1,2}$ fields to the leading order in T (equation 2.6) and the expression of $\langle A_\mu A^\mu \rangle$ from equation 2.15, in equation 2.14 we obtain,

$$\lambda \left[\phi_0^2 - \frac{3g^3 T \phi_0}{4\pi\lambda} + \left(\frac{1}{3} + \frac{g^2}{4\lambda} \right) T^2 - v^2 \right] \phi_0 = 0. \tag{2.16}$$

Integrating equation 2.16 we find the effective potential of ϕ_0:

$$V_{eff}(\phi_0) = \frac{1}{2} \left[\left(\frac{\lambda}{3} + \frac{g^2}{4} \right) T^2 - \lambda v^2 \right] \phi_0^2 - \frac{g^3 T}{4\pi} \phi_0^3 + \frac{\lambda}{4} \phi_0^4 \tag{2.17}$$

From equation 2.17 we can understand the behavior of ϕ_1 as a function of temperature. Its behavior is shown in the following figure 2.2. Unlike the effective potential for the second order phase transition, in case of first order phase transition, the effective potential has a ϕ^3 term. This cubic term gives rise to a local maxima. As the temperature drops, a local maxima develops as a potential barrier which keeps the field trapped near the origin. At the critical temperature, all the three minima of the potential become degenerate. As the temperature drops below critical temperature minima corresponding to $\phi \neq 0$ becomes energetically more favourable than the minimum corresponding to $\phi = 0$. However, because of the potential barrier, field remains trapped in the false vacuum (vacuum corresponding to $\phi = 0$). Classically the field cannot roll down to the true vacuum (vacuum corresponding to $\phi \neq 0$), however, quantum mechanically field can tunnel through the barrier. But this tunneling probability is small. As the temperature drops below the nucleation temperature T_n, the potential barrier becomes smaller and the probability for the field to tunnel to the true vacuum becomes larger in the presence of fluctuations. Eventually, the field rolls

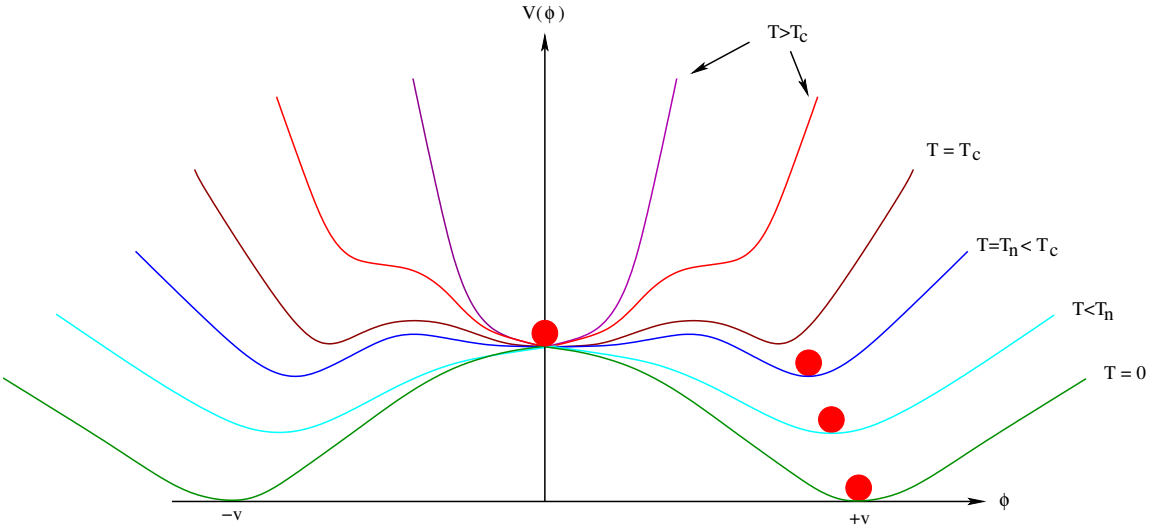

Figure 2.2: Toy model potential for a real scalar field with two degenerate local minima used to illustrate a first order transition phase transition. It is clear from the figure that at transition temperature degenerate vacua exist. These vacua are separated by a potential barrier. For $T < T_c$, $\phi = 0$ is the metastable vacuum.

down to the true minimum and completes the phase transition. (This simple picture of only using ϕ_1 was used as illustration of the dynamics of a first order transition. ϕ in equation 2.9 is complex, hence full effective potential will be in terms of a complex field with degenerate vacuum being $U(1)$ symmetric.)

2.3 False Vacuum Decay

In the section 2.2.2 we have elaborately discussed how cubic term in scalar field can give rise to first order phase transition. However in this toy model we have used finite temperature corrections to construct the effctive potential. But in general ϕ^3 term can arise in a scalar field Lagrangian without finite temperature corrections, e.g. the following potential of a real scalar field can give rise to first order phase transition,

$$V(\phi) = \frac{\lambda}{2}\phi^2(\phi - \phi_0)^2 - \lambda\epsilon_0\phi_0\phi^3. \tag{2.18}$$

The potential is shown in the figure 2.3. Here the metastable vacuum is at $\phi = 0$

and the true vacuum appears at,

$$\phi = \sigma = \phi_0 \left[\frac{3(1+\epsilon_0) + \sqrt{(3(1+\epsilon_0))^2 - 8}}{4} \right]. \tag{2.19}$$

As pointed out earlier ϕ^3 term in the potential gives rise to a potential barrier between metastable and true vacuum. Note that, as $\epsilon_0 \to 0$, the global minimum σ approaches ϕ_0 and the vacuum at $\phi = 0$ and $\phi = \sigma$ becomes degenerate. In the case of a first order phase transition, the field ϕ evolves from the metastable vacuum $\phi = 0$ (false vacuum) to $\phi = \sigma$ (true vacuum). Transition to the true vacuum state by quantum tunneling occurs through the nucleation of bubbles of the energetically favored phase $\phi = \sigma$, which then expand outward nearly at the speed of light. The semiclassical theory of quantum tunneling at zero temperature was given in [6] and the finite temperature extension of this theory was proposed by Linde [7]. We will discuss below semi-classical theory of false vacuum decay given by Coleman (for details see, [8–10]). As we will see, the tunneling solution will require consideration of a particle moving in potential $-V(\phi)$. For the later purpose we also show, in Fig. 2.4 the inverted potential $-V(\phi)$.

False vacuum decay at zero temperature is a problem of quantum tunneling from one vacuum state to the other. To illustrate the physics of the tunneling, we will first consider a particle mechanics problem where a particle of mass m is moving in potential $V(x)$ in 1D, with the Lagrangian,

$$\mathcal{L} = \frac{1}{2} m \dot{x}^2 - V(x). \tag{2.20}$$

In general transition amplitude from a state $|x_i, t_i\rangle$ to a state $|x_f, t_f\rangle$ is given as,

$$\langle x_f, t_f | x_i, t_i \rangle = N \int \mathcal{D}x \, e^{\frac{i}{\hbar} S[x]}, \tag{2.21}$$

where $S[x]$ is the action of the system. It is important to note that in Minkowski space this integral is oscillatory. However, in such a case we can rotate to Euclidean space (imaginary time) to make the integral well behaved. This point will be clear in the subsequent discussions. One can continue to use real time description keeping in

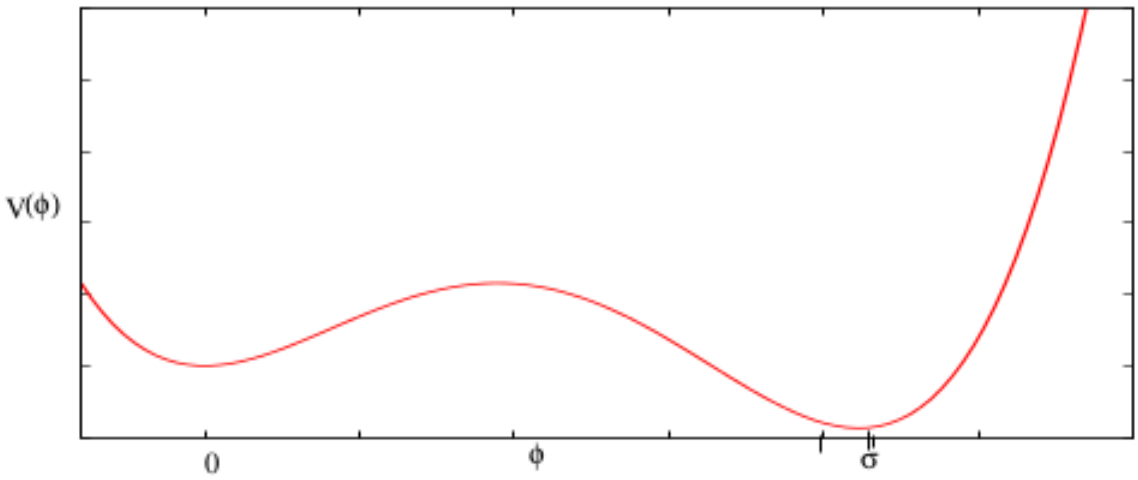

Figure 2.3: Potential for a first order phase transition [10].

mind the fact that the actual calculations are done in Euclidean space and the results are rotated back to Minkowski space.

In path integral formalism, we can expand the action around the classical trajectory (path which satisfy classical equation of motion),

$$x(t) = x_{cl}(t) + \eta(t), \tag{2.22}$$

where classical trajectory x_{cl} satisfies,

$$\left(\frac{\delta S[x]}{\delta x(t)}\right)_{x=x_{cl}} = 0. \tag{2.23}$$

Then, we have

$$\begin{aligned} S[x] &= S[x_{cl} + \eta] \\ &= S[x_{cl}] + \frac{1}{2}\int\int dt_1 dt_2 \eta(t_1) \frac{\delta^2 S[x_{cl}]}{\delta x_{cl}(t_1)\delta x_{cl}(t_2)} \eta(t_2) + \mathcal{O}(\eta^3). \end{aligned} \tag{2.24}$$

Substituting the expression of $S[x]$ back into the equation 2.21 , one can show that,

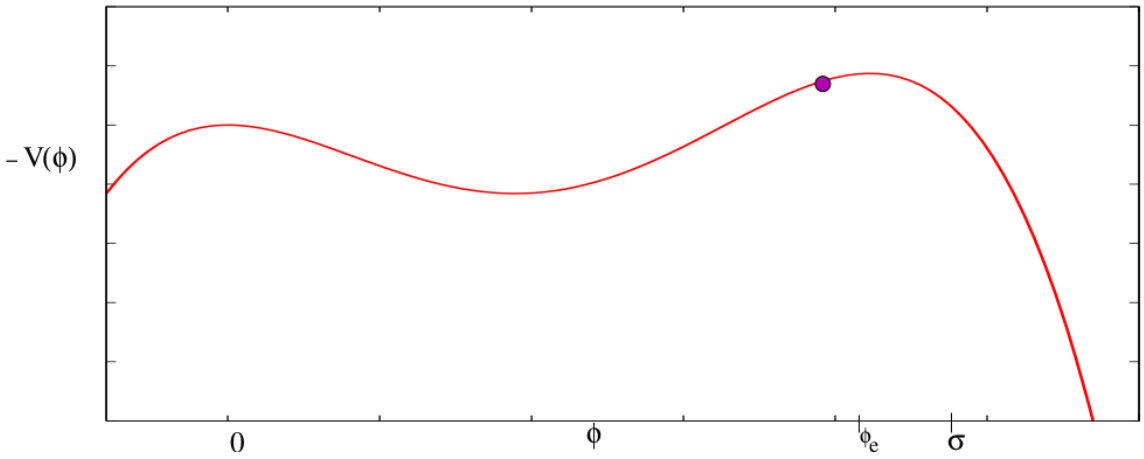

Figure 2.4: Inverted potential in Minkowski space [10].

$$\begin{aligned}\langle x_f, t_f | x_i, t_i \rangle &= N \int \mathcal{D}\eta e^{\frac{i}{\hbar}\left(S[x_{cl}]+\frac{1}{2}\int\int dt_1 dt_2 \eta(t_1)\frac{\delta^2 S[x_{cl}]}{\delta x_{cl}(t_1)\delta x_{cl}(t_2)}\eta(t_2)+\mathcal{O}(\eta^3)\right)} \\ &\simeq N e^{\frac{i}{\hbar}S[x_{cl}]} \int \mathcal{D}\eta e^{\frac{i}{2\hbar}\int\int dt_1 dt_2 \eta(t_1)\frac{\delta^2 S[x_{cl}]}{\delta x_{cl}(t_1)\delta x_{cl}(t_2)}\eta(t_2)} \\ &= \frac{N}{\sqrt{\det\left(\frac{1}{\hbar}\frac{\delta^2 S[x_{cl}]}{\delta x_{cl}(t_1)\delta x_{cl}(t_2)}\right)}} e^{\frac{i}{\hbar}S[x_{cl}]}. \end{aligned} \tag{2.25}$$

It is important to note that the above derivation breaks down if,

$$\det \frac{\delta^2 S[x_{cl}]}{\delta x_{cl}(t_1)\delta x_{cl}(t_2)} = 0, \tag{2.26}$$

normally this happens when there is some underlying symmetry of the system. This determinant is also known as determinant of fluctuations and in general it is very difficult to calculate. There are only some systems e.g., double well potential, where one can get the closed form exact expression of this determinant. However, in general case one can use dimensional arguments to estimate this factor.

As already discussed, how a particle evolves from one position to another can be expressed as the transition amplitude for a particle that starts at x_i at $t_0/2$ to ends at x_f at $t_0/2$ as,

$$\langle x_f|e^{-iHt_0}|x_i\rangle = N\int \mathcal{D}x\, e^{\frac{i}{\hbar}S[x]}. \tag{2.27}$$

we can set $\hbar = 1$ as we are working in natural units. The left hand side of the equation 2.27 can be expanded in energy eigenstates,

$$H|n\rangle = E_n|n\rangle, \tag{2.28}$$

which implies,

$$\langle x_f|e^{-iHt_0}|x_i\rangle = \sum_n e^{-iE_nt_0}\langle x_f|n\rangle\langle n|x_i\rangle. \tag{2.29}$$

We have already said that path integral as given in equation 2.27 is oscillatory. To make this integral well behaved we have to go to Euclidean space, where the time t is rotated to the complex axis $t \to -i\tau$. In the $\tau_0 \to \infty$ limit all the states with energy higher than E_0 are exponentially suppressed in comparison to the term involving $|0\rangle$. This gives us,

$$e^{-E_0\tau_0}\langle x_f|0\rangle\langle 0|x_i\rangle \equiv e^{-E_0\tau_0}\psi_0(x_f)\psi_0^*(x_i), \tag{2.30}$$

where ψ_0 is the ground state wave function at position x. The action on the right hand side of equation 2.27 under the Wick rotation takes the form,

$$iS[x(t)] \to -S_E = \int_{-\tau_0/2}^{\tau_0/2}\left(-\frac{1}{2}\left(\frac{dx}{d\tau}\right)^2 - V(x)\right)d\tau, \tag{2.31}$$

where S_E is the Euclidean action. Therefore the equation 2.27 becomes,

$$\langle x_f|e^{-iHt_0}|x_i\rangle = N\int \mathcal{D}x\, e^{-S_E}. \tag{2.32}$$

The techniques that we have already discussed to get the equation 2.25 can also be used in this case to get the closed form expression for the transition amplitude,

$$\langle x_f|e^{-iHt_0}|x_i\rangle \propto Ne^{-S_E}, \tag{2.33}$$

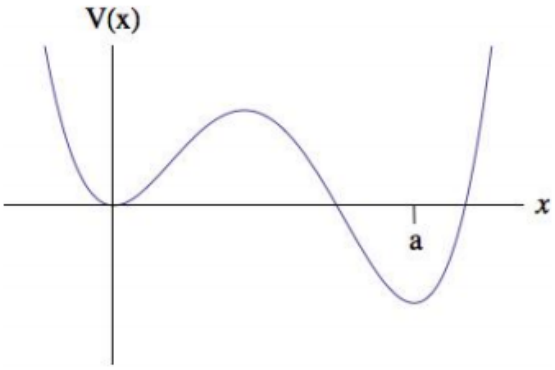

Figure 2.5: Double well potential with unstable vacuum [10].

where leading contribution to S_E comes from classical trajectory and the proportionality includes determinant of fluctuations.

Let us consider a potential of the form in figure 2.5 . It has a false vacuum at $x = 0$ and a true minima at $x = a$. In the classical case, if a particle is trapped at $x = 0$ then the escape is impossible, apart from external effects (such as thermal excitations). In the quantum case, however, the phenomena of tunneling will eventually cause the particle to escape and evolve to the true minimum. The probability of this occurring is given by the width of the state, which is in turn given by the complex component of the energy. This can be understood in the following way, The probability of remaining in a state at time t is,

$$|\psi(t)|^2 = |U(t)\psi(0)|^2 = |e^{-iEt}\psi(0)|^2 = e^{-\Gamma t}, \tag{2.34}$$

where $\Gamma = -2\mathrm{Im}(E)$ is the width of the state and in these units its inverse is the lifetime [10] . By considering the determinant of fluctuations about the instanton solution (which mediates the tunneling), one can show that for this double well potential the width of the state is,

$$\Gamma = -2\mathrm{Im}E_0 = \left(\frac{S_E}{2\pi}\right)^{1/2} e^{-S_E} \left|\frac{\det'[-\Box_E + V''(\phi)]}{\det[-\Box_E + V''(0)]}\right|^{-1/2}, \tag{2.35}$$

where '$\prime$' indicates that zero modes of the operator are to be omitted when computing

the determinant. This is important as we have discussed that zero modes in the determinant of fluctuations arise due to the symmetry of the system. In this case the system has one dimensional translation symmetry in time direction (this is separately integrated in terms of the position of the instanton in the time direction). So the zero mode corresponding to that has to be removed. Another important feature of the above equation in the prefactor $\left(\frac{S_E}{2\pi}\right)^{1/2}$. This term comes because of the symmetry of the system. In a (3+1) dimensional field theory system, which we will discuss later, has four translational symmetries. Hence there will be four such factors of $\left(\frac{S_E}{2\pi}\right)^{1/2}$.

Now let us consider the field theory systems. Similar to the quantum mechanical system, the rate of the false vacuum decay is given by [9] ,

$$\Gamma = A\, e^{-S_E(\phi)}, \tag{2.36}$$

where ϕ is a solution of the Euclidean field equation which extremises the Euclidean action S_E given by,

$$S_E(\phi) = \int d^3x dt_E \left[\frac{1}{2}\left(\frac{d\phi}{dt_E}\right)^2 + \frac{1}{2}(\vec{\nabla}\phi)^2 + V(\phi)\right], \tag{2.37}$$

where, $V(\phi)$ is given in equation 2.18 and,

$$A = \left(\frac{S_E}{2\pi}\right)^2 \left|\frac{\det'[-\Box_E + V''(\phi)]}{\det[-\Box_E + V''(0)]}\right|^{-1/2}. \tag{2.38}$$

At zero temperature, the least action Euclidean solution has $O(4)$ symmetry. In this case ϕ is only a function of r, where $r^2 = |\vec{x}|^2 + t_E^2$. The $O(4)$ Euclidean equation of motion for $\phi(r)$ is given by,

$$\frac{d^2\phi}{dr^2} + \frac{3}{r}\frac{d\phi}{dr} - V'(\phi) = 0, \tag{2.39}$$

and the Euclidean action in terms of r can be expressed as,

$$S_E = 2\pi^2 \int_0^\infty r^3 dr \left[\frac{1}{2}\left(\frac{d\phi}{dr}\right)^2 + V(\phi)\right]. \tag{2.40}$$

The boundary conditions for the $O(4)$ solution are $\phi = 0$ at $r = \infty$ and $\frac{d\phi}{dr} = 0$ at $r = 0$. The value of ϕ at $r = 0$ is decided by the two boundary conditions. Starting with $\phi = \phi_e$ and $\frac{d\phi}{dr} = 0$ at $t_E = 0$, ϕ will evolve to $\phi = 0$ at $t_E = \infty$. Here ϕ_e is somewhere in between $\phi = 0$ and $\phi = \sigma$. The technique to find ϕ_e can be illustrated with the negative of the potential $V(\phi)$ as shown in the figure 2.4 . If we interpret ϕ to be the "position" of a particle of unit mass and r to be the "time" variable, then equation 2.39 describes the classical motion of a particle under the influence of the inverted potential $-V(\phi)$ with a velocity dependent "friction" force. If ϕ starts at rest from a specific point, the escape point ϕ_e , it will have just enough energy to overcome the friction force and come to rest at $\phi = 0$. If ϕ is released at rest from the left of the escape point ϕ_e , it will undershoot the desired final configuration. That is, after some finite r, ϕ will come to rest and then reverse direction at some point before reaching $\phi = 0$. If ϕ is released at rest from the right of the escape point ϕ_e , it will overshoot the point $\phi = 0$ and go to negative ϕ. The escape point ϕ_e can thus be identified by trial, and this is the solution for $\phi(r)$ for the bubble profile. Then we can calculate Euclidean action for this solution.

In general analytic solution of equation 2.39 is not available. However, in thin wall approximation it is possible to find a simple approximate analytic expression for S_E. In thin wall approximation, the difference in energy between the metastable and true vacua is small compared to the height of the barrier. In the thin wall limit ($\epsilon_0 \to 0$), the minima are nearly degenerate. In order to overcome the friction term, ϕ_e must be very close to σ. The form of the solution can be understood by again using the particle analogy. For $\epsilon_0 << 1$, the particle sits near $\phi = \sigma$ or a very long time (i.e up to a large value of r) making the dissipation term ineffective. Then at some large value of r, say $r \sim R$, the particle rapidly makes the transition across the 'dip' in $-V(\phi)$, and finally slowly comes to rest at $\phi = 0$. Here $\phi(r)$ corresponds to the bubble profile and R is the bubble radius. In thin wall approximation, the Euclidean action for $O(4)$ symmetric instanton can be shown to be [8],

$$S_E(\phi) = 2\pi^2 R^3 S_1 - \pi^2 \frac{R^4}{2}\epsilon, \tag{2.41}$$

where $\epsilon = V(\phi_0) = \frac{-\epsilon_0 \lambda \phi_0^4}{2}$, S_1 is the action of one dimensional instanton. We can determine radius R by extremising Euclidean action $\frac{dS_E}{dR} = 0$. From this we find critical radius $R_c = \frac{3S_1}{\epsilon}$. In the thin wall limit, bubble radius is much larger than the wall thickness. The extremum action in this limit becomes $S_E = \frac{27\pi^2 S_1^4}{2\epsilon^3}$. Once we have the estimates of the Euclidean action we can calculate the rate of false vacuum decay provided we also know the determinant of fluctuations. We have already mentioned that the exact calculations of the determinant of fluctuations is very difficult. However one can use dimensional arguments to estimate this factor. At finite temperature one can replace this factor by T^4 for rough estimate. In this thesis we have considered only zero temperature quantum tunneling. In this case determinant of fluctuations can be estimated as R_c^{-4}.

After this general discussion of phase transition and simple illustration of phase transition dynamics in quantum field theory systems using simple toy models, we will now focus on QCD phase transitions. The QCD confinement deconfinement transition takes place in the early universe when the temperature of the universe was ~ 100 MeV. It is the only particle physics transition of the early universe that can be studied experimentally. However, the transition cannot be fully understood within the framework of perturbative quantum field theory. QCD phase transition can be characterized in two different ways. It can be viewed as a transition from a deconfined phase to a confined phase as well as a spontaneous breaking of the chiral symmetry. In the next sections we will discuss the confinement deconfinement transition and after that, we will discuss the chiral symmetry breaking.

2.4 Confinement Deconfinement Phase Transition

In this section, we will briefly discuss confinement-deconfinement phase transition. We follow [11] to construct the order parameter for the phase transition which is

known as Polyakov loop. We will write the effective potential for the order parameter and we will also discuss the symmetry properties of Polyakov loop. In the present case, we will consider pure QCD with no dynamical quarks are in the picture.

2.4.1 Polyakov Loop Order Parameter

Consider $SU(N)$ gauge theory at finite temperature without dynamical quarks. Let $|s_G\rangle$ denote the states of the system. The partition function of the system can be written as,

$$\mathcal{Z} = e^{-\beta F} = \sum_{s_G} \langle s_G | e^{-\beta H} | s_G \rangle. \tag{2.42}$$

To determine whether the system is in confined phase or not we use an infinitely heavy static test quark at position $\vec{x_0}$, as a probe. This test quark has no dynamics and it produces no back reaction on the system. In the presence of the test quark the state of the system is not $|s_G\rangle$. Now we denote the state by $|s\rangle = \psi_a^\dagger(\vec{x_0}, 0)|s_G\rangle$. The field creation operators $\psi_a^\dagger(\vec{x_0}, t)$ create a quark with color a at a position $\vec{x_0}$ and time t. These fermionic operators satisfy their usual anti commutation relations,

$$\{\psi_a(\vec{x_1}, t), \psi_b^\dagger(\vec{x_2}, t)\} = \delta_{ab}\delta^3(\vec{x_1} - \vec{x_2}). \tag{2.43}$$

Then the partition function can be written as,

$$\begin{aligned} \mathcal{Z}_q = e^{-\beta F(\vec{x_0})} &= \frac{1}{N} \sum_s \langle s | e^{-\beta H} | s \rangle, \\ &= \frac{1}{N} \sum_{s_G} \langle s_G | \sum_a \psi_a(\vec{x_0}, 0) e^{-\beta H} \psi_a^\dagger(\vec{x_0}, 0) | s_G \rangle, \end{aligned} \tag{2.44}$$

where N is the number of colors. $N = 3$ for QCD. Thus the sum over a is on all the possible color states. Here the sum is over all states $|s_G\rangle$ with no quarks, that is, over states of pure gauge theory. Time translation of any operator in the Euclidean space is given as,

$$e^{\beta H} O(t) e^{-\beta H} = O(t+\beta), \tag{2.45}$$

which implies

$$\begin{aligned} e^{\beta H}\psi_a(\vec{x_0},0)e^{-\beta H} &= \psi_a(\vec{x_0},\beta), & (2.46)\\ \Rightarrow \mathcal{Z}_q &= \frac{1}{N}\sum_{s_G}\langle s_G|\sum_a e^{-\beta H}\psi_a(\vec{x_0},\beta)\psi_a^\dagger(\vec{x_0},0)|s_G\rangle. & (2.47) \end{aligned}$$

Time evolution of the wave function is given by the Dirac equation in Euclidean space,

$$\left(-i\partial_0\delta^{ab} - gA_0^{ab}(\vec{x_0},\tau)\right)\psi_b(\vec{x_0},\tau) = 0, \tag{2.48}$$

where $A_0 = A_0^i\lambda_i$, with λ_i being the Gell-Mann matrices. Solution of the above equation is,

$$\psi_a(\vec{x_0},\beta) = \mathbf{P}\left[\exp\left(ig\int_0^{\tau=\beta} d\tau A_0(\vec{x_0},\tau)\right)\right]_{ab}\psi_b(\vec{x_0},0), \tag{2.49}$$

where $\mathbf{P}$ denotes path ordering forward in time. In the above equation, one can immediately see that the time evolved field is related to the initial field value by an overall phase factor. This overall phase is known as Wilson line, which is nothing but the non-abelian analog of Arhanov-Bohm phase factor. It is a loop in the Euclidean space due to the periodicity in the Euclidean time direction. The trace of this quantity over all color degree of freedom is known as Polyakov Loop. It is defined as

$$L(\vec{x}) = \frac{1}{N}\mathrm{Tr}\left\{\mathbf{P}\left[\exp\left(ig\int_0^{\tau=\beta} d\tau A_0(\vec{x_0},\tau)\right)\right]\right\}. \tag{2.50}$$

Using eq. (2.49) and eq. (2.50) in eq. (2.47) we get

$$\mathcal{Z}_q = \sum_{s_G}\langle s_G|e^{-\beta H}L(\vec{x})|s_G\rangle. \tag{2.51}$$

After we introduce the test quark, partition function of the system changes. Change in the free energy of the system is given as,

$$\frac{\mathcal{Z}_q}{\mathcal{Z}} \equiv e^{-\beta\Delta F} = \langle L(\vec{x})\rangle, \tag{2.52}$$

where $\langle ... \rangle$ denotes thermal expectation value. Since our test quark is static and infinitely massive it does not have any dynamics. So there is no such notion of free energy for this static, heavy quark. However, with a quark and an antiquark pair at positions $\vec{x}$ and $\vec{y}$ respectively, one can show that the free energy of the system is a function of the distance between the pair. Thus

$$\langle L^{\dagger}(\vec{y})L(\vec{x})\rangle \propto e^{-\beta F_{q\bar{q}}}. \tag{2.53}$$

If the distance between the quark and antiquark pair is very large then the fields are uncorrelated over a distance scale larger than the correlation length. In this case $\langle L^{\dagger}(\vec{y})L(\vec{x})\rangle \longrightarrow \langle L^{\dagger}(\vec{y})\rangle\langle L(\vec{x})\rangle = |\langle L(\vec{x})\rangle|^2$. Then the equation 2.53 becomes,

$$|\langle L(\vec{x})\rangle|^2 \propto e^{-\beta F_{q\bar{q}}}. \tag{2.54}$$

In the confining phase the free energy required to separate a quark- antiquark pair is infinite. Thus $F_{q\bar{q}} \to \infty$. This implies that in the confining phase $\langle L(x)\rangle = 0$. However in the deconfined phase, $F_{q\bar{q}}$ is finite, hence $\langle L(x)\rangle$ is finite in the deconfined phase. Thus the Polyakov loop can serve as a good order parameter and it can be used to distinguish between different phases of the system. In the high temperature limit $|\langle L(\vec{x})\rangle|$ can be normalized to 1.

2.4.2 Spontaneous Breaking of $Z(3)$ Symmetry

Let's understand the symmetry properties of the order parameter. QCD Lagrangian is invariant under $SU(3)$ gauge transformations. Let $U(x,\tau)$ be an arbitrary matrix belonging to $SU(3)$ gauge group. Under $SU(3)$ gauge transformations the gauge fields transform as,

$$A_{\mu}(x,\tau) \to A'_{\mu}(x,\tau) = U(x,\tau)A_{\mu}(x,\tau)U(x,\tau)^{-1} + iU(x,\tau)\partial_{\mu}U(x,\tau)^{-1}, \tag{2.55}$$

and the Polyakov loop transforms as,

$$L(\vec{x}) \to L(\vec{x})' = \frac{1}{N}\mathrm{Tr}\left\{U(x,\beta)\mathbf{P}\left[\exp\left(ig\int_0^{\tau=\beta} d\tau A_0(\vec{x_0},\tau)\right)\right]U^{\dagger}(x,0)\right\}. \tag{2.56}$$

The gauge fields should be periodic in the direction of Euclidean time, i.e. $A_\mu(x,0) = A_\mu(x,\beta)$. Thus, only gauge transformations are allowed which preserve the periodic boundary conditions of the gauge fields. With $A_\mu(x,0) = A_\mu(x,\beta)$, if we choose $U(x,\beta) = U(x,0)$, then using equation 2.55 one can show that $A'_\mu(x,0) = A'_\mu(x,\beta)$. Under these transformations equation 2.56 tells us that the Polyakov Loop remains invariant due to the cyclic properties of the trace and also $U^\dagger U = 1$. Now if we consider $U(x,\beta) = ZU(x,0)$ such that $Z \in SU(N)$, commutes with all the $SU(N)$ generators and is space-time independent, then also the periodic condition is satisfied. Z is called the center group of $SU(N)$ and is denoted as $Z(N)$. The elements of $Z(N)$ are

$$Z = e^{i\phi}\mathbf{1}; \quad \phi = 2\pi m/N; \quad m = 0, 1...(N-1) \tag{2.57}$$

Under the $Z(N)$ transformation the gauge field remains periodic and the pure gauge action remains invariant. However using $U(x,\beta) = ZU(x,0)$ in equation 2.56 we get,

$$L(\vec{x}) \to ZL(\vec{x}). \tag{2.58}$$

For QCD $N = 3$ and according to equation 2.58 $\langle L(\vec{x})\rangle \to Z\langle L(\vec{x})\rangle$. Since in the confined phase $\langle L(\vec{x})\rangle = 0$, thus $\langle L(\vec{x})\rangle$ does not change. However, in the deconfined phase $\langle L(\vec{x})\rangle \neq 0$, thus it is not invariant under $Z(3)$ transformations. Thus $Z(3)$ symmetry is spontaneously broken in the high temperature deconfined phase (QGP) and there are 3 equivalent phases viz $\langle L(\vec{x})\rangle$, $Z\langle L(\vec{x})\rangle$ and $Z^2\langle L(\vec{x})\rangle$. $Z(3)$ symmetry is restored in the low temperature confined phase.

2.5 Chiral Symmetry Breaking

Apart from the $SU(3)$ color gauge symmetry, QCD possesses two important global symmetries, these are isospin symmetry and chiral symmetry [12]. For a pedagogical

discussion on chiral symmetry and related topics see [13]. Isospin symmetry is very important in the context of the development of the Quark model. Here we will not discuss the isospin symmetry of QCD. For details of isospin symmetry and the quark model see [14–21]. The full chiral symmetry of QCD arises in the vanishing mass limit of quark flavors. But quarks are not massless, however certain quark flavors, in particular, the u and the d quarks have masses which are small compared to the QCD scale. In this small quark mass limit, chiral symmetry is not exact, rather approximate.

To understand the origin of chiral symmetry and its breaking in QCD let us start with the QCD Lagrangian for u and d quarks in the massless limit.

$$\begin{aligned}\mathcal{L} &= \sum_{f=u}^{d} \bar{\psi}_f \left(i\gamma^\mu D_\mu \right) \psi_f - \frac{1}{4} Tr\, F_{\mu\nu} F^{\mu\nu} \\ &= \bar{\psi} \left(i\gamma^\mu D_\mu \right) \psi - \frac{1}{4} Tr\, F_{\mu\nu} F^{\mu\nu}, \qquad \psi = \begin{pmatrix} u \\ d \end{pmatrix}. \end{aligned} \tag{2.59}$$

The above Lagrangian remains invariant under the following $SU(2)$ chiral transformations,

$$\begin{aligned}\psi_L \to \psi'_L &= e^{-i\frac{\vec{\tau}}{2}.\vec{\theta_L}} \psi_L \\ \psi_R \to \psi'_R &= e^{-i\frac{\vec{\tau}}{2}.\vec{\theta_R}} \psi_R, \end{aligned} \tag{2.60}$$

where $\vec{\tau}$ are the Pauli matrices, $\vec{\theta_{L,R}}$ arbitrary constant parameters and $\psi_{L,R}$ are left and right chiral part of the field ψ, given as,

$$\psi_{L,R} = \frac{1}{2} \left(1 \mp \gamma_5 \right) \psi. \tag{2.61}$$

The QCD Lagrangian 2.59 is invariant not only under $SU(3)$ color gauge transformations, but also under the global chiral transforms 2.60. Thus global $SU(2)_L \times SU(2)_R$ is an additional symmetry of the massless QCD Lagrangian, it is known as

chiral symmetry. One can get vector and axial vector currents using the linear combinations of the conserved currents associated with $SU(2)_L \times SU(2)_R$ global transformations. These conserved vector and axial vector currents are associated with the following transformations of the field ψ,

$$\begin{aligned} \text{Vector transformation } SU(2)_V: \quad \psi \rightarrow \psi' = e^{-i\frac{\vec{\tau}}{2}.\vec{\theta}}\psi \\ \text{Axial vector transformation } SU(2)_A: \quad \psi \rightarrow \psi' = e^{-i\gamma_5\frac{\vec{\tau}}{2}.\vec{\theta}}\psi \end{aligned} \tag{2.62}$$

QCD Lagrangian is symmetric under the global $SU(2)_V \times SU(2)_A$ transformations. These transformations are different representations of $SU(2)_L \times SU(2)_R$ transformations. Thus $SU(2)_V \times SU(2)_A$ or $SU(2)_L \times SU(2)_R$ are an additional global symmetry of the massless QCD Lagrangian. However the presence of mass term in the Lagrangian (equation 2.59) breaks the chiral symmetry explicitly because fermion mass term $m\bar{\psi}\psi = m\bar{\psi_L}\psi_R + \bar{\psi_R}\psi_L$ couples left and right chiral part of the fermionic field ψ. Hence the mass term is not invariant under $SU(2)_L \times SU(2)_R$ or $SU(2)_V \times SU(2)_A$ transformations. However, u and d quarks have masses which are small with respect to the characteristic QCD scale $\Lambda_{QCD} \simeq 200MeV$. So for the two flavor case, the massless approximation is quite good and the chiral symmetry is almost exact. If the ground state of the system also respects this symmetry then one expects degenerate multiplets of particles corresponding to the irreducible representations of the group $SU(2)_L \times SU(2)_R$. For example, as a manifestation of chiral symmetry triplet pseudo-scalar mesons (pions) should be accompanied by their parity partners. But experimentally we have not seen such parity partners in nature. Thus the absence of the chiral multiplets can be explained if the QCD vacuum is not invariant under $SU(2)_L \times SU(2)_R$ global chiral transformations. However, we do see the multiplet structure of $SU(2)$ isospin in nature. Thus the vacuum of QCD must be invariant under $SU(2)$ isospin global symmetry. All this implies that in QCD the $SU(2)_L \times SU(2)_R$ chiral symmetry is spontaneously broken to the $SU(2)$ isospin subgroup with the generation of pseudo-scalar Goldstone bosons as pions. However, pions are not massless; they have nonzero masses arising from nonzero masses of

quarks. Thus chiral symmetry is also explicitly broken by a small amount.

A simple phenomenological model which implements the idea of chiral symmetry breaking is the linear sigma model [22] originally constructed to study chiral symmetry in pion-nucleon system. This simple model contains some crucial features of low-energy QCD. Here the Lagrangian is constructed out of the iso-triplet pion $\pi = (\pi_1, \pi_2, \pi_3)$ fields and an iso-scalar σ field. The Lagrangian in terms of these fields, in the chiral limit with zero quark masses, is [23]

$$\mathcal{L} = \frac{1}{2}\left[(\partial_\mu \sigma)^2 + (\partial_\mu \pi)^2\right] - V(\sigma, \pi), \tag{2.63}$$

with the potential $V(\sigma, \pi)$ describing the self-interaction of the scalars and is given by

$$V(\sigma, \pi) = \frac{\mu^2}{2}(\sigma^2 + \pi^2)^2 + \frac{\lambda}{24}(\sigma^2 + \pi^2)^4. \tag{2.64}$$

The Lagrangian given in equation 2.63 along with the potential given in equation 2.64 can be shown to invariant under $SU(2)_V \times SU(2)_A$. For this we have to consider the mesons as combinations of quark fields. σ meson which is isoscalar-scalar can be considered as $\bar{\psi}\psi$ and the isovector-pseudo scalar π mesons can considered as $i\bar{\psi}\vec{\tau}\gamma_5\psi$. Using the transformation properties of ψ under $SU(2)_V$ and $SU(2)_A$ one can derive the transformation properties of the mesons under $SU(2)_V$ and $SU(2)_A$ transformations. Under $SU(2)_V$ transforms, σ and π fields transform as follow [13]:

$$\begin{aligned} &SU(2)_V \text{ transformation of } \sigma : \bar{\psi}\psi \rightarrow \bar{\psi}\psi \\ &\Rightarrow \sigma \rightarrow \sigma \\ &SU(2)_V \text{ transformation of } \pi_i : i\bar{\psi}\tau_i\gamma_5\psi \rightarrow i\bar{\psi}\tau_i\gamma_5\psi + i\theta_j\epsilon_{ijk}\bar{\psi}\tau_k\gamma_5\psi \\ &\Rightarrow \vec{\pi} \rightarrow \vec{\pi} + \vec{\theta} \times \vec{\pi}. \end{aligned} \tag{2.65}$$

Similarly one can show that,

$$\begin{aligned} SU(2)_A \text{ transformation of } \sigma : \ \sigma \rightarrow \sigma - \vec{\theta}.\vec{\pi} \\ SU(2)_A \text{ transformation of } \pi : \ \vec{\pi} \rightarrow \vec{\pi} + \vec{\theta}\sigma \end{aligned} \tag{2.66}$$

Equation 2.65 and 2.66 can be used to show that the Lagrangian of the linear sigma model is invariant under $SU(2)_V \times SU(2)_A$. Since the transformations of the mesons 2.65,2.66 are linear in fields hence the name linear sigma model.

When the mass term μ^2 is negative the minima of the potential is given by

$$\sigma^2 + \pi^2 = -\frac{6\mu^2}{\lambda}. \tag{2.67}$$

This set of minima defines the vacuum manifold $\mathcal{M}$ which is a 3-sphere (S^3) in the four-dimensional field space. Now, to determine the particle spectrum of the theory one has to choose a vacuum state and rewrite the fields in terms of fluctuations around it. A convenient choice of ground state is,

$$< \sigma >= v = -\frac{6\mu^2}{\lambda}, \quad \langle \pi \rangle = 0. \tag{2.68}$$

Note that the vacuum is the condensate of the sigma field. According to the transformation laws, sigma field remains invariant under $SU(2)_V$ isospin symmetry. However, sigma field transforms non trivially under $SU(2)_A$ transformations. Hence the vacuum is isospin symmetric and $SU(2)_A$ symmetry is spontaneously broken. So the spontaneous breaking of the chiral symmetry is well encoded in the linear sigma model.

Expanding the sigma field around the minimum as $\sigma = v + \zeta$, the Lagrangian 2.63 becomes,

$$\mathcal{L} = \frac{1}{2}\left[(\partial_\mu \sigma)^2 + (\partial_\mu \pi)^2\right] + \mu^2\zeta^2 - \frac{\lambda v}{6}\zeta(\zeta^2 + \pi^2) - \frac{\lambda}{24}(\zeta^2 + \pi^2)^2. \tag{2.69}$$

From the above equation is clear that σ is a massive excitation and pions are massless excitation. Pions are the Goldstone bosons associated with the spontaneous breaking of symmetry. In this case, $SU(2)_V \times SU(2)_A \rightarrow SU(2)_V$ leads to the appearance of three massless (the number of broken generators being three) pions.

In summary, chiral symmetry is an exact global symmetry of QCD only in the massless limit. Current quark masses, however, are not zero. But, compared to hadronic scales (Λ_{QCD}), the two lightest quarks have negligible masses. So chiral

symmetry can be regarded as an approximate symmetry of QCD. Since chiral symmetry is only approximate, the pions get a finite but small mass, compared to other hadrons, in the chiral symmetry broken phase.

2.6 Results from Lattice QCD

For a system in thermal equilibrium, various thermodynamic quantities can be obtained once we know the partition function of the system. In QCD, thermal expectation value of any operator can be expressed as,

$$\langle \hat{\mathcal{O}} \rangle = \frac{\int \mathcal{D}A_\mu(\mathbf{x},\tau)\mathcal{D}\psi(\mathbf{x},\tau)\mathcal{D}\bar{\psi}(\mathbf{x},\tau)\hat{\mathcal{O}}[A_\mu,\psi,\bar{\psi}]e^{-\mathcal{S}_E}}{\int \mathcal{D}A_\mu(\mathbf{x},\tau)\mathcal{D}\psi(\mathbf{x},\tau)\mathcal{D}\bar{\psi}(\mathbf{x},\tau)e^{-\mathcal{S}_E}}, \tag{2.70}$$

where $\mathcal{S}_E$ is the Euclidean Action. For free field theory, one can evaluate the corresponding path integral using Gaussian integrals. However, due to the presence of interaction, it is not always possible to carry out the path integral analytically. In that case, one can use numerical techniques to evaluate the path integral. This is how one uses Lattice QCD (LQCD) techniques to solve the path integral numerically. Apart from this fact, we are also interested to understand the phase structure of QCD. Furthermore, since the equilibrium phases and the phase transition involve quarks and gluon interacting over a large distance scale, they need to be studied within the framework of nonperturbative QCD. Lattice QCD requires discretization of space-time into space-time lattice with a lattice constant or lattice spacing and it includes nonperturbative aspects of QCD. Although Lattice QCD works well for a system at high temperature and zero baryon chemical potential, for nonzero baryon chemical potential due to fermion "sign problem" LQCD loses its predictability. Thus LQCD describes a quark gluon plasma with vanishing net baryon density, which is approximately the situation in the Early Universe. However, QGP formed in heavy ion collision experiment has small but non-zero baryon chemical potential. LQCD and its extension to non-zero baryon chemical potential are areas of current research.

Significant progress has been made and LQCD results for hadronization phase transition in a QGP with non-zero baryon chemical potential have been reported (see, [24] and references therein). In LQCD framework one typically studies thermodynamic quantities e.g. energy density, pressure and behavior of the expectation value of the Polyakov loop (order parameter for confinement deconfinement phase transition) and chiral condensate (order parameter for chiral phase transition).

Quark masses plays an important role in these calculations. In the infinite quark mass limit, QCD has a first order confinement-deconfinement phase transition, while the chiral phase transition for three flavor is first order in the vanishing quark mass limit. QCD phase transition as a function of the light and strange quark masses is shown in the figure 2.6 . An interesting aspect of this phase diagram is the occurrence of a second order transition line in the light quark mass regime, the boundary of the region of first order phase transitions. The features of this diagram are richer than what we have mentioned here. For details of this phase diagram see [25].

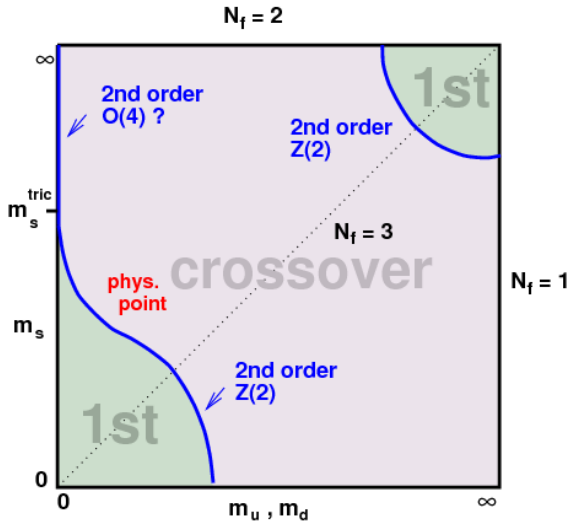

Figure 2.6: QCD phase transition at finite temperature and zero chemical potential as a function of quark masses [26]. Physical point in the figure denotes the transition for the physical quark masses.

In the presence of quark mass, Polyakov Loop is not a correct order parameters, but it can be used as indication of phase transition. Lattice results for the order

parameters and associated susceptibilities are shown in figure 2.7 [25, 27] . In this figure, m_q denotes the light quark mass. Figure 2.7 shows the variation of the thermal expectation value of Polyakov Loop $\langle L \rangle$, which is the order parameter for deconfinement in the pure gauge limit ($m_q \to 0$) and $\langle \bar{\psi}\psi \rangle$, which is the order parameter for chiral symmetry breaking in the chiral limit ($m_q \to 0$). This figure also shows the corresponding susceptibilities as a function of the coupling $\beta = 6/g^2$. It is interesting to note that smooth change in Polyakov Loop and chiral condensate happens around same β. Also the corresponding susceptibilities peaks at same β. These strongly indicate that both the transitions happen almost simultaneously.

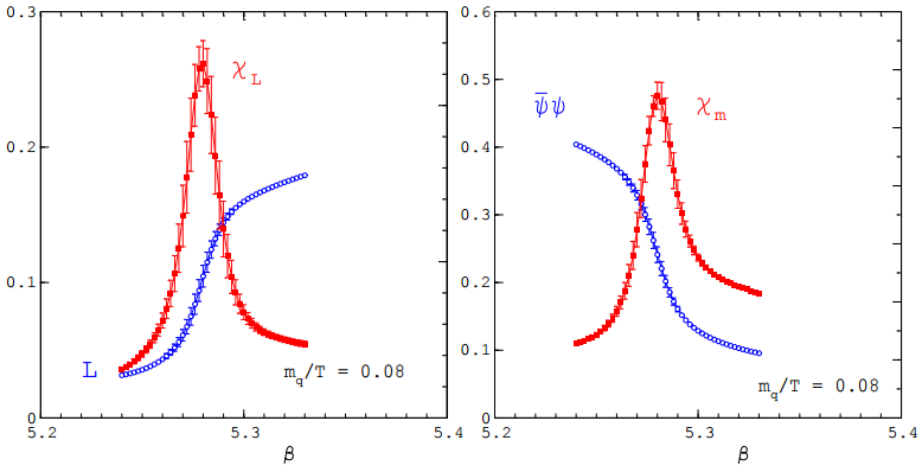

Figure 2.7: Deconfinement and chiral transition in two light flavor case. Left figure shows the variation of Polyakov Loop and the associated susceptibility as a function of gauge coupling. Right figure shows the behavior of chiral order parameter and associated susceptibility [25]

.

Figure 2.8 shows the smooth variation of energy density for QCD with dynamical quarks [28]. The energy density is larger for three light flavors relative to the two light flavor case. The increment in the energy density of the system above the transition temperature is due to the generation of new degrees of freedom, which is consistent with the notion of deconfinement. It is now believed that the confinement deconfinement transition is a crossover for physical quark masses. Similarly, the

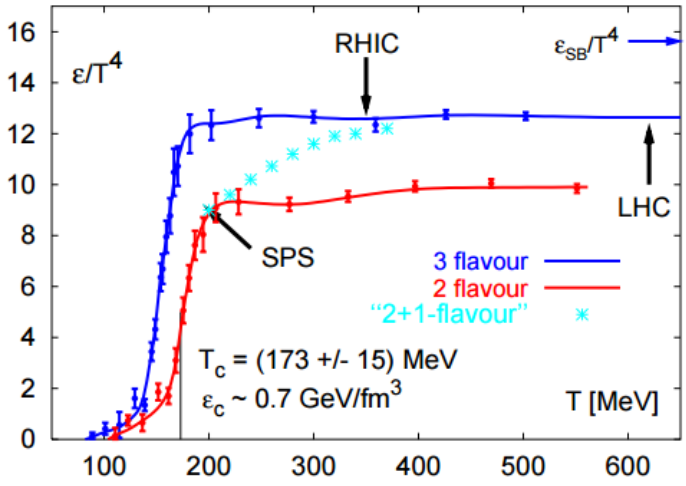

Figure 2.8: Lattice results showing the variation of the energy density for QCD with quarks [28].

.

chiral transition at low chemical potential and for small quark masses is a smooth crossover [24].

2.7 Effective potential for Polyakov Loop Order Parameter

In this section we make the following notational changes - we suppress the arrow on $\vec{x}$ and denote the thermal expectation of the Polyakov loop by the symbol $l(x)$.

A possible effective Lagrangian of the Polyakov loop which encodes the physics of confinement deconfinement transition was proposed by Pisarski [29, 30].

$$\mathcal{L} = \frac{N}{g^2}|\partial_\mu l|^2 T^2 - V(l), \tag{2.71}$$

where

$$V(l) = \left(-b_2|l|^2 + b_3(l^3 + (l^*)^3) + |l|^4\right) b_4 T^4, \tag{2.72}$$

where $l(x)$ is the thermal expectation value of the Polyakov Loop. l is dimensionless and the factor T^4 determines the dimensions of the potential. In mean field theory, b_4 is taken as constant and b_2 varies with temperature. b_3 term gives

a $cos(3\theta)$ term, leading to $Z(3)$ degenerate vacua when $b_3 \neq 0$. The parameters are fitted in ref. [31–33] such that that the effective potential reproduces the thermodynamics of pure $SU(3)$ gauge theory on lattice [34, 35]. The coefficients are $b_2 = (1 - 1.11/x)(1 + 0.265/x)^2(1 + 0.300/x)^3 - 0.478$, (with $x = T/T_c$ and $T_c \sim 182$ MeV), $b_3 = 2.0$ and $b_4 = 0.6061 \times 47.5/16$. With the coefficients chosen above, the expectation value of the order parameter approaches to $y = b_3/2 + \frac{1}{2} \times \sqrt{b_3^2 + 4b_2(T = \infty)}$ as $T \longrightarrow \infty$. Various quantities are normalized such that the expectation value of the order parameter goes to unity for $T \longrightarrow \infty$. Hence the fields and the coefficients of the potential are rescaled as,

$$l(x) \rightarrow \frac{l(x)}{y}, \quad b_2 \rightarrow \frac{b_2}{y^2}, \quad b_3 \rightarrow \frac{b_3}{y}, \quad b_4 \rightarrow b_4 y^4. \tag{2.73}$$

$l(x)$ has the value zero at low temperatures and the potential has only one minimum. For $T > T_c$, $l(x)$ picks up a non-vanishing vacuum expectation value l_0, and the cubic term gives rise to $Z(3)$ vacua. The structure of these $Z(3)$ vacua has been discussed in the literature.

It is important to mention that other parametrizations of the effective potential for the Polyakov loop have been given in the literature, e.g. in refs. [36,37]. The effective potential of the Polyakov loop as provided by Fukushima [36] has the following form,

$$V[L]/T^4 = -2(d-1)e^{-\sigma_a/T}|TrL|^2 - ln[-|TrL|^4 + 8Re(TrL)^3 - 18|TrL|^2 + 27], \tag{2.74}$$

where $\sigma = (425\text{MeV})^2$ is the string tension and $2(d-1)e^{-\sigma_a/T_d} = 0.5153$ with $T_d = 270$ MeV and $d = 4$ (number of space-time dimensions). T_d is the transition temperature. Lattice spacing $a = (272\text{MeV})^{-1}$. For a discussion on the phenomenology of the $Z(3)$ vacua and the associated $Z(3)$ domaim walls see [38–45] and references therein.

2.8 Topological Defects

Topological defects emerge as a consequence of symmetry breaking phase transitions. Formation of such objects during the phase transition is not necessarily restricted

to a model of particle physics only. Whenever there is a phase transition based on spontaneous symmetry breaking, topological defects are produced if they are allowed by the structure of the vacuum manifold. Common examples of such defects in condensed matter systems are the vortices in superfluid Helium [46], flux tubes in type II superconductor [47], and line and point defects in liquid crystals [48, 49]. Topological defects formation occurs after the symmetry breaking transition because of the random choice of the order parameter among the many possible ground states in the different region of space. These regions form domains in space. During the further evolution of the system, the order parameter may get 'locked' in the symmetric state, while the remaining system will be in the symmetry broken phase. These locked regions are in general called defects. If these defects are produced due to non-trivial topology of the vacuum manifold, these are called topological defects.

Kibble in 1976 proposed the mechanism for the production of topological defects in phase transitions in the context of early universe [50]. After a spontaneous symmetry breaking phase transition, the physical space consists of regions, called domains. In each domain, the configuration of the order parameter field (or the Higgs field) can be taken as nearly uniform while it varies randomly from one domain to another. The order parameter field configuration in between domains is assumed to be such that the variation of the order parameter field is the minimum on the vacuum manifold. With this simple construction, topological defects arise at the junctions of several domains if the variation of the order parameter in those domains traces a topologically non-trivial configuration in the vacuum manifold.

Let us consider a simple model with a single real scalar field having double well potential. This model gives rise to planer topological defect, known as domain wall. The Lagrangian is given by,

$$\mathcal{L} = \frac{1}{2}\left(\partial_\mu \phi\right)^2 - \frac{\lambda}{4}\left(\phi^2 - \eta^2\right)^2 . \tag{2.75}$$

This Lagrangian is symmetric under $\phi \to -\phi$. Thus $Z(2)$ is the symmetry of the Lagrangian. This potential has two minima at $\phi = \pm\eta$ and a local maximum at

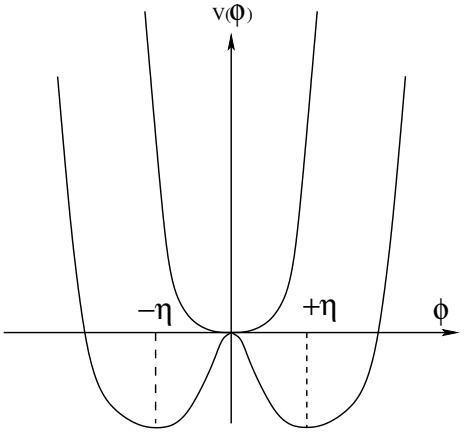

Figure 2.9: Double well potential

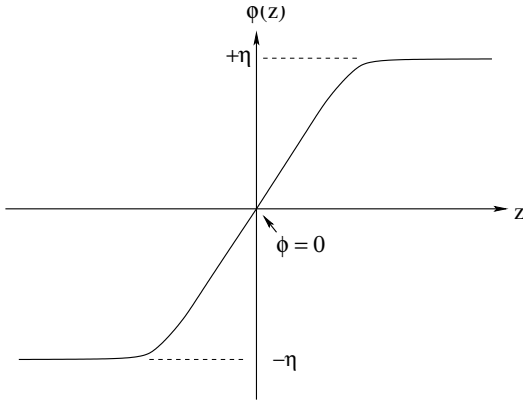

Figure 2.10: Domain wall or Kink solution

$\phi = 0$ (see figure 2.9). The Z_2 symmetry is spontaneously broken when the field chooses one of the vacua. The field equation has the analytic solution under the following boundary condition, and $\phi \to \pm\eta$ at $z \to \pm\infty$. This analytic solution is,

$$\phi(z) = \eta \tanh\left[\left(\frac{\lambda}{2}\right)^{1/2} \eta z\right], \tag{2.76}$$

the profile of the solution is also shown in the figure 2.10,

In the figure $\phi = -\eta$ on the far left, while $\phi = \eta$ on far right. ϕ also needs to vary from $-\eta$ to η continuously, because the energy of the system has to be finite. This would mean that ϕ must pass through zero as it goes from far left to far right. This solution is known as kink solution. Similar to kink solution, an anti-kink solution is also possible with opposite boundary condition. It is important to note that $\phi = 0$ is the local maximum of the potential. Thus the system has an energetically unstable region after the symmetry breaking. However, the stability of the kink solution is a consequence of a topological conservation law. Kink or anti-kink solutions are topologically stable and these cannot be removed by local operation. In three dimension these solutions lead to domain wall. These defects occur in the system where vacuum manifold has disconnected sectors.

In a formal language topological defects arise because of the topology of the vacuum manifold. The vacuum manifold or the order parameter space is defined as the set of distinct ground states and is denoted by $\mathcal{M}$. In technical terms, if a group G

Table 2.1: Topological classification of defects with homotopy group $\pi_n(\mathcal{M})$

Topological Defects	Dimension	Classification
Domain Wall	2	$\pi_0(\mathcal{M})$
String defect	1	$\pi_1(\mathcal{M})$
Monopole	0	$\pi_2(\mathcal{M})$
Texture/Skyrmion	-	$\pi_3(\mathcal{M})$

breaks down to H spontaneously, then vacuum manifold is $\mathcal{M} \equiv G/H$. It is precisely the topology of $\mathcal{M}$ which determines the type of defects which may arise during symmetry breaking transition. The necessary conditions for the formation of such defects depend on the existence of non-trivial mapping from physical space to the vacuum manifold. If the vacuum manifold has two or more disconnected pieces, then it can be shown that zeroth homotopy group of vacuum manifold, $\pi_0(\mathcal{M}) \neq 1$. In such case, domain walls form as topological defects. Domain walls are two dimensional topological defects. Similarly, other topological defects like string defects (one dimension), monopoles (point defects) may arise when the first and second homotopy group of $\mathcal{M}$ are non-trivial respectively.

Different classes of homotopy groups and the different types of topological defects associated with these groups are listed in the table 2.1 . For a comprehensive review of topological defects see [51]. Some examples of topological defects which arise in different physical systems is given below,

- **2D Spins**: The order parameter space is $\mathcal{M} = S^1$. First non-trivial homotopy group of S^1 is π_1, $\pi_1(S^1) = Z$. Hence, in this case, the topological defects are string defects in three space dimensions (vortices in two space dimensions).
- **3D Spins**: The order parameter space is $\mathcal{M} = SO(3)/SO(2) \equiv S^2$. First non-trivial homotopy group of S^2 is π_2. $\pi_1(S^2) = 1$ and $\pi_2(S^2) = Z$. Hence there are point like topological defects.

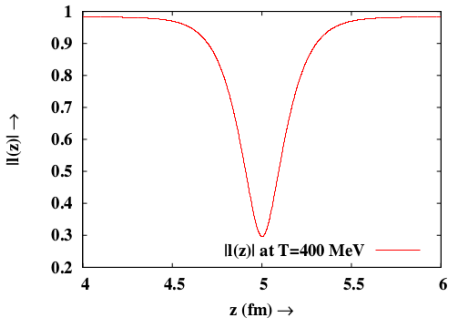

Figure 2.11: Domain wall between two $Z(3)$ domains [38].

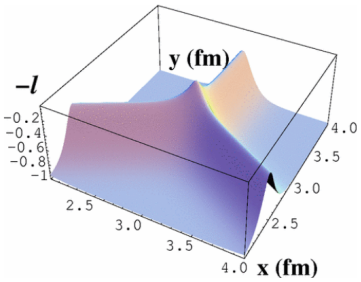

Figure 2.12: QGP string at the junction of $Z(3)$ walls.

- **Superfluidity of** He^4: The order parameter space is $\mathcal{M} = U(1) \equiv S^1$. First non-trivial homotopy group of S^1 is π_1. $\pi_1(S^1) = Z$. Hence there are string defects. These are superfluid vortices.

- **Topological defects in Quark Gluon Plasma**: In the pure QCD gauge theory Z_3 symmetry is spontaneously broken. Thus the vacuum manifold has disconnected pieces. In this case, domain walls appear as the topological defects. At the junction of three domain walls, one will have a string defect [52]. Figure 2.11 and figure 2.12 shows $Z(3)$ interfaces and associated string respectively.

Bibliography

[1] E. Witten, Phys.Rev. **D30** (1984).

[2] A. Rajantie, (2003), hep-ph/0311262, Lectures given at COSLAB Workshop on Cosmological Phase Transitions and Topological Defects, Porto, Portugal, 22-24 May 2003.

[3] Doru Sticlet, "Phase Transitions in the Early Universe", http://fyzika.uniza.sk/ melo/DoruSticlet.pdf

[4] J. I. Kapusta, " Finite temperature Field Theory", (Cambridge University Press, Cambridge, UK), 1989.

[5] F.Halzen, A.D Martin, "Quarks And Leptons" (John Wiley and Sons); D.Griffiths, " Introduction to Elementary Particles" (John Wiley and Sons), 1987; D.H.Perkins, " Introduction to High Energy Physics" (Addison-Wesley Publishing Company), 1982; Fayyazuddin, Riazuddin, " A Modern Introduction to Particle Physics" (World Scientific, Singapore), 2000.

[6] S. Coleman, Phys. Rev. **D 15**, 2929 (1977); I. Yu. Kobzarev, L.B. Okun and M.B. Voloshin, Sov. Jrnl. Nucl. Phys.**20**, 644 (1975).

[7] A.D. Linde Nucl. Phys. **B 216**, 421 (1983).

[8] S. Coleman, "The Uses of instantons".

[9] R. K. Mohapatra," Investigating Formation and Evolution of $Z(3)$ Walls and Flow Anisotropies in Relativistic Heavy-Ion Collision", (Ph.D. thesis, Homi Bhabha National Institute, India, 2012).

[10] M. Citron, " Spontaneous and induced false vacuum decay", (M.Sc thesis, Imperial College London, 2013).

[11] L. D. McLerran and B. Svetitsky, Phys. Rev. **D 24**, 450 (1981); L. D. McLerran, Rev. Mod. Phys. **58**, 1021 (1986).

[12] T. Hatsuda and T. Kunihiro, Phys. Rept. **247**, 221 (1994); R.Rapp and J. Wambach, Adv. Nucl. Phys. **25**, 1 (2000).

[13] P. Finelli, " Chiral Symmetry", Nuclear Physics Course, Physics Department, University of Bologna, 2012.

[14] M. Gell-Mann, Phys. Rev. **92**, 833 (1953)

[15] T. Nakano and K. Nishijima, Prog. Theor. Phys. **10**, 581 (1953).

[16] M. Gell-Mann, CTSL-20.

[17] Y. Ne'eman, Nucl. Phys. **26**, 222 (1961).

[18] M. Gell-Mann, Phys. Lett. **8**, 214 (1964).

[19] G. Zweig, development in the Quark Theory of Hadrons, Volume 1. Edited by D. lichtenberg and S. Rosen. pp. 22-101.

[20] O. W. Greenberg, Phys. Rev. Lett. **13**, 598 (1964).

[21] M. Y. Han and Y. Nambu, Phys. Rev. **139**, B1006 (1965).

[22] M. Gell-Mann and M. Levy, Nuovo Cimento, **16**, 705 (1960).

[23] T. Cheng and L. Li, " Gauge Theory Of Elementary Particles", (Oxford University Press), 2005.

[24] C. DeTar and U. M. Heller, Eur. Phys. J. **A 41**, 405 (2009) (arXiv: 0905.2949).

[25] F. Karsch, arXiv: hep-lat/0106019

[26] P. de Forcrand, arXiv:1005.0539

[27] F. Karsch and E. Laermann, Phys. Rev. **D 50**, 6954 (1994),(arXiv: hep-lat/9406008).

[28] F. Karsch and E. Laermann, arXiv: hep-lat/0305025.

[29] R. D. Pisarski, Phys. Rev. **D 62**, 111501 (2000) [hep-ph/0006205].

[30] R. D. Pisarski, hep-ph/0203271.

[31] A. Dumitru and R. D. Pisarski, Phys. Lett. **B 504**, 282 (2001) [hep-ph/0010083].

[32] A. Dumitru and R. D. Pisarski, Nucl. Phys. **A 698**, 444 (2002) [hep-ph/0102020].

[33] A. Dumitru and R. D. Pisarski, Phys. Rev. **D 66**, 096003 (2002) [hep-ph/0204223].

[34] G. Boyd, J. Engels, F. Karsch, E. Laermann, C. Legeland, M. Lutgemeier and B. Petersson, Nucl. Phys. **B 469**, 419 (1996) [hep-lat/9602007].

[35] M. Okamoto *et al.* [CP-PACS Collaboration], Phys. Rev. **D 60**, 094510 (1999) [hep-lat/9905005].

[36] K. Fukushima, Phys.Lett. **B 591**, 277 (2004), hep-ph/0310121.

[37] S. Roessner, C. Ratti and W. Weise, Phys.Rev. **D 75**, 034007 (2007), hep-ph/0609281.

[38] A. Atreya, A. M. Srivastava and A. Sarkar, Phys.Rev. **D 85**, 014009 (2012).

[39] A. Atreya, A. M. Srivastava and A. Sarkar, J.Phys.Conf.Ser. **484**, 012053 (2014).

[40] A. Atreya, P. Bagchi and A. M. Srivastava, Phys.Rev. **C 90**, 034912 (2014).

[41] A. Atreya, A. M. Srivastava and A. Sarkar, Phys.Rev. **D 90**, 045010 (2014).

[42] A. Atreya, P. Bagchi, A. Das and A. M. Srivastava, Phys.Rev. **D 90**, 125016 (2014).

[43] A. Atreya, " Spontaneous CP Violation In Quark Scattering From QCD $Z(3)$ Domains and Its Cosmological Implications", (Ph.D. thesis, Homi Bhabha National Institute, India, 2015).

[44] U. S. Gupta, R. K. Mohapatra, A. M. Srivastava and V. K. Tiwari, Phys.Rev. **D 82**, 074020 (2010).

[45] A. Atreya, P. Bagchi and A. M. Srivastava, Phys.Rev. **C 90**, 034912 (2014).

[46] W. H. Zurek, Nature **317**, 505 (1985); Phys. Rept. **276**, 177 (1996).

[47] H. B. Nielsen and P. Olesen, Nucl. Phys. **B 61**, 45 (1973).

[48] M. J. Bowick, L. Chandar, E. A. Schiff and A. M. Srivastava, Science **263**, 943 (1994).

[49] S. Digal, R. Ray and A. M. Srivastava, Phys. Rev. Lett. **83**, 5030 (1999); R. Ray and A. M. Srivastava, Phys. Rev. **D 69**, 103525 (2004).

[50] T.W.B. Kibble, J. Phys. **A 9**, 1387 (1976), Phys. Rep. **67**, 183 (1980).

[51] N. D. Mermin, Rev. Mod. Phys. **51**, 591 (1979).

[52] B. Layek, A. P. Mishra and A. M. Srivastava, Phys. Rev. **D 71**, 074015 (2005).

Chapter 3

Neutron Star

In this chapter we will give a general qualitative overview of neutron star physics. After a general introduction to the Neutron star we will discuss its structural properties, e.g. mass and radius, properties of matter in the crust and in the core of neutron stars etc. This discussion will be followed by the discussion of the superfluid phase in the core of the neutron star and its effects on the pulsar dynamics e.g. glitch and recently observed antiglitch. In this discussion we will not go into the details of the neutron star physics rather we will focus on the concepts which will be necessary for this thesis. Large part of this discussion is mainly based on [1] and references therein.

3.1 General overview

The behavior of nuclear matter at extreme conditions is still not understood completely. This led to the speculations about the appearance of new phases of matter. Under conditions of high density and/or high temperature, the hadronic matter is expected to undergo a phase transition to deconfined quark matter known as Quark Gluon Plasma (QGP). We have mentioned earlier that QGP phase can also be achieved in ultra relativistic heavy ion collision experiments. However, very high density environment, which exists in the interior of neutron stars, can also provide a perfect condition for QGP phase. We will discuss the presence of deconfined phases of QCD matter in the core of neutron star and how the presence of these phases can

influence the dynamics of neutron stars, pulsars etc. In this chapter we will discuss general features of neutron star, different QCD phases inside it and influence of these phases on the dynamics of pulsars e.g. glitch mechanism etc.

Stars are dynamical, self-gravitating masses of hot gas supported by the nuclear furnace at their center. Stars forms due to the gravitational collapse of clouds of dust and gas and evolve from protostars through a contracting phase leading to nuclear ignition and onto the main sequence. Main sequence stars spend their lives burning their nuclear fuel, fusing hydrogen into helium. Nuclear fusion provides enough thermal energy to balance the gravitational collapse. But, when the nuclear fuel is depleted, the pressure gradients can not balance the gravity anymore and the interior of the star starts to collapse. The star can collapse either to a white dwarf, or neutron star or black hole. For the details of astrophysical aspects of stellar evolution see [2]. For a general discussion on neutron star, its evolution, its matter content etc. see [3,4].

When the stellar evolution ends in a supernova explosion, the hot core with a temperature of the order of tens of MeV, cools down to a temperature of the order of 1 MeV or less by neutrino emission [5]. Meanwhile, the collapsed core becomes an equilibrated system of neutrons, protons, hyperons, leptons and possibly quarks. Thus a neutron star is born. Neutron star radius is about ten kilometers and the average density in the core can be $5 - 10\,\rho_0$, where ρ_0 is the nuclear saturation density, i.e. $3 \times 10^{14} g\,cm^{-3}$. Their surface temperature is of the order of 10^6 Kelvin and the surface magnetic field strength is around $10^8 - 10^{12}$ Gauss. Observed masses of different neutron stars are generally of the order of $1.5 M_\odot$, where $M_\odot$ denotes Solar mass ($\sim 2 \times 10^{30}$ Kg). Neutron star mass is dependent on the equation of state. For a review on the observational constraints of the equation of state in a neutron star see [6]. Neutron stars could exist and can be observed as an isolated star or in a binary system. Measurements of Keplerian and post-Keplerian parameters of the orbit can give the estimate of the mass of the neutron stars in a binary system [7, 8]. Isolated neutron stars are observed as pulsars. Pulsars are rotating neutron stars with

magnetic field axis oriented towards the observer. In pulsars, the magnetic field axis is misaligned with the axis of rotation. Isolated neutron stars can also be observed by the thermal radiation emitted by it [9].

In 1934, W. Baade and F. Zwicky first proposed the idea of the neutron star as an end stage of stellar evolution [10]. They speculated the connection between supernova and the origin of neutron stars. However, after the discovery of the neutron by Chadwick [11], Landau had first suggested that at high densities, neutron matter would be energetically favored over a mixture of protons and neutrons [12]. He also suggested that very massive objects with high densities would consist almost entirely of neutrons in chemical equilibrium [13]. In 1939, Tolman, Oppenheimer, and Volkoff gave the formalism of full general relativistic equation of hydrostatic equilibrium for spherically symmetric objects (TOV equation) [14, 15]. Assuming matter consists of non-interacting neutrons, Oppenheimer and Volkoff found the maximally allowed mass to be $\sim 0.7 M_{\odot}$. However interaction of neutrons can increase this value [16,17].

Observational proof of neutron star started with the beginning of X-ray astronomy during the '60s [18]. Although several X-ray sources were discovered, but these were not the conclusive proof for the existence of neutron stars (see [7, 19, 20]). In 1965, Wheeler pointed out that it would be extremely difficult to detect the neutron stars due to their tiny radii and hence low luminosity [21]. In that period a lot of theories were proposed to suggest how to discover neutron stars (e.g. [22,23]). One of the suggestions [24] was that a rapidly rotating neutron star with a strong dipolar magnetic field could convert its rotational energy into electromagnetic radiation and accelerate particles to high energies. In 1967, J. Bell and A. Hewish detected sources of pulsating radio beams during a galactic survey [25]. At first, the sources were thought of as extra-terrestrial communications. However when they searched for Doppler shift due to extra-terrestrial planetary orbital motion, they found Doppler shift due to the earth's motion only. Meanwhile, other sources were detected emitting pulsating

signals having the same radio wavelength and the idea of extra-terrestrial communication was abandoned. During that time many proposals were put forward which can describe the observed signal. The simple vibration was one such proposal, but is was ruled out because vibrations always contain some kind of damping, whereas the pulsar period remained constant. A binary stellar system was discarded as a source because these systems emit gravitational radiation and speed up, while pulsars were observed to slow down on very large time scales. Rotating white dwarfs were ruled out because to obtain an observed signal, the source region would have to be very small, but white dwarfs are not that small. Also, observed data gave an indication for high rotation frequencies. A white dwarf can not have very high rotation frequency [26], otherwise, they would be ripped apart by the centrifugal force generated at the equator. Hence the white dwarfs were also ruled out. In 1968 T. Gold first proposed that only rotating neutron star can explain the pulsar phenomenon [27]. To date, more than 2500 neutron stars have been detected as radio pulsars.

3.2 The Structure of Neutron Stars

3.2.1 Mass and Radius

Physical parameters such as mass, radius of an isolated neutron star can not be measured directly. Using theoretical considerations Rhodes and Ruffini in 1974 gave the bound on neutron star mass: $0.2M_{\odot} \leq M \leq 3.5M_{\odot}$ [17]. However, measurement of pulsar masses is possible in certain binary systems. In 1999, Thorsett and Chakrabarty constrained this mass range to very close to $1.4M_{\odot}$ using the measurements from 14 pulsar binary systems [28]. Figure 3.1 shows their result. Fitting blackbody spectra to neutron stars with sufficient X-ray flux, their radii was constrained in the range 8-15 km [29]. Alternatively, one can determine the radii and masses of neutron stars using the relevant equation of states in Tolman-Volkoff-Oppenheimer (TOV) equation. A typical example of mass radii relationship for different equation

of states is shown in the figure 3.2. However, one can use non-relativistic and Newtonian equations for hydrostatic equilibrium to get the mass radii relationship. In this thesis, we have used this approach to determine density profile as well as mass and radius of a neutron star having polytropic equation of state. In this thesis although we have used Newtonian approximation and non-rotating case to determine the density profile for a polytropic equation of state, but we have used the results for a rotating neutron star. This is an approximation, however we expect only small correction to our results in a realistic situation.

Let us consider a spherical star in a hydrostatic equilibrium. Its structure is described by two first order ODEs:

$$\frac{dP(r)}{dr} = -\frac{Gm(r)\rho(r)}{r^2}, \tag{3.1}$$

$$\frac{dm(r)}{dr} = 4\pi r^2 \rho(r), \tag{3.2}$$

where $\rho(r), P(r), m(r)$ are mass density, pressure, and mass as a function of radial coordinate r. G is the Newton's constant.

From equation 3.1 we get,

$$\frac{dm(r)}{dr} = -\frac{1}{G}\frac{d}{dr}\left(\frac{r^2}{\rho(r)}\frac{dP(r)}{dr}\right). \tag{3.3}$$

Comparing LHS of equations 3.2 and 3.3 we get second order Poisson equation,

$$\frac{1}{r^2}\frac{d}{dr}\left(\frac{r^2}{\rho(r)}\frac{dP(r)}{dr}\right) = -4\pi G\rho(r). \tag{3.4}$$

We assume that there is a polytropic relation between pressure and density:

$$P = K\rho^{1+\frac{1}{n}}, \tag{3.5}$$

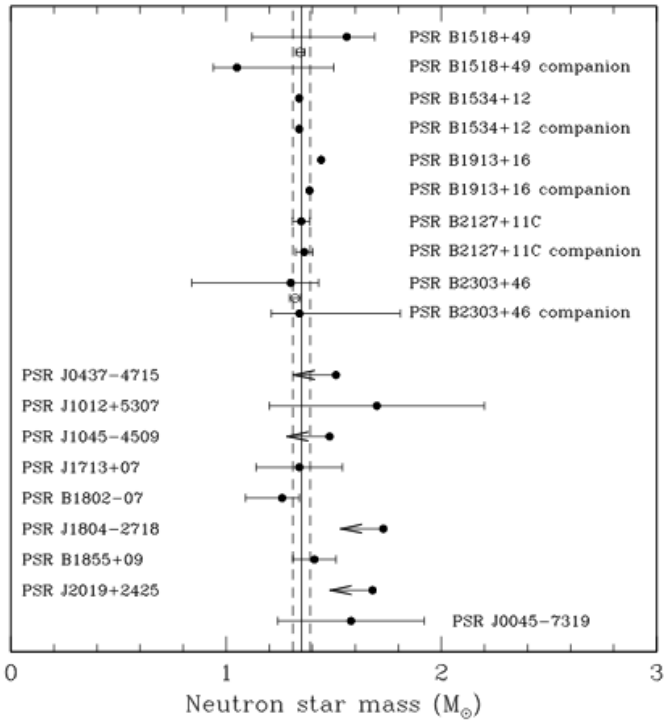

Figure 3.1: Figure showing neutron star mass results for fourteen pulsar binary systems. The dotted lines contain the region which has values agreeing with all measurements, i.e. $M = 1.35 \pm 0.4 M_{\odot}$ [28].

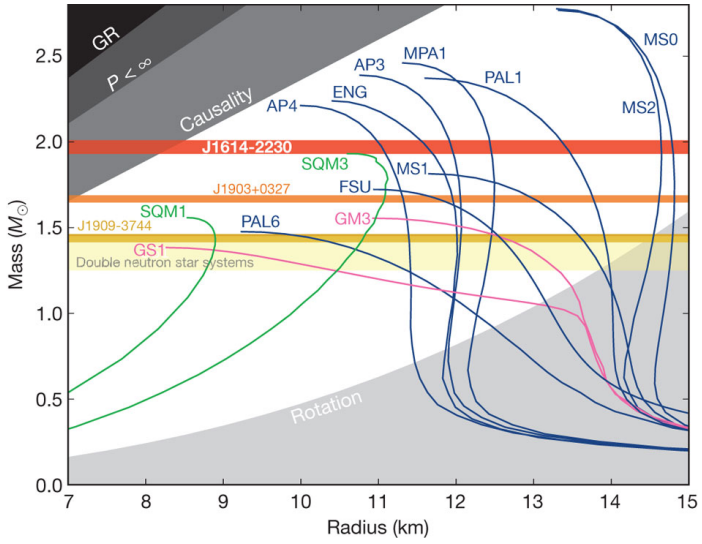

Figure 3.2: The plot shows non-rotating mass versus physical radius for several typical EOSs. For details see [30].

where K and n are real, positive constants. n is called the polytropic index. We introduce first a dimensionless variable θ, such that,

$$\rho = \rho_c \theta^n \qquad P = P_c \theta^{n+1}, \tag{3.6}$$

where ρ_c is the central density, θ is the "polytropic temperature". In terms of these new variables equation 3.4 can be written in the following form,

$$\frac{1}{r^2}\frac{d}{dr}\left(\frac{r^2 K(n+1)\rho_c^{\frac{1}{n}}}{4\pi G\rho_c}\frac{d\theta(r)}{dr}\right) = -\theta^n(r). \tag{3.7}$$

Again introducing another dimensionless variable ξ, where,

$$r = \alpha\xi, \qquad \alpha^2 = \frac{n+1}{4\pi G} K \rho_c^{\frac{1-n}{n}}. \tag{3.8}$$

Now the equation 3.7 becomes completely dimensionless,

$$\frac{1}{\xi^2}\frac{d}{d\xi}\left(\xi^2\frac{d\theta(\xi)}{d\xi}\right) = -\theta^n(\xi). \tag{3.9}$$

This is known as the Lane-Emden equation [31] for polytropic stars. This is a second order ODE, so we need two boundary conditions to solve this equation.

1. At the center of the star $\rho = \rho_c \Rightarrow \theta(r=0) = 1$.

2. At $r = 0, \frac{dP}{dr} = 0$ (because there is no mass inside zero radius). Using dimensionless variables as defined in the equations 3.6, 3.8 and using the polytropic equation of state(equation 3.5) one can show that:

$$\frac{dP}{dr} \propto \theta^n \frac{d\theta}{d\xi}$$
$$or, \left(\frac{dP}{dr}\right)_{r=0} = 0 \Rightarrow \left(\frac{d\theta}{d\xi}\right)_{\xi=0} = 0 \tag{3.10}$$

Hence hydrostatic equilibrium equations for a spherically symmetric star with polytropic equation of state reduces to Lane-Emden equation 3.9, with the following boundary conditions:

$$\theta(\xi = 0) = 1 \tag{3.11}$$

$$\left(\frac{d\theta}{d\xi}\right)_{\xi=0} = 0. \tag{3.12}$$

As both boundary conditions are at the same point, they are in fact initial conditions. Therefore, for every value of a polytropic index n, there is only one solution of equation 3.9. The solution has a physical meaning as long as $\theta \geq 0$. The surface of a polytropic star is at $\xi = \xi_1$. At $\xi = \xi_1$, $\theta = 0$ and according to equation 3.6 density and pressure also goes to zero.

One can find three analytical solutions for different values of n. These are,

1. $n = 0, \qquad \theta = 1 - \frac{\xi^2}{6}, \qquad \xi_1 = \sqrt{6} \simeq 2.45,$
2. $n = 1, \qquad \theta = \frac{\sin\xi}{\xi}, \qquad \xi_1 = \pi \simeq 3.14,$
3. $n = 5, \qquad \theta = \left(1 + \frac{\xi^2}{3}\right)^{-1/2}, \qquad \xi_1 = \infty.$

Once we know θ as a function of ξ we can calculate the mass(M) and radius(R) of the star. In fact, one can show that,

$$R = \alpha\xi_1 = \left(\frac{K}{G}\frac{n+1}{4\pi}\right)^{1/2} \rho_c^{\frac{1-n}{n}} \xi_1, \tag{3.13}$$

$$\begin{aligned} M = \int_0^R 4\pi r^2 \rho(r) dr &= 4\pi\alpha^3\rho_c \int_0^{\xi_1} \xi^2\theta^n d\xi \\ &= 4\pi \left(\frac{K}{G}\frac{n+1}{4\pi}\right)^{3/2} \rho_c^{\frac{3-n}{2n}} \left(-\xi^2\frac{d\theta}{d\xi}\right)_{\xi=\xi_1}. \end{aligned} \tag{3.14}$$

It is important to note that it is not always possible to find analytic solution of Lane-Emden equation with appropriate boundary conditions for any polytropic

equation of state. In that case, we have to solve hydrostatic equations using numerical techniques. In this thesis, we have used a complicated polytropic equation of state and we have used numerical techniques to find the density profile of a neutron star. We will discuss this in the later chapters. In this section, we have talked about non-rotating spherical polytrope in Newtonian approximation. For rotating deformed polytropes mathematical treatment will be different, e.g. see [32–34]. For a detailed discussion on polytropes and their properties see [35].

3.2.2 Atmosphere and Outer Crust

Very little is known about the surrounding atmosphere of a neutron star. In this thesis, neutron star atmosphere is not relevant. However for completeness, one can see [36, 37] and references therein.

Below this atmosphere, there exists a solid crust. Nuclear theory shows that under normal circumstances ^{56}Fe is most stable due to the maximum binding energy per nucleon. Hence the outer layer of solid crust is made of ^{56}Fe lattice. Matter density increases with decreasing radius of the neutron star. Due to large pressure and density, electrons in this region becomes relativistic and degenerate. These high energy electrons can participate in inverse beta decay process. As a result protons and electrons convert into neutrons. This regions of the crust contains lattice of heavier, neutron-rich nuclei, such as ^{78}Ni, ^{76}Fe, ^{118}Kr etc. [38–40]. Typically the crust layer exists up to a density of the order of 4×10^{11}g cm^{-3}. This density is also known as neutron drip density.

3.2.3 Inner Crust, Outer core, and Superfluidity

Below the outer crust, at densities greater than the neutron drip density, the neutrons begin to leak out of the nuclei. These neutrons form a neutron fluid which interpenetrates the crusts lattice. At nuclear density $\rho_0 = 2.7 \times 10^{14}$g cm^{-3}, the crust lattice dissolves altogether, leaving only bulk fluid, mostly made out of neutrons. However,

a small amount of ($\sim$5%) protons and electrons remain in this bulk fluid. The bulk of the neutron star is in a superfluid phase. The superfluid occurs in both the outer core and the inner crust.

Migdal pointed out the possible existence of superfluidity inside neutron star [41]. In case of electromagnetic superconductor electrons form cooper pairs due to electron phonon interaction. It is expected that nucleons in neutron star at a sufficiently high density and low temperature can also form Copper pairs due to the long-range attractive nuclear force and lead to superfluidity and superconductivity. However, nucleonic superfluidity is quite different from electron Cooper pair formation. Formation of electron Cooper pairs only happens in the presence of lattice, but nucleonic superconductivity and superfluidity do not require any lattice. Also, the excitation energy of electron Cooper pair is much smaller than the nucleonic superconductivity and superfluidity, because relevant energy scales are very different. In this thesis we are not interested in proton superconductivity inside a neutron star, so we will not discuss it further.

There exist three types of superfluids inside the neutron star. These are neutron superfluidity of type $^1S_0$ in the inner crust region, neutron superfluidity of type $^3P_2$ and proton superconductivity of type $^1S_0$ in the outer core (where $\rho \sim 2\rho_0$). As mentioned earlier because of low density, nucleons are bound inside the nucleus and are not free to move. Hence there is no superfluidity in the outer crust. In the inner crust region due to large nuclear density, inverse beta decay takes place. With more and more neutrons present, eventually, extra neutrons go to continuum states giving rise to neutron Fermi sea. Neutrons near the Fermi surface interact through long-range attractive interaction and form Cooper pairs (see, [42] and references therein). Typical temperature of a neutron star is much smaller than the estimated critical temperature for superfluidity. Although we have neutron superfluidity in the inner crust, protons are still not free and locked inside the nucleus. As we go towards the outer core, density becomes so large that neutrons and protons are free. In this high

density, neutrons become superfluid, however of different type. Due to extremely high density, short range repulsion of nuclear force will come into play, neutron superfluid will no longer be $^1S_0$. However $^3P_2$ partial wave nucleon-nucleon interaction becomes attractive at high density [43]. Thus in this region neutron superfluid is of type $^3P_2$. However, proton number is much less than that of neutron and the short range nuclear force repulsion is not dominant for protons. They will form $^1S_0$ superconductor similar to conventional superconductor [44]. The presence of superfluidity is very important for the explanation of pulsar glitch mechanism. We will discuss this topic shortly.

3.2.4 Inner Core

In the inner core density can be as large as 10^{15}g cm^{-3}. There are many hypotheses regarding the matter present in the inner core. One of the speculations is the presence of hadronic matter besides nucleons. It can contain charged mesons like pions or kaons or other hyperons such as Σ^- or Λ. However, the interaction between hyperons and nucleons and between kaons and nucleons are not well known. Hence the transition densities of nuclear matter(NM) to hadronic matter(HM) are not well understood.

Due to the attractive interaction between K^- and nucleons the kaon energy decreases with increasing density and eventually, it drops below electron chemical potential (μ_e) in NM. Hence K^- will condense [45]. Kaon condensation requires very high density core inside the neutron star. Like Kaon condensation pion condensation is also possible when their chemical potential becomes lower than μ_e [46]. For studies on the hyperonic matter see [47]. Apart from pion, kaon etc, QGP phase can also exist under extreme conditions. Exotic phase of QCD e.g 2SC phase, CFL phase can exist in the dense inner core of the neutron star. We will briefly discuss CFL phase in the next section.

3.2.5 Quark Matter and Color superconductivity

As we have already mentioned because of asymptotic freedom, at high temperature and/or high density, QCD phases are readily described in terms of quarks and gluons. In QCD phase diagram (figure 1.6) at low temperature and high density, there is a first order phase transition line separating hadronic phase (low chemical potential phase) and a degenerate system of deconfined quarks and gluons (high chemical potential phase) [48–54]. Speculations about the existence of a quark matter phase at high density was made a long time back even before the understanding of asymptotic freedom of QCD [55–59].

At very high densities (far to the right on the phase diagram in figure 1.6 , in the deconfined phase of quarks and gluons) the ground state of QCD is the color-flavor-locked (CFL) color superconductor [48, 49, 60–67], for review see [68–78]. In this high density regime deconfined quarks fill the Fermi sea and the interesting physics is that of quarks near their Fermi surface. Quark-quark scattering amplitude in the one gluon exchange approximation is proportional to [78]:

$$\sum_{A=1}^{N_c^2-1} T^A_{aa'} T^A_{b'b} = -\frac{N_c+1}{4N_c}(\delta_{aa'}\delta_{b'b} - \delta_{ab'}\delta_{a'b}) + \frac{N_c-1}{4N_c}(\delta_{aa'}\delta_{b'b} + \delta_{ab'}\delta_{a'b}). \qquad (3.15)$$

In the quark-quark interaction (equation 3.15) first term corresponds to attractive antitriplet channel, which is antisymmetric, responsible for Cooper pairing, whereas the second term corresponds to repulsive sextet channel, which is symmetric. Because a quark-quark condensate cannot be a color singlet object, the quark-quark BCS condensate breaks color gauge symmetry, hence it is called color superconductivity. At very high densities along with the u and d quarks, strange quark mass can also be neglected and flavor $SU(3)$ is a good symmetry of the QCD Lagrangian (recall chiral symmetry). $SU(3)$ color and $SU(3)$ flavor both are important for the existence of CFL phase. However at lower densities strange quark mass can not be neglected, hence $SU(3)$ flavor symmetry is explicitly broken. However quark-quark pairing only

requires attractive channel, which is possible even in non-CFL phase. Any quark-quark pairing breaks color symmetry so the system remains as an "unlock" non-CFL color superconductor. Thus moving down the chemical potential axis in QCD phase diagram (figure 1.6) from very high density towards relatively low density, there is a possibility of "unlocking" transition [53, 79–84].

It is important to note that non-CFL phases can be of different nature depending upon the symmetry properties of quark-quark condensate. 2SC color superconductivity, crystalline color superconductivity, gapless 2SC(g2SC) etc are candidates for non-CFL superconductivity. The properties of the vacuum are very different in these phases. In 2SC phase only two flavors (u, d) participate in Cooper instability. The unpaired massive strange quarks introduce a $U(1)_S$ symmetry. In this phase $SU(3)_c$ gauge symmetry is broken down to $SU(2)_{rg}$ red-green gauge symmetry. No global symmetries are broken in a 2SC pairing. The condensate is symmetric under $SU(2)_L \times SU(2)_R$ flavor symmetry. However, baryon number symmetry $U(1)_B$ is broken to $U(1)_{\tilde{B}}$, where $\tilde{B}$ is a linear combination of B (baryon number) and T_8 (color generator). Electromagnetism is also partially broken in a complicated manner, for details see [74]. 2SC quark matter is a color superconductor but it is neither a superfluid nor an electromagnetic superconductor. In the crystalline phase, Cooper pairs forms with non-zero total momentum. Condensates of this type spontaneously break translation and rotational invariance, leading to gaps which vary periodically in a crystalline pattern. For details of these exotic phases see [74, 78] and references therein.

At extremely high densities, the quarks at the Fermi surface have very large momenta and their interactions are asymptotically weak. Due to medium effects long range interactions are screened, hence no bad infrared behavior. Due to these properties of QCD a rigorous theoretical analysis of the QCD ground state is possible under extreme condition [60, 80, 85–92]. This analysis predicts that at an asymptotically high density where u, d and s quarks are massless, color flavor locked (CFL)

is preferred ground state of QCD. All nine quarks (three flavors each comes in three colors) together form diquark condensate of the form [64, 73] ,

$$\langle \psi_{i\alpha a}(\vec{x})\psi_{j\beta b}(\vec{x})\rangle \propto \triangle_0 \epsilon_{abA}\epsilon_{ijA}(\mathcal{C}\gamma_5)_{\alpha\beta}, \tag{3.16}$$

where (α, β) are spin indices, (a, b) are color indices, (i, j) are flavor indices, index A is summed and it locks color and flavor in the vacuum. $\mathcal{C}$ is the Dirac chrage conjugation matrix and $\triangle_0$ is the CFL gap calculated in the asymptotic limit for one gluon exchange. The ϵ_{abA} term indicates that the condensate is an $SU(3)_{color}$ antitriplet. We have already mentioned that the antitriplet channel is attractive and gives rise to quark-quark condensate. The ϵ_{ijA} term indicates that the condensate is an $SU(3)$ flavor antitriplet. One can show that the condensate is rotationally invariant, parity even and spin singlet. Symmetry breaking pattern of CFL phase is:

$$G \equiv SU(3)_{color} \times SU(3)_L \times SU(3)_R \times U(1)_B \rightarrow H \equiv SU(3)_{color+L+R} \times Z_2, \tag{3.17}$$

where the first group of G is the color gauge symmetry, $SU(3)_L$ and $SU(3)_R$ belong to chiral symmetry and the last factor is due to baryon number conservation. Along with these symmetries, there is also electromagnetism $U(1)_Q$ which is not written here. Due to the formation of condensate the color and chiral flavor symmetries are broken to a diagonal global symmetry group $SU(3)_{color+L+R}$. Chiral symmetry is spontaneously broken and there is an octet of massless pseudoscalar bosons associated with eight broken generators. Breaking of $SU(3)_{color}$ and $U(1)_Q$ is complicated. The vacuum is not invariant under original $U(1)_Q$, however, there is a residual $U(1)_{\tilde{Q}}$ symmetry remains after the symmetry breaking. $U(1)_{\tilde{Q}}$ is a combination of original $U(1)_Q$ and one of the diagonal $SU(3)_{color}$ generator $T_8 \equiv \frac{1}{\sqrt{3}}$ diagonal$(-2, 1, 1)$ in (r, g, b) color space. Vacuum is symmetric under the new $U(1)_{\tilde{Q}}$ symmetry and the corresponding conserved charge is $\tilde{Q} = Q + \frac{1}{\sqrt{3}}T_8$. This new rotated photon is massless and can be represented as $A^*_\mu = \cos(\alpha)A_\mu + \sin(\alpha)G^8_\mu$, where A_μ and G^8_μ are the gauge fields associated with the original $U(1)_Q$ and T_8 color generator respectively. Mixing angle α is given by $\cos(\alpha) = g/\sqrt{e^2/3 + g^2} \sim 1$. So the new photon is almost the usual photon with a very small admixture of the gluon. The orthogonal combination

of A^*_μ and the other seven QCD gauge fields becomes massive after the symmetry breaking, due to Meissener-Higgs mechanism. Baryon number is broken to a discrete Z_2 symmetry. Breaking of $U(1)_B \to Z_2$ has non-trivial topological implication. This symmetry breaking gives rise to superfluid vortices. Presence of these vortices can have non-trivial effects on neutron star dynamics and also on low energy heavy ion collisions at FAIR and NICA, see [93, 94].

3.3 Pulsar Glitch Mechanism

The rotation period of pulsars increases slowly. It was pointed out that the rotational energy of a rotating neutron star would decrease due to magnetic dipole radiation, resulting in the pulsar slowing down. This spin down is gradual and largely predictable. However, there exist timing irregularities such as a "Glitch", when rotational frequency of pulsar exhibits a sudden increase, followed by a slow exponential relaxation. The relaxation time scale can vary from days to months for different pulsars. The following figure 3.3 shows the observational data of pulsar glitch of Vela pulsar. The standard theory of pulsar glitch mechanism in intimately related with nuclear superfluidity inside the neutron stars. Superfluid vortex pinning and vortex creep model is widely used for the explanation of glitch mechanism. Two fluid model of a neutron star which is based upon the existence of superfluid phase in the interior of a neutron star can explain the post-glitch relaxation mechanism. Apart from this there are other models which were also proposed to explain glitch phenomenon, e.g. crust driven glitch mechanism by Ruderman in 1976 [95], thermally driven glitch model by Link and Epstein in 1996 [96], flux-tube model by Ruderman, Zhu, and Chen in 1998 [97], centrifugal buoyancy model by Carter, Langlois, and Sedrakian in 2000 [98] etc. In this section, we will discuss the two fluid model and vortex creep model for glitch mechanism. For a detailed discussion on pulsar glitch mechanisms and some other topics which we have already discussed, see [1, 42] and references therein. QCD phase transitions can also play a very important role in pulsar glitch mechanism [93] and this is one of the main topics of this thesis. After introducing

the glitch mechanism we will discuss how QCD phase transitions can affect pulsar dynamics in a later chapter. In this section we will first review the basic physics of superfluid vortices, then we will discuss the physics of vortex creep model of glitch mechanism and two fluid model of glitch relaxation.

3.3.1 Superfluid Vortex

The bulk of the neutron star is believed to be in a superfluid state. The superfluidity occurs in the outer core and the inner crust. Superfluid is a macroscopic coherent quantum system. Superfluidity was first observed in helium II. Macroscopic behaviour of superfluid can be described by a condensate wave function. In the interior of neutron star due to Cooper instability arising from the attractive nuclear force, superfluid neutrons are paired together like Cooper pairs in a superconductor. Paired neutrons are bosons and the fluid obtains bosonic properties giving rise to Bose Einstein Condensate. The superfluid condensate can be described by a complex order parameter,

$$\Psi(\vec{r},t) = \Psi_0(\vec{r},t)e^{iS(\vec{r},t)}, \tag{3.18}$$

$|\Psi_0|^2$ gives the density of superfluid and the superfluid velocity can be given as,

$$\vec{v_s} = \frac{\hbar}{m_{np}}\nabla S. \tag{3.19}$$

S is the phase of the condensate and m_{np} is the mass of the neutron pair. Using the above equation one can reach Landau criterion of superfluidity,

$$\nabla \times \vec{v_s} = 0, \quad \text{if} \quad \vec{v_s} \neq 0, \tag{3.20}$$

detailed derivation of this criterion can be found in any standard textbook, e.g. see [99].

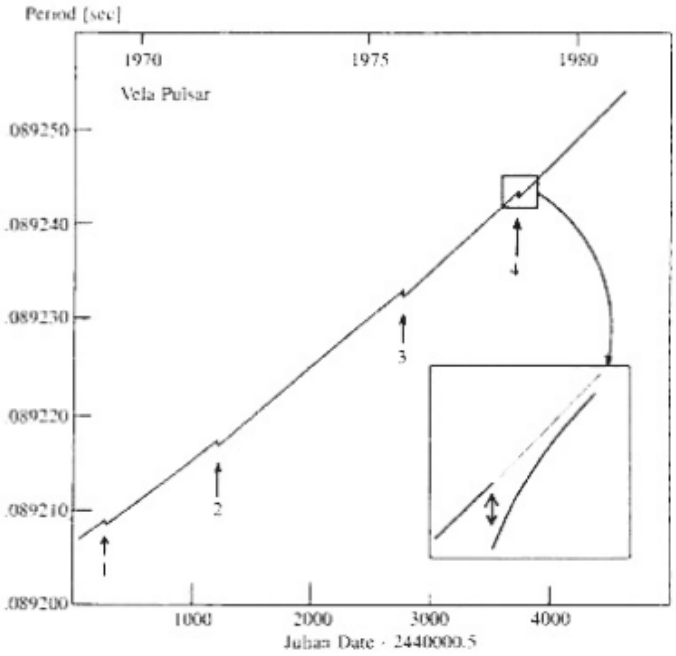

Figure 3.3: Observed period of Pulsar Vela. x-axis in given in Julian year and y axis gives the period showing the sudden decrease in time period or increase in rotational frequency. Inset figure shows the exponential relaxation. This figure is taken from [42].

Landau's criterion is important for the rotation of the superfluid. The circulation which is a measure of fluid rotation is defined as,

$$\kappa = \oint_L \vec{v_s}.d\vec{l}, \tag{3.21}$$

where L is the integration contour, which is entirely in the superfluid. Using Stokes theorem and the Landau criterion in equation3.21 we get,

$$\kappa = \oint_L \vec{v_s}.d\vec{l} = \int_A (\nabla \times \vec{v_s}).d\vec{A} = 0. \tag{3.22}$$

Equation 3.22 tells us that due to the Landau criterion pure superfluid can not have circulation, hence no rotation. Landau criterion and the observed rotation of superfluid can be reconciled by allowing a multiply connected region inside the integration contour. This gives rise to the concept of vortex core, which is a hole in the superfluid having cylindrical symmetry and either empty of fluid or containing normal fluid. For the vortex core $\nabla \times \vec{v_s} \neq 0$. The vortex core is surrounded by pure superfluid matter having irrotational flow.

Using equation 3.21 and 3.19 we get,

$$\kappa = \frac{\hbar}{m_{np}} \oint_L \nabla S.dl = \frac{\hbar}{m_{np}} (\Delta S)_L. \tag{3.23}$$

Since the wavefunction in equation 3.18 is singled valued S can only be either 0 or integer multiple of 2π. Hence,

$$\kappa = n\frac{h}{m_{np}}, \tag{3.24}$$

for $n = 0$ we get back Landau criterion. $n \neq 0$ gives non-zero circulation applicable for vortices. Due to the criterion given in equation 3.24 superfluid circulation is quantized. Thus rotation of superfluid is manifested by quantized vortices. In fact one can also show that both velocity and angular momentum of the fluid around a vortex line are quantized. These quantized vortices exist in HeII and also in rotating

neutron star due to the superfluid phase in the interior. Note that in this case we have considered the vortex formation entirely due to the rotation of the superfluid. However these superfluid vortices can also be formed via Kibble mechanism in a normal to superfluid transition [100].

3.3.2 Vortex creep model

The presence of the superfluid vortices has been exploited in one of the most recognized models of glitch mechanism, known as vortex pinning and vortex creep, model, first proposed by Anderson and Itoh in 1975 [101]. The basic idea of vortex creep model is pinning and unpinning of the superfluid vortices in the inner crust layer of a neutron star and the transfer of angular momentum from superfluid core to non-superfluid crust. We have already shown that for rotating superfluid we have quantized vortices having quantized rotation. Thus, for a fixed number of vortices, the rotation frequency of superfluid is also fixed. It has been shown that it is energetically favorable for the vortex to pin nucleus in the crust. As we have already discussed due to radiation energy loss rotational frequency of the crust layer decrease with time. However, the rotation of the superfluid part remains the same. This differential rotation between the core and the crust gives rise to a magnus force which tries to unpin the vortices from the crust. Pinning force can sustain some differential rotation and it acts as an angular momentum reservoir. When the magnus force exceeds the pinning force unpinning occurs, as a result huge angular momentum will be transferred to crust, thus the angular momentum of the crust increases suddenly resulting in a glitch.

3.3.3 Post glitch relaxation: Two component model

Like the glitch mechanism, relaxation after the glitch can also be explained in the presence of superfluid core in the interior of a neutron star. Two component model

was proposed [102]to predict the post glitch behavior of a pulsar. It is important to note that the observed rotation frequency of a neutron star is the frequency of crust layer. We do not have a direct observation on the frequency of superfluid core. The two components are the solid crust and the nuclear superfluid in the core, having moment of inertia I_c and I_n and angular velocities Ω_c and Ω_n respectively. The angular acceleration of crust is given by the total torque divided by its moment of inertia,

$$\dot{\Omega_c} = \frac{-\alpha - N_{int}}{I_c}, \tag{3.25}$$

where α and N_{int} are external torque and internal torque respectively. External torque term is arising from the electromagnetic braking of the pulsar. Internal torque is due to coupling between crust layer and superfluid core and can be assumed to be of the following form [103],

$$N_{int} = I_n\dot{\Omega_n} = I_c\frac{\Omega_c - \Omega_n}{\tau_c}. \tag{3.26}$$

Hence equations of motion of the two components after a glitch event:

$$I_c\dot{\Omega_c} = -\alpha - I_c\frac{\Omega_c - \Omega_n}{\tau_c}, \tag{3.27}$$

$$I_n\dot{\Omega_n} = I_c\frac{\Omega_c - \Omega_n}{\tau_c}, \tag{3.28}$$

here τ_c is the crust-core coupling time, which is model dependent. In this analysis I_c, I_n, α, τ_c are constant over the timescales of interest. Equation 3.27 and 3.28 can be solved to give (for details see [19]),

$$\Omega_c = -\frac{\alpha}{I}t + \frac{I_n}{I}Ae^{-t/\tau} + B, \tag{3.29}$$

$$\Omega_n = \Omega_c - Ae^{-t/\tau} + \frac{\alpha\tau}{I_c}, \tag{3.30}$$

where $I = I_c + I_n$, $\tau = \tau_c I_n/I$. A and B are integration constants. One can verify that Ω_c and Ω_n as given in the equations 3.29, 3.30, actually satisfy equation 3.27 and 3.28. Using equation 3.30 it is straight forward to show that, the steady state solution ($t/\tau \to \infty$) is,

$$\alpha = \frac{I_c}{\tau}(\Omega_n - \Omega_c). \tag{3.31}$$

If the integration constants are known in terms of $\Delta\Omega_0$ (i.e. the absolute magnitude of the glitch) and Q (known as 'healing parameters'), then one can get the following equation,

$$\Omega_c(t) = \Omega_0(t) + \Delta\Omega_0[Qe^{-t/\tau} + (1 - Q)], \tag{3.32}$$

where Ω_0 is the frequency without a glitch. The healing parameter Q describes the degree to which the angular velocity relaxes back towards its extrapolated value. When $Q = 1$, we have $\Omega_c(t) \to \Omega_0(t)$ as $t \to \infty$. The behavior indicated by equation 3.32 is illustrated in the figure 3.4. A crucial test for this simple phenomenological model is to test whether or not the fitted post glitch functions give the same values of Q and τ for all the glitches of a single pulsar. Although this model was successful, however plenty of observation data show violations of the two-component model [104].

Vortex creep model of glitch and two component model of post glitch relaxation tells us that microphysics of superfluidity is necessary to understand properties of neutron stars.

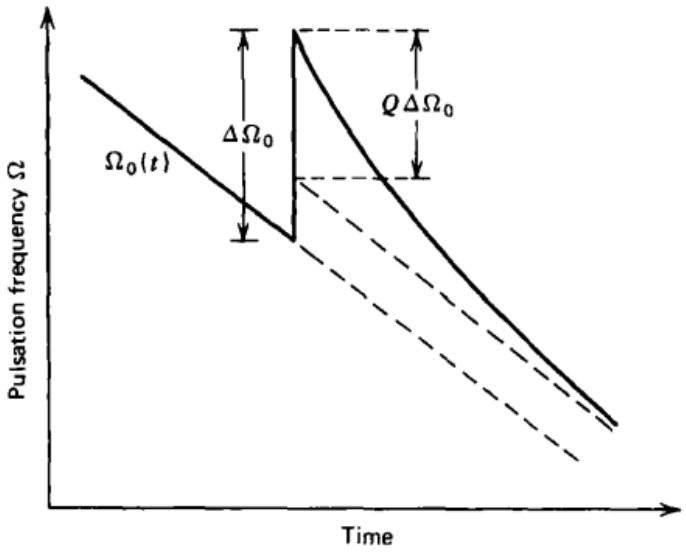

Figure 3.4: Time dependence of the pulsar angular frequency $\Omega_c(t)$, followed by a glitch. This figure is taken from [19].This figure also shows exponential relaxation after pulsar glitch from two-components model.

3.4 Anti-glitch: a new observation

Like conventional radio pulsars, magnetars also exhibit glitches phenomenon. There are several hundred observed glitches in radio pulsars and magnetars (magnetars have huge magnetic field) where astronomers have observed sudden spin-up (increase in the angular velocity) of the star. As we discussed above, a possible explanation of this glitch phenomenon is the vortex creep model which assumes the rotation of superfluid in the interior is faster than the crust. However, Archibald and collaborators have reported an 'anti-glitch' [105]. Instead of an abrupt spin-up, the star abruptly spun down. Astronomers have searched for surrounding afterglow, which rules out the possibility of sudden particle outflow that could have carried off the angular momentum. Observation of anti-glitch put forward a great challenge for the theorists. The well-tested models like vortex creep, model, two component model of pulsar glitch necessarily requires a superfluid core. In these model superfluid rotation is larger than the crust rotation, which is very natural to assume. These simple models cannot explain the anti-glitch. However some of the possible solutions of anti-glitch

have already been proposed, see [106–108]. Though, some of the models also assume superfluid core but the models are complicated with respect to the vortex creep or two component model e.g. one models [107] assumes that the collision of a small solid body with a pulsar can lead to an observable glitch/anti-glitch. Although theorists are trying to get the possible explanation of the anti-glitch phenomenon, it will be nice to have a simple unified framework for glitch/anti-glitch mechanism. In this thesis, we will introduce a simple unified model, which can give rise to glitch as well as anti-glitch.

Bibliography

[1] G. B. McDonald, "A Review of Pular Glitch Mechanisms", University of Johannesburg, 2007.

[2] F. Shu, "The Physical Universe: An Introduction to Astronomy", University Science Books, Sausalito, California, 1989.

[3] Ágnes Nyíri, "Quark-Gluon Plasma in Neutron Stars", M. Phil. Thesis 2001, Theoretical and Computational Physics Section, Dept. of Physics, University of Bergen.

[4] Martin Urbanec, "Equations of state and structure of neutron stars", 2010, Silesian University in Opava, Faculty of Philosophy and Science, Institute of Physics.

[5] A. Burrows and J. M. Lattimer, Astrophys. J. **307**, 178 (1986).

[6] J. Lattimer and M. Prakash, Phys. Rep., **442**, 109-165 (2007); arXiv:astro-ph/0612440.

[7] P. Ghosh, "Rotation and Accretion Powered Pulsars", World Scientific, Singapore, 2007.

[8] M. Kramer and N. Wex, Class. Quantum Grav., **26**, 073001 (2009).

[9] F. M. Walter, S. J. Wolk and R. Neuhäuser, Nature, **379**, pp. 233235, January 1996.

[10] W. Baade and F. Zwicky, Phys. Rev., **45**, 138 (1934).

[11] J. Chadwick, Nature, **129**, 312 (1932).

[12] L. D. Landau, Phys. Z. sowietunion,**1**, 285 (1932).

[13] R. X. Xu, ACTA Astronomica Sinica,**44**, 245 (2003).

[14] J. Oppenheiemer and G. Volkoff, Phys. Rev., **55**, 374 (1939).

[15] R. Tolman, Phys. Rev., **55**, 364 (1939).

[16] A. G. W. Cameron ApJ,**130**, 916 (1959).

[17] C. E. Rhoades, R. Ruffini, Physical Review Letters, **32**, 324 (1974).

[18] R. Giacconi, H. Gursky, F. R. Paolini, B. B. Rossi, Physical Review Letters, **9**, 439 (1962).

[19] S. L. Shapiro and S. A. Teukolsky, " Black holes, white dwarfs and neutron stars", John Wilery and Sons, New York, 1983.

[20] P. Haensel, A. Y. Potekhin, D. G. Yakovlev, "Neutron Stars 1: Equation of State and Structure" , volume 326 of Astrophysics and Space Science Library, 2007.

[21] J. A. Wheeler, Ann. Rev. Astron. and Astrophys. **4**, 428 (1966).

[22] Y. B. Zeldovich and I. D. Novikov, "Relativistic astrophysics. Vol.1: Stars and relativity", University of Chicago Press, 1971.

[23] A. G. Lyne and F. Graham-Smith, "Pulsar astronomy", Cambridge University Press, 1998.

[24] F. Pacini, Nature, **216**, 567 (1967).

[25] A. Hewish, S. J. Bell, J. D. H. Pilkington, P. F. Scott and R. A. Collins, Nature, **217**, 709 (1968); J. D. H. Pilkington, A. Hewish, S. J. Bell and T. W. Cole, Nature, **218**, 126 (1968).

[26] J. M. Comella , H. D. Craft, R. V. E. Lovelace, J. M. Sutton, Nature, **221**, 453 (1969).

[27] T. Gold, Nature,**218**, 731 (1968).

[28] S. E. Thorsett and D. Chakrabarty, ApJ, **512**, 288 (1999).

[29] J. M. Lattimer and M. Prakash, ApJ, **550**, 426 (2001).

[30] P. B. Demorest, T. Pennucci, S. M. Ransom, M. S. E. Roberts and J. W. T. Hessels, Nature, **467**, 1081 (2010).

[31] H. J. Lane, Am. J. Sci., **50**, 57-74 (1870).

[32] S. Chandrasekhar, MNRAS, **93**, 390 (1933).

[33] R. A. James, Astrophysical Journal, **140**, 552 (1964).

[34] F. F. Monaghan and I. W. Roxburgh, MNRAS,**131**, 13 (1965).

[35] S. Chandrasekhar, "An Introduction to the Study of Stellar Structure", Dover Publications, Inc. (1939).

[36] M. C. Miller, MNRAS, **255**,129 (1992).

[37] M. Rajagopal, R. W. Romani and M. C. Miller, The Astrophysical Journal, **479**, 347 (1997).

[38] C.J. Pethick, D. G. Ravenhall, NYASA, **647**, 503 (1991).

[39] C. P. Lorenz, D. G. Ravenhall and C. J. Pethick, Phys.Rev.Lett., **70**, 379 (1993).

[40] C.J. Pethick, D. G. Ravenhall and C. P. Lorenz, Nucl. Phys. **A 584**, 675 (1995).

[41] A. B. Migdal, Soviet Physics JETP **10**, 176 (1960).

[42] K. W. Lo,"Neutron Star and Superfluidity", Department of Physics, University of Illinois at Urbana-Champaign, 2010.

[43] Ø. Elgarøy, L. Engvik, M. Hjorth-Jensen and E. Osnes, Nucl. Phys. A607, 425 (1996).

[44] J. M. C. Chen, J. W. Clark, R. D. Dave and V. V. Khodel, Nucl. Phys. **A555**, 59 (1993).

[45] D. B. Kaplan abd A. E. Nelson, Phys. Lett. **B 291**, 57 (1986); G. Brown, C. Lee, M. Rho and V. Thorsson, Nucl. phys. **A 572**, 693 (1994); T. Waas, M. Rho and W. Weise, Nucl. Phys. **A 617**, 449 (1997).

[46] A. B. Migdal, ReV. Mod. Phys. **50**, 107 (1978); T. Kunihiro, T. Muto, T. Takatsuka, R. Tamagaki and T. Tatumi, Prog. Theor. Phys. supplement, **112**, 1 (1993).

[47] Th. A. Rijiken, V. G. J. Stokes and Y. Yamamoto, phys. Rev. **C 59**, 21 (1998); V. G. J. Stokes and T. S. H. Lee, Phys. Rev. **C 60**, 024006 (1999).

[48] M. Alford, K. Rajagopal and F. Wilczek, Phys. Lett. **B422**, 247 (1998) (hep-ph/9711395).

[49] R. Rapp, T. Sch afer, E. V. Shuryak and M. Velkovsky, Phys. Rev. Lett.**81**, 53 (1998) (hep-ph/9711396).

[50] J. Berges and K. Rajagopal, Nucl. Phys. **B 538**, 215 (1999) (hep-ph/9804233).

[51] M. A. Halasz, A. D. Jackson, R. E. Shrock, M. A. Stephanov, and J. J. Verbaarschot, Phys. Rev. **D 58**, 096007 (1998).

[52] M. Stephanov, Phys. Rev. Lett.**76** 4472 (1996).

[53] M. Buballa and M. Oertel, hep-ph/0202098; Nucl. Phys. **A 703**, 770 (2002) (hep-ph/0109095).

[54] A. Barducci, R. Casalbuoni, S. DeCurtis, R. Gatto and G. Pettini, Phys. Lett. **B231**, 463 (1989); Phys. Rev. **D41**, 1610 (1990); S. P. Klevansky, Rev. Mod. Phys.**64**, 649 (1992); A. Barducci, R. Casalbuoni, G. Pettini and R. Gatto, Phys. Rev. **D49**, 426 (1994).

[55] Boccaletti, D., V. de Sabbata and C. Gualdi, Nuovo Cim. **45**, 513 (1966).

[56] P. Carruthers, Coll. Phen.**1**, 147 (1973)

[57] N. Itoh, Prog. Theor. Phys. **44**, 291 (1970).

[58] D. D. Ivanenko and D. F. Kurdgelaidze, Astrophysics **1(4)**, 479 (1965).

[59] F. Pacini, Nature **209**, 389 (1966).

[60] B. C. Barrois, Nucl. Phys. **B129**, 390 (1977); B. C. Barrois, "Non-perturbative effects in dense quark matter", 1979, Ph.D. thesis, California Institute of Technology, Pasadena, California, UMI 79-04847.

[61] Frautschi, S. C., 1978, presented at Workshop on Hadronic Matter at Extreme Energy Density, Erice, Italy, Oct 13-21, 1978.

[62] D. Bailin, and A. Love, J. Phys. **A12**, L283 (1979); D. Bailin, and A. Love, Phys. Rept.**107**, 325 (1984).

[63] M. Iwasaki, Prog. Theor. Phys. Suppl. **120**, 187 (1995); M. Iwasaki, and T. Iwado, Phys. Lett. **B350**, 163 (1995).

[64] M. Alford, K. Rajagopal and F. Wilczek, Nucl. Phys. **B537**, 443 (1999) (hep-ph/9804403).

[65] R. Rapp, T. Schafer, E. V. Shuryak and M. Velkovsky, Annals Phys.**280**, 35 (2000) (hep-ph/9904353).

[66] T. Schafer and F. Wilczek, Phys. Rev. Lett.**82**, 3956 (1999) (hep-ph/9811473)

[67] M. G. Alford, Ann. Rev. Nucl. Part. Sci.**51** (2001) 131 (hep-ph/0102047);

[68] Alford, M. G., and K. Rajagopal, arXiv: hep-ph/0606157, K. Rajagopal and F. Wilczek, hep-ph/0011333;

[69] T. Schafer and E. V. Shuryak, Lect. Notes Phys. **578**, 203 (2001) (nucl-th/0010049);

[70] D. K. Hong, Acta Phys. Polon. **B 32**, 1253 (2001) (hep-ph/0101025);

[71] S. D. Hsu, hep-ph/0003140;

[72] D. H. Rischke and R. D. Pisarski, nucl-th/0004016;

[73] J. A. Bowers, hep-ph/0305301;

[74] M. G. Alford, A. Schmitt, K. Rajagopal and T. Schafer, arXiv: 0709.4635;

[75] M. Buballa, Phys. Rept. **407**, 205 (2005);

[76] M. Huang, Int. J. Mod. Phys. **E14**, 675 (2005);

[77] D. H. Rischke,Prog. Part. Nucl. Phys. **52**, 197 (2004).

[78] I. A. Shovkovy, arXiv: nucl-th/0410091

[79] M. Alford, J. Berges and K. Rajagopal, Nucl. Phys. **B558**, 219 (1999) (hep-ph/9903502).

[80] T. Sch afer and F. Wilczek, Phys. Rev. **D60**, 074014 (1999) (hep-ph/9903503).

[81] K. Rajagopal and F. Wilczek, Phys. Rev. Lett.**86**, 3492 (2001) (hep-ph/0012039).

[82] P. Bedaque, Nucl. Phys. **A697**, 569 (2002) (hep-ph/9910247).

[83] M. G. Alford, K. Rajagopal, S. Reddy and F. Wilczek, Phys. Rev. **D64**, 074017 (2001) (hep-ph/0105009).

[84] M. Alford and K. Rajagopal, JHEP **0206**, 031 (2002) (hep-ph/0204001).

[85] D. T. Son, Phys. Rev. **D59**, 094019 (1999) (hep-ph/9812287).

[86] R. D. Pisarski and D. H. Rischke, Phys. Rev. Lett. **83**, 37 (1999) (nucl-th/9811104); Phys. Rev.**D60**, 094013 (1999) (nucl-th/9903023); Phys. Rev.**D61**, 051501 (2000) (nucl-th/9907041); R. D. Pisarski and D. H. Rischke, Phys. Rev.**D61**, 074017 (2000) (nucl-th/9910056).

[87] I. A. Shovkovy and L. C. Wijewardhana, Phys. Lett. **B470**, 189 (1999) (hep-ph/9910225).

[88] D. K. Hong, Phys. Lett.**B473**, 118 (2000) [hep-ph/9812510]; Nucl. Phys.**B582**, 451 (2000) [hep-ph/9905523]; D. K. Hong, V. A. Miransky, I. A. Shovkovy and L. C. Wijewardhana, Phys. Rev. **D61**, 056001 (2000); erratum Phys. Rev. D62, 059903 (2000) [hep-ph/9906478].

[89] W. E. Brown, J. T. Liu and H. Ren, Phys. Rev. **D61**, 114012 (2000) [hep-ph/9908248]; Phys. Rev. **D62**, 054016 (2000) [hep-ph/9912409]; Phys. Rev.**D62**, 054013 (2000) [hep-ph/0003199].

[90] S. D. Hsu and M. Schwetz, Nucl. Phys. **B572**, 211 (2000) [hep-ph/9908310].

[91] T. Sch afer, Nucl. Phys. **B575**, 269 (2000) [hep-ph/9909574].

[92] S. Beane, P. Bedaque and M. Savage, Nucl. Phys. **A688**, 931 (2001) [nucl-th/0004013]; S. Beane and P. Bedaque, Phys. Rev. **D62**. 117502 (2000) [nucl-th/0005052].

[93] P. Bagchi, A. Das, B. Layek and A. M. Srivastava, Phys.Lett. **B 747**, 120 (2015) [arXiv:1506.03287]; P. Bagchi, A. Das, B. Layek and A. M. Srivastava, arXiv: 1412.4279.

[94] A. Das, S. S. Dave, S. De and A. M. Srivastava, arXiv:1607.00480.

[95] M. Ruderman, The Astrophysical Journal, **203**, 213 (1976); M. Ruderman, The Astrophysical Journal, **366**, 261 (1991).

[96] B. K. Link, R. I. Epstein, The Astrophysical Journal, **457**, 844 (1996).

[97] M. Ruderman, T. Zhu, K. Chen,The Astrophysical Journal, **492**, 267 (1998).

[98] B. Carter, D. Langlois and D. M. Sedrakian, **A& A, 361**, 795 (2000).

[99] L. D. Landau, E. M. Lifshitz, "Fluid Mechanics", 2nd Edition, (Pergamon Press) (1987).

[100] T.W.B. Kibble, J. Phys. **A 9**, 1387 (1976), Phys. Rep. **67**, 183 (1980).

[101] P. W. Anderson, N. Itoh, Nature **256**, 25 (1975).

[102] G. Baym, C. Pethick, D. Pines, M. Ruderman, Nature **224**, 872 (1969).

[103] D. Pines, M. A. Alpar, Nature **316**, 27 (1985).

[104] P. E. Boynton,Prac. IAU Symp. No. **95**, 279 (1981).

[105] R. F. Archibald, V. M. Kaspi, C. Y. Ng, K. N. Gourgouliatos, D. Tsang, P. Scholz, A. P. Beardmore, N. Gehrels, J. A. Kennea, Nature **497**, 591 (2013).

[106] C. Thompson et al. Astrophys. J.**543**, 340 (2000); R. C. Duncan, Nature **497**, 574 (2013).

[107] Y. F. Huang, J. J. Geng, Z. B. Zhang, arXiv:1506.04888

[108] E. Kantor, M. Gusakov, arXiv: 1411.2777

Chapter 4

Effects of Phase Transition induced density fluctuations on pulsar dynamics

In the chapter 3 we have discussed the physics of neutron stars. The core of the neutron star can have deconfined QCD matter and some other exotic QCD phases. However we can not observe these phases directly, but these phases can affect the dynamics of a neutron star. Thus analyzing neutron star dynamics we can extract information regarding the different QCD matter in the core. We have also introduced the phenomenon of pulsar glitch and antiglitch. Superfluid phase in the core of the pulsar plays a very important role in the glitch mechanism. Superfluid vortex creep model is a well established model of glitch mechanism. However this simple models does not account for anti-glitches. Although new models are proposed to explain the observation of anti-glitches, these models are not simple and elegant as the vortex creep model. These models also do not explain glitch and anti-glitch in a unified simple framework. In this chapter we introduce a relatively simple way by which one can probe the interior of the neutron star. During the evolution of a pulsar, various phase transitions may occur in its dense interior, such as superfluid transition, as well as transition to various exotic phases of quantum chromodynamics (QCD). We propose a technique which allows to probe these phases and associated transitions by

detecting changes in rotation of the star arising from density changes and fluctuations during the transition affecting stars moment of inertia. In this chapter we have also discussed how QCD phase transition and different QCD phases at extremely high density can explain phenomena of glitch and anti-glitch in a simple unified manner.

4.1 Introduction

The core of an astrophysical compact dense object, such as a neutron star, provides physical conditions where transition to exotic phases of quantum chromo dynamics (QCD) [1] may be possible. Superfluid phases of nucleons are also believed to exist inside neutron stars with vortex de-pinning associated with glitches (though it may not provide a viable explanation for anti-glitches). In this chapter we propose a technique to probe the dynamical phenomena happening inside the neutron star, which may also account for glitches and anti glitches in a unified framework.

We consider density fluctuations which invariably arise in any phase transition. We show that even with relatively very small magnitudes, these density fluctuations may be observable with accurate measurement of pulsar timings which can detect very minute changes in the moment of inertia (MI) of the pulsar. This provides a very sensitive probe for density changes and density fluctuations (especially due to formation of topological defects) during phase transitions in the pulsar core. Non-zero off-diagonal components of moment of inertia arising from density fluctuations imply that a spinning neutron star will develop wobble leading to modulation of the peak intensity of pulses (as the direction of the beam pointing towards earth undergoes additional modulation). This is a unique, falsifiable, prediction of our model, that rapid changes in pulsar timings should, most often, be associated with modulations in changes in peak pulse intensity. It is important to note that the vortex de-pinning model of glitches is not expected to lead to additional wobble as the change in rotation caused by de-pinning of vortex clusters remains along the rotation axis. Density fluctuations will also lead to development of rapidly changing quadrupole moment which can provide a new source for gravitational wave emission due to extremely

short time scales involved (despite small magnitude of this new contribution to the quadrupole moment) .

The effect of phase changes on the moment of inertia has been discussed in literature. For example, moment of inertia change arising from a phase change to high density QCD phase (such as to the QGP phase) is discussed in ref. [2]. In the scenario of ref. [2], the transition is driven by slow decrease in the rotation speed of the pulsar, leading to increasing central density causing the transition as the central density becomes supercritical. It is assumed that as the supercritical core grows in size (slowly, over the time scale of millions of years), it continuously converts to the high density QGP phase (even when the transition is of first order). Due to very large time scale, the changes in moment of inertia are not directly observable, but observations of changes in the braking index may be possible.

Our work differs from these earlier works primarily in our focus on the *rapidly evolving density fluctuations* arising during the phase transitions. This has not been considered before as far as we are aware. (Though effects of density inhomogeneities in a rotating neutron star have been discussed [3].) Density fluctuations inevitably arise during phase transitions, e.g. during a first order transition in the form of nucleated bubbles, and may become very important in the critical regime during a continuous transition. The density fluctuations arising from a phase transition become especially prominent if the transition leads to formation of topological defects. Extended topological defects can lead to strong density fluctuations which can last for a relatively long time (compared to the phase transition time). It is obvious that such randomly arising density fluctuations will affect the moment of inertia of the star in important ways. Most importantly, it will lead to development of transient non-zero off-diagonal components of the moment of inertia, as well as transient quadrupole moment. Both of these will disappear after the density fluctuations decay away and the transition to a uniform new phase is complete. Net change in moment of inertia will have this transient part as well as the final value due to change to the new phase. It seems clear that this is precisely the pattern of a glitch or anti-glitch where rapid change in pulsar rotation is seen which slowly and *only partially* recovers to the

original value. As we mentioned above, transient change in quadrupole moment will be important for gravitation wave emission. It is important to realize that the net change in MI (as discussed previously, e.g. in [2]) is only sensitive to the difference in the free energies of the two phases, and cannot distinguish different types of phase transitions. In contrast, density fluctuations arising during phase transitions crucially depend on the nature of phase transition, especially on the symmetry breaking pattern (e.g. via topological defects). Identification of these density fluctuations via pulsar timings (and gravitational waves) can pin down the specific transition occurring inside the pulsar core.

We consider the possibility of rapid phase transition in a large core of a neutron star. The scenario of slow transition as discussed in [2] is applicable for slowly evolving star (e.g. by accretion), with a transition which is either a weak first order, or a second order (or a crossover). If the transition is strongly first order then strong supercooling can lead to extremely suppressed nucleation rate, with transition occurring suddenly after the supercritical core becomes macroscopic in size. (This is similar to the situation of low nucleation rate leading to nucleation distance scales of the order of meters in the early universe as discussed by Witten [4].) Rapid transition in a large core of neutron star is naturally expected during the early stages of evolution of neutron star due to rapid cooling of star. It could also be driven by rapid accretion on a neutron star, coupled with a first order transition.

We will not discuss any detailed scenario of such a rapid transition in this chapter, and rather just note the possibility of such transitions. Our focus will be that once such a rapid transition occurs, what are its observational implications. Clearly, change in phase will lead to net change in MI of star, affecting its rotation. This has been discussed earlier, e.g. in [2]. We will focus on additional effects associated with presence of density fluctuations which lead to qualitatively new effects, not included in the earlier investigations. These effects are, a transient component of change in MI, development of the off-diagonal components of MI, and a transient, rapidly evolving quadrupole moment.

4.2 Effects of density fluctuations due to bubble nucleation

A rough estimate of change in the moment of inertia due to phase change can be taken from ref. [2] using Newtonian approximation, and with the approximation of two density structure of the pulsar. If the density of the star changes from ρ_1 to a higher density ρ_2 inside a core of radius R_0, then the fractional change in the moment of inertia is of order (from ref [2], we have for $R_0 << R$),

$$\frac{\Delta I}{I} \simeq \frac{5}{3}(\frac{\rho_2}{\rho_1} - 1)\frac{R_0^3}{R^3}, \tag{4.1}$$

where, $I \simeq (2/5)MR^2$. Here R is the radius of the star in the absence of the dense core. For a QCD phase transition, density changes can be of order one. We take the density change to be about 30% as an example. If we take the largest rapid fractional change in the moment of inertia of neutron stars, observed so far (from glitches), to be less than 10^{-5}, then Eq.4.1 implies that $R_0 \leq 0.3$ Km (taking R to be 10 Km). For a superfluid transition, we may take change in density to be of order of superfluid condensation energy density $\simeq 0.1$ MeV/fm^3 (see, ref. [5]). In such a case, R_0 may be as large as 5 Km. These constraints on R_0 arise from observed data on glitches/anti-glitches. These estimates may also be taken as prediction of possible large fractional changes in the moment of inertia (hence pulsar spinning rate) of order few percent when a larger core undergoes rapid phase transition. For example, R_0 may be of order 2-3 km for QCD transition (from estimates of high density core of neutron star [6]), or it may be only slightly smaller than R for superfluid transition. For a detail description on how rapid QCD phase transtion can affect the pulsar dynamics see section 5.2, where we have discussed the change in moment of inertia due to rapid QCD phase transition in the core of a non rotating neutron star. Although the discussion on the rapid phase transition in the section 5.2 is in the context of non rotating neutron star, but the results are applicable to a rotating neutron star if we ignore small general relativistic corrections .

We now discuss density fluctuations during phase transitions. First we consider fluctuations arising simply from a first order transition. Consider nucleation of relatively large number of bubbles (several thousand) inside the supercritical core. This is possible due to nonuniformities, even of purely statistical origin (e.g. from fluctuations in temperature [7]).

4.2.1 Parameters for bubble nucleation and Results

We simulate random nucleation of bubbles filling up a core of size R_0 (= 300 meters). Effects of bubble nucleations will be characterized in terms of the following parameters. Bubble radius r_0 will be taken to vary from 5 meters to 20 meters, with bubble separation being of same order as bubble size (close packing). Density change in bubble nucleation is taken to be about the nuclear saturation density $\simeq 160$ MeV/fm^3 (e.g. for QCD scale).

We find that density fluctuations lead to fractional change in MI, $\Delta I/I \simeq 4\times 10^{-8}$ for $r_0 = 20$ meters implying similar changes in pulsar timings. Change in MI remains of same order when r_0 is changed from 20 meter to 5 meter. Due to random nature of bubble nucleation, off-diagonal components of the moment of inertia, as well as the quadrupole moment become nonzero and the ratio of both to the initial moment of inertia are found to be of order $I_{xy}/I_0 \simeq Q/I_0 \simeq 10^{-11} - 10^{-10}$.

This aspect of our model is extremely important, arising entirely due to density fluctuations generated during the transition. As these density fluctuations homogenize, finally leading to a uniform new phase of the core, both these components will dissipate away. The off-diagonal component of moment of inertia will necessarily lead to wobbling (on top of any present initially), which will get restored once the density fluctuations die away. This will lead to transient change not only in the pulse timing, but also in the pulse intensity (as the angle at which the beam points towards earth gets affected due to wobbling). We again emphasize that the conventional vortex depinning model of glitches is not expected to lead to additional wobble as the change in rotation caused by de-pinning of vortex clusters remains along the rotation axis.

Thus, the presence of intensity modulations associated with a glitch can distinguish between our model and the vortex de-pinning model.

Generation of quadrupole moment has obvious implication for gravitational wave generation. One may think that a quadrupole moment of order $Q/I_0 \simeq 10^{-10}$ is too small for any significant gravity wave emission. However, note that the gravitation power depends on the (square of) third time derivative of the quadrupole moment [8]. The time scales will be extremely short here compared to the time scales considered in literature for the usual mechanisms of change in quadrupole moment of the neutron star. Here, phase transition dynamics will lead to changes in density fluctuations occurring in time scales of microseconds (or even shorter as we will see below in discussions of topological defects generated density fluctuations). This may more than compensate for the small amplitude of quadrupole moment and may lead to these density fluctuations as an important source of gravitational wave emission from neutron stars, as we will discuss below.

4.3 Density fluctuations from topological defects

Topological defects form during spontaneous symmetry breaking transitions via the so called *Kibble mechanism* [9]. These defects can be source of large density fluctuations depending on the relevant energy scales, and their formation and evolution shows universal characteristics, (e.g. scaling behavior). This may lead to reasonably model independent predictions for changes in MI, and quadrupole moment and subsequent relaxation. As bubbles, strings, domain walls, all generate different density fluctuation, with specific evolution patterns, high precision measurements of pulsar timings and intensity modulations (from wobbling) and its relaxation may be used to identify different sources of fluctuations, thereby pinning down the specific phase transition occurring. Specific phase transitions expected inside pulsars lead to different types of topological defects. Important thing is that a random network of defects will arise in any phase transition, and resulting defect distribution can be determined entirely using the symmetry breaking pattern. For example, superfluid transition leads to

formation of random network of vortices. Confinement-deconfinement QCD transition can lead to formation of a network of domain walls and global strings arising from the spontaneous breaking of Z(3) center symmetry [10]. QCD transition may also give rise to only global strings, e.g. in the color flavor locked (CFL) phase with $SU(3)_c \times SU(3)_L \times SU(3)_R \times U(1)_B$ symmetry (for 3 massless flavors) is broken down to the diagonal subgroup $SU(3)_{c+L+R} \times Z_2$ [1]. As the resulting density fluctuations are mostly dominated by the nature of defect (domain walls, or strings, or both), we will model formation of these different defect networks in the following using correct energy scale and try to estimate resulting density fluctuations.

4.3.1 Results of model simulation of defect network

We model formation of U(1) strings and Z_2 domain walls by using correlation domain formation in a cubic lattice, with lattice spacing ξ representing the correlation length, as in ref. [11]. It is not possible to carry out these simulation covering length scales of km (for star) to fm (QCD scale). Hence these simulations are necessarily restricted to very small system sizes. Each lattice site is associated with an angle θ randomly varying between 0 and 2π (to model U(1) global string formation), or two discrete values 0,1 (when modeling Z_2 domain wall formation). For string case, winding of θ on each face of the cube is determined using the geodesic rule. For a non-zero winding, a string segment (of length equal to ξ) is assumed to pass through that phase (normal to the phase). For domain wall case, any link connecting two neighboring sites differing in Z_2 value is assumed to be intersected by a planar domain wall (of area ξ^2, and normal to the link). The mass density (i.e. mass per unit length) of the string was taken as 3 GeV/fm, and the domain wall tension is taken to be 7 GeV/fm^2. These values are taken as order of magnitude estimates from the numerical minimization results in ref. [10] for the pure gauge case. (Note that logarithmic dependence of global strings on inter-string separation may lead to much larger density fluctuations than considered here.)

We consider spherical system of size R and confine defect network within a spherical core of radius $R_c = \frac{0.3}{10}R$. This is in view of the constraints on the supercritical core size R_c being of order 0.3 km for a neutron star with radius $R = 10$ km. Of course, in our simulations, R is extremely small, with maximum value of 4000 fm. For $\xi \simeq 10$ fm, we find the resulting value of $\frac{\delta I}{I_i} \simeq 10^{-12} - 10^{-13}$ implying similar changes in the rotational frequency. Here $I_i, i = 1, 2, 3$ are the three diagonal values of the MI tensor. As we increase R_c from 5 ξ to about 400 ξ, we find that the value of $\frac{\delta I}{I_i}$ stabilizes near $10^{-13} - 10^{-14}$ as shown in the table below. This change in ξ amounts to change in the number of string and wall segments by a factor of 10^6. This gives a strong possibility that the same fractional change in the MI may also be possible when R is taken to have the realistic value of about 10 Km, especially when we account for statistical fluctuations in the core. For the formation of domain walls we find fractional change in MI components (as well as quadrupole moments) to be larger by about a factor of 40. With accurate measurements, these small changes may be observable. Also, for a larger core size undergoing transition these changes can be larger. We are only presenting change in MI due to transient density fluctuations during phase transition, which as we see, can have either sign. (As we discussed above, the net change in MI will include the very large contribution of order 10^{-5} due to net phase change of the core [2].) This suggests that the phase transition dynamics may be able to account for both glitch and anti-glitch events (with associated wobbling from off-diagonal components leading to pulse intensity modulation).

We now consider superfluid transition. A rapid superfluid transition could occur after transient heating of star (either due to another transition releasing latent heat, or due to accretion etc). (In this work we neglect any possible effect of star rotation on this mechanism of random vortex formation which is expected to lead to a much denser network than the one arising from star rotation.) We take the vortex energy per unit length to be 100 MeV/fm and correlation length for vortex formation of order 10 fm (ref. [5]). Table 4.1 shows that the string induced transient fractional change in MI is of order 10^{-10} (compared to net fractional change in MI of order 10^{-5} as discussed in Sect.4.2). Ratios of the quadrupole moment and off-diagonal components

of MI to the net MI of the pulsar are also found to be of order 10^{-10}. The transient change in the MI decays away when the string system coarsens, thereby restoring less than few percent of the original value. We note that this pattern (and numbers) are similar to that of a glitch (or anti-glitch).

Table 4.1: Fractional change of various moments of the pulsar caused by inhomogeneities due to defects, with the correlation length ξ = 10 fm. For QCD scale strings, the string tension is taken as 3 GeV/fm, while the QCD Z(3) wall tension is taken as 7 GeV/fm^2 (from simulations in ref. [10]). For the superfluid vortices, the energy per unit length is taken to be 100 MeV/fm [5].

	QCD Strings			QCD Walls			Superfluid Strings		
$\frac{R_c}{\xi}$	$\frac{\delta I_{xx}}{I}$	$\frac{\delta I_{xy}}{I}$	$\frac{Q_{xx}}{I}$	$\frac{\delta I_{xx}}{I}$	$\frac{\delta I_{xy}}{I}$	$\frac{Q_{xx}}{I}$	$\frac{\delta I_{xx}}{I}$	$\frac{\delta I_{xy}}{I}$	$\frac{\delta Q_{xx}}{I}$
5	5E-10	-3E-10	-1E-10	2E-8	-1E-8	-8E-10	2E-6	-1E-6	-4E-7
50	5E-12	-2E-12	2E-12	1E-10	-8E-11	-1E-11	2E-8	-7E-9	7E-9
200	1E-13	2E-14	-7E-14	5E-12	-4E-12	-6E-12	5E-10	6E-11	-2E-10
400	-3E-15	-5E-14	-9E-14	3E-12	-2E-12	3E-14	-1E-11	-2E-10	-3E-10

4.3.2 Field theory simulations for QCD transition

As a further support for these estimates, we have also carried out field theory simulations of confinement-deconfinement (C-D) QCD transition using effective field theory Polyakov loop model. This leads to spontaneously broken Z(3) symmetry (for the SU(3) color group) in the QGP phase giving rise to topological domain wall defects in the QGP phase and also string defects forming at wall junctions. We carry out a field theory simulation for the C-D transition using a quench (quench is used for simplicity as only domain formation is relevant here), see ref. [10] for details. It is not possible to carry out field theory simulation covering length scales of km (for star) to fm (QCD scale). Hence these simulations are necessarily restricted to system sizes of tens of fm only. The physical size of the lattice is taken as (7.5 fm)^3 and (15 fm)^3. We use periodic boundary conditions and take a spherical region with radius R_c (representing star's core) to study change of MI, with $R_c = 0.4 \times$ lattice size. We mention that the model of ref. [10] does not directly apply to the case of neutron star which has

large baryonic chemical potential. However, the most relevant features of the model are formation of Z(3) defects with similar energy scale as in the neutron star case. Hence we use those simulations [10] to estimate defect induced density fluctuations for the present neutron star case. We also use dissipation to relax density fluctuations but total energy is kept fixed by adding the dissipated energy. Thus we only focus on re-distribution of energy in defect network and the background. For the net change in the MI, we will use the estimates of $\Delta I/I$ from Sect.4.2 (refs. [2]). QCD transition may also give rise to only global strings, e.g. in the color flavor locked (CFL) phase with $SU(3)_c \times SU(3)_L \times SU(3)_R \times U(1)_B$ symmetry (for 3 massless flavors) is broken down to the diagonal subgroup $SU(3)_{c+L+R} \times Z_2$ [1]. For this case, we modify the model studied in ref. [10] by removing terms which correspond to Z(3) structure of the vacuum manifold. This gives rise to string defects only without any domain walls, with energy scale of QCD.

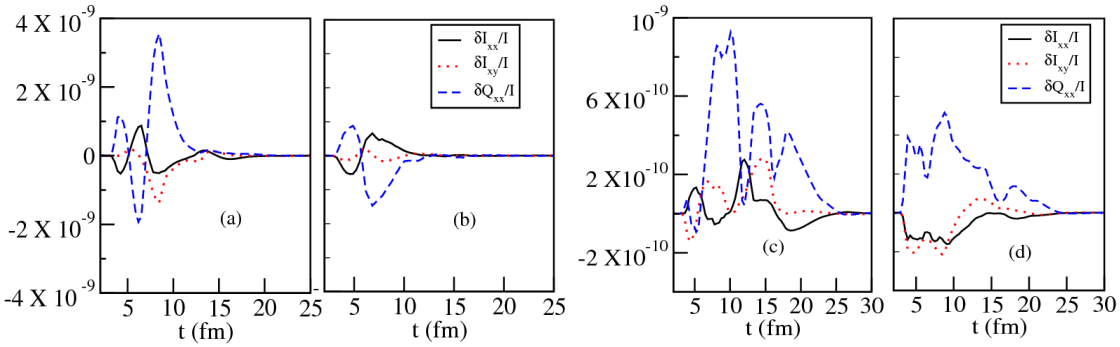

Figure 4.1: Fractional change in MI and quadrupole moment during phase transitions. (a),(b) correspond to lattice size (7.5 fm)^3, and (c),(d) correspond to lattice size (15 fm)^3 respectively. Plots in (a) and (c) correspond to the C-D phase transition with Z(3) walls and strings, while plots in (b) and (d) correspond to the transition with only string formation as for the CFL phase.

Plots in Fig.4.1 show the time evolution of the resulting fractional change in the MI and the quadrupole moment of the core relative to the initial total MI for these field theory simulations. Here we have taken dense core of fractional size 0.3/10 (in view of transition in core size of 300 meter for a 10 km star). We add the MI of a shell

outside the core so that total system size = $\frac{10}{0.3}$ of the core size, and the shell has the same uniform density as the core. Fractional changes for all components of MI as well as the ratio of quadrupole moment to MI are found to be of similar order. We are only presenting change in MI due to transient density fluctuations during phase transition, which as we see, can have either sign. (Net fractional change in MI will include the very large contribution of order 10^{-5} due to net phase change of the core [2].) This suggests that the phase transition dynamics may be able to account for both glitch and anti-glitch events (with associated wobbling from off-diagonal components leading to pulse intensity modulation). As discussed above, rapid changes in the quadrupole moment will lead to gravitational wave emission.

4.4 Gravitational wave generation due to density fluctuations

Despite the small values of quadrupole moments in Table 4.1, the power emitted in gravitational waves may not be small due to very short time scales in the present case. The defect coarsening will be governed by microphysics with time scale being of order tens of fm/c. Even with extremely dissipative motion of strings, and much larger length scales, the change in quadrupole moment due to strings can happen in an extremely short time scale (during string formation, and/or during string decay), thereby boosting the rate of quadrupole moment change. Even a very conservative value of the time scale of microseconds (e.g. for nucleation of bubbles with nucleation sites few meters apart, as discussed above) for the evolution of density fluctuations will still be 1000 times smaller than fastest pulsar rotation time of milliseconds, resulting in huge enhancement in the gravitational power, as can be seen from the following expression for the power [8]

$$\frac{dE}{dt} = -\frac{32G}{5c^5}\Delta Q^2\omega^6 \simeq -(10^{33}J/s)(\frac{\Delta Q/I_0}{10^{-6}})^2(\frac{10^{-3}sec.}{\Delta t})^6 \tag{4.2}$$

Here I_0 is the MI of the pulsar, and ΔQ is the change in the quadrupole moment

occurring in time interval Δt. For the present case, we can take $\Delta Q/I_0$ of order $10^{-14} - 10^{-10}$ from Table 4.1 (which is much smaller than the value of 10^{-6}, typically used for deformed neutron stars). Even though $\Delta Q/I_0$ is very small here, the relevant time scale Δt is also very small. Thus, even with a conservative estimate of the time scale for the transition (e.g. bubble coalescence), $\Delta t = 10^{-6} - 10^{-5}$ sec., the power in gravitational wave can be significant due to large enhancement from the $(\frac{10^{-3} sec.}{\Delta t})^6$ factor. A shorter time scale may make this source as potentially very prominent for gravitational waves. For an estimate of the expected strain amplitude from a pulsar at a distance r, we use the following expression [8]

$$h = \frac{4\pi^2 G \Delta Q f^2}{c^4 r} \simeq 10^{-24} (\frac{\Delta Q/I_0}{10^{-6}})(\frac{10^{-3} sec.}{\Delta t})^2 (\frac{1 kpc}{r}) \tag{4.3}$$

With $\Delta Q/I_0$ of order 10^{-10} and a time scale for the transition (e.g. bubble coalescence), $\Delta t = 10^{-6} - 10^{-5}$ sec. we can have $h \simeq 10^{-24} - 10^{-22}$ for a pulsar at 1 kpc distance. As we mentioned above, the time scale for evolution of density fluctuations may be even shorter, leading to larger strain amplitudes (even if much smaller values of $\Delta Q/I_0$ are taken from Table 4.1), and much larger power emitted in gravitational waves. Since the wave emission is only for a single burst, lasting for only duration Δt, net energy lost by the star remains small fraction of the star mass.

4.5 Conclusions

To summarize our results, we have shown that density fluctuations arising during a rapid phase transition lead to transient change in the MI of the star. Such density fluctuations in general lead to non-zero off-diagonal components of moment of inertia tensor which will cause the wobbling of pulsar, thereby modulating the peak intensity of the pulse. This is a distinguishing and falsifiable signature of our model. The conventional vortex de-pinning model of glitches is not expected to lead to additional wobble as the change in rotation caused by de-pinning of vortex clusters remains along the rotation axis. We find that moment of inertia can increase or decrease, which gives the possibility of accounting for the phenomenon of glitches and

anti-glitches in a unified framework. Development of nonzero value of quadrupole moment (on a very short time scale) gives the possibility of gravitational radiation from the star whose core is undergoing a phase transition. Net change in MI (as discussed previously, e.g. in [2]) is only sensitive to the difference in the free energies of the two phases, and cannot distinguish different types of phase transitions. In contrast, density fluctuations arising during phase transitions crucially depend on the nature of phase transition, especially on the symmetry breaking pattern (e.g. via topological defects). Identification of these density fluctuations via pulsar timings (and gravitational waves) can pin down the specific transition occurring inside the pulsar core. This is an entirely new way of probing phase transitions occurring inside the core of a neutron star. Though our estimates suffer from the uncertainties of huge extrapolation involved from the core sizes we are able to simulate, to the realistic sizes, they strongly indicate that expected changes in moment of inertia etc. may be well within the range of observations, and in fact may be able to even account for the phenomena of glitches and anti-glitches.

One aspect of glitches which may raise concern in our model is multiple occurrences of glitches. For vortex de-pinning model multiple glitches seem natural due to formation of vortices due to star rotation with glitches occurring with de-pinning of clusters of vortices. In our model, multiple occurrence of glitches will require multiple phase transitions. This is not very improbable, though, when the transition happens due to accretion from companion star causing heating, with subsequent cooling down. Essentially, in this case, the matter in the neutron star core will continue to remain in the vicinity of the phase boundary in the $T - \mu$ plane (in the QCD phase diagram). Accretion will move the system across the boundary by increasing μ, causing a phase transition, and subsequent cooling will move the system back through the phase boundary with another transition. Such processes could in principle repeat for certain neutron stars leading to multiple glitches. One should also allow the possibility that glitches could occur due to multiple reasons. Some glitches/anti-glitches could occur due to the model proposed here, that is due to phase transition induced density fluctuations, while other glitches could occur due to the conventional de-pinning of

vortex clusters. Main point of our work is to emphasize that if and when a transition happens in the core of a neutron star, it invariably leads to density fluctuations which manifest itself in glitch/anti-glitch like behavior, along with other implications such as wobbling of star, gravitational wave emission etc.

It is thus important to investigate this interesting possibility further. With much larger simulations, and accounting for statistical fluctuations of temperature, chemical potential etc. in the core, more definitive patterns of changes in moment of inertia tensor/quadrupole moment etc. may emerge which may carry unique signatures of specific phase transitions involved. (For example, continuous transitions will lead to critical density fluctuations, and topological defects will induce characteristic density fluctuations depending on the specific symmetry breaking pattern.) If that happens then this method can provide a rich observational method of probing the physics of strongly interacting matter in the naturally occurring laboratory, that is interiors of neutron star. It will be interesting to see if any other astrophysical body, such as white dwarf, can also be probed in a similar manner.

Bibliography

[1] M.G. Alford, A. Schmitt, K. Rajagopal and T. Schfer, Rev. Mod. Phys. **80**, 1455(2008).

[2] H. Heiselberg and M. Hjorth-Jensen, Phys. Rev. Lett. **80**, 5485 (1998).

[3] D.M. Sedrakian, M. Benacquista, K.M. Shahabasian, A.A. Sadoian and M.V. Hairapetian, Astrophysics **46**, 445 (2003).

[4] E. Witten, Phys.Rev. **D 30**, 272 (1984).

[5] R. W. Richardson, Phys. Rev. **D 5**, 1883 (1972); C.-H. Yang and J.W. Clark, Nucl. Phys. **A 174**, 49 (1971).

[6] J. M. Lattimer and M. Prakash, Astrophys. J. **550**, 426 (2001).

[7] L.D. Landau and E.M. Lifshitz, " Statistical Physics" 3rd Ed. Pergamon Press (1980).

[8] K. Riles, Prog. Part. Nucl. Phys. **68**, 1 (2013); S. Weinberg, " Gravitation and cosmology", John Wiley and Sons Inc., 1972, USA.

[9] T.W.B. Kibble, J. Phys. A **9**, 1387 (1976); Phys. Rept. **67**, 183 (1980).

[10] U.S. Gupta, R.K. Mahapatra, A.M. Srivastava and V.K. Tiwari; Phys. Rev. **D82**, 074020 (2010).

[11] T. Vachaspati and A. Vilenkin, Phys. Rev. **D 30**, 2036 (1984).

Chapter 5

Probing Dynamics of Phase Transitions occurring inside a Pulsar

In the last chapter, we have seen that density change and fluctuations originating from various phase transitions, e.g. superfluid transition or transition to various exotic phases of QCD, affect star's moment of inertia. Our result suggests that these changes may be observable and may possibly account for glitches and anti-glitches. In this chapter, we will carry out detailed calculations of a first order transition dynamics for the quark-hadron transition in the core of a neutron star. We will calculate the density profile in the neutron star and will calculate bubble nucleation probability for the transition. We will also discuss specific field theory models which lead to topological defect induced density fluctuations as discussed in chapter 4.

5.1 Introduction

Exotic phases of quantum chromo dynamics (QCD), viz., quark-gluon plasma (QGP), color flavor locked (CFL) phase, [1] etc. are possible at very high baryon density. The core of an astrophysical compact dense object, such as a neutron star, provides physical conditions where a transition to these phases may be possible. Superfluid phases

of neutrons (as well as of protons) are also believed to exist inside neutron stars. Also, relatively young pulsars show the phenomenon of glitches [2] and, recently observed anti-glitches [3], where the spinning rate of the pulsar rapidly changes, and then slowly relaxes. Conventional understanding of a glitch in terms of depinning of a cluster of superfluid vortices in the core of a neutron star (which transfers angular momentum to the crust) does not seem viable for explaining anti-glitch, though external body impact has been proposed as a possible cause for anti-glitches.

In the last chapter, we have proposed a technique to probe the dynamical phenomena happening inside the neutron star, which seems to be capable of also accounting for the phenomena of glitches and anti glitches in a unified framework. Basic physics of our approach is based on the fact that phase transitions are typically associated with density changes as well as density fluctuation. Density fluctuation in the core of a star will in general lead to transient changes in its moment of inertia (MI), along with a permanent change in MI due to phase transformation. This will directly affect its rotation and hence the pulsar timings. As accuracy of measurement of pulsar timings is extremely high ($\frac{\triangle\nu}{\nu} \sim 10^{-9}$), very minute changes of the moment of inertia of star may be observable, providing a sensitive probe for phase transitions in these objects. Non-zero off-diagonal components of the moment of inertia arising from density fluctuations imply that a spinning neutron star will develop wobble leading to modulation of the peak intensity of pulses (as the direction of the beam pointing towards earth undergoes additional modulation). This is a unique, falsifiable, prediction of our model, that rapid changes in pulsar timings should, most often, be associated with modulations in changes in peak pulse intensity. It is important to note that the vortex depinning model of glitches is not expected to lead to additional wobble as the change in rotation caused by depinning of the vortex, clusters remains along the rotation axis. Density fluctuations will also, lead to a development of rapidly changing quadrupole moment which can provide a new source of gravitational wave emission due to extremely short time scales involved (despite the small magnitude of this new contribution to the quadrupole moment).

Moment of inertia change arising from a phase change to high density QCD phase

(such as to the QGP phase) is discussed in ref. [4]. The transition is driven by a slow decrease in rotation speed of the pulsar, leading to increasing central density causing the transition as the central density becomes supercritical. It is assumed that as the supercritical core grows in size (slowly, over the time scale of millions of years), it continuously converts to the high density QGP phase (even when the transition is of the first order). Due to very large time scale, the changes in the moment of inertia are not directly observable, but observations of changes in the braking index may be possible.

As we have mentioned that hadronic phase to QGP phase transition is first order. In the case of strong first order phase transition with large latent heat transition from hadronic phase to quark matter phase may not happen continuously via bubble nucleation. In this case, transition can take place in superdense core of macroscopic size e.g. large nucleation distances, of the order of meters, could be possible in the original discussion of Witten [5] in the context of quark hadron transition in the early universe. In this chapter, we discuss how in a neutron star supercritical core can grow to macroscopic size. Phase transition from hadronic to QGP phase in the supercritical bubble can occur in very short time (see [6] for rapid transitions in the context of *hot* neutron stars during its very early stages). Subsequently, we will also discuss specific field theory models which can lead to density fluctuations via topological defects as discussed in the previous chapter.

5.2 Change in moment of inertia due to a first order transition

As we mentioned above, the discussions in ref. [4] about the change in moment of inertia due to a phase transition assumed that the phase conversion happens continuously in the supercritical region of the core. This will happen for a second order transition, or a crossover, or for a weak first order transition with very large bubble nucleation rate. However, for a strong first order phase transition, this may not happen. As we

mentioned above, for very low nucleation rates, the supercritical core may become macroscopically large before a single bubble of new phase nucleates. Once nucleated, the bubble will expand fast sweeping entire supercritical core and converting it to the new phase. This will lead to the change in the moment of inertia of the pulsar in a very short time which may be directly observable. Using the constraints from glitches, that the fractional change in the moment of inertia of the neutron star be less than about 10^{-5}, we had argued in chapter 4 that the core size (R_0) undergoing quark-hadron transition should be less than about 300 meters. For superfluid transition, R_0 could be as large as $5Km$.

Let us now discuss the conditions which will allow such a rapid phase transition in a large core. As an example, we consider a simple case of zero temperature transition (as appropriate for late stages of neutron star) between a nucleonic phase and a QGP phase with pressures (P) and energy densities (ϵ) of the two phases given as follows [7].

$$P_{nucleon} = \frac{M^4}{6\pi^2}\left(\frac{\mu}{M}\left(\frac{\mu^2}{M^2}-1\right)^{1/2}\left(\frac{\mu^2}{M^2}-\frac{5}{2}\right)+\frac{3}{2}ln\left[\frac{\mu}{M}+\left(\frac{\mu^2}{M^2}-1\right)^{1/2}\right]\right) \quad (5.1)$$

$$\epsilon_{nucleon} = \frac{2\mu}{3\pi^2}(\mu^2-M^2)^{3/2} - P_{nucleon} \quad (5.2)$$

$$P_{QGP} = \frac{\mu_q^4}{2\pi^2} - B \quad (5.3)$$

$$\epsilon_{QGP} = 3P_{QGP} + 4B \quad (5.4)$$

Here μ_q and $\mu(=3\mu_q)$ are the baryon chemical potentials for quarks and nucleons respectively, M is the mass of the relevant hadron (nucleon), and B is the bag pressure. Note that with this simple *Bag model* equation of state, the transition to QGP phase requires absorption of latent heat which should be provided by the release of gravitational potential energy from the compression of the core. For other equations of state (see, e.g. [6]), or for other QCD transitions (say from QGP to CFL phase) the transition may release latent heat which will be rapidly dissipated by the star.

The nucleation rate appropriate for zero (low) temperature is dominated by quantum tunneling mediated by O(4) symmetric instantons, and is given by [8].

$$\Gamma = A\frac{S_0^2}{4\pi^2}exp(-S_0) \tag{5.5}$$

where A is the determinant of fluctuations around the instanton configuration and S_0 is the Euclidean action of the instanton. In our case, we will be interested in the situation of extremely low nucleation rates, corresponding to very large values of action S_0. The nucleation rate, then will be completely dominated by the exponential factor, and the pre-exponential factor can be approximated by dimensional estimates using $A = R_c^{-4}$ where R_c is the radius of the critical bubble (size of the instanton in Minkowski space). Recall, that at finite temperature T, dimensional estimates use $A = T^4$. The action S_0 for the instanton can be obtained from the action for an O(4) symmetric configuration written as follows,

$$S = -\frac{1}{2}\pi^2 R^4 \Delta P + 2\pi^2 R^3 S_1 \tag{5.6}$$

where ΔP is the pressure difference between the two phases and S_1 is the action of a one-dimensional instanton giving the contribution of the surface term of the bubble to the action. Extremization of S gives the critical radius $R_c = 3S_1/(\Delta P)$ with which the action of the instanton S_0 is found to be

$$S_0 = \frac{27\pi^2 S_1^4}{2(\Delta P)^3} \tag{5.7}$$

For our case, $\Delta P = P_{QGP} - P_{nucleon}$ (Eqns. 5.2,5.4). For calculation of S_1, one needs the free energy functional (e.g. Landau-Ginzburg free energy). In the absence of that, we simply consider a range of values of surface tension S_1 ranging from 0.01 MeV/fm^2 to 5 MeV/fm^2. As we discussed above, for QCD scale phase transitions, observations constrain the critical core size to be less than about 0.3 Km. We calculate the number of bubbles nucleated in 300 meter radius core in one million year time duration as a function of core density. This is given in Fig.5.1a. For this, we have used parameters $B^{1/4} = 177.9$ MeV, surface tension $S_1 \equiv \sigma = 0.05$ MeV/fm^2 and $M =$

1087.0 MeV (taken as the mean of the nucleon and delta mass, ref. [7]). The value of surface tension is unusually small here. With the simple equations of state for the two phases used here, nucleation rate rapidly drops with much larger values of σ. For a more realistic equation of state, larger values of surface tension may be possible. (Note that we are considering homogeneous nucleation here. There may be inhomogeneities in the core region enhancing the nucleation probability via heterogeneous nucleation.) With these choices, the critical density for the transition is found to be $\rho_c = 2.500\rho_0$ (where $\rho_0 \simeq 0.15 m_{nucleon}$ is the nuclear saturation density). Fig.5.1 shows that at a density $\rho_{nucl} \simeq 2.502\rho_0$ the number of nucleated bubble is one. The critical radius of the bubble $R_c = 50$ fm at this density. Nucleation rate changes sharply as a function of density and is insignificant at lower values of ρ. For example, with a decrease in density by only 0.01%, the number of bubbles nucleated is about 10^{-10}.

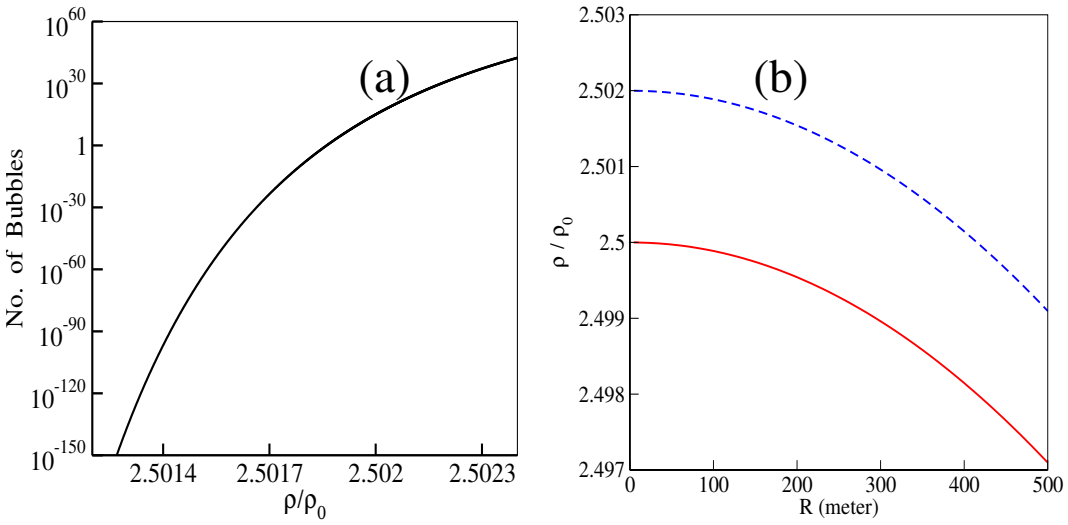

Figure 5.1: (a) Plot of the number of bubbles nucleated in 300 meter radius core in one million year time duration as a function of core density for a QCD transition. (b) Solid plot shows the density profile of the core region of the neutron star with neutron star mass is $M_1 = 1.564 M_0$. Density at $r = 0$ has just reached the critical value ρ_c. The dashed plot shows the density profile when the supercritical core size (with $\rho > \rho_c$) has increased to about 300 meter. The mass of the neutron star at this stage is $M_2 = 1.567 M_0$.

For density change of the neutron star, we consider the case of accretion driven change. Typical data shows that neutron stars in a binary system accrete matter at

the rate of about $10^{15}-10^{18}$ grams/sec [9]. With accretion rate of 10^{17} grams/sec, for a solar mass neutron star, this will mean about 0.1% change in its mass in one million years. We calculate density profile of a non-rotating star (this approximation will be valid for slowly rotating pulsars) in Newtonian approximation using a polytropic equation of state $P = K\rho^{\alpha}$. We take $\alpha = 2.54$ with $K = 0.021\rho_0^{-1.54}$ (as in ref. [4]) and solve the following equation for density profile [4].

$$\frac{1}{\rho}\frac{dP}{dr} = -\frac{Gm}{r^2} \; ; \quad dm = 4\pi r^2 \rho dr \tag{5.8}$$

With central density $\rho = 2.5\rho_0$ ($= \rho_c$, the critical density for hadron-QGP transition) we get neutron star mass to be 1.564 M_0 (M_0 is the solar mass) and its radius to be about 13.7 Km. We consider the situation when a neutron star with sub-critical central density accretes matter such that its central density becomes super-critical. Consider the stage when the central value of the density of the neutron star (at radius $r = 0$) just reaches the critical density ρ_c by mass accretion. We calculate the density profile with $\rho = \rho_c$ at the center $r = 0$. This situation is shown by the (solid) plot in Fig.5.1 b showing the density profile of the core region of the neutron star. Mass of the star at this stage (with our choice of parameters) is $M_1 = 1.564M_0$. Subsequently, the continued accretion increases the size of the core region where the density is supercritical ($\rho > \rho_c$). The dashed plot in Fig.5.1 b shows the density profile of the core region when the supercritical core size has increased to about 400 meters. The mass of the neutron star at this stage is $M_2 = 1.567M_0$. Taking the accretion rate of 10^{17} grams/sec. it will take about one million years for the supercritical core size to increase to this size. Nucleation rate in Fig.5.1 a shows that at this stage there can be just about one bubble nucleation possible in this supercritical core. (Actually core needs to be somewhat larger as in regions away from the center of the supercritical core, nucleation rate is smaller. This difference is unimportant for our rough estimates).

Once the bubble is nucleated, it will sweep through the entire supercritical core. Typical speed of bubble wall propagation will be relativistic, and one may take the

speed of sound in a relativistic plasma ($c/\sqrt{3}$) as an estimate. Thus the transition will be completed in a time of order microsecond. The resulting transition is therefore completed in a very short time, even though the supercritical core grew over a million year time. We again point out that this scenario is very similar to the one discussed by Witten [5] for the the early universe where bubble nucleation is insignificant until the age of the universe is few microseconds (many orders of magnitude larger than the strong interaction time scale), and inter-bubble separation of order centimeters or even meters is possible. As discussed above, such a rapid transition in a macroscopically large core of the neutron star will lead to the fractional change in moment of inertia of order $10^{-5} - 10^{-6}$ which may be observed as a pulsar glitch. The supercritical core size (in which a single bubble can nucleate) may be larger (for appropriate values of parameters such as bubble surface tension). In that case, the fractional change in moment of inertia of even few percent (occurring in a very short time of order micro seconds) may be possible and this can be taken as a prediction of our model suggesting lookout for such candidates.

One more consequence of the scenario discussed above has implication for the superfluid phase of the neutron star. We consider the above discussed transition such that latent heat of order few hundred MeV/fm^3 is released in the QCD scale transition. Assuming that most of the neutron star is in the neutron superfluid phase (and/or proton superconducting phase) at this stage, with the free energy density scale for the superfluid transition being of order 0.1 MeV/fm^3, the latent heat released by the QCD transition will heat up the superfluid phase to the normal phase. Simple volume ratio will tell that the latent heat released in a 300 meter core undergoing QCD transition will convert about 3 km radius region from a superfluid to the normal phase as the heat pulse sweeps through the neutron star. Subsequent cooling will again lead to transition to the superfluid phase for all that region. Our estimates of change in moment of inertia above suggest that even this superfluid transition happening in a radius of about 3 km will again lead to fractional change in moment of inertia of order $10^{-5} - 10^{-6}$. Again, a larger core will lead to a larger change in moment of inertia.

5.3 Effect of Density fluctuations on the neutron star dynamics

The core of a neutron star may go through a transition from hadronic matter to QGP due to gradual slowing down of the rotating neutron star [4], or due to accretion of matter. Or a QGP core formed during early hot and dense phase of neutron star may undergo a transition to hadronic matter after a relatively longer time as the core cools. At these baryon densities, the transition is very likely a first order transition which proceeds via bubble nucleation. Bubble nucleation can give rise to density fluctuations. As we discussed above, for strong first order case, a core of size few hundred meters (or larger) can become supercritical without any bubble nucleation taking place inside the core. With further accretion of matter, the density may become *sufficiently* large so that bubble nucleation can take place. We discussed the case above when a single bubble nucleation takes place. However, there can the situations when density change is such that no bubbles are nucleated until density increases to a value when a reasonably large number of bubbles (several thousand) can nucleate inside the supercritical core. With strictly ideal, monotonic decrease in density with radial distance such a scenario looks unlikely. However, we emphasize that in general the core region will be expected to have minute nonuniformities, even of purely statistical origin. For example, the temperature of different parts of the core (even at the same radial distance, but in different directions) cannot have exactly the same value. Purely from statistical fluctuations, there will be fluctuations in temperature in these regions (similarly in chemical potential) which will depend on properties such as specific heat [10]. In fact, such density fluctuations can lead to large enhancement in our estimates of density fluctuations from defect formations. This is because the density of defects is entirely determined by the correlation length which sensitively depends on parameters like temperature, chemical potential etc. Varying correlation length will lead to an additional source of fluctuation in the density of defects, hence for density fluctuations. We will not get into such details here, but only conclude that a situation where many bubbles may nucleate in different parts of

the supercritical core may not be unreasonable for a realistic case. After nucleation, bubbles (with initial critical size being microscopic, of order tens of fm) rapidly expand and coalesce. At the time of coalescence, the supercritical core region will consist of a close packing of bubbles of a new phase, embedded in the old phase. We assume that the latent heat is released from the star which either contributes to a uniform background in energy density (contributing to the net moment of inertia of the star as a homogeneous sphere), or it is simply dissipated away from the star. In either case, the latent heat will not affect the off-diagonal component of the moment of inertia and the quadrupole moment.

Such Random nucleation of spherical bubbles filling up a spherical bubble can give rise to change in moment of inertia $\Delta I/I \simeq 10^{-8}$. The radius of such random bubble can have a range from 5 meters to 20 meters. Quadrupole moment generated due to the random distribution of the bubbles in the interior can be of the order of $10^{-11}-10^{-10}$ (see section 4.2.1 for details). As we have already discussed in the section 4.2.1 we again emphasize that the off-diagonal component of the moment of inertia will necessarily lead to wobbling, which will get restored once the density fluctuations die away. Non zero quadrupole moment has obvious implication for gravitational wave generation (see section 4.4) . Although in this case quadrupole moment of order 10^{-10}, but the time scales of the fluctuations are of the order of Fermi. Due to this small time scale involved gravitation power can be large (large compared to the usual mechanisms of change in quadrupole moment of the neutron star) [11] .

As we have already discussed density can give rise to observable effect in neutron star dynamics. Phase transitions naturally introduce density fluctuations. Topological defects [12] which are the outcome of symmetry breaking phase transitions, can be a source of large density fluctuations depending on the relevant energy scales. The defect network resulting from a phase transition and its evolution shows universal characteristics, e.g. defects have initial densities which basically depend only on the correlation length and on the relevant symmetries and the evolution of string defects and domain wall defects show scaling behavior. This has important implications, as the universal properties of defect network and scaling during evolution may

lead to reasonably model independent predictions for changes in moment of inertia (hence glitches/anti-glitches) and quadrupole moment, and subsequent relaxation to the original state of rotation.

Most important aspect of these changes in moment of inertia components (especially the off-diagonal ones) and the quadrupole moment arising from density fluctuations during phase transition is the following. The specific pattern of density fluctuation and the manner in which it decays (to eventual uniform new phase) crucially depends on the nature of the source of the fluctuations. Bubbles, strings, domain walls, all generate different density fluctuations, and detailed simulations can determine the nature of resulting changes in pulsar timings and intensities (due to wobbling as discussed above) resulting from these. High precision measurements have the potential of distinguishing between different sources of fluctuations, thereby pinning down the specific phase transition occurring inside the core of a neutron star. Similarly, the evolution of density fluctuation also depends on the specific case being considered. For example, the bubble generated density fluctuations discussed above will decay away quickly in time scale of coalescence of bubbles, while domain wall network and the string network may coarsen on much larger time scales (and differently from each other). Thus the relaxation of the pulsar spinning (and wobbling etc.) can also provide important information about the specific transition (leading to corresponding defect formation) occurring inside the neutron star.

Various kinds of symmetry breaking phase transition and the associated topological defects are possible in the interior of the neutron star. The inner core of a neutron star can have nucleonic superfluid phase and the associated superfluid vortices. We have discussed the implication of these superfluid phases in the context of the glitch mechanism. Deconfined quark matter can exist in the core of the neutron star. Confinement-deconfinement transition in QCD gives rise to $Z(3)$ domain walls and QCD string defects. Phase structure of deconfined quark matter at very high density is very rich. One of the possible QCD phases at very high density regime is the color flavor locked (CFL) phase. Symmetry breaking pattern of the CFL transition is very complex (see section 3.2.5) . Symmetry breaking in the case of CFL transition

gives rise to global strings. One can use numerical methods to simulate these defect with proper energy scale and can estimate the change in moment of inertia.

We have already discussed that the expectation value of the Polyakov loop, $l(x)$, is the order parameter for this transition [13]. $l(x)$ is zero in the hadronic phase and is non-zero in the QGP phase breaking Z(3) center symmetry (for the SU(3) color group) spontaneously as $l(x)$ transforms non-trivially under $Z(3)$. This gives rise to topological domain wall defects in the QGP phase which interpolate between different $Z(3)$ vacua and also string defects (QGP strings) forming at the junction of these $Z(3)$ walls [14–16]. We point out that in the presence of quarks, $Z(3)$ symmetry is also explicitly broken and it affects the dynamics (especially at late times) of $Z(3)$ walls and the QGP string in important manner [16]. However for an order of magnitude estimate, we focus on very early stages of evolution of defect network and neglect these quark effects. We carry out a field theory simulation of the evolution of $l(x)$ from an initial value of zero (appropriate for the hadronic phase) as the system is assumed to undergo a rapid transition (quench) to the QGP phase (as in [17]). Use of quench is not an important point here is the formation of defects only requires formation of uncorrelated domains, and the size of the domains in this model has to be treated as a parameter.

We mention that the estimates of change in moment of inertia due to the formation of the QGP string and $Z(3)$ domain walls etc. require microphysics governed by QCD scale of order 10^{-15} meters, while the star radius is in km. It is not possible for us to carry out simulation covering such widely different scales of length and time. Results with appropriate length scales are not possible for the general case and one has to resort to simulations. We now discuss detailed field theory simulations, which are necessarily restricted to very small system sizes. To simulate the domain walls the effective Lagrangian proposed in [18] can be used.

$$L = \frac{N}{g^2}|\partial_\mu l|^2 T^2 - V(l). \tag{5.9}$$

Here, $N = 3$ and $V(l)$ is the effective potential for the Polyakov loop given by,

$$V(l) = \Big(-\frac{b_2}{2}|l|^2 - \frac{b_3}{6}\big(l^3 + (l^*)^3\big) + \frac{1}{4}\big(|l|^2\big)^2\Big)b_4 T^4. \tag{5.10}$$

l_0 is given by the absolute minimum of $V(l)$ and the normalization of $l(x)$ is chosen such that $l_0 \to 1$ as $T \to \infty$. Values of various parameters in Eq. 5.10 are fixed with lattice result following Ref. [18] (see refs. [15, 16] for these details). Time evolution of $l(x)$ is governed by the field equations obtained from Lagrangian in Eq.5.9 . We use leap frog algorithm with periodic boundary conditions for the simulation (for details see section 4.3) . The actual simulation is done for the physical size of the lattice is taken as $(7.5 \text{ fm})^3$ and $(15 \text{ fm})^3$ with lattice spacing, $\Delta x = 0.025$ fm and time step, $\Delta t = \frac{0.9 \times \Delta x}{\sqrt{3}}$. To minimize the effects of periodic boundary conditions, a spherical region with radius R_c is chosen to study change of moment of inertia, with $R_c = 0.4$(lattice size). This represents the core of the neutron star. Although in the simulation T = 400 MeV is used as a sample value, the temperature of few hundred MeV is needed to get correct energy scale of QCD transition for field theory model of Eqn.5.9 which corresponds to lattice data at zero chemical potential. Please note that this value of T has nothing to do with the actual temperature of the neutron star where QCD transition can occur at very small temperatures due to high baryon density. A dissipation term is added to enable relaxation of density fluctuations so that finally homogeneous phase is reached completing the phase transition. The decrease in energy due to dissipation term is added as a uniform background to the core energy to keep the total energy fixed. Note that with this assumption the change in the moment of inertia due to the net change in the phase of the core is ignored. The reason for this is there are numerical errors (of order few percent) in evolving a field theory configuration via leapfrog algorithm. Since we are looking for fractional changes of order 10^{-6} or even smaller, numerical errors will mask any such changes. Thus we keep the net energy fixed and only focus on redistribution of energy in defect network and the background. For the net change in the moment of inertia, we will use the estimates from Eqn.4.1 ([4]).

In the case of color flavor locked (CFL) phase inside the core of a pulsar the QCD

symmetry for three massless flavors, $SU(3)_c \times SU(3)_L \times SU(3)_R \times U(1)_B$ is broken down to the diagonal subgroup $SU(3)_{c+L+R} \times Z_2$ at very high baryon density [1] by the formation of a condensate of quark Cooper pairs. This transition will give rise to global strings (vortices). To roughly estimate resulting change in MI, we consider a simplified case by replacing the cubic term $(l^3 + l^{*3})$ in Eq.5.10 by $(|l|^2 + |l^*|^2)^{3/2}$ term. This modification in the potential will give rise to string defects only without any domain walls, as appropriate for the transition from (say) QGP phase to the CFL phase, while ensuring that we have the correct energy scale for these string defects.

The results of field theory simulations for C-D phase transition and the transition with only string formation as appropriate for the CFL phase are summarized in Fig.4.1 in section 4.3.2 . The magnitudes of the fractional changes due to density fluctuations for all the diagonal components, I_{xx}, I_{yy} and I_{zz} are found to be of the same order, though the changes for different components may be positive or negative. Net change in MI will include the very large contribution of order 10^{-5} due to net phase change of the core ([4]). The change due to fluctuations is the transient one and will dissipate away as star core achieves uniform new phase. As we see, the transient change have either sign, similarly the net change can also have either sign depending on the nature of the transition (QGP to CFL, or reverse transition, or hadronic to QGP etc.). Thus, this evolution pattern of fractional changes in MI suggests that the phase transition dynamics may be able to account for both glitch and anti-glitch events. The small change in the off-diagonal components, $I_{xy}, I_{xz}\&I_{yz}$ will cause the pulsar to wobble about its axis of rotation. This will lead to modulation of the peak intensity of pulse. This is a definitive, falsifiable, prediction of this model. Such phenomenon, if observed will be a signal for random density fluctuations occurring inside the star, strongly indicating a phase transition. Changes in the quadrupole moment will lead to gravitational wave emission.

Instead of doing dynamical field theory approach to estimate the effects of fluctuations due to topological defects, one could take a static approach in which one produces a network of defects inside the core of the pulsar by modeling the correlation domain formation in a cubic lattice, with lattice spacing ξ representing the

correlation length [19]. For the details of this approach and estimates of the fractional change in moment of inertia, see section 4.3.1 .

Thus we have shown that with simple equation of state for quark hadron transition, one can get a first order transition dynamics via mass accretion by a neutron star allowing for bubble nucleation. The estimates of critical bubble nucleation rate at density profile of the neutron star show that the transition can proceed after significant supercooling so that a single bubble nucleates at the centre sweeping through the entire supercritical core, thereby leading to a rapid change in the moment of inertia of the neutron star. Such macroscopic bubble nucleation can lead to density fluctuation as discussed in chapter 4 which can lead to glitches / anti-glitches. We have also discussed specific field theory realization of topological defect induced density fluctuations.

Bibliography

[1] M. Alford, K. Rajagopal and F. Wilczek, Phys. Lett. **B422** 247, (1998); M.G. Alford, A. Schmitt, K. Rajagopal and T. Schfer, Rev. Mod. Phys. **80**, 1455(2008).

[2] P.W. Anderson and N. Itoh, Nature **256**, 25 (1975); D. Pines and M.A. Alpar, Nature **316**, 27 (1985); B. Link, R.I. Epstein and K.A. van Riper, Nature **359**, 616 (1992).

[3] R. F. Archibald et al. Nature **497**, 591 (2013).

[4] H. Heiselberg and M. Hjorth-Jensen, Phys. Rev. Lett. **80**, 5485 (1998).

[5] E. Witten, Phys.Rev. **D 30**, 272 (1984).

[6] M.L. Olesen and J. Madsen, Phys. Rev. **D 49**, 2698 (1994)

[7] J. Cleymans, R.V. Gavai and E. Suhonen, Phys. Rep. **130**, 217 (1986).

[8] M.B. Voloshin, I.Yu. Kobzarev, and L.B. Okun, Yad. Fiz. **20**, 1229 (1974) [Sov. J. Nucl. Phys. **20**, 644 (1975)]; S. Coleman, Phys. Rev. **D15**, 2929 (1977).

[9] M. S. Ouellette, Thesis " Heating and cooling of neutron star crusts", UMI-31-71508, Michigan State University, 2005

[10] L.D. Landau and E.M. Lifshitz, "Statistical Physics" 3rd Ed. Pergamon Press (1980).

[11] L. Ju, D. G. Blair and C. Zhao, Rep. Prog. Phys. **63**, 1317 (2000).

[12] T.W.B. Kibble, J. Phys. **A 9**, 1387 (1976); Phys. Rept. **67**, 183 (1980).

[13] L.D. McLerran and B. Svetitsky, Phys. Rev. **D24**, 450 (1981); B. Svetitsky, Phys. Rept. **132**,1 (1986).

[14] T. Bhattacharya, A. Gocksch, C.K. Altes, and R.D. Pisarski, Nucl. Phys. **B383**, 497 (1992).

[15] B.Layek, A.P. Mishra and A.M. Srivastava; Phys. Rev. **D71**, 074015(2005)

[16] U.S. Gupta, R.K. Mahapatra, A.M. Srivastava and V.K. Tiwari; Phys. Rev. **D82**, 074020 (2010); *ibid*, Phys. Rev. **D 86**, 125016 (2012).

[17] R.K. Mohapatra and A.M. Srivastava, Phys.Rev. **C 88**, 044901 (2013).

[18] A. Dumitru and R.D. Pisarksi, Phys. Lett. **B 504**, 282 (2001); Phys. Rev. **D 66**, 096003 (2002); Nucl. Phys. **A698**, 444 (2002).

[19] T. Vachaspati and A. Vilenkin, Phys. Rev. **D 30**, 2036 (1984).

Chapter 6

Inflation

Cosmological inflation is a phase of exponential expansion assumed to have taken place in the very early universe. Inflation was introduced [1] as a solution to the cosmological problems which appear in the standard big bang model. Inflation provides correct initial conditions for the standard big bang cosmology. As it turned out, inflation also provides the seed of structure formation. However, there are two main unresolved questions concerning inflation. These are, realistic elementary particle physics model which can give rise to inflation, and the initial conditions for inflation. Till date many models of inflation have been proposed [2] which are in good agreement with the observational data, however issue of initial conditions for inflation is still a debatable issue. What is meant by initial conditions for inflation is that, whether inflation is generic or it requires special fine tuned initial conditions? This question is very important because inflation was initially proposed to solve similar initial condition problems of big bang model. If inflation itself requires fine tuned initial condition then the issue of initial conditions is not solved and the existence of our universe is not generic. In this thesis we will argue how to generate inflation from a generic initial condition. In this chapter, the cosmological standard model will be discussed first, after that the inflationary paradigm will be introduced. For a brief review on cosmology and inflation, also see [3–7] and references therein.

6.1 Standard Model of Cosmology

The hot big bang model assumes that the universe has been expanding and gradually cooling from an initial state of singularity (hot big bang). It also assumes that the universe is homogeneous and isotropic on large scale (today these scales are of the order of 100 Mpc). Both assumptions are justified by the observation of the cosmic microwave background radiation (CMBR), a relic of the earlier hot era.

The universe is, therefore, described to a good approximation by the Friedmann-Robertson-Walker (FRW) metric which is the most general metric of a homogeneous and isotropic spacetime,

$$ds^2 = dt^2 - a(t)^2 \left[\frac{dr^2}{1 - kr^2} + r^2 \left(d\theta^2 + \sin^2 \theta \, d\phi^2 \right) \right], \tag{6.1}$$

where the coordinates (r, θ, ϕ) are comoving coordinates independent of t, and the time coordinate t is the cosmological time, time measured by a comoving observer. In the line element 6.1, $a(t)$ is the scale factor which encodes the expansion of the universe. The evolution of the scale factor $a(t)$ determines the evolution of the universe which is in turn determined by the matter content of the universe through Einstein equations. Here k represents the curvature of the spatial part of the FRW metric. k can take three values: k=1 for a positively curved closed universe, k=0 for a flat universe and k=-1 for a negatively curved open universe. For a homogeneous and isotropic universe as given by equation 6.1, the Eienstein equations lead to Friedmann equations [8–10],

$$\left(\frac{\dot{a}}{a} \right)^2 + \frac{k}{a^2} = \frac{8\pi G}{3} \rho, \tag{6.2}$$

$$\dot{\rho} + 3 \frac{\dot{a}}{a} (\rho + P) = 0, \tag{6.3}$$

$$\frac{\ddot{a}}{a} = -\frac{4\pi G}{3} (\rho + 3P), \tag{6.4}$$

where ρ is the total energy density, P is the total pressure, G is the gravitational constant and an over-dot is a derivative with respect to cosmological time t. For the homogeneous and isotropic metric, ρ, P and $a(t)$ are only functions of t. For a multi component universe total energy density and pressure can be written as the sum of the energy density and pressure of all the individual components,

$$T_{\mu\nu} = \sum_{\alpha} T^{(\alpha)}_{\mu\nu} \Rightarrow \rho = \sum_{\alpha} \rho^{(\alpha)}, \quad P = \sum_{\alpha} P^{(\alpha)}, \tag{6.5}$$

where α denotes different components like, radiation, matter etc. Equation 6.3 is satisfied for all the individual components. The underling assumption is that interactions among individual components are not significant for the background evolution. Although in this case we neglect the interaction between different components, however these interactions are really important for whatever cosmological structure we see today e.g. CMB, galaxy etc. Equation 6.3 can also be derived from the conservation of total energy momentum tensor,

$$\nabla_{\mu} T^{\mu\nu} = 0. \tag{6.6}$$

This is very interesting that equation 6.3 which is derived using only the curvature part of the Einstein equation, can also be derived using the conservation of energy momentum tensor. This happens due to the Bianchi identity, which is an alternative way to derive Einstein equations.

To quantify the change in the scale factor, it is useful to define the Hubble parameter,

$$H(t) = \frac{\dot{a}}{a}, \tag{6.7}$$

H^{-1} is called the Hubble radius.

The energy momentum tensor can be assumed to have ideal fluid form with equation of state $P = \omega\rho$ for constant ω. For different components the value of ω can be given as,

- Dust/cold non relativistic matter: $\omega = 0$, so $P = 0$.
- Radiation/hot matter: $\omega = \frac{1}{3}$, so $P = \frac{1}{3}\rho$.
- Vacuum energy: $\omega = -1$, so $P = -\rho$.

Substituting the equation of state $P = \omega\rho$ in the equation 6.3 and integrating it, we get the following normalized equation,

$$\rho = \rho_0 \left(\frac{a_0}{a}\right)^{3(1+\omega)}, \tag{6.8}$$

where a_0 is the scale factor for energy density ρ_0. Scale factor can be normalized in such a way that $a_0 = 1$, is the present value of the scale factor. After substituting different values of ω in the equation 6.8 we get,

- Dust/cold non relativistic matter: $\omega = 0$, $\rho(t) \sim a^{-3}(t)$, so matter dilutes because of the change in the number density due to the expansion,
- Radiation/hot matter: $\omega = \frac{1}{3}$, so $\rho(t) \sim a^{-4}(t)$. Energy density of the radiation changes not only because of the change in number density, but also due to the change in the energy (cosmological redshift).
- Vacuum energy: $\omega = -1$, $\rho =$ constant.

Form the time evolution of the different components of the universe it is clear that radiation energy density falls more rapidly than the matter energy density. So towards the beginning of the universe when the temperature was very high, evolution of the universe was dominated by the radiation energy density (Radiation dominated era). However as the universe expanded there was an epoch when the radiation energy density became equal to the matter energy density. This epoch is known as radiation-matter equality. For cosmological evolution radiation-matter equality is very important, CMB power spectrum, large scale structure formations etc. depend on this epoch. After this epoch matter energy density takes control over radiation

(Matter dominated era). For the growth of the density perturbations matter dominated era is very important. Radiation dominated era does not allow for the growth of the primordial density perturbations due to the radiation pressure, on the other hand, matter dominated era allows for the non-linear growth of density perturbations. Eventually, matter density also fades away and the vacuum energy or the cosmological constant (Λ) takes control. Our universe has recently (w.r.t the age of the universe) entered the Λ dominated era. For the behavior of the energy densities of different components it is clear that once the universe is dominated by the cosmological constant, it will always be the dominating component. So in the early universe, the fraction of the cosmological constant in the total energy density must be very small.

The key characteristics of our universe today are determined by the following parameters,

- Hubble parameter H_0 determines the expansion rate of the universe.
- Deceleration parameter q_0 determines the rate of expansion. Historically it was assumed that the expansion of the universe will eventually slow down due to the attractive nature of gravity, hence the name 'deceleration parameter', but observations of type Ia supernovae tell us that our universe is not decelerating, on the contrary, the expansion rate is increasing.
- Dimensionless density parameter $\Omega(t)$ and its value today Ω_0.

In terms of density parameter first Friedmann equation can be written as,

$$\Omega(t) - 1 = \frac{k}{a^2 H^2}, \quad \Omega(t) \equiv \frac{\rho(t)}{\rho_c(t)} = \frac{8\pi G\rho}{3H^2}, \quad \rho_c(t) = \frac{3H^2}{8\pi G}. \tag{6.9}$$

It is clear from the equation 6.9 that $\Omega(t)$ is the measure of the spatial curvature of the universe. There are three possible cases,

- $\Omega(t) = 1$ implies $k = 0$ and $\rho = \rho_c \longrightarrow$ flat universe (just expands forever).
- $\Omega(t) > 0$ implies $sign(k) > 0$ and $\rho > \rho_c \longrightarrow$ closed universe (re-collapses),

- $\Omega(t) < 0$ implies $sign(k) < 0$ and $\rho < \rho_c \longrightarrow$ open universe (expands forever).

From the first expression in equation 6.9 it is clear that the right hand side does not change sign under cosmological evolution, hence e.g. if the universe started with $\rho > \rho_c$ then, during the evolution $\rho(t)$ will always be greater than $\rho_c(t)$.

After this brief discussion lets come to the ΛCDM model. This model is a parametrization of the Big Bang cosmological model of our Universe with a cosmological constant (Λ)/dark energy, cold dark matter (CDM) and radiation. This is the widely accepted model for our Universe, and till date this model is consistent with all the observational data e.g. CMB [11], large scale structures [12], Hubble constant measurement and the expansion of the universe [13, 14]. All the observational data indicates that our universe is spatially flat (k = 0) to a great accuracy, $\Omega_0 = 1.0005 \pm 0.00333$ [11], with $\Omega_m \simeq 0.3$ and $\Omega_\Lambda \simeq 0.7$. Value of H is around 70 Km s^{-1} Mpc^{-1}. Here we are not giving exact recent numbers, because that is not necessary for this thesis. However one can see recent Planck results for exact values of cosmological parameters [15].

For spatially flat universe, using the Friedmann equation 6.2 and equation 6.8 one can show that for a single component characterized by equation of state parameter ω,

$$(\dot{a})^2 \propto a^{-(1+3\omega)}. \tag{6.10}$$

Further if we assume $a(t)$ has power law behaviour, $a(t) \propto t^q$, then it can be shown that, the scale $a(t)$ has the following time dependence,

$$a(t) \sim t^{2/(3+3\omega)}, \quad \text{when} \quad \omega \neq 1, \tag{6.11}$$

hence for radiation dominated era ($\omega = 1/3$), $a(t) \sim t^{1/2}$ and for matter dominated era ($\omega = 0$), $a(t) \sim t^{2/3}$.

One very important comoving distance is the comoving horizon, which is defined as the distance travelled by the light since $t = 0$. This is given by,

$$\eta = \int_0^t \frac{dt'}{a(t')}. \tag{6.12}$$

Since the beginning of the universe at $t = 0$, no information could have propagated beyond a comoving distance η. The proper size of the horizon could then be written as $a(t)\eta$. It is important to note that there are two length scales associated with cosmology, these are proper horizon and the Hubble radius. However using the time dependence of the scale factor $a(t)$ in radiation and matter dominated era, one can show that both length scales are, $\sim \frac{1}{t}$. Hence in radiation and matter dominated era one uses Hubble length and horizon interchangeably. As we will discuss later for inflationary era Hubble and horizon have different time dependencies.

In the expanding universe, the light traveling towards us from a distance sources will be red shifted since these sources are moving away from us. The red shift z is defined as,

$$1 + z \equiv \frac{\lambda_{observed}}{\lambda_{emitted}} = \frac{1}{a}, \tag{6.13}$$

where we have used the fact that today the scale factor is normalized to 1. Since in a given cosmological model $a(t)$ is a monotonic function of t, we can also use the redshift as an equivalent of time.

6.2 Short Comings of Big Bang Cosmology

We have already mentioned that standard hot big bang cosmology model is very successful and in accordance with different observational data. It has successfully predicted experimentally verified observable, e.g. cosmic microwave background, an abundance of light elements etc. But the hot big bang cosmology has some short comings, these are,

- The flatness problem,
- The monopole problem,
- The horizon problem.

6.2.1 The Flatness Problem

Let us assume that Einstein equations are valid since the Planck era. Einstein equations are classical field equations and at the Planck era quantum gravity effects will be dominating. Hence this assumption is a tremendous extrapolation. At the Planck era the temperature of the universe is $T_{pl} \sim m_{pl} \sim 10^{19}$GeV. It is clear from equation 6.9 if the universe is perfectly flat today, then $\Omega = 1$ at all times. But if there is a small curvature term present today, then $\Omega \neq 1$ and in that case, $(\Omega - 1)$ has a non-trivial time dependence.

During radiation dominated era $H^2 \propto \rho_R \propto a^{-4}$ and in matter dominated era $H^2 \propto \rho_M \propto a^{-3}$. Hence, in radiation dominated era the evolution of Ω as a function of scale factor can be written as,

$$\Omega - 1 \propto \frac{1}{a^2 H^2} \propto \frac{1}{a^2 a^{-4}} \propto a^2, \tag{6.14}$$

and in the matter dominated era,

$$\Omega - 1 \propto \frac{1}{a^2 H^2} \propto \frac{1}{a^2 a^{-3}} \propto a, \tag{6.15}$$

In both the cases $\Omega - 1$ decreases as we go backwards in time. Since we know $(\Omega - 1)$ today we can track $(\Omega - 1)$ at the epoch of BBN using single component approximation,

$$\frac{|\Omega - 1|_{T=T_N}}{|\Omega - 1|_{T=T_0}} \simeq \left(\frac{a_N^2}{a_0^2}\right) \simeq \left(\frac{T_0^2}{T_N^2}\right) \sim \mathcal{O}(10^{-16}), \tag{6.16}$$

where we have used, $T \sim \frac{1}{a}$, $T_0 \sim 10^{-13}$ GeV is the present temperature of CMB radiation and nucleosynthesis happened at a temperature $T_N \sim 1$ MeV [5]. Simple extrapolation of this analysis to the Planck scale will give,

$$\frac{|\Omega - 1|_{T=T_{pl}}}{|\Omega - 1|_{T=T_0}} \simeq \left(\frac{a_{pl}^2}{a_0^2}\right) \simeq \left(\frac{T_0^2}{T_{pl}^2}\right) \sim \mathcal{O}(10^{-64}), \tag{6.17}$$

where we have used, Planck scale temperature $T_{pl} \sim 10^{19}$ GeV.

Even in a multi component universe one can show that in early stages universe was remarkabley more spatially flat than today. In order to get the correct value of $(\Omega - 1)$ today, its value must be fine tuned to extremely close to zero at early times. But there is no reason for such fine tuned value of $(\Omega - 1)$ in the early universe.

6.2.2 The Monopole Problem

Our universe has gone through symmetry breaking transitions many times. One of such transitions is the GUT scale symmetry breaking phase transition. The energy scale associated with the GUT phase transition is $E_{GUT} \sim 10^{12}$TeV, and the associated time scale $t_{GUT} \sim 10^{-36}$sec. Grand Unified Theories predict that the GUT phase transition creates point-like topological defects, known as magnetic monopoles.The rest mass of the magnetic monopoles created in the GUT phase transition is predicted to be, $m_M \sim E_{GUT} \sim 10^{12}$ TeV. If we assume that number of magnetic monopoles in a Hubble volume at the GUT scale ($H_{GUT}^{-1} = 2t_{GUT}$)is atleast one, then the lower bound on the number density and the energy density of these magnetic monopoles at the time of their creation would be $n_M(t_{GUT}) \sim 10^{82}\text{m}^{-3}$ and $\rho_M(t_{GUT}) \sim 10^{94}$TeV m^{-3}, respectively. However, Energy density of radiation at the time of the GUT phase transition was $\rho_\gamma(t_{GUT}) \sim 10^{104}$ TeV m^{-3}. We also know that, $\rho_\gamma \propto a^{-4}$ and $\rho_M \propto a^{-3}$. Thus the magnetic monopoles would have dominated the energy density of the universe when the age of the universe was only $t \sim 10^{-16}$sec. However today the universe is apparently free of magnetic monopoles, this puzzle is known as the monopole problem.

6.2.3 The Horizon Problem

In the early universe when the cosmological red shift was around $z \sim 1100$, there were three closely related epochs. First, is the epoch of recombination, when ionized baryonic component of the universe (atomic nucleus, free electron etc.) formed neutral atoms. Before this era, photon energy was higher than the binding energy of the neutral atoms (mainly Hydrogen atoms). So, there were no neutral atoms before this era. But as the temperature of the universe decreases due to expansion, photon became less energetic and eventually for the first time, neutral atoms are formed. Primary interaction between photons and the free electrons is the Thomson scattering and the interactions between free electrons and photons are dominant over the nucleus photon interactions. Due to the formation of neutral atoms the number density of the free electrons became less and the Thomson scattering rate, which is proportional to the number density of free electron, also became less. Once the Thomson scattering rate dropped sufficiently below the Hubble expansion rate, photons decoupled from the rest of the plasma. This was the era of photon decoupling. The photon decoupling was not a rapid event, however, there was a time when the Thomson scattering rate became so low that photons suffered the last scattering and after that their momentum distribution became frozen. This is the epoch of the last scattering. After last scattering photon did not scatter with the free electrons and today we observe these photons as Cosmic Microwave Background Radiation. Since there momentum space distribution was not altered after the last scattering (apart from overall refshift), they carry pristine information about the physics at the surface of the last scattering.

CMB sky as measured by WMAP is shown in the figure 6.1. The average temperature of CMB is around 2.7K. Temperature fluctuations in CMB are shown as red spots and blue spots. The temperature fluctuations in the CMB result from the density fluctuations that existed at the time of the last scattering. In this plot blue spots corresponds to over densities and red spots correspond to under densities. Temperature fluctuations are of the order of $\delta T/T \sim 10^{-5}$, as shown in the figure 6.2. Angular separation between two points in the CMB sky is related to the multipoles

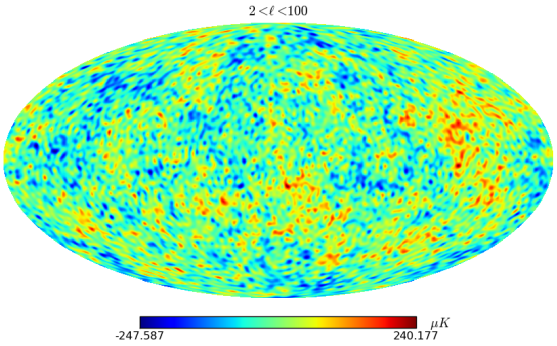

Figure 6.1: CMB sky as measured by WMAP

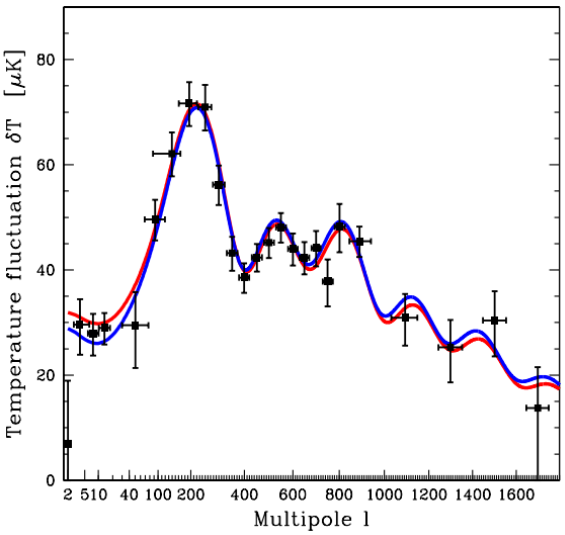

Figure 6.2: Temperature fluctuations as a function of multipoles.

as, $\theta \sim 180/l$.

It can be shown that the angular separation corresponding to the horizon distance at the last scattering surface as seen from the Earth today is $\theta_{hor} \simeq 2^\circ$ [5]. Points on the last scattering surface separated by an angle $\theta > 2^\circ$ were out of contact with each other at the time the temperature fluctuations were stamped upon the CMB. But in the figure 6.2 we find $\delta T/T$ is as small as 10^{-5} on scales $\theta > 2^\circ$. How can the average temperature and fluctuations in causally disconnected regions be of the same order, this is known as the horizon problem.

Horizon problem and its solution can be understood easily in the conformal diagram because in an expanding space-time the propagation of light (photons) is best studied using conformal time. The line element in conformal time coordinate becomes,

$$ds^2 = a^2(\tau)[d\tau^2 - d\chi^2]. \tag{6.18}$$

For null geodesics, $\Delta\chi(\tau) = \pm\Delta\tau$, and the light cone diagram is shown in the figure 6.3. In this figure dotted lines show the worldlines of comoving objects. The event horizon is the maximal distance to which we can send signal. The particle horizon is the maximal distance from which we can receive signals. Mathematically

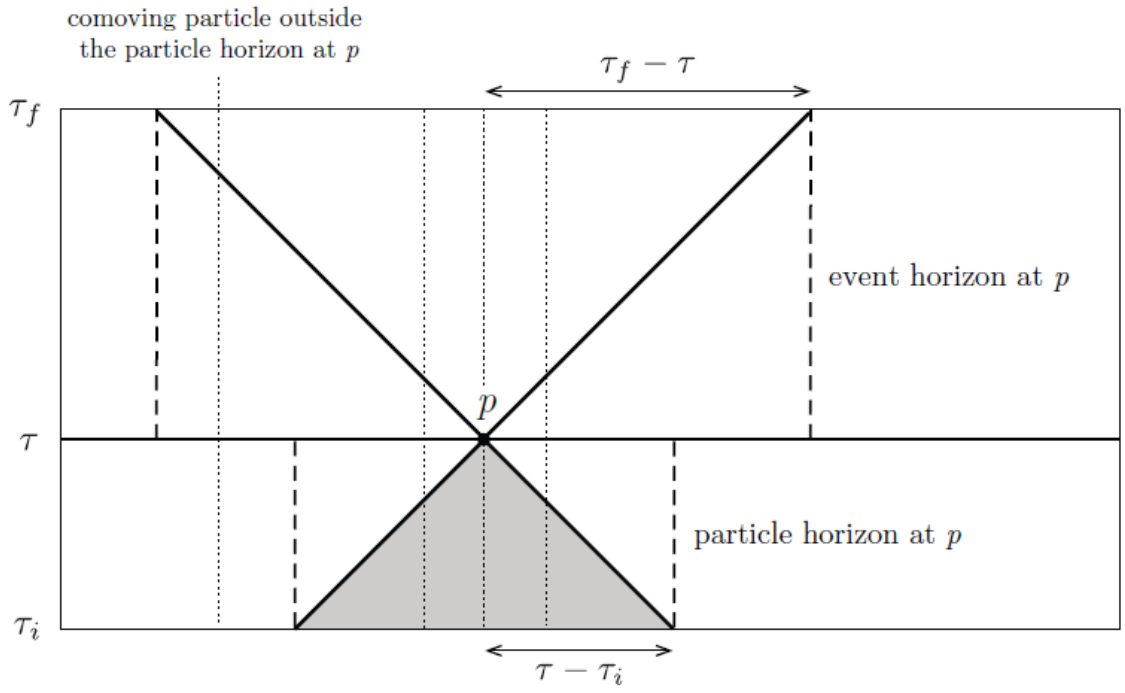

Figure 6.3: Spacetime diagram illustrating the concept of horizons [6]. Horizontal axis and vertical axis corresponds to comoving distance χ and conformal time respectively.

particle horizon can be written as,

$$\chi_{ph}(\tau) = \tau - \tau_i = \int_{t_i}^{t} \frac{dt}{a(t)} = \int_{\ln a_i}^{\ln a} (aH)^{-1} d\ln a. \tag{6.19}$$

For a universe dominated by a fluid with constant EOS: $P = \omega\rho$,

$$a(t) = \left(\frac{t}{t_0}\right)^{2/3(1+\omega)}, \quad (aH)^{-1} = H_0^{-1} a^{\frac{1}{2}(1+3\omega)}, \quad H_0^{-1} = \frac{2}{3(1+\omega)} t_0. \tag{6.20}$$

Hence, with strong energy condition, $(1 + 3\omega > 0)$, the comoving Hubble radius $(aH)^{-1}$ increases as the universe expands. So in this case contribution in particle horizon is dominated by the late times and early time contributions are negligible.

$$\chi_{ph}(a) = \frac{2H_0^{-1}}{1+3\omega}[a^{\frac{1}{2}(1+3\omega)} - a_i^{\frac{1}{2}(1+3\omega)}] \equiv \tau - \tau_i, \tag{6.21}$$

where, $\tau_i \equiv \frac{2H_0^{-1}}{1+3\omega} a_i^{\frac{1}{2}(1+3\omega)}$. If $(1 + 3\omega) > 0$, then $\tau_i \to 0$ as $a_i \to 0$.

Since in the standard big bang Model radiation and matter satisfy the strong energy condition, universe begins when $a_i = 0$ and $\tau_i = 0$. Thus in the standard big bang Model of universe the age of the universe is finite in the conformal coordinate as illustrated in the figure 6.4,

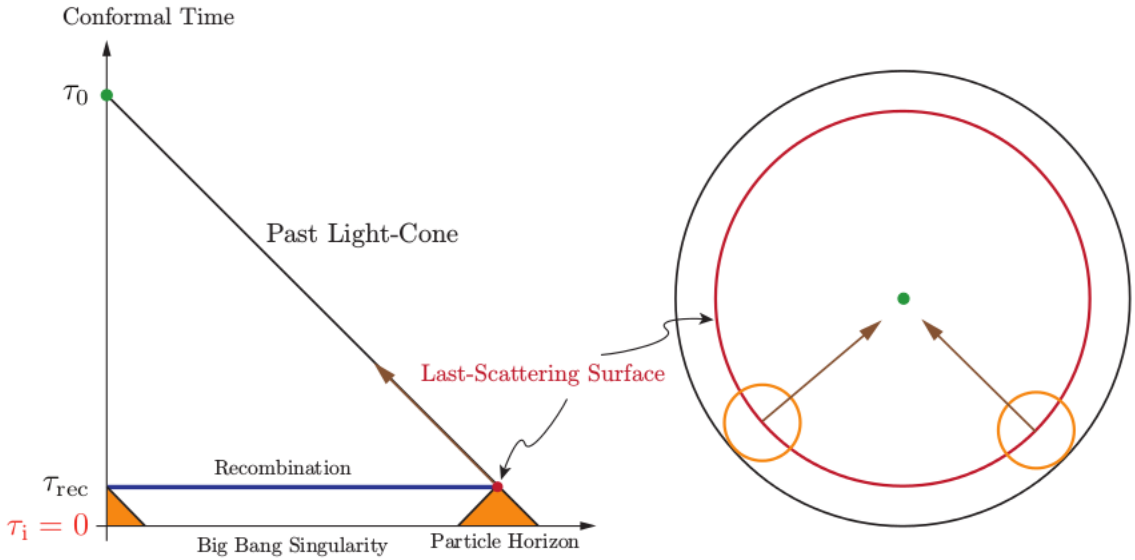

Figure 6.4: Conformal diagram of Big Bang cosmology. [6].

It is clear from the figure 6.4 that finite value of τ_i is the reason of the horizon problem. So, if the the big bang singularity can be pushed to negative conformal time, then the horizon problem can be solved (figure 6.5). This can be achieve in the following way,

$$\tau_i \equiv \frac{2H_0^{-1}}{1+3\omega} a_i^{\frac{1}{2}(1+3\omega)} \to -\infty, \quad \text{as} \quad a_i \to 0, \quad \text{iff} \quad (1+3\omega) < 0. \tag{6.22}$$

It is clear from this discussion that horizon problem can be solved if the strong energy condition is violated: $(1+3\omega) < 0$. This also translates into the fact that a phase of decreasing Hubble radius in the early universe can solve the horizon problem. Hence,

$$\frac{d}{dt}(aH)^{-1} = -\frac{\ddot{a}}{(\dot{a})^2} < 0 \Rightarrow \ddot{a} > 0. \tag{6.23}$$

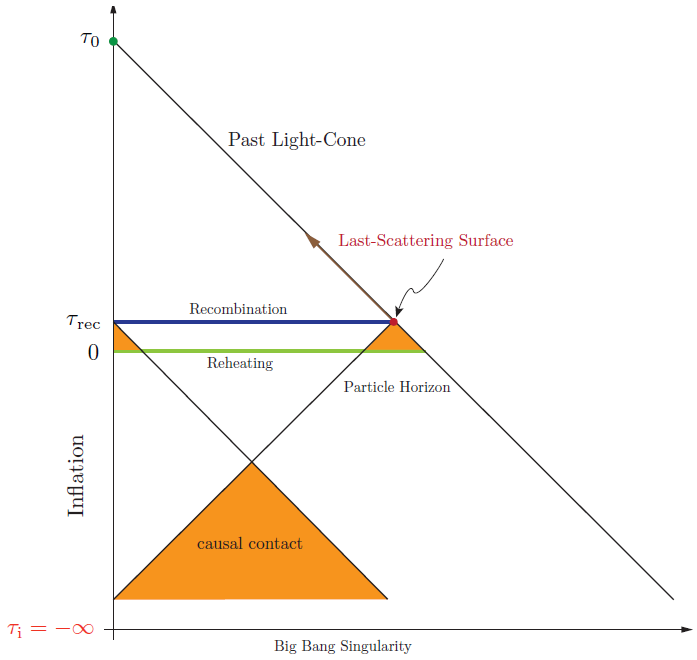

Figure 6.5: Conformal diagram of inflationary cosmology [6].

Thus a phase of accelerating universe in the early universe can solve the horizon problem. This epoch of accelerating expansion is known as Inflation. Cosmological constant with $P = -\rho$ can give rise to Inflation. For cosmological constant, Friedmann equation 6.4 gives,

$$\frac{\ddot{a}}{a} = \frac{8\pi G\rho}{3} = \frac{\Lambda_i}{3} \Rightarrow \ddot{a} > 0, \tag{6.24}$$

other Friedmann equation 6.2 for $k = 0$,

$$\left(\frac{\dot{a}}{a}\right) = \frac{\Lambda_i}{3} = H_i^2 \Rightarrow a(t) \propto e^{H_i t}. \tag{6.25}$$

In the case inflation driven by cosmological constant, H is constant and the scale factor grows as $e^{H_i t}$. Thus in this case $|1 - \Omega(t)| \propto 1/a^2(t) \propto e^{-2H_i t}$. The relation between the density parameter before and after inflation,

$$|1 - \Omega(t_f)| = e^{-2N}|1 - \Omega(t_i)|, \tag{6.26}$$

where $N = H_i(t_f - t_i)$. t_i is the start of inflation and t_f is the end of inflation. N is the number of e-folding. If $N = 100$, then $|1 - \Omega(t_f)| \sim 10^{-87}$, even if $|1 - \Omega(t_i)| \sim 1$. Thus the value of density parameter $\Omega(t)$ close to 1 can be easily achieved naturally. Also, During the period of exponential expansion number density of the magnetic monopoles decreases as, $n_M(t_f) = e^{-3N} n_M(t) \sim 10^{-49}\mathrm{m}^{-3}$. Thus inflation which was introduced to solve horizon problem can also solve flatness problem and monopole problem. However inflationary paradigm became more important because inflation can give rise to correct initial conditions for structure formation [16].

6.3 Inflationary Models

Inflationary cosmology started to emerge around the 1970s. Cosmological constant can give rise to inflation, but it is not a good candidate for inflation, because in cosmological constant model inflation never ends. So one needs a dynamical field which can give rise to inflation and also there is a way to achieve the graceful exit. It became apparent that the energy density of a scalar field is equivalent to the vacuum energy/cosmological constant [17], but changing due to cosmological phase transitions [18]. For first order phase transitions, these changes can occur discontinuously [19]. The first model of inflation was proposed by Starobinksy [20]. First particle physics motivated model was proposed by Guth [1]. This model is known as "old inflation" based on supercooling during cosmological phase transitions. Till date there are many models of inflation proposed, e.g. Power Law model [21], Hilltop model [22], Natural inflation [23, 24], D-brane inflation [25–27], Exponential potential in supergravity inspired models [28–32], Hybrid model [33,34], α attactors [35], Higgs inflation [36–39] etc. For good reviews of the inflationary models and their current status see, [2,40–43].

6.3.1 Old Inflation

The old inflation model assumed general relativity plus a single scalar field which is trapped in a metastable vacuum state of nonzero potential energy. At high temperature, field is localized in the vicinity of the origin. This constant vacuum energy gives rise to inflation. In this model inflation proceeds exponentially with $a(t) \propto \exp(\sqrt{\frac{V_0}{3M_{pl}^2}}t)$, where V_0 is the potential energy of metastable vacuum.

In this model classically stable inflation ends by quantum tunneling of the field into the true vacuum, nucleating a bubble of true vacuum in the sea of false vacuum. However to reheat the universe the bubbles must collide. The Universe is expanding at an exponential rate while the bubbles are nucleating. Even though the bubbles nucleate at a constant rate per volume per time, they will be unable to meet and percolate unless the nucleation rate is high enough. On the other hand, if the nucleation rate is high enough then the phase transition will be completed almost immediately, failing to provide sufficient inflation. Thus achieving the correct amount of inflation and also graceful exit of inflation are two contradictory requirements. Guth himself noticed this problem. This problem was solved by Linde in the so called new inflation picture. Schematic diagram of old and new inflation is shown in the figure 6.6

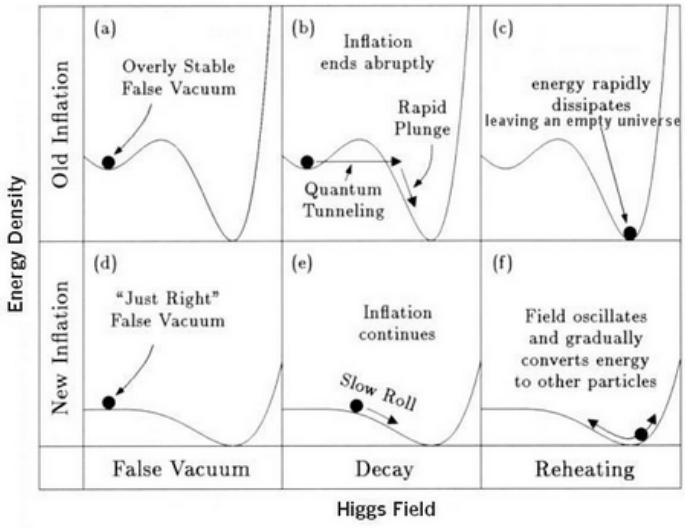

Figure 6.6: Schematic visualization of old and new inflation [44].

6.3.2 New Inflation

A new inflation theory emerged between 1981-1982 [45, 46]. In this model, inflation can be achieved due to an unstable state at the top of the potential as shown in the figure 6.6. The inflation field ϕ then rolls down to the minimum of its effective potential, where it oscillates and reheats the universe. This new scenario explained the homogeneity of the Universe and it does not occur in the false vacuum state. This model requires the effective potential to have a very flat plateau near $\phi = 0$. For discussion on the generation of density perturbation during slow roll inflation in this model see, [47].

6.3.3 Single Field Slow-Roll Theories of Inflation

The central feature in slow-roll models of inflation is that the potential energy of the inflaton field dominates the energy density of the field and changes slowly during inflation epoch due to an almost flat potential (see figure 6.7). Ordinary fields such as matter and radiation fields also exist during this period but their contributions are negligible with respect to the inflaton field. In later stages of inflation, potential energy decreases as the kinetic energy of the inflaton field increases. Once the energy of the inflaton field is no longer sufficiently dominated by potential energy, inflation ends. At the end of the inflation, inflaton field oscillates in the true vacuum of the potential and reheats the universe.

For single scalar field models, the energy density and pressure of the homogeneous background scalar field can be expressed as,

$$\rho_\phi = \frac{1}{2}\dot{\phi}^2 + V(\phi), \tag{6.27}$$

$$P_\phi = \frac{1}{2}\dot{\phi}^2 - V(\phi). \tag{6.28}$$

Equation of motion of the inflaton field is,

$$\ddot{\phi} + 3H\dot{\phi} + V' = 0, \tag{6.29}$$

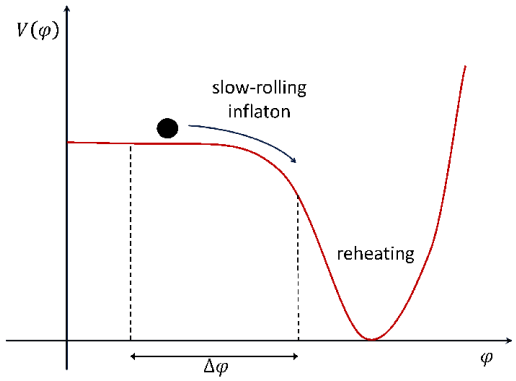

Figure 6.7: Example of inflationary potential with a "flat" region. After the slow-roll of the inflaton field ϕ the reheating phase starts, the field oscillates around the minimum of the potential and decays to other particles [48].

where $\dot{\phi}$ is the derivative of homogeneous inflaton field with respect to t and V' is the derivative of the potential with respect to the field ϕ. It can be shown that a convenient way to assess whether a given potential $V(\phi)$ can lead to slow-roll inflation is to compute the potential slow-roll parameters [6],

$$\epsilon_V \equiv \frac{M_{pl}^2}{2}\left(\frac{V'}{V}\right)^2, \qquad |\eta_V| \equiv M_{pl}^2\frac{|V''|}{V}, \tag{6.30}$$

where $M_{pl}^2 = \frac{1}{8\pi G}$.

Successful slow-roll inflation occurs when these parameters are small, $\epsilon_V << 1$ and $|\eta_V| << 1$. The first condition tells that for inflation to occur $\dot{\phi}^2$ term has to be negligible compared to $V(\phi)$. Under this condition, the equation of state of single scalar field model becomes $P(\phi) \simeq -\rho(\phi)$ and it can give rise to inflation. The second condition comes from the fact that, for sufficient inflation, the first condition has to be satisfied for a sufficient amount of time during the field evolution. This is achieved by assuming $\ddot{\phi}$ term in the equation of the motion of the scalar field is small compared to the $\dot{\phi}$ term. Due to this condition the inflaton field moves towards the true vacuum slowly and hence produces sufficient inflation. Inflation stops when $\epsilon_V \sim \mathcal{O}(1)$ and $|\eta_V| \sim \mathcal{O}(1)$. Number of e-foldings in the slow roll inflation model can be written as,

$$N = \frac{1}{M_{pl}^2} \int_{\phi_{end}}^{\phi} \frac{V}{V'} d\phi. \tag{6.31}$$

The lower bound for sufficient inflation is in the range $N = 50 - 60$ [49].

6.3.4 Evolution of Scales

We have already introduced the notion of conformal time, which is defined as,

$$d\tau = \frac{dt}{a(t)}. \tag{6.32}$$

In this coordinate system spatially flat FRW metric becomes,

$$ds^2 = a^2(\tau) \left(-d\tau^2 + \delta_{ij} dx^i dx^j \right). \tag{6.33}$$

In this coordinate system one of the Friedmann equations 6.4 reduces to,

$$\mathcal{H}' = -\frac{1}{2} \mathcal{H}^2 (1 + 3\omega), \tag{6.34}$$

where $\mathcal{H} \equiv aH$ is the comoving Hubble parameter and '$\prime$' denotes the derivative with respect to conformal time. We have already discussed that inflation occurs when $(1 + 3\omega) < 0$. Thus in case of inflation equation 6.34 clearly shows that comoving Hubble $\mathcal{H}$ increases or the comoving Hubble radius $\mathcal{H}^{-1}$ decreases with time. For standard radiation and matter dominated era $(1 + 3\omega) > 0$ and comoving Hubble $\mathcal{H}$ decreases or the comoving Hubble radius $\mathcal{H}^{-1}$ increases with time. All the other comoving scales always remains unchanged. Comoving Hubble radius and the other comoving scales are shown in the figure 6.8 .

In figure 6.8 λ_1 and λ_2 are some covoming wavelengths and $\lambda_1 > \lambda_2$. The fluctuations corresponding to the wavelengths λ_1 and λ_2 are originated deep inside the horizon (Hubble) before the inflation. As the inflation starts the comoving Hubble decreases, however, the comoving wavelengths remains unchanged. The epoch when a wavelength crosses the comoving Hubble radius is known as 'Horizon exit'. This epoch can be quantified as $\lambda = aH$. After the end of the inflation comoving Hubble radius increases. Thus the wavelengths which are outside the Hubble volume start to

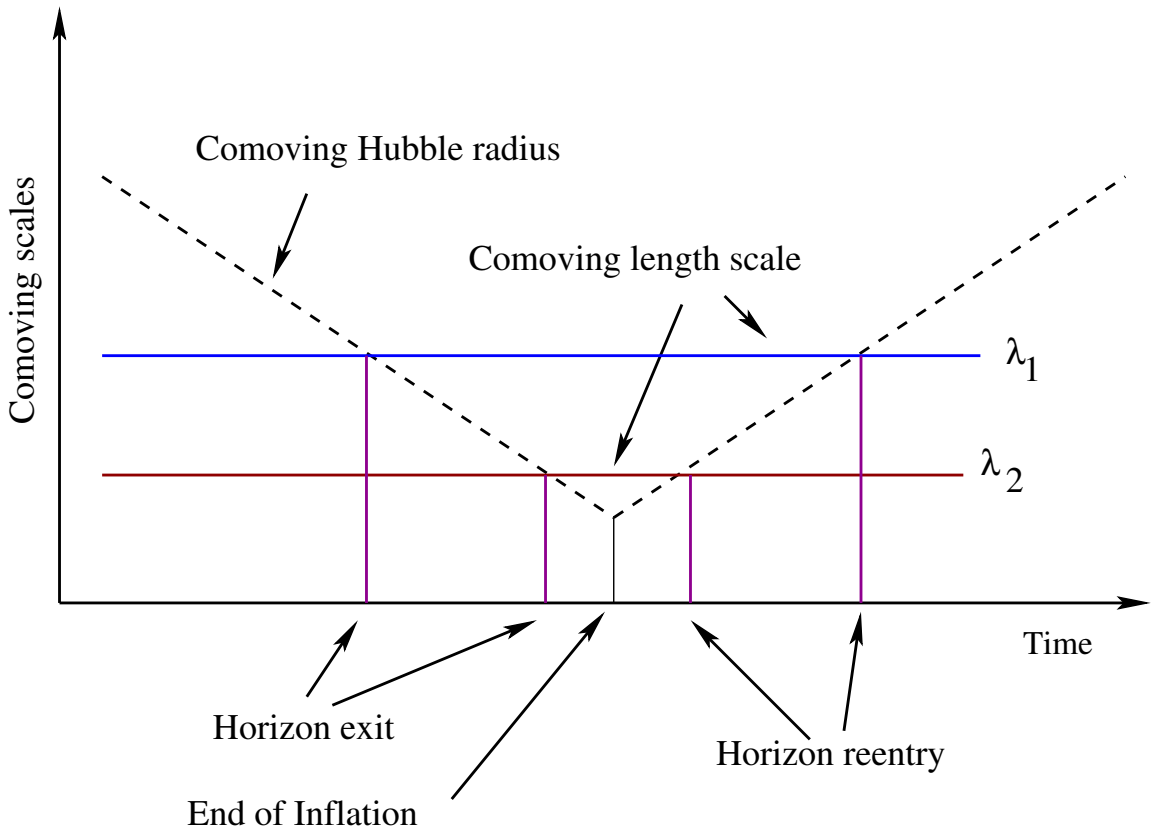

Figure 6.8: Evolution of scale during and end of the inflation

reenter the Hubble volume. For the figure 6.8 it is clear that large wavelengths get out of the Hubble volume first and they re-enter the Hubble volume late. It is important to note that 'horizon exit' for the large wavelengths happen very early, within a couple of e-foldings. Smaller wavelengths leave the Hubble volume late but they re-enter very early. When the wavelengths representing some fluctuation is outside the Hubble volume their evolution cannot happen by any causal dynamics. These wavelengths are 'frozen' outside the horizon. But once they re-enter the Hubble volume they again start to evolve. The first acoustic peak that we observe in the CMB power spectrum corresponds to the wavelength which just entered the Hubble volume at the time of the last scattering. All the other wavelengths smaller than this entered the Hubble volume much earlier and they went through an evolution in the cosmic plasma. These small wavelengths give rise to the subsequent peaks in the CMB power spectrum (for details see [3]), known as acoustic peaks.

6.3.5 Constraints on Models of Inflation

As we have seen in the figure 6.2, apart from a smooth background, CMB also has temperature fluctuations. According to the current understanding seed of these fluctuations were generated in the inflationary era. We will not discuss cosmological perturbation theory in this thesis, for details of cosmological perturbation theory and the derivations of different constraints, see [4, 6, 50, 51]. It can be shown that due to homogeneity and isotropy of the background, different Fourier modes (momentum space) of fluctuations evolve independently in linear order perturbation theory. Also, Fourier modes of different helicity (scalar, vector, and tensor perturbations) evolve independently. Due to these simplifications inflationary perturbations can be split into scalar, vector and tensor modes. Vector modes are not important because in an expanding universe these modes decay quickly. However, imprints of the scalar and tensor perturbations can be observed as temperature fluctuations in CMB and primordial gravitational wave. Using initial condition given by the Bunch Davis vacuum, power spectrum (two point correlation in momentum space) of these fluctuations can be calculated. Every power spectrum is associated with two important parameters, these are amplitude and spectral index. In the slow roll approximation the scalar power spectrum or the power spectrum of curvature perturbation $\mathcal{R}$ can be expressed as,

$$\mathcal{P}_{\mathcal{R}}(k) \propto A_s k^{n_s - 1}, \tag{6.35}$$

where A_s is the amplitude of the power spectrum and n_s is the corresponding spectral index. Similarly one can also define the tensor power spectrum as,

$$\mathcal{P}_t(k) \propto A_t k^{n_t}, \tag{6.36}$$

In slow roll inflationary model using slow roll approximation one can calculate $\mathcal{P}_{\mathcal{R}}(k)$, $\mathcal{P}_t(k), r, n_s, n_t$ where $r = \frac{\mathcal{P}_t}{\mathcal{P}_{\mathcal{R}}}$ [52]. In the slowroll approximation $\mathcal{P}_{\mathcal{R}}(k), r, n_s, n_t$ can be completely expressed by the potential and its derivatives,

$$n_s = 1 + 2\eta_V - 6\epsilon_V, \qquad \text{(1st order in slow roll)}, \tag{6.37}$$

$$n_t = -2\epsilon_V, \qquad \text{(1st order in slow roll)}, \tag{6.38}$$

$$\mathcal{P}_{\mathcal{R}}(k) = \frac{1}{12\pi^2 M_{pl}^6}\frac{V^3(\phi)}{(V')^2} \qquad \text{(zeroth order in slow roll)}, \tag{6.39}$$

$$r = -8n_t \qquad \text{(consistency relation)}. \tag{6.40}$$

$\mathcal{P}_{\mathcal{R}}(k)$ and $\mathcal{P}_t(k)$ should be calculated for each k mode at the time of horizon crossing ($k = aH$). Given any slow roll single scalar field model, we can calculate $\epsilon_V, \eta_V, n_s, n_t$, $\mathcal{P}_{\mathcal{R}}(k), r$ to compare them with measured values. In this way, inflationary models can be constrained. However it is important to note that till date tensor power spectrum is not observed, so there are only upper bounds available for tensor perturbations. It is important to mention that A_t can be shown to be directly proportional to the height of the potential. Thus measurement of A_t will give us the scale of inflation. Figure 6.9 shows the predictions of various slow-roll models as well as the latest constraints from measurements by the Planck satellite, for details see [53]

6.4 Issue of initial conditions

Recall the old inflationary model, where the assumption is that universe was in thermal equilibrium from Planck scale to GUT scale and at GUT scale a first order phase transition happened. Since in the first order phase transition, there is a metastable vacuum at $\phi = 0$, the field ϕ gets stuck at the false vacuum. Once the field is in the false vacuum it can give rise to inflation and the inflation ends once the field makes a transition from false vacuum to true vacuum by bubble nucleation. However in the new inflationary model, there was no false vacuum at $\phi = 0$ and in this case, the potential is of the second order phase transition. For second order phase transition, the field ϕ always sit in the true vacuum as soon as the temperature goes below the

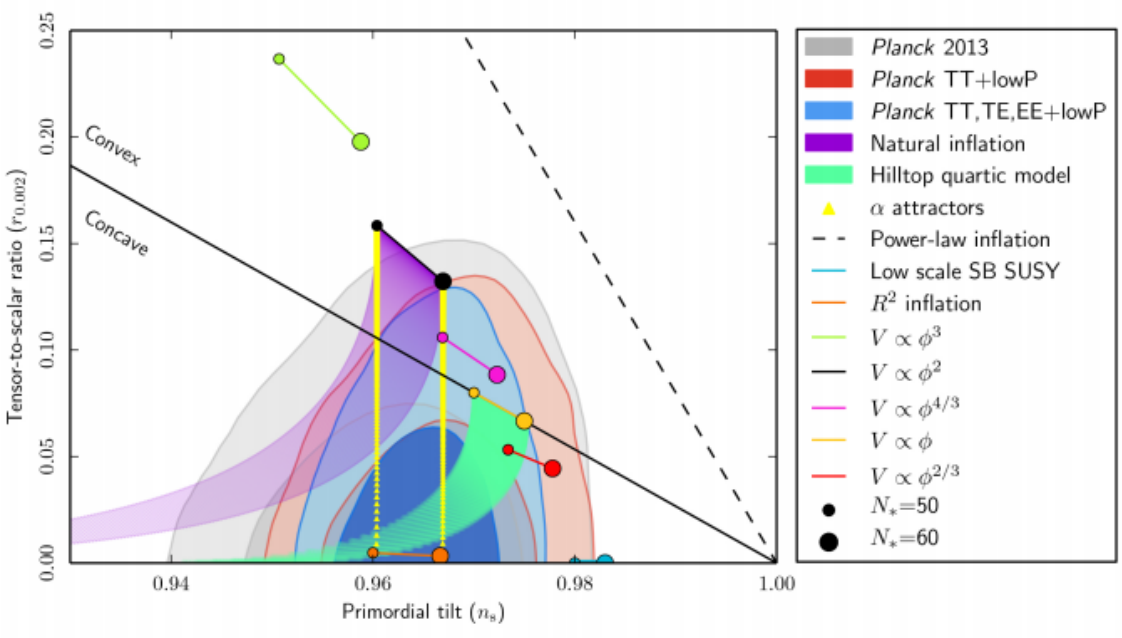

Figure 6.9: Latest constraints on the scalar spectral index n_s and the scalar to tensor ratio r [53].

transition temperature. But in the new inflationary model, the assumption is that the field ϕ is initially close to $\phi = 0$ and eventually it goes towards the vacuum. In this case, there is no false vacuum which can hold the value of ϕ close to zero. Thus there is no justification for the field to start close to $\phi = 0$. Again evolution equation of the inflating field is only applicable to length scales comparable to Hubble scale. Thus for sufficient inflation to happen the field ϕ should be close to zero, over the Hubble scale. However one can show that at the GUT scale there are 10^9 thermally uncorrelated domains within the Hubble volume. The argument is as follows,

Let us consider GUT scale inflation. Also assume that the universe was in thermal equilibrium from the Planck scale to GUT scale. In radiation dominated era $H \sim \frac{1}{t}$ and $T \sim \frac{1}{a(t)} \sim t^{-1/2}$. Hence,

$$H_{GUT}^{-1} = \frac{T_{pl}^2}{T_{GUT}^2} H_{pl}^{-1}. \tag{6.41}$$

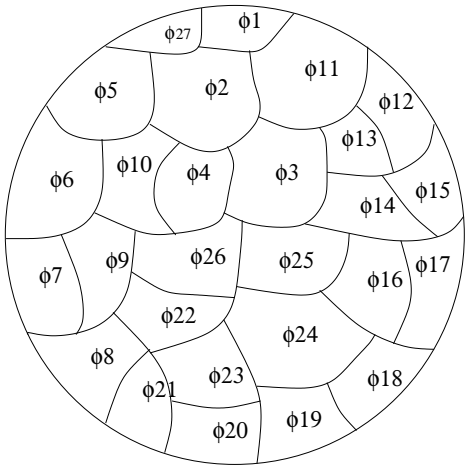

Figure 6.10: Uncorrelated domains within the Hubble volume. Within each correlation domain field value ϕ is same but different domains have different values of ϕ.

On the other hand correlation length $\xi \sim T^{-1}$. Hence,

$$\xi_{GUT} = \frac{T_{pl}}{T_{GUT}} \xi_{pl}. \tag{6.42}$$

However at the Planck scale there was only one length scale $M_{pl}^{-1} \sim T_{pl}^{-1}$. So at the GUT scale $H_{pl}^{-1} = \xi_{pl}$,

$$\frac{H_{GUT}^{-1}}{\xi_{GUT}} = \frac{T_{pl}}{T_{GUT}} \times \frac{H_{pl}^{-1}}{\xi_{pl}} \sim 10^3$$

Thus at the GUT scale Hubble volume contains about 10^9 uncorrelated domains as represented in the figure 6.10. Within a correlation domain field value ϕ can be taken to have uniform value. But the probability, that all the correlation domains have the same field value ϕ is very small (we will give an estimate of this probability for Natural inflation). Thus over the Hubble volume, initial value of the field might not be $\phi = 0$ or close to zero. Thus Initial homogeneity of the inflating field is fine tuned!

6.5 Natural Inflation

For a general class of inflation models involving a single slowly-rolling field the ratio of change in the height of the potential and the corresponding change in the field must satisfy [54],

$$\chi \equiv \Delta V/(\Delta\phi)^4 \leq 10^{-6} - 10^{-8}, \tag{6.43}$$

where ΔV is the change in the potential $V(\phi)$ and $\Delta\phi$ is the change in the field ϕ during the slow rolling portion of the inflationary epoch. Thus the inflating field must be very weakly coupled. However from particle physics point of view very small coupling is another problem of "fine-tuning" because there is no guaranty that the small coupling constant will remains small after the radiative correction. However, the smallness of the coupling constant can be protected by symmetry, e.g. SUSY. In this case, the small coupling may arise from a small ratio of mass scales. However, it is not clear how the mass hierarchy will generate at the first place.

In Natural inflation [23, 24] this mass hierarchy and thus inflation itself arise dynamically in a particle physics model. In particle physics models Nambu-Goldstone bosons (NGB) arise whenever a global symmetry is spontaneously broken. The potential of Goldstone bosons is exactly flat due to a shift symmetry under $\phi \rightarrow \phi + \text{constant}$, for example, recall the shape of the potential of electroweak symmetry breaking or the spontaneous chiral symmetry breaking in QCD and the associated massless excitation. As long as the shift symmetry is exact, the inflaton field can not roll because every vacuum state is degenerate. So, for inflation to happen there must be additional explicit symmetry breaking, e.g. explicit breaking of chiral symmetry in QCD. Then these particles become pseudo-Nambu Goldstone bosons (PNGBs), with "nearly" flat potential and a true vacuum, which can give rise to inflation. In these models required mass hierarchy is generated dynamically, e.g. in the axion model [55, 56]. In axion models, a global $U(1)$ symmetry is spontaneously broken at some large mass scale f, due to the vacuum expectation value of a complex scalar field, $\langle\Phi\rangle = f\exp(ia/f)$. a is the massless axion field, the angular Nambu-Goldstone mode around the bottom of the Φ potential. At energies below the scale f, the only relevant degree of freedom is the massless axion field a. However, at much lower energy scale the symmetry is softly broken by loop corrections, e.g. in QCD case due to chiral anomaly axion gets a mass from instanton processes. Instanton processes

give rise to a periodic potential of height Λ_{QCD}^4 for QCD axion. In invisible axion model where Peccei-Quinn symmetry breaking scale is $f_{PQ} \sim 10^{15}$ GeV, the axion self coupling is $\lambda \sim (\Lambda_{QCD}/f_{PQ})^4 \sim 10^{-64}$.

Interestingly pseudo-Nambu-Goldstone bosons (PNGBs) like the axions are routinely available in particle physics models, whenever an approximate global symmetry is spontaneously broken e.g. pions are pseudo-Goldstone bosons due to the explicit chiral symmetry breaking. These Goldstone bosons originate naturally and have sufficiently flat but tilted potential. So they can be a good candidate for inflaton. In Natural inflation model [23,24] it is assumed that a global symmetry is spontaneously broken at a scale f, with soft explicit symmetry breaking at a lower scale Λ. These two scales completely characterize the model and will be specified by the requirements of successful inflation. Many types of candidates have subsequently been explored for natural inflation, e.g. natural chaotic inflation in SUGRA [57], natural inflation in extra dimensional model [58], PNGB in braneworld scenario [59, 60] etc.

The potential of the PNGB in the Natural inflation model is generally of the form,

$$V(\phi) = \Lambda^4 \left(1 \pm \cos(N\phi/f)\right). \tag{6.44}$$

In the original model [23] positive sign was taken and $N = 1$ was assumed. So the height of the potential is $2\Lambda^4$. $\phi = \pi f$ is the unique minimum of the potential. It is assumed that the inflation is initiated from thermal equilibrium state. This is assumed keeping in mind that PNGB potential is arising from a phase transition associated with spontaneous symmetry breaking. For temperatures $T \leq f$, the global symmetry is spontaneously broken, and the field ϕ describes the phase degree of freedom of the vacuum manifold. Initially, the field ϕ is randomly distributed between 0 and $2\pi f$ in different regions. Within the Hubble volume, the evolution of the field is described by,

$$\ddot{\phi} + 3H\dot{\phi} + \Gamma\dot{\phi} + V'(\phi) = 0, \tag{6.45}$$

where Γ is the decay width of inflaton field and is neglected in the rest of the analysis

below. For $\Lambda \leq T \leq f$ Hubble term is dominant over the potential term. Hence in this region potential is dynamically irrelevant. At $T \leq \Lambda$, the region of the universe with ϕ close to the top of the potential starts to roll down the hill towards the minimum. This gives rise to inflation.To successfully solve the cosmological puzzles of the standard cosmology, this model should satisfy the following constraints coming from the requirements of slow roll regime, sufficient inflation, density fluctuations etc.

In the slow roll regime $\ddot{\phi}$ term can be neglected with respect to $\dot{\phi}$ and $V'(\phi)$ term in the inflaton evolution equation. Hence under slow roll approximation,

$$3H\dot{\phi} + V'(\phi) = 0. \tag{6.46}$$

After taking time derivative of equation 6.46, dividing both sides by $9H^2\dot{\phi}$ and after so rearrangements, one can get the following equation,

$$\frac{\ddot{\phi}}{3H\dot{\phi}} = -\frac{V''(\phi)}{9H^2} - \frac{\dot{H}}{3H^2}, \tag{6.47}$$

where $-\frac{\dot{H}}{3H^2}$ is a slow roll parameter which can also be written as $\frac{1}{2}M_{pl}^2\left(\frac{V'}{V}\right)^2$ and $M_{pl}^2 = m_{pl}^2/8\pi$. Also note that V'' is negative in this case. Thus the equation 6.47 becomes,

$$\frac{\ddot{\phi}}{3H\dot{\phi}} = \left|\frac{V''(\phi)}{9H^2}\right| + \frac{m_{pl}^2}{48\pi}\left(\frac{V'}{V}\right)^2. \tag{6.48}$$

Neglecting $\ddot{\phi}$ with respect to $3H\dot{\phi}$ implies,

$$|V''(\phi)| \leq 9H^2, \qquad and \qquad \left|\frac{V'm_{pl}}{V}\right| \leq \sqrt{48\pi}. \tag{6.49}$$

In this model with $V(\phi) = \Lambda^4\left(1 + \cos(\phi/f)\right)$ and $H^2 \simeq \frac{24\pi}{3m_{pl}^2}V(\phi)$,

$$|V''(\phi)| \leq 9H^2 \Rightarrow \left(\frac{2|\cos(\phi/f)|}{1+\cos(\phi/f)}\right)^{1/2} \leq \frac{\sqrt{48\pi}f}{m_{pl}}, \tag{6.50}$$

and,

$$\left|\frac{V'm_{pl}}{V}\right| \leq \sqrt{48\pi} \Rightarrow \frac{\sin(\phi/f)}{1+\cos(\phi/f)} \leq \frac{\sqrt{48\pi}f}{m_{pl}}. \tag{6.51}$$

Apart from $\phi/f = \pi$, where the inflation ends, left hand side of equation 6.50 and 6.51 are of $\mathcal{O}(1)$. Thus,

$$\mathcal{O}(1) \leq \frac{\sqrt{48\pi}f}{m_{pl}} \Rightarrow f \geq \frac{m_{pl}}{\sqrt{48\pi}}. \tag{6.52}$$

Inflation ends when the inequalities 6.50 and 6.51 are violated. This happens when $\phi = \pi f$. If ϕ_2 is the field value when the inflation ends, then from equation 6.51 one can see $\phi_2/f \simeq 2.98$ when $f = m_{pl}$ and $\phi_2/f \simeq 1.9$ when $f = m_{pl}/\sqrt{24\pi}$. Thus as f grows ϕ_2/f approaches π. Hence if f is small inflation ends quickly.

If we demand the lower bound on the number of e-foldings during inflation is 60 then in slowroll approximation we can show that,

$$\begin{aligned} N(\phi_1, \phi_2, f) \equiv \ln(a_2/a_1) &= \int_{t_1}^{t_2} H dt \\ &= -\frac{8\pi}{m_{pl}^2}\int_{\phi_1}^{\phi_2} \frac{V(\phi)}{V'(\phi)} d\phi = \frac{16\pi f^2}{m_{pl}^2} \ln\left(\frac{\sin(\phi_2/2f)}{\sin(\phi_1/2f)}\right) \geq 60, \end{aligned} \tag{6.53}$$

where the inflation begins at a field value $0 < \phi_1/f < \pi$. Once ϕ_2/f is fixed we can calculate ϕ_1/f from the equation 6.53. For a given ϕ_2/f there is a maximum value of ϕ_1/f above which the inequality in equation 6.53 is not satisfied. Thus for just enough inflation with $N(\phi_1, \phi_2, f) = 60$, ϕ_1/f should lie within $(0, \phi_{1_{max}}/f)$. We also assume that ϕ_1/f is uniformly distributed between 0 and π from one horizon to the other. For $f = m_{pl}$ and $\phi_2/f = 2.98$, $\phi_{1_{max}}/f = 0.61$ with probability 0.2. For $f = m_{pl}/\sqrt{24\pi}$ and $\phi_2/f = 1.9$, $\phi_{1_{max}}/f \sim 10^{-40}$ with probability $\sim 10^{-40}$. From the above analysis it is clear that probability of getting a Hubble volume with ϕ_1/f close to zero is very small. Thus if one starts with the initial condition with $\phi \simeq 0$ at the beginning of the inflation, then this initial condition is not generic. Thus from the above analysis it is clear that $f \sim m_{pl}$ allows more natural initial conditions for enough inflation.

The amplitude and spectrum of density fluctuations produced in the natural inflation model can be compared with microwave background data in order to constrain the height and width of the potential. Density perturbation in this model using the

slow roll approximation can be expressed as [6],

$$\frac{\delta\rho}{\rho} \simeq \frac{0.3\Lambda^2 f}{m_{pl}^3}\left(\frac{8\pi}{3}\right)^{3/2}\frac{[1+\cos(\phi_1^{max}/f)]^{3/2}}{\sin(\phi_1^{max}/f)}. \tag{6.54}$$

This expression has to be calculated at the time of horizon crossing of the fluctuations [61]. Measured value of $\delta\rho/\rho \sim 10^{-5}$. For $f = m_{pl} \sim 10^{19}$GeV one gets $\Lambda \sim 10^{16}$ GeV or GUT scale. Thus the two parameters of the model f and Λ can be constrained by sufficient inflation and the amplitude of density fluctuations.

However as we have already discussed, this model also suffers the initial condition problem. We have shown that at the GUT scale there are about 10^9 uncorrelated domains present within the Hubble volume. Again in Natural inflation model with $0 \leq \phi/f \leq \pi m_{pl}$, ϕ/f should be close to zero for sufficient inflation. If one take a modarate value $\phi/f = 0.1$ then the probability of having the the field value over entire Hubble volume is 0.1^{10^9} which is practically zero. Thus the initial condition of the field is not generic. Although in this chapter we have discussed the issue of initial condition in the context of Natural inflation, but this problem will arise in other models of inflation, where the scale of inflation in well below planck scale. In the later chapter, we will discuss how to achieve inflation from a generic initial condition where we will not assume same value of the inflaton field over all such domains within a Hubble volume.

Bibliography

[1] A.H. Guth, Phys. Rev. **D 23**, 347 (1981).

[2] J. Martin, C. Ringeval and V. Vennin, arXiv:1303.3787.

[3] B. Rayden, "Introduction to Cosmology", (Cambridge University Press, 2017).

[4] A. Tee, "Cosmic Inflation: An Overview of the Current Themes", Theoretical Physics Group, Department of Physics,2016.

[5] A. Riotto, arXiv:hep-ph/0210162.

[6] D. Baumann, Cosmology lecture notes, www.damtp.cam.ac.uk/user/db275/Cosmology/Lectures.pdf.

[7] D. S. Goldwirth and T. Piran, Phys. Reports **211**, 223 (1992).

[8] R. H. Brandenberger, arXiv:hep-ph/9702217.

[9] S. Dodelson, "Modern Cosmology" (Academic Press, India, 2006).

[10] S. Weinberg, "Cosmology", Oxford University Press (2008).

[11] P.A.R. Ade et al. (Planck Collaboration 2013 XVI), arXiv:1303.5076v1

[12] Lauren Anderson et al. The clustering of galaxies in the SDSS-III Baryon Oscillation Spectroscopic Survey: baryon acoustic oscillations in the Data Releases 10 and 11 Galaxy samples. Mon. Not. Roy. Astron. Soc., **441(1)**:2462, 2014.

[13] W. L. Freedman, B. F. Madore, V. Scowcroft, C. Burns, A. Monson, S. E. Persson, M. Seibert and J. Rigby. Carnegie Hubble Program: A Mid-infrared Calibration of the Hubble Constant. apj,**758**:24, October 2012.

[14] A. G. Riess, L. Macri, S. Casertano, H. Lampeitl, H. C. Ferguson, A. V. Filippenko, S. W. Jha, W. Li and R. Chornock. A 3% Solution: Determination of the Hubble Constant with the Hubble Space Telescope and Wide Field Camera 3. apj, **730**:119, April 2011.

[15] P.A.R. Ade et al. (Planck Collaboration 2015 XIII) Cosmological parameters, arXiv:1502.01589

[16] D. H. Lyth and A. R. Liddle. "The Primordial Density Perturbation". Cambridge University Press, 2009.

[17] A. D. Linde, JETP Lett.**19**, 183 (1974).

[18] D.A. Kirzhnits, JETP Lett. **15**,529 (1972).

[19] D.A. Kirzhnits and A. D. Linde, Annals. Phys. **101**, 195 (1976).

[20] A. A. Starobinsky, JETP Lett.**30**, 682 (1979).

[21] A. D. Linde, Phys.Lett. **B 129**, 177, 1983.

[22] L. Boubekeur and D. Lyth, JCAP, **0507**, 010, (2005) [arXiv:hep-ph/0502047].

[23] K. Freese, J. A. Frieman and A. V. Olinto, Phys. Rev. Lett. **65**, 3233 (1990); F. Adams, J.R. Bond, K. Freese, J. Frieman and A. Olinto, Phys. Rev. **D 47**, 426 (1993) [arXiv:hep-ph/9207245].

[24] J. E. Kim, H. P. Nilles and M. Peloso, JCAP, **0501**, 005 (2005) [arXiv:hep-ph/0409138].

[25] S. Kachru, R. Kallosh and A. D. Linde, et al., JCAP, **0310**, 013 (2003) [arXiv:hep-th/0308055].

[26] G. Dvali, Q. Shafi and S. Solganik, arXiv:hep-th/0105203.

[27] J. Garcia-Bellido, R. Rabadan and F. Zamora, JHEP,**0201**, 036 (2002) [arXiv:hep-th/0112147].

[28] A. Goncharov and A. D. Linde, Sov.Phys.JETP, **59**, 930 (1984).

[29] E. D. Stewart, Phys.Rev., **D 51**, 6847 (1995) [arXiv:hep-ph/9405389].

[30] G. Dvali and S. H. Tye, Phys.Lett., **B 450**, 72 (1999) [arXiv:hep-ph/9812483].

[31] C. Burgess, et. al., JHEP, **0203**,052 (2002) [arXiv:hep-th/0111025].

[32] M. Cicoli, C. Burgess and F. Quevedo, JCAP, **0903**, 013 (2009) [arXiv:0808.0691].

[33] E. J. Copeland, et. al., Phys.Rev., **D 49**, 6410 (1994) [arXiv:astro-ph/9401011].

[34] A. D. Linde, Phys.Rev., **D 49**, 748 (1994) [arXiv:astro-ph/9307002].

[35] R. Kallosh, A. Linde and D. Roest, JHEP, **1311**, 198 (2013) [arXiv:1311.0472].

[36] F. Bezrukov and M. Shaposhnikov, Phys.Lett. **B 659**, 703706 (2008) [arXiv:0710.3755].

[37] F. L. Bezrukov, A. Magnin and M. Shaposhnikov, Phys.Lett. **B 675** 8892 (2009) [arXiv:0812.4950].

[38] F. Bezrukov and M. Shaposhnikov, JHEP **0907**, 089 (2009) [arXiv:0904.1537].

[39] J. Garcia-Bellido, J. Rubio, M. Shaposhnikov and D. Zenhausern, Phys.Rev. **D 84**, 123504 (2011) [arXiv:1107.2163].

[40] Jerome Martin, Christophe Ringeval, Roberto Trotta and Vincent Vennin, arXiv:1312.3529

[41] D. H. Lyth and A. Riotto, arXiv:hep-ph/9807278.

[42] R. Rangarajan, arXiv:1506.07433.

[43] A. Linde, arXiv:1402.0526.

[44] https://antimatter.ie/2009/03/18/the-mechanism-of-inflation/

[45] A. D. Linde, Phys.Lett.**B 108**, 389 (1982).

[46] A. D. Linde, Phys.Lett.**B 114**, 431 (1982).

[47] A. A. Starobinsky, Phys.Lett. **B 117**, 175 (1982).

[48] M. C. Guzzetti et al. Riv.Nuovo Cim. **39**, 399 (2016).

[49] J. E. Lidsey, A. R. Liddle, E. W. Kolb, E. J. Copeland and T. Barreiro, Rev.Mod.Phys.**69**, 373 (1997).

[50] V. F. Mukhanov, H. A. Feldman and R. H. Brandenberger, Phys. Reports **215**, 203 (1992).

[51] P. A. Farago, "ΛCDM Cosmology + Chaotic Inflation", Virginia Commonwealth University (2015).

[52] H. V. Peiris, et al., Astrophys. J. Suppl. **148**, 213 (2003) [arXiv:astro-ph/0302225].

[53] P.A.R. Ade et al. (Planck 2015 results. XX. Constraints on inflation), arXiv:1502.02114.

[54] F. C. Adams, K. Freese and A. H. Guth, Phys. Rev. **D 43**, 965 (1991).

[55] H. Quinn and R. Peccei, Phys. Rev. Lett. **38**, 1440 (1977); S. Weinberg, Phys. Rev. Lett. **40**, 223 (1978); F. Wilczek, Phys. Rev. Lett. **40**, 279 (1978).

[56] J. E. Kim, Phys. Rev. Lett. **43**, 103 (1979); M. Dine, W. Fischler and M. Srednicki, Phys. Lett. **B 104**, 199 (1981); M. Wise, H. Georgi and S. L. Glashow, Phys. Rev. Lett. **47**, 402 (1981).

[57] M. Kawasaki, M. Yamaguchi and T. Yanagida, Phys. Rev. Lett. **85**, 3572 (2000).

[58] N. Arkani-Hamed, H. Cheng, P. Creminelli and L. Randall, [arXiv:hep-th/0301218] and [arXiv:hep-th/0302034].

[59] H. Firouzjahi and S.H. H. Tye, [arXiv: hep-th/0312020].

[60] J.P. Hsu and R. Kallosh, hep-th/0402047.

[61] K. Freese, W. H. Kinney, arXiv:hep-ph/0404012.

Chapter 7

Reaction-Diffusion Equations

In this chapter, we take a detour and talk about a particular class of non-linear differential equations, known as the reaction-diffusion equations. After a brief introduction to reaction diffusion equation, we will discuss some specific examples in the context of high energy particle physics model to understand its applicability.

7.1 The Diffusion Equation

In this section, we will discuss the well-known diffusion equation in some details. We will consider the mass balance approach to get the diffusion equation. For simplicity, we first consider only a one-component system, after that we will extend the analysis to multicomponent systems. This discussion can be found in any statistical mechanics book, for example, [1]. Let $\rho_m(\vec{r}, t)$ be the local mass density of the system at position $\vec{r}$ at time t and let $\vec{u}(\vec{r}, t)$ be the corresponding velocity. The total mass in an arbitrary fixed volume V enclosed by the surface area S within the fluid is

$$M = \int_V \rho_m(\vec{r}, t)\, dV. \tag{7.1}$$

The rate of change of mass due to the change in the density within the volume V is

$$\frac{dM}{dt} = -\int_V \frac{\partial \rho_m}{\partial t}\, dV. \tag{7.2}$$

where V is fixed in space. Now, according to the mass conservation, the rate of change of mass in V must be the same as the rate at which mass flows through the surface

S. Since the local flow rate of mass is $\rho_m \vec{u}$, therefore

$$\frac{dM}{dt} = -\int_S \rho_m \vec{u} \cdot \vec{n}\, dS, \tag{7.3}$$

where $\vec{n}$ is a unit outward normal (local) to S. Using Gauss's divergence theorem we have

$$\frac{dM}{dt} = -\int_V \nabla \cdot (\rho_m \vec{u})\, dV. \tag{7.4}$$

From equations 7.2 and 7.4 we have

$$\int_V \left[\frac{\partial \rho_m}{\partial t} + \nabla \cdot (\rho_m \vec{u}) \right] dV = 0. \tag{7.5}$$

Since equation 7.5 is true for any arbitrary volume V, then we must have

$$\frac{\partial \rho_m}{\partial t} + \nabla \cdot (\rho_m \vec{u}) = 0. \tag{7.6}$$

This is the equation of continuity for mass. By using the vector identity we can rewrite the above in the following form

$$\frac{D\rho_m}{Dt} + \rho_m \nabla \cdot \vec{u} = 0, \tag{7.7}$$

where the convective derivative is given by,

$$\frac{D}{Dt} = \frac{\partial}{\partial t} + \vec{u} \cdot \nabla. \tag{7.8}$$

We now apply equation (7.5) to a Fick's law of diffusion, where the rate of flow of mass is proportional to the gradient of the density. This is an empirical law and this is valid when the gradient of the density is small. Mathematically,

$$\rho_m \vec{u} = -\mathcal{D} \nabla \rho_m, \tag{7.9}$$

where $\mathcal{D}$ is known as the diffusion constant. Substituting this into the equation 7.6 and also assuming spatially constant $\mathcal{D}$, we get the diffusion equation

$$\frac{\partial \rho_m}{\partial t} = \mathcal{D} \nabla \cdot (\nabla \rho_m) = \mathcal{D} \nabla^2 \rho_m. \tag{7.10}$$

The diffusion equation is generally applied to the diffusion of one species through some medium. If c is the concentration of some species then according to diffusion equation,

$$\frac{\partial c}{\partial t} = \mathcal{D} \nabla^2 c. \tag{7.11}$$

The solution of the diffusion equation depends upon the initial distribution of concentration and the geometry of the boundary confining the system. However, once the Green function of the equation 7.11 is known, solution for any geometry and initial conditions can be constructed.

Let us consider the simple situation of isotropic diffusion in three dimensional spherical polar coordinates. The diffusion equation is,

$$\frac{\partial c}{\partial t} = \mathcal{D}\,\nabla^2\, c, \tag{7.12}$$

and the initial condition is

$$c(\,\vec{r},\,0) = c_0\,\delta(\vec{r}), \tag{7.13}$$

where $\delta(\vec{r})$ is the 3-d Delta function centred at the origin.

We perform this analysis in Fourier space. 3-dimensional Fourier transform of $c(\vec{r},\,t)$ can be expressed in the following way,

$$\hat{C}(\,\vec{k},\,t) = (2\,\pi)^{-\,3/2} \int_{-\infty}^{\infty}\int_{-\infty}^{\infty}\int_{-\infty}^{\infty} e^{i\,\vec{k}\cdot\vec{r}}\, c(\,\vec{r},\,t)\, d^3\vec{r}, \tag{7.14}$$

the inverse Fourier transform is,

$$c(\,\vec{r},\,t) = (2\,\pi)^{-\,3/2} \int_{-\infty}^{\infty}\int_{-\infty}^{\infty}\int_{-\infty}^{\infty} e^{-i\,\vec{k}\cdot\vec{r}}\, \hat{C}(\,\vec{k},\,t)\, d^3\vec{k}. \tag{7.15}$$

Hence

$$\nabla\, c(\,\vec{r},\,t) = -\frac{i}{(2\,\pi)^{\,3/2}} \int_{-\infty}^{\infty}\int_{-\infty}^{\infty}\int_{-\infty}^{\infty} \vec{k}\, e^{-i\,\vec{k}\cdot\vec{r}}\, \hat{C}(\,\vec{k},\,t)\, d^3\vec{k}, \tag{7.16}$$

and

$$\begin{aligned} \nabla\cdot\nabla\, c(\,\vec{r},\,t) &= \nabla^2 c(\,\vec{r},\,t) \\ &= -\,\frac{1}{(2\,\pi)^{\,3/2}} \int_{-\infty}^{\infty}\int_{-\infty}^{\infty}\int_{-\infty}^{\infty} k^2\, e^{-i\,\vec{k}\cdot\vec{r}}\, \hat{C}(\,\vec{k},\,t)\, d^3\vec{k} \end{aligned} \tag{7.17}$$

Thus in the Fourier space the diffusion equation 7.12 becomes,

$$\frac{\partial \hat{C}(\vec{k},t)}{\partial t} = -\mathcal{D}\,k^2\,\hat{C}(\vec{k},t)\,, \tag{7.18}$$

with the initial condition

$$\hat{C}(\,\vec{k},\,0) = (2\,\pi)^{-\,3/2}\, c_0 \equiv \hat{C}_0. \tag{7.19}$$

The solution to (7.18) is

$$\hat{C}(\,\vec{k},\,t) = \hat{C}_0\, e^{-\mathcal{D}\,k^2\,t}. \tag{7.20}$$

Using equation 7.20 and 7.15 we get,

$$\begin{aligned} c(\,\vec{r},\,t) &= (2\,\pi)^{-\,3/2} \int_{-\infty}^{\infty}\int_{-\infty}^{\infty}\int_{-\infty}^{\infty} e^{-i\,\vec{k}\cdot\vec{r}}\,\hat{C}(\,\vec{k},\,t)\,d^3\vec{k}, \\ &= c_0\,(2\,\pi)^{-3} \int_{-\infty}^{\infty}\int_{-\infty}^{\infty}\int_{-\infty}^{\infty} e^{-i\,\vec{k}\cdot\vec{r}}\,e^{-\mathcal{D}\,k^2\,t}\,d^3\vec{k}, \\ &= \frac{c_0}{8\,(\pi\,\mathcal{D}\,t)^{3/2}}\,e^{-\,r^2\,/4\,\mathcal{D}\,t}. \end{aligned} \tag{7.21}$$

This solution of the diffusion equation 7.12 shows that the diffusing material which was initially concentrated at the origin, spreads out in time and initial delta function concentration becomes a Gaussian profile of concentration.

As a check one can verify that

$$\int_0^{\infty} c(r,t)\,4\,\pi\,r^2\,dr = c_0. \tag{7.22}$$

The solution to the one-dimensional diffusion equation can be shown to be

$$c\,(\,x,\,t) = \frac{c_0}{2\,(\pi\,\mathcal{D}\,t)^{1/2}}\,e^{-\,x^2\,/4\,\mathcal{D}\,t}. \tag{7.23}$$

7.2 Reaction-Diffusion Equations

Despite the appearance of the diffusion equation in realistic situations, it has some limitations. The typical time to convey information in the form of a changed concentration over a distance L is $O\,(L^2/D\,)$. Simple dimensional arguments can give this estimate. However, contrary to many processes involved in real-life situations, the diffusion time estimated using dimensional arguments is large. Hence diffusion can not be the only mechanism for the information to travel over significant distances. In contrast, it can be shown that if the reaction kinetics and diffusion are coupled then traveling waves of concentration exist. This traveling waves can boost the propagation of concentration in a much faster way than the only diffusion-driven processes. It is important to emphasize that reaction diffusion equation is not a wave equation, so the

solution of this equation is not of the form $e^{(\pm ikx - vt)}$. The exact form of this solutions will be clear in later discussions. The diffusion equation, which belongs to class of parabolic equations, does not have a physical realistic travelling wave solutions for assymptotic boundary conditions (i.e. where concentration does not diverge at spatial infinity). To see this behaviour let us assume a travelling wave solution of the form,

$$u(\,x,t\,) = u(\,x - vt\,) = u(\,z\,), \quad z = x - v\,t, \tag{7.24}$$

where concentration is denoted by u and v denotes the wave speed. Due to the change of variables $z = x - v\,t$, the diffusion equation becomes,

$$\mathcal{D}\,\frac{d^2u}{dz^2} + v\,\frac{du}{dz} = 0 \quad \Rightarrow \quad u(z) = A + B\,e^{-v\,z/\mathcal{D}}, \tag{7.25}$$

where A, B are integration constants. Now, since u has to be bounded for all z, B must be zero, otherwise the exponential part of the solution as given in equation 7.25 blows up as $z \to -\infty$. Therefore, $u(z) = A$, a constant, is not a propagating wave solution. However, reaction-diffusion equations can give rise to traveling wave solutions, depending on the nature of interaction/reaction term with appropriate boundary conditions.

For a formal derivation of reaction-diffusion equations see [2, 3]. Here we will go through the main steps of the derivation. We consider diffusion in three dimensions for an arbitrary volume V in a medium bounded by the surface S. Mass conservation principles require that the rate of change of matter content in V is equal to the rate at which matter flows out of or into V through S plus the rate of creation/destruction of matter in V. Thus

$$\frac{\partial}{\partial\,t}\,\int_V u(\,\vec{x},t\,)\,dV = -\int_S \vec{J}\,\cdot\,d\vec{s} + \int_V f\,dV, \tag{7.26}$$

where $\vec{J}$ is the matter flux and f represents source/sink term. In the most general situation f can be a function of u, $\vec{x}$, and t. Using Gauss's divergence theorem, the equation 7.26 becomes,

$$\int_V \left[\,\frac{\partial\,u}{\partial\,t} + \nabla\,\cdot\,\vec{J} - f\,(\,u,\vec{x},t\,)\right]\,dV = 0. \tag{7.27}$$

Since the equation 7.27 is true for any arbitrary volume V the integrand must be zero and so we get the conservation equation for u as

$$\frac{\partial u}{\partial t} + \nabla \cdot \vec{J} = f(u, \vec{x}, t). \tag{7.28}$$

This equation holds for a general flux transport $\vec{J}$.

If the process under study is diffusion then according to Fick's law, we have

$$\vec{J} = -\mathcal{D} \nabla u, \tag{7.29}$$

and equation 7.28 becomes

$$\frac{\partial u}{\partial t} = f + \nabla \cdot (\mathcal{D} \nabla u), \tag{7.30}$$

where $\mathcal{D}$ may be a function of $\vec{x}$ and u. f can also depends on u, $\vec{x}$, and t. Equation 7.30 is the general form of reaction-diffusion equation, where term involving $\mathcal{D}$ is the diffusion term and f is the reaction term.

The reaction-diffusion equation 7.30 can be further generalized to multicomponent systems consisting of several interacting species/chemicals/particles. A multicomponent systems can be described by the concentration/density vector $u_i(\vec{x}, t)$, $i = 1, \cdots, m$ along with the corresponding diffusion coefficients $\mathcal{D}_i$ and interaction vector source term $\vec{f}$. The reaction-diffusion equation (7.30)then generalizes to

$$\frac{\partial \vec{u}}{\partial t} = \vec{f} + \nabla \cdot (\mathcal{D} \nabla \vec{u}), \tag{7.31}$$

where $\mathcal{D}$ is a matrix of diffusivities and if cross diffusivities are small then this matrix is essentially a diagonal matrix. Without any loss of generality the physics of reaction-diffusion equation can be understood in the simple case where the matrix $\mathcal{D}$ is diagonal and $\vec{f}$ a function of u only. Note that $\nabla \vec{u}$ is a tensor so $\nabla \cdot (\mathcal{D} \nabla \vec{u})$ is a vector.

There exists a large variety of reaction-diffusion equations. Here we mention only some of them relevant to our works [4, 5]. These are [6] :

- The Fisher-Kolmogoroff equation or logistic equation

$$u_t = u_{xx} + u\,(1-u) \tag{7.32}$$

which serves as a deterministic model for the spread of an advantageous gene in a population. This model admits the wavefront solution of the form

$$f(\xi) = \left[1 + \exp(\xi/\sqrt{6})\right]^{-2}, \tag{7.33}$$

where $\xi = x - vt$ with $v = 5/\sqrt{6}$.

- The Newell- Whitehead equation or amplitude equation

$$u_t = u_{xx} + u\,(1-u^2) \tag{7.34}$$

which arises in the study of thermal convection of a fluid heated from below.This model admits the wavefront solution of the form

$$f(\xi) = \left[1 + \exp(\xi/\sqrt{2})\right]^{-1} \qquad \text{with,} \qquad v = 3/\sqrt{2}, \tag{7.35}$$

$$f(\xi) = -\left[1 + \exp(-\xi/\sqrt{2})\right]^{-1} \qquad \text{with,} \qquad v = -3/\sqrt{2}, \tag{7.36}$$

$$f(\xi) = -\tanh(\xi/\sqrt{2}) \qquad \text{with,} \qquad v = 0. \tag{7.37}$$

- The Nagumo equation or bistable equation

$$u_t = u_{xx} + u\,(1-u)\,(u-a) \quad \text{with} \quad 0 < a < 1, \tag{7.38}$$

which arises as one of a set of equations modeling the transmission of electrical pulses in a nerve axon.This model admits the wavefront solution of the form

$$f(\xi) = \left[1 + \exp(\xi/\sqrt{2})\right]^{-1} \qquad \text{with,} \qquad v = (1-2a)/\sqrt{2}, \tag{7.39}$$

$$f(\xi) = a\left[1 + \exp(a\xi/\sqrt{2})\right]^{-1} \qquad \text{with,} \qquad v = (a-2)/\sqrt{2}, \tag{7.40}$$

$$f(\xi) = a + (1-a)\left[1 + \exp\{(1-a)\xi/\sqrt{2}\}\right]^{-1} \qquad \text{with,} \qquad v = (a+1)/\sqrt{2}. \quad (7.41)$$

7.3 RD Equations in Field Theory Systems

In the last section, we have discussed diffusion equation and reaction-diffusion (RD) equations for non-relativistic systems essentially in the context of statistical mechanics. It turns out that equation of motion in various field theory systems in certain approximations have exactly the same form as RD equation. For example, field evolution equation with standard kinetic term and in the presence of dissipation term is,

$$\ddot{\phi} - \nabla^2\phi + \eta\dot{\phi} = -V'(\phi). \quad (7.42)$$

This dissipation term $\eta\dot{\phi}$ is introduced phenomenologically in the presence of thermal dissipation. In the case of thermal dissipation, this term cannot be generated from Lagrangian dynamics. However in an expanding universe $\eta\dot{\phi}$ term comes due to Hubble expansion. In the absence of $\ddot{\phi}$ term or in the large η limit the field evolution equation becomes RD equation.

As an example let us consider the chiral sigma model [7] in the context of relativistic heavy ion collision experiments. In these experiments one studies the transition from a chiral symmetry restored phase (QGP) to chiral symmetry broken phase (hadronic phase). The field equation for the sigma field is, (setting other components of the chiral field to zero)

$$\ddot{\phi} - \nabla^2\phi + \eta\dot{\phi} = -4\lambda\phi^3 + m(T)^2\phi + H,$$
$$m(T)^2 = \frac{m_\sigma^2}{2}\left(1 - \frac{T^2}{T_c^2}\right). \quad (7.43)$$

T is the temperature and the time derivatives are with respect to the proper time τ in an expanding plasma. H is the explicit chiral symmetry breaking term. All the

other parameter values are given in [7], however in this discussion the exact values are not important. The dissipation term η is not constant for expanding plasma formed in heavy ion collision experiments. For the early stages in a heavy-ion collisions one normally takes Bjorken 1D scaling solution with $\eta = 1/\tau$, which eventually turns into a 3D spherical expansion for which $\eta = 3/\tau$.

To get the exact correspondence with the RD equation we neglect the H term and also consider high dissipation case to neglect $\ddot{\phi}$ term. For the resulting equation we rescale the variables as: $x \to m(T)x$, $\tau \to \frac{m^2(T)}{\eta}\tau$ and $\phi \to 2\frac{\sqrt{\lambda}}{m(T)}\phi$. The resulting equation is,

$$\dot{\phi} = \nabla^2\phi - \phi^3 + \phi. \tag{7.44}$$

In one dimension with $\nabla^2 = \frac{d^2\phi}{dx^2}$, this equation is exactly the same as the Newell-Whitehead equation. $\frac{d^2\phi}{dx^2}$ is the diffusion term and other polynomial terms in ϕ are reaction terms. Now if we impose the boundary condition $\phi = 0$ and 1 at $x \to \pm\infty$, then the analytical solution has the form,

$$\phi(z) \sim [1 + \exp(z/\sqrt{2})]^{-1}, \tag{7.45}$$

where $z = x - v\tau$ and $v = 3/\sqrt{2}$ is the velocity of the front. Travelling front solution of the Newell-Whitehead equation is shown in the figure 7.1 .

In this case, we have used some approximation to show the direct correspondence between the field theory system and reaction diffusion equation. In an actual model there may not be an exact correspondence between the field evolution equation and reaction diffusion equation, however, in that case also the reaction diffusion dynamics will play its role in the field evolution.

The basic features of reaction-diffusion equations can be represented as follows. Let us consider that some continuous symmetry of the field theory system is spontaneously broken, hence after the symmetry breaking the shape of the potential is shown in the figure 7.2 . Let us consider an inhomogeneous initial field profile as shown in the figure 7.3 . Φ_0 is the field value corresponding to the true vacuum and

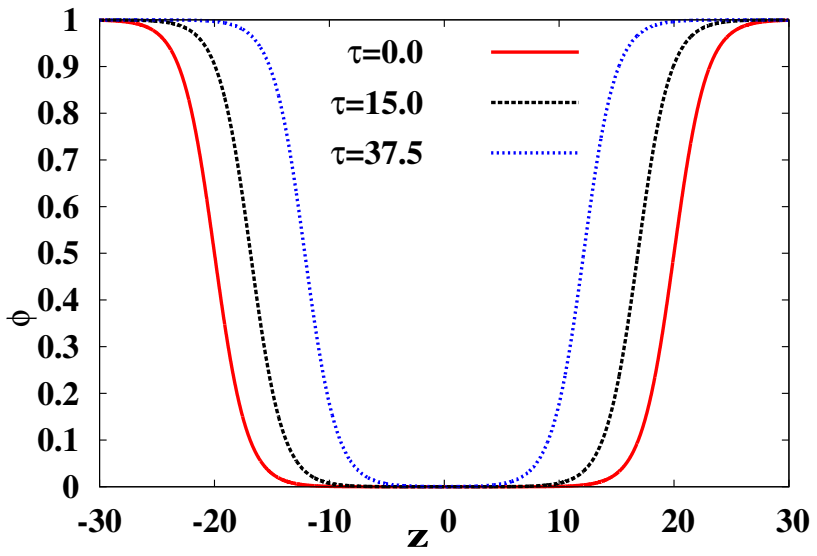

Figure 7.1: Plot of the numerical solution for the travelling front of Newell-Whitehead equation at different times. Note that the form of the propagating front solution of equation 7.45 corresponds to the profile of the front on the left part (negative z), with the origin selected at the midpoint of the left profile [4]

.

$\Phi = 0$ is the local maxima. In the coordinate space, we have an inhomogeneous initial condition, where some region of space is filled with the field value corresponding to the true vacuum and some other region has different field value. If we do not consider the reaction diffusion dynamics, then we expect the evolution of the field in a natural way where the field value will start to lift towards Φ_0 in the region, where the field value is different from Φ_0. Eventually, the field will roll down to the true vacuum in all regions. After the roll down of the field value in the entire region, ϕ will become Φ_0 and the entire region will turn into the true vacuum. This evolution is shown in the figure 7.4.

However in the presence of reaction diffusion dynamics, field evolution is quite different. In this case first a travelling front develops interpolating between $\Phi = \Phi_0$ and $\Phi = 0$. This traveling front moves towards the false vacuum and during its motion more and more regions in false vacuum get converted into the true vacuum. Eventually, the whole space becomes filled with the field value corresponding to the

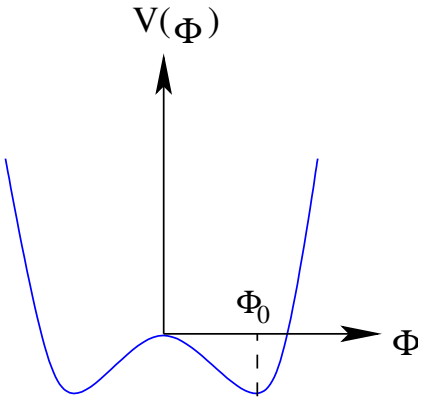

Figure 7.2: Spontaneously symmetry broken potential.

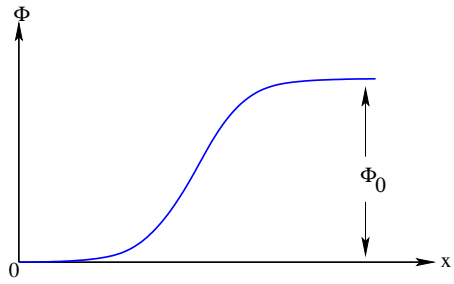

Figure 7.3: Field configuration in coordinate space.

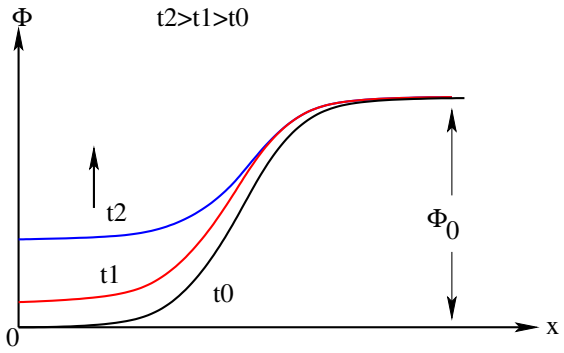

Figure 7.4: Standard expected field evolution.

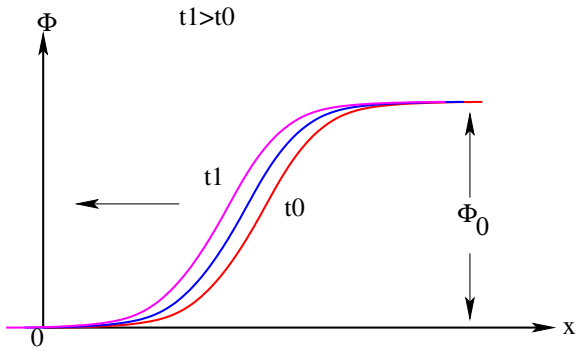

Figure 7.5: Field evolution in RD equation.

true vacuum. This evolution dynamics is shown in the figure 7.5 . In reaction diffusion dynamics there is always a boundary between false and true vacuum irrespective of the nature of the phase transition. Note that this dynamics is essentially the same as that of a first order transition (when $\phi = 0$ is a metastable vacuum) where the transition is completed by nucleation of bubbles. Importance of RD equation for quark hadron transition becomes immediately clear. Earlier it used to be believed that the quark-hadron transition is first order in the early universe. This led to a very important conjecture by Witten [8] about the possibility of the formation of quark nuggets due to the concentration of quarks by moving phase boundaries at the quark-hadron transition. However, Lattice QCD results show that quark-hadron transition is not first order rather it is a smooth crossover. Due to these results, Witten's idea about quark nugget formation became irrelevant. However, RD equations give rise

to propagating front solution which acts as phase separating boundary. Thus RD equations can have phenomenological implications in a quark hadron transition if appropriate boundary conditions can be achieved.

But if the potential is symmetric, as shown in the figure 7.6, then the field evolution is almost standard (see figure 7.7). In this case, the vacuum is at $\phi = 0$. In any region where the field value is different from $\phi = 0$, field simply rolls down to true vacuum. Though due to the diffusion dynamics, the roll down of the field is slower than the situation when there is no diffusion dynamics. But in this case, no propagating front solution develops. Thus we conclude that even if one starts with an inhomogeneous initial field profile, the presence of propagating front depends on the shape of the potential.

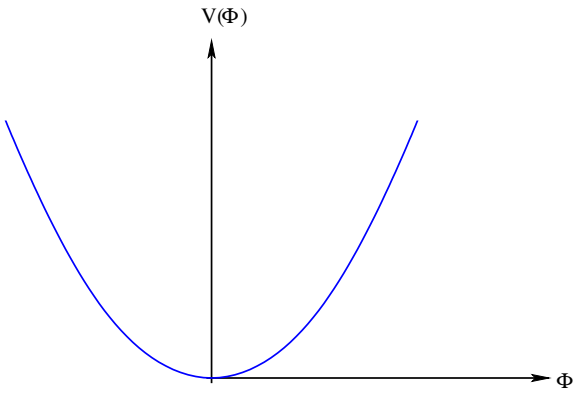

Figure 7.6: Potential with only minimum at $\phi = 0$.

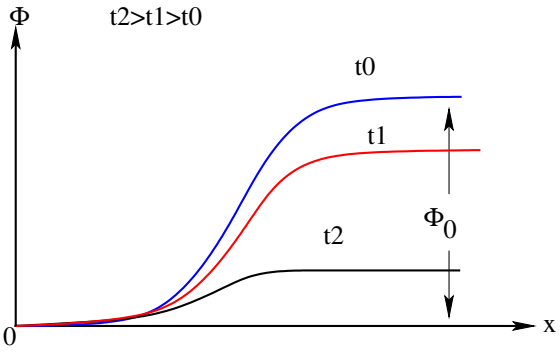

Figure 7.7: Field evolution via RD equation for potential in figure 7.6.

7.4 Reaction-Diffusion Equation for Chiral Transition

From the earlier discussions, it is clear that, traveling front solutions will exist when the underlying potential allows for a non-zero order parameter in the vacuum state, along with a local maximum of the potential [3–5, 9, 10]. The corresponding values of the order parameter provide the required boundary conditions for the propagating

front solution. In ref. [4] we were interested in the dynamics of chiral-symmetry-breaking transition in the context of relativistic heavy ion collisions. In this case, the boundary conditions required for the propagating solution of equation 7.43 naturally arise due to the spatial profile of the energy density of the plasma. The highest temperature T_{centr} is at the center of the plasma, which smoothly decreases to a temperature below the chiral transition temperature T_c in the outer regions of the plasma. Thus when $T_{centr} > T_c$, the chiral field will take a chirally symmetric value at the center at $r = 0$ and will take a symmetry broken value at large distances. For the case with a non-zero value of H as in Equation 7.43, the value of the field (ϕ) at one boundary was taken to be the (true) vacuum expectation value $\phi = \xi$ while the other boundary field value corresponded to the shifted central maximum of the potential $\phi = \phi_0$ (note that due to the explicit symmetry breaking term central maximum is not at $\phi = 0$, see figure 7.8). The propagating front solution in equation 7.45, suitably modified for these changed boundary conditions is,

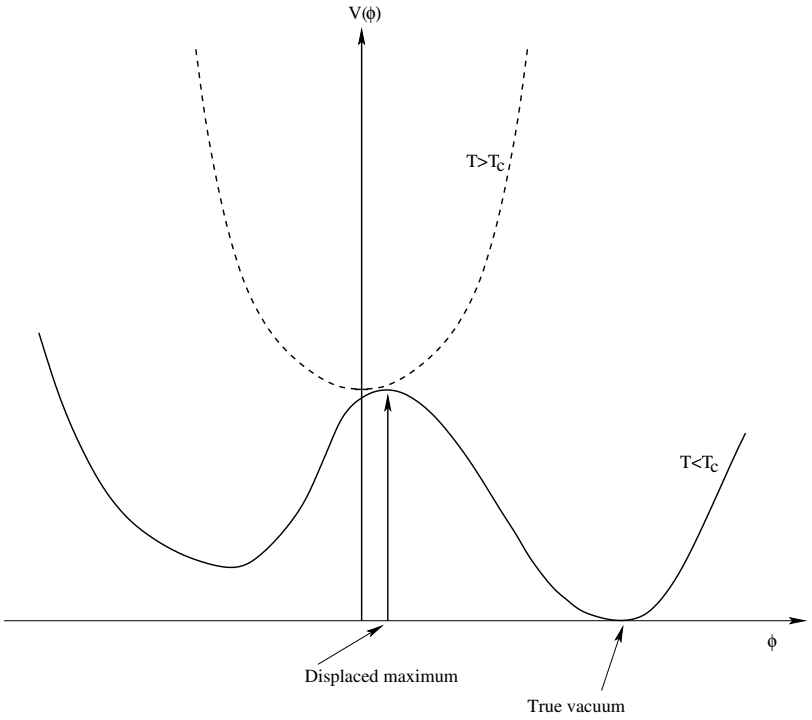

Figure 7.8: Effective potential of chiral field with explicit chiral symmetry breaking

.

$$\phi(z) = -\frac{(\xi - \phi_0)}{A_0}[1 + exp(\frac{m(T)(|z| - R_0)}{\sqrt{2}})]^{-1} + \xi, \tag{7.46}$$

where the normalization factor $A_0 = [1 + exp(\frac{-m(T)R_0}{\sqrt{2}}]^{-1}$. Here, we have restored the original, unscaled, variable z. $|z|$ was used in order to have a symmetric front on both sides of the plasma for the 1D case with R_0 representing the width of the central part of the plasma. For the 3D case, due to spherical symmetry, one can replace $|z|$ by the radial coordinate r.

In ref. [4] we calculated numerical solutions for the full equation 7.43 , retaining all the terms. We also took proper time dependence of T and η for expanding QGP (still retaining the assumption of uniform temperature for studying front propagation as with a spatially varying T the effective potential also has to vary spatially and correspondence with the reaction-diffusion equation becomes more complicated). We showed that the propagating front solution still exists with little modifications (see figure 7.9). Instead of taking the initial profile as given in equation 7.45, we took a completely different interpolation between the boundary values (see figure 7.10). But even in this case, we found the propagation front behavior. This really shows the robustness of the reaction diffusion dynamics, for a detailed discussion, see [4].

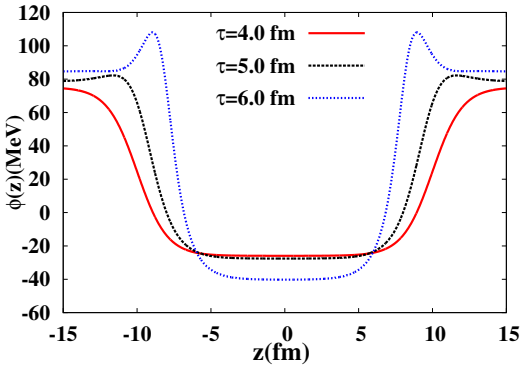

Figure 7.9: Solution of equation 7.43, with realistic values of time dependent η and T [4].

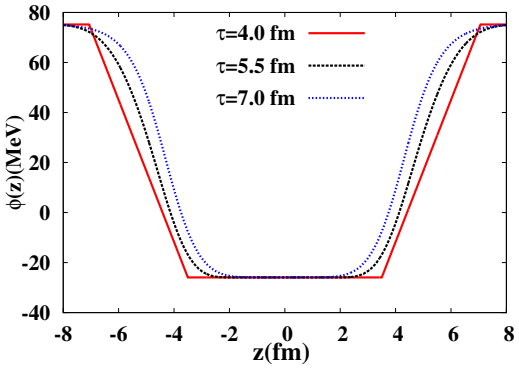

Figure 7.10: Initial profile consisting of linear segments also rapidly evolves into a well-defined propagating front [4].

7.5 DCC Formation via the Reaction-Diffusion Equation

In this section, we discuss disoriented chiral condensates (DCC) in the context of chiral transition in high multiplicity proton- proton collisions. The concepts introduced in this section is important for the application of reaction diffusion equation in the case of inflation. The physics of the formation of DCC domain in our model will exactly correspond to an inflating region, as we will discuss in the next section.

DCC refers to the formation of a chiral condensate in an extended domain, such that the direction of the condensate is misaligned from the true vacuum direction. It is expected that DCC will lead to the coherent emission of pions. A motivation for the formation of such domains came from Centauro events in cosmic ray collisions [11]. It was suggested that the anomalous fluctuations in neutral to charge pion ratio observed in the Centauro (and anti-Centauro) events in cosmic ray collisions could be due to the formation of a large region of DCC [12]. The formation of DCC was extensively investigated in high multiplicity hadronic collisions as well as in heavy-ion collision experiments [12–15].

As we have already discussed, linear sigma model provides a simple way to model chiral symmetry restoration at high temperatures. Thus it can be used to explain the formation of DCC. At high temperature, the chiral symmetry is restored. However, as the temperature drops down through the critical temperature, the chiral field can pick up random directions in the vacuum manifold in different regions in the physical space. The Lagrangian density of linear sigma model is given by [16, 17]),

$$L = \frac{1}{2}\partial_\mu \Phi \partial^\mu \Phi - V(\Phi, T), \tag{7.47}$$

where the finite temperature effective potential $V(\Phi, T)$ at one loop order is given by [16],

$$V = \frac{m_\sigma^2}{4}\left(\frac{T^2}{T_c^2} - 1\right)|\Phi|^2 + \lambda|\Phi|^4 - H\sigma. \tag{7.48}$$

Here the chiral field Φ is an $O(4)$ vector with components $\Phi = (\vec{\pi}, \sigma)$, and T is the temperature. H is the explicit chiral symmetry breaking term with which leads to non-zero mass for pions. Pions are pseudo-Goldstone bosons. The values of the different parameters are given in reference [17].

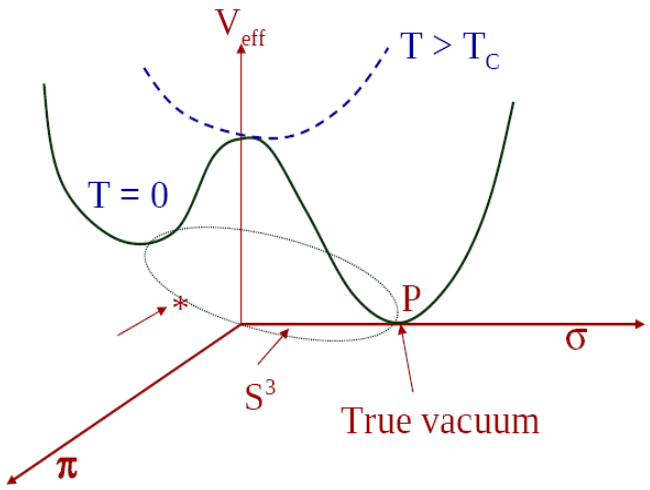

Figure 7.11: Effective potential for the chiral field Φ. P denotes the true vacuum on the (approximately degenerate) vacuum manifold while $*$ marks the value of the chiral field inside a DCC domain which is disoriented from the true vacuum direction.

In the exact chiral limit, vacuum manifold is S^3. Chiral symmetry is spontaneously broken at $T < T_c$. All the points on S^3 are equally likely. However due to the explicit symmetry breaking term, there is a unique vacuum state as shown in figure 7.11 . However, one may expect that due to rapid cooling during very early stages of the evolution of the fireball produced in heavy ion collision, chiral field will assume some arbitrarily chosen value in the (approximately degenerate) vacuum manifold within a correlation size domain. If this value differs from the true vacuum direction (as marked by $*$ in figure 7.11) then this domain will correspond to a DCC which will subsequently decay by emission of coherent pions as the chiral field rolls down to the true vacuum.

Although there was a lot of interest in exploring the possibility of the formation of DCC in high multiplicity hadronic collisions or in heavy ion collisions, after intensive

experimental searches no clear signals for its formation were found. There was in general a consensus among the scientists that in a heavy-ion collisions experiments, chiral symmetry breaking transition will likely lead to the formation of many DCC domains. But the expected size of such DCC domains was too small. Typically the size of these DCC domains are of the order of a fm. On the other hand, the radial dimension of the nuclei in heavy ion collisions are of the order of 10 fm. Thus in the central collisions size of the thermalized medium is much larger than single DCC domain. Thus the numbers of DCC domains in such collisions is too large in any given event. Due to this reason, standard DCC signals were washed out. Thus heavy-ion collisions were not ideally suited for the detection of DCC. With a large volume system undergoing chiral symmetry breaking transition, multiple DCC domains necessarily result, and a clean signal of coherent pion emissions becomes very unlikely.

In comparison, a *pp* collision system size is much smaller and this could in principle, lead to a single DCC domain with a relatively cleaner signal of coherent pion emission. However, at the previously attained center of mass energies, it was not clear whether chiral symmetry restoration was ever achieved which is a necessary condition for DCC formation. Further, even if chiral symmetry was restored in *pp* collisions, the resulting DCC domains could have been too small of the order of a few fm^3. This will lead to emission of only a few coherent pions and the signal would be hard to detect with the background of thermal pions. However, the conditions of chiral symmetry restoration seem much more favorable for the very high multiplicity pp collisions at LHC energy. There are strong indications for the production of thermalized medium and chiral symmetry restoration in these high multiplicity *pp* collisions [18]. We have shown in one of our works [5] that the problem of rapid roll down of the chiral field to the true vacuum is alleviated due to a rapid three-dimensional expansion of the system which makes reaction-diffusion equation applicable for governing the dynamics of the chiral field for this system (with appropriate boundary conditions naturally arising in these events).

The basic picture of DCC formation, in this case, is as follows [5]. In a high multiplicity pp collision, thermalized medium can be created and one can achieve

chiral symmetry restoration. Due to the very small size of the initial system, it undergoes a rapid 3D spherical expansion after a very short time of order 1-2 fm. The resulting rapid cooling of the system leads to the chiral symmetry breaking with the chiral field taking some value in the vacuum manifold. Due to the smallness of the explicit breaking term for the chiral effective potential, any value in the vacuum manifold will be roughly equally likely. This leads to the formation of a DCC domain where the chiral field is likely to be initially misaligned from the true vacuum. The typical size of this domains will be expected to be of the order of 1fm. The field will also be expected to roll down to the true vacuum rapidly in time of the order few fm. It is very difficult to detect such small DCC domains because a very small numbers of coherent pions come out from these domains.

This is where reaction-diffusion equation plays a very important role. Reaction-diffusion equation with proper boundary conditions gives rise to propagating front solutions. We have also discussed that chiral field evolution equation in the presence of dissipation term and proper boundary conditions give rise to propagating front solution. Such dissipation arises due to plasma expansion in the form of Hubble term and also from thermal dissipation. We have also argued that the appropriate boundary conditions which are suitable for the existence of propagating front solutions in the context of chiral transition, naturally arises in the heavy ion collision experiments. The initial field profile, in this case, is as follows, the chiral field in the interior of the system takes some arbitrary value on the (approximately degenerate) vacuum manifold. We considered the case of maximal disorientation when the field in the center of the parton system takes the value at the saddle point opposite to the true vacuum on the vacuum manifold. Outside the system, the chiral field was always in the true vacuum. The field in between is taken to smoothly interpolate along the vally of the potential. This constitutes the initial profile of the chiral field. Note that it is not immediately obvious that such boundary conditions should lead to a propagating front solution. Recall that for reaction-diffusion equations, which we have already discussed the condition is set to a local maximum of the potential, and not for a saddle point. However, it appears that the importance of the maximum of

the potential is in delaying the roll-down of the field from that point due to vanishing field derivative. In that situation, a saddle point will also satisfy this requirement and a propagating front solution should result. We will see that, indeed this expectation is correct and a propagating front solution exists with these boundary conditions. Propagating front solution delays the roll down of the chiral field in the interior of the region towards the true vacuum. At the same time, rapid expansion stretches the interior to a size of several Fermi radius before the field significantly rolls down towards the true vacuum. The resulting system constitutes a single large DCC domain which should lead to a relatively clear signal of coherent pion emission.

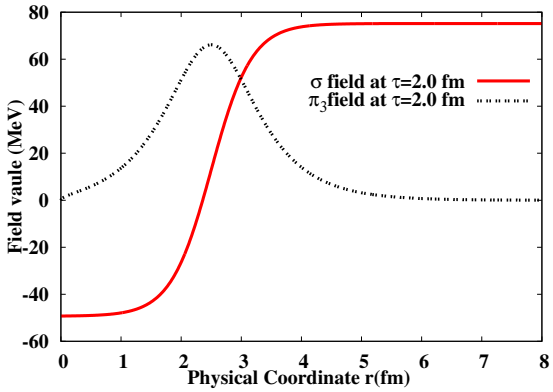

Figure 7.12: The initial profile of the chiral field. Solid (red) curve shows the profile of the σ field which interpolates between the true vacuum value and the saddle point opposite to the true vacuum. Corresponding variation of π_3 is shown by the dashed (black) curve [5].

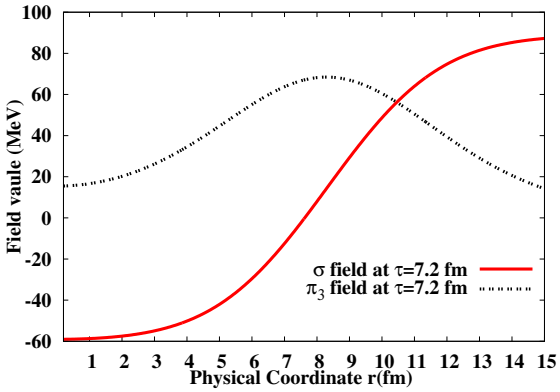

Figure 7.13: Chiral field profile at later time. Solid (red) curve shows the profile of the σ field which interpolates between the true vacuum value and the saddle point opposite to the true vacuum . Corresponding variation of π_3 is shown by the dashed (black) curve [5].

All these discussions can be summarized in the figures 7.12 and 7.13. The profile of the chiral field in between the two boundary values (as discussed above) lie on $\sigma - \pi_3$ plane, for simplicity. It would lead to emission only of neutral pions. For the 3-dimensional expansion, with spherical symmetry, will use the field equations in spherical polar coordinates,

$$\ddot{\Phi}_i - \frac{d^2\Phi_i}{dr^2} - \frac{2}{r}\frac{d\Phi_i}{dr} + (\frac{3}{\tau} + \eta'(T))\dot{\Phi}_i = -4\lambda|\Phi|^2\Phi_i + m(T)^2\Phi_i + H\delta_{i4}, \qquad (7.49)$$

where Φ_i denote components of the O(4) vector Φ (for details see [5]). Figure 7.12 shows the initial field profile in $\sigma - \pi_3$ plane. The solid (red) curve shows the profile of the σ field. The corresponding variation of π_3 is shown by the dashed (black) curve. Normally one would have expected that the field from the saddle point will roll down towards the true vacuum in a time scale of a couple of fm within the whole system of the size of 2-3 fm. Here we see the importance of the front solution of the reaction-diffusion equation. The front solution delays this roll down dramatically. The field retains its value close to the saddle point in a significant region for a long duration of time (due to the slow movement of the front). During this period, the rapid expansion of the plasma stretches the whole system. Thus the disoriented region where the chiral field is close to the saddle point stretches. This leads to a DCC domain which is expanding and getting bigger without the chiral field in the interior rolling down towards the true vacuum. This is shown in the figure 7.13, where σ field clearly showing DCC domain has increased in size retaining the disoriented field value.

Above discussion on DCC is very suggestive of a possible resolution of the problem of initial condition in inflation, which we have already discussed in section 6.4. In this thesis we have considered the issue of initial condition in the Natural Inflation model (see section 6.5) . Although we have only considered a specific model of inflation, the issue of initial condition still holds for other inflationary models an effective potential with a metastable vacuum. It is clear from all these discussions that propagating front solution of reaction diffusion equation makes the roll down of the field very slow from an unstable local maximum to the true vacuum of the underlying potential. Along with this if the system is expanding, then by the time field slightly rolls down from the local maxima the domain in the physical space, where the field value is disoriented from the true vacuum becomes larger in size. In this way, one can achieve a large domain in the physical space where the field value is disoriented from the

true vacuum. This interesting feature of the propagating front solution can be used to resolve the initial condition problem of inflation. It is important to note that the physics of chiral symmetry breaking in low energy physics is exactly similar to the symmetry breaking pattern in the axion model which we have discussed in the Natural Inflation model, e.g. the pions are the pseudo Goldstone bosons in the case of chiral symmetry breaking, on the other side axions are pseudo Goldstone bosons in the axion model. It is the potential of the axion which drives inflation. In the DCC case, we have demonstrated that a single fermi size DCC domain becomes larger due to the reaction diffusion driven dynamics. Similarly, in the next chapter in the context of Natural inflation, we will show how a tiny initial domain having field value close to the local maxima of the axion potential, stretches to a Hubble scale retaining its value close to the local maxima. Once we have understood the stretching of DCC domains having field value close to the saddle point of the chiral potential, stretching of domains in the Natural inflation model is straight forward.

Bibliography

[1] Donald A. McQuarrie, " Statistical Mechanics", (Harper and Row), 1976.

[2] J.D.Murray, " Mathematical Biology, I : An Introduction, Third Edition", (Springer), 2002; J.D.Murray, "Lectures on Nonlinear-Differential-Equation Models in Biology, (Clarendon Press), 1977.

[3] B.Bradshaw-Hajek, " Reaction-diffusion Equations for Population Genetics", (Ph.D. thesis, School of Mathematics and Applied Statistics, University of Wollongong), 2004, (http://ro.uow.edu.au/thesis/201).

[4] P. Bagchi, A. Das, S. Sengupta and A. M. Srivastava, Phys.Rev. **C92**, 034902 (2015) [arXiv:1507.01015].

[5] P. Bagchi, A. Das, S. Sengupta and A. M. Srivastava, Phys.Rev. **C93**, 024914 (2016) [arXiv:1508.07752].

[6] B.H.Gilding and R.Kersner, " Travelling Waves in Nonlinear Diffusion Convection Reaction", (Springer Basel AG, Switzerland), 2004.

[7] D. Boyanovsky, H. J. de Vega, R. Holman and S. Prem Kumar, Phys. Rev. **D56**, 3929 (1997).

[8] E. Witten, Phys. Rev. **D** 30, 272 (1984).

[9] A.G. Nikitin and T.A. Barannyk, Central European Journal of Mathematics **2(5)**, 840 (2004);

[10] "Progress in Nonlinear Differential Equations and Their Applications", Editor H. Brezis, Springer Basel AG, Switzerland (2004).

[11] C. M. G. Lattes, Y. Fujimoto and S. Hasegawa, Phys. Rep. **65**, 151 (1980); L. T. Baradzei et al., Nucl. Phys. **B370**, 365 (1992), and references therein.

[12] J.D. Bjorken, K.L. Kowalski and C.C. Taylor, in " Results and Perspectives in Particle Physics 1993"; Proceedings of the 7th Rencontres de Physique de la Vallee d'Aoste, La Thuile, Italy, 1993, edited by M. Greco (Editions Frontieres, Gif-sur-Yvette, France, 1993).

[13] A. A. Anselm, Phys. Lett. **B217** (1989) 169; J.-P. Blaizot and A. Krzywicki, Phys. Rev. **D46** (1992) 246.

[14] J. P. Blaizot and D. Diakonov, Phys. Lett. **B315** (1993) 226.

[15] K. Rajagopal and F. Wilczek, Nucl. Phys. **B399** (1993) 395; *ibid* **B404** (1993) 577.

[16] D. Boyanovsky, H. J. de Vega, R. Holman, and S. Prem Kumar, Phys. Rev. **D 56**, 3929 (1997).

[17] A.M. Srivastava, Pramana 55, 53 (2000).

[18] P. Ghosh, S. Muhuri, J.K. Nayak, and R. Varma J.Phys. **G 41**, 035106 (2014); I.B. Bashir, R.A. Bhat, and S. Uddin, arXiv: 1502.04185.

Chapter 8

Setting Initial Conditions for Inflation with Reaction-Diffusion Equation

In chapter 6 we have discussed the issue of initial conditions for inflation. We have pointed out that for any inflation at energy scale much below the Planck scale, assuming homogeneous field configuration over entire Hubble scale is not reasonable. In this chapter we will revisit the issue of initial condition in details for a specific model of inflation e.g. Natural inflation and we will argue how the use of travelling front solution of reaction dissusion equation can resolve the issue of initial condition.

8.1 Introduction

We again review briefly the physics of inflationary model. The hot big-bang model of the Universe is described by Friedmann-Robertson-Walker (FRW) metric [1] , which is based on large-scale homogeneity and isotropy of the observed universe. It provides reliable and tested description of the history of the Universe from about 1 sec after the big-bang till today. Despite the self-consistency and remarkable success of the early hot big-bang model, a number of unanswered questions remained regarding the initial state of the Universe. These are known as flatness problem, horizon problem

and monopole problem [2] . To resolve these problems inflationary universe model was proposed. The main ingredient of the inflation is the accelerated expansion of the Universe at a very early stage. If the duration of the inflation $\Delta t \geq 60H^{-1}$, where H is the Hubble parameter during inflation, then one can explain the observed homogeneity and isotropy of the Universe, the absence of the magnetic monopoles and the spatial flatness. Although it was known that inflation can resolve the shortcomings of the hot big-bang cosmology, the first particle physics motivated model of inflation was suggested by Guth [3] , which is known as the old inflationary model. In this model, the Universe is assumed to be initially in thermal equilibrium and undergoes a strong first order phase transition (typically at the GUT scale). Inflation occurs when the scalar field (inflaton) gets trapped in the metastable vacuum. In this model inflation ends by quantum tunneling of the field into the true vacuum via bubble nucleation. In his own paper, Guth pointed out the graceful exit problem of this model. In old inflation model, the Universe expands at an exponential rate while the bubbles nucleate at a constant rate. Until and unless the nucleation rate is high enough, the bubbles will not collide with each other, which is necessary for the end of the inflation and subsequent reheating. However, if the nucleation rate is large then phase transition will be completed quickly and it will not give enough inflation. Thus old inflationary model suffers graceful exit problem. This problem was addressed in the new inflation model [4–6] , where the shape of the finite temperature effective potential is such that either there is no potential barrier, so the phase transition is second order, or there is a very tiny potential barrier. In this model, the potential must have a very flat portion in between the origin and the true minimum. The field starts very close to $\phi = 0$ and slowly rolls to the true minimum. During the slow roll, the energy density is dominated by the potential energy which gives rise to inflation. In new inflation when the classical field reaches the end of the flat part of the potential, it rapidly rolls down to the true vacuum and starts to oscillate. This is the stage of reheating of the Universe at the end of inflation. Other inflationary models are also proposed like chaotic inflation [7] , stochastic inflation [8] , inflation with pseudo Goldstone boson [9] , inflation with modified gravity [10] , warm inflation [11] etc.

Inflationary models can be broadly classified depending upon initial conditions, behavior of the scale factor and the end of the inflation. (Warm inflation is a separate category where dissipative dynamics of the inflaton field leads to continued particle production during the entire inflationary phase. We will comment on that later.) For example, the old and new inflationary models were based on the assumption that the Universe was in a state of thermal equilibrium at very high temperature, on the other hand, chaotic inflation models can be applied for generic initial conditions including no thermal equilibrium for the pre-inflationary stage. Again time dependence of the scale factor during inflation can be different in different models e.g. exponential inflation, power-law inflation etc. Inflationary models can also be classified according to the change in the scalar field during inflation, e.g. the large field and small field models where the change in the scalar field is of the order of m_{pl} (Planck mass), or smaller respectively (see, ref. [12] for different definitions used in the literature for the term large field inflation).

In the original old inflation model, although the model does not work due to graceful exit problem, $\phi = 0$ is naturally set because of the presence of the metastable vacuum at $\phi = 0$. For new inflation it was hard to justify initial value of field being close to zero when the transition is second order (which requires field always remaining at the minimum of the potential) [13] . For this, versions of new inflation invoked a metastable vacuum with tiny potential barrier, along with a very flat top for the potential [4, 5, 14] . With that, the initial value of ϕ could be set precisely (e.g. equal to zero) due to the false vacuum at that value of ϕ. The field tunnels through the barrier via nucleation of a bubble which undergoes inflation as the field inside the bubble rolls slowly over the flat top of the potential. The inflation ends when the field reaches the end of flat part of the potential and rolls down to the true vacuum rapidly. Thus the entire observed universe is inside one very large bubble, with other such bubbles constituting different parts of the Universe disconnected from our universe by regions which are constantly undergoing inflation. For other models like chaotic inflation and natural inflation, the initial value of the field is not set in this manner. Rather, it is supposed to explore entire allowed (relevant) range of field

values. Inflation occurs wherever the field has the correct initial value.

For definiteness we will discuss natural inflation model with field varying from 0 to the vacuum expectation value (vev). For inflation, (e.g. for natural inflation with the field starting near $\phi = 0$) the requirement of appropriate field values over several Hubble volumes is very hard to justify. We will discuss this in some detail in the next section. Important point is that correct field value is required not just as an average, one cannot allow significant field values anywhere inside the region of interest (several Hubble volumes) as the field will rapidly roll down to the true vacuum in those regions. The issue of initial conditions for inflaton field has been extensively discussed in the literature [15–20] . In particular, it has been investigated that starting with inhomogeneous field configurations, how a homogeneous component, appropriately localized near the origin can arise. Recently, fluctuation-dissipation dynamics has been used in this context by Bastero-Gil et al. [16] . This is of importance to us as dissipative dynamics plays very crucial role in our model also. However, there are crucial differences between this work and our model , as we will discuss below. In a numerical simulation of full Einstein field equations coupled to scalar inflaton field, it is shown by East et al. [19] that inflation can occur with highly inhomogeneous initial conditions, as long as the average value of the field, as well as the fluctuation of the field in a Hubble region remains within the slow roll region of the potential. Otherwise, as we discussed above, the field generically rolls down quickly to the minimum, being pulled down by the field values outside the slow roll regime. For earlier works with highly inhomogeneous conditions, see ref. [15, 17] . For a recent review on the issue of initial conditions, see ref. [18] (see, also [21]) .

We attempt to address this issue of initial conditions for inflation using specific features of the reaction-diffusion (RD) equations [22–26] using a natural inflation model with field varying between 0 and vev. In our model, the field is close to zero only in a very small region inside the Hubble volume and varies smoothly to a large value (vev) over a region, which we will call as the *field domain*. The size of this *field domain* is taken to be much smaller than the Hubble size at GUT scale. In principle, it may be possible to take the size of the *field domain* to be of order of the correlation

size, but in the present chapter we are only able to provide results when it is much bigger than the correlation domain, though still much smaller than the Hubble region at GUT scale. Domain sizes we take provide examples where inflation can be shown to occur. Due to long time required for each simulation we have not been able to optimize the domain sizes for different cases. Important thing is that the field is not homogeneous at all in our model, and the variation of the field lies well outside the slow roll region, in fact all the way upto the vacuum value. One would have expected this field to rapidly roll down to the true vacuum everywhere. This is where the special features of reaction-diffusion equation become relevant. With appropriate boundary conditions, with field interpolating between $\phi = 0$ at the top of the potential and the minimum of the potential (the true vacuum), specific solutions of reaction diffusion equation exist which represent slowly propagating fronts just like interfaces in a first order transition [22, 24–26] . This happens even though the potential corresponds to a second order transition, or even a cross-over. This holds up the field near $\phi = 0$ for sufficiently long time such that vacuum energy starts dominating compared to the kinetic energy (from the time derivative of the field), the gradient energy, as well as the radiation energy, in the entire Hubble volume signaling beginning of inflation. Duration of inflation will be governed by the exact profile of the field inside this field domain, and its size.

Though still we are unable to show inflation beginning from a single correlation-size domain, it is important to appreciate that we are able to obtain inflation using a reasonable field profile over a region much smaller than the GUT scale Hubble region. In fact in some cases we are even able to get field domain to be smaller than the Hubble size including energy density of the field variation (which has large contributions from the gradient energy). Important point is that one can get inflation even when the field profile inside the Hubble volume is highly inhomogeneous with field varying from the top of the potential to the vev. All that is required is that contributions of field kinetic energy as well as gradient energy, along with background radiation energy density etc., become sub-dominant compared to the potential energy contribution. Even a single small field domain can achieve that if it retains its shape

during evolution. Normally one expects that any inhomogeneous field will quickly roll down to true vacuum. However, as we will see, special solutions of the RD equations provide field profiles which retain their shape for very long time, allowing inflation to occur. We emphasize that we take natural inflation model here just as an example to illustrate the importance of RD equation solutions in providing initial conditions for inflation. Our discussion naturally applies to any inflation model with such boundary conditions, and can also be straightforwardly extended to other models if the potential has appropriate extrema. The only requirement for the applicability of RD analysis is that the potential should have one maximum and a minimum, the corresponding values of field providing appropriate boundary conditions for the RD front profile. The non-trivial role of RD equation solutions in delaying the roll down of the field from the top of the potential clearly has very general applicability and should be explored for a wide class of inflation models.

Small field domains with the field profile as discussed above will be expected to arise naturally during a thermal phase transition. For example, in a second order transition (or after a rapid first order transition), due to thermal fluctuations, small regions will generically be found where the field remains near the top of the potential while the field settles to the true vacuum in the neighboring regions. This is especially true for a continuous transition in the critical regime where fluctuations of a correlation domain to the top of the potential are unsuppressed with the correlation length becoming very large. (Though, with rapid expansion at the GUT scale, large correlation domains may not be realistic due to critical slowing down.) Once such a field profile is achieved, and the universe cools down below the Ginzberg temperature, rest of the dynamics of the field will be governed by RD equation as we discussed above. One may expect similar small domains to arise from quantum fluctuations also for a non-equilibrium transition (say a quench), or possibly even without any thermal history of the universe just as one expects in the conventional picture of inflation, except that one needs much smaller domains here. (This is important as achieving thermal equilibrium for the inflaton field during pre-inflation stages is far from clear in view of various constraints on the couplings [27]. Effects of any pre-inflation equilibrium

stage on CMBR has been discussed in ref. [28] .)

We mention here one of the important limitations of our analysis. We have not taken into account the self gravity of the field domain for its evolution. The field in this region is assumed to undergo evolution by the FRW equations appropriate for the average energy density in that Hubble region even though energy density is highly inhomogeneous. The evolution of such a localized field domain has to be studied using full Einstein equations in that region like the analysis in [19] . In that sense our results should be taken in the spirit of providing a new possibility of beginning the inflationary phase which needs to be verified by more detailed simulations. Our main purpose in this work is to demonstrate the role of RD equation solutions in slowing down the roll down of the field from the top of the potential even when spatial derivatives of the field are significantly non-zero. This aspect will not be affected by the self gravity of the domain, though certainly the expansion rate of the domain will be affected. Another limitation of our model is that in studying the evolution of the field profile, though dissipation plays an important role, fluctuation part has been ignored. Fluctuations can clearly affect the propagation of the fronts, and should be considered (as we noted in our earlier works ([24–26]) . For example, in [16] , the role of fluctuation-dissipation dynamics has been found to play crucial role in setting the homogeneous component of the field appropriately near the origin. However, there are important differences in that work and our model as role of special solutions of field equation (namely RD equations here) along with proper boundary conditions, play no role in the analysis of ref. [16] . Though we have considered high dissipation here, with special propagating front solutions of RD equation having very small velocities, even smaller dissipation may work in our model. Highly inhomogeneous initial conditions have also been considered by Albrecht et al. [17] where role of dissipation has been emphasized (see, also [15]) . However, role of special boundary conditions and special solutions of propagating front (which may allow for smaller dissipation) were not considered there.

This chapter is organized in the following manner. In Section 8.2 we will revisit the issue of requirement of initial fine tuned field value for natural inflation. We will

argue that it appears virtually impossible to satisfy this requirement over a Hubble volume. In Section 8.3 we will introduce the Reaction-diffusion equation where we will also briefly mention our earlier application of RD equation in the context of Heavy ion collision experiment and formation of misaligned chiral field domains, the so called *disoriented chiral condensate* (DCC) in pp collisions at LHC energies. The reason we present this discussion is that the physics of DCC domain formation using RD equation in the context of chiral sigma model very closely resembles the issue of initial condition for inflation. In fact in our model, DCC formation is exactly equivalent to an inflating field domain in the expanding universe. In some ways, this picture of DCC formation in heavy-ion collisions can be taken as possible experimental test of the basic picture underlying the model we are proposing for inflation based on RD equation solutions. Section 8.4 discusses application of RD equation solutions to the case of inflation in the early universe. Section 8.5 presents numerical results and conclusions are presented in Section 8.6 .

8.2 Initial Conditions For Inflation

As we mentioned above, we will discuss the case of a natural inflation model with pseudo Nambu-Goldstone boson inflaton field [9] . Nambu- Goldstone bosons naturally arise in particle physics models with a spontaneous breaking of some global continuous symmetry. If there is explicit symmetry breaking in addition to spontaneous symmetry breaking then one gets Pseudo-Nambu-Goldstone Bosons (PNGB). In the case of QCD axion model with Pecci-Quinn symmetry breaking two very different scales naturally arises, these are Pecci-Quinn scale f_{PQ} which can be as high as the GUT scale $\sim 10^{15} GeV$, and QCD scale $\Lambda_{QCD} \sim 200 MeV$. In this case axion self-coupling is $\lambda_a \sim (\Lambda_{QCD}/f_{PQ})^4 \sim 10^{-64}$. The same situation arises in low energy QCD theory with chiral sigma model, where pions are PNGB.

For natural inflation, we take the potential of the form $V(\phi) = \Lambda^4(1 \pm cos(\phi/f))$. We take the plus sign and take the inflation to occur when ϕ rolls from a value near

$\phi = 0$ to the vev ($\phi = \pi f$). (Our analysis will equally well apply to other choices of potential maximum. See, for example the analysis of DCC formation with chiral sigma model in ref. [25] .) This potential contains two scales which naturally comes from particle physics model. One can show that if $f \sim m_{pl}$ and $\Lambda \sim m_{GUT} \sim 10^{15} GeV$, then the PNGB field ϕ can drive inflation. Note Λ is the scale of the potential and f is the vacuum expectation value of the field after the symmetry breaking, which also set the scale of the field ϕ. The values of f and Λ are constrained by the requirements of the slow-rolling regime, sufficient inflation and observed magnitude of density contrast of CMBR. In the temperature range $T \leq f$, the global symmetry is spontaneously broken and Nambu-Goldstone boson describes the angular degree of freedom of the symmetry broken potential. Initially, the value of NGB is distributed uniformly between 0 and $2\pi f$ in different causally connected regions, or rather, different correlation volumes. At temperature range $T \leq \Lambda$ additional explicit symmetry breaking comes into the picture because of which the original *Mexican Hat* potential becomes tilted. Now the PNGB field ϕ starts rolling down to the unique true vacuum. If one starts from any arbitrary value of ϕ then sufficient inflation is not guaranteed. Although one can get sufficient inflation if the initial field value is localized suitably near $\phi = 0$.

In order to achieve sufficient inflation, the PNGB field has to start close to $\phi = 0$ and one assumes that somewhere in the entire universe such a condition was achieved initially in a region which is at least of Hubble size (more like several times the Hubble size). Let us examine how reasonable this requirement is. For definiteness, let us assume the Universe to be in equilibrium and radiation dominated before inflation. Inflaton field fluctuations will be determined by the correlation length. Let us consider a GUT scale inflation at, say, 10^{16} GeV scale. If one assumes that the Universe was radiation dominated between the Planck epoch and the GUT scale, then at the GUT scale $H_{GUT}^{-1} = \frac{T_{pl}^2}{T_{GUT}^2} H_{pl}^{-1}$ (though it may be hard to argue that the inflaton field can be in equilibrium above the GUT scale [27]) . We take the equilibrium correlation length at the GUT temperature scale, ζ_{GUT} to be of the order of the inverse of the temperature, $\zeta_{GUT} = (T_{GUT})^{-1}$. Ignoring factor of order 1, with $H_{pl} \simeq T_{pl}$,

we find that the Hubble volume at the GUT scale contains about 10^9 uncorrelated domains (10^{12} domains if GUT scale is taken to be 10^{15} GeV). Within one correlation volume, one can assume homogeneous conditions for the magnitude of ϕ, but different correlation volumes will have ϕ magnitude varying over the entire allowed range for ϕ at that temperature. If the probability of required value of ϕ in a single correlation domain is p, then the probability of N correlation domains all having the required value of ϕ is p^N. Required value of ϕ for natural inflation can be extremely close to $\phi = 0$, with $p < 10^{-30}$ (depending on the scale of f). Even if we take very liberal values of $p \simeq 0.1$, the probability of one single Hubble volume having the required value of ϕ is 10^{-10^9} which is practically zero. We thus conclude that the requirement of appropriate value of ϕ over the entire Hubble volume is extremely fine tuned, requiring tuning much stronger than the one inflation was intended to solve. Even if we do not take thermal initial conditions, the problem remains as the quantum fluctuations of ϕ will also be governed by an appropriate zero temperature correlation length (which again will be determined by the potential parameters of GUT scale leading to similar estimates). One will still need to allow that in different correlation domains field explores the full range of values upto vev, especially when one needs field values near the top of the potential.

One may argue that one should estimate the probability of the required value of ϕ over the Hubble size to be given by the decay of correlation over the Hubble size $= e^{-H_{GUT}^{-1}/\zeta_{GUT}}$ which will be of order e^{-1000} and not the absurdly small number we obtained above. However, this estimate is hard to justify. The correlation length relates to the correlation of the field magnitude on the average. So, this estimate corresponds to the *average* value of the field being within the required limit over the entire Hubble volume. This is not enough for inflation as wherever the field departs from this required range significantly (with some other region having compensating value of the field so that the correct average of the correlation of the field is obtained), the field will roll down much faster to the true vacuum. The main point is that we require the exact value of the field to be within the required range over the entire Hubble volume (containing 10^9 correlation volumes), and not the average value of

the field. (By average we mean spatial average. If one invokes time average then the meaning of field rolling down the potential via field equations itself becomes ambiguous as one will require addition of *noise* term.) The only way to get this is to say that each correlation volume must have the correct value of the field (assuming, of course, that at least the correlation length size region can be taken to have the correct value of the field). This gets us back to the earlier estimate of the probability being less than 10^{-10^9}.

This is a serious problem in assuming a reasonable initial condition for inflation. Although, the issue of initial conditions has been extensively investigated in the literature [15–20] , and inhomogeneous field configurations have been considered, generally an almost homogeneous component is taken to start the inflationary phase. Even for large field inflation models, there is a constraint on acceptable variations of the field. For example, in a recent numerical simulation of full Einstein field equations coupled to scalar inflaton field, East et al. have discussed [19] when inflation can arise from a general class of highly inhomogeneous initial conditions. It is then shown that for inflation one requires, not just the average value of the field, but also the fluctuation of the field in a Hubble region to remain within the slow roll region of the potential. Otherwise, the field quickly rolls down to the minimum, being pulled down by the large field regions. This is in accordance with the discussion above. As we mentioned, restricted variations of the field is hard to justify from the picture of correlation domains where full range (allowed by the energy/temperature considerations) of random variations of the field occurs across different correlation regions.

We will address this issue of initial conditions for inflation using specific features of the reaction -diffusion equations. We start the discussion of our model by briefly introducing reaction-diffusion (RD) equations in the next section, with focus on special propagating front solutions of RD equations.

8.3 Reaction-Diffusion Equations In Field Theory

Reaction-diffusion equations are studied typically in the context of biological systems, e.g. population genetics, chemical systems etc. RD equation with appropriate boundary condition gives traveling front with a well-defined profile. This profile mimics the profile of the phase boundary in a first order phase transition. Propagating front solutions of RD equations exist irrespective of the underlying phase transition dynamics [22,24] . Earlier some of us have shown the existence of propagating front solution in the context of chiral phase transition and confinement-deconfinement (C-D) transition in QCD even when the underlying transition is a cross-over or a continuous transition [24–26] . We have applied reaction-diffusion dynamics in relativistic field theory exploiting the fact that classical equation of motion of relativistic field in the presence of thermal bath has a similar form like RD equation except for second order time derivative term in the first case. In the strong dissipation limit, the first order time derivative term in the field equation dominates over the second time derivative term and the resulting field equation of motion directly maps to reaction-diffusion equation. In the case of heavy ion collision experiments, a large $\dot{\phi}$ term can arise from the plasma expansion (as well as from thermal dissipation), and the required boundary conditions for the existence of traveling front arise from collision geometry. We find that even in the presence of second time derivative term, approximate propagating front solutions of the RD equation exist, again leading to a first order transition like dynamics.

To demonstrate briefly how RD equation works for relativistic field theories, let us consider the case of a spontaneous chiral symmetry breaking transition for two flavor case where the chiral order parameter can be represented as $\Phi = (\sigma, \vec{\pi})$. The field equation for chiral field in chiral sigma model is,

$$\ddot{\phi} - \bigtriangledown^2\phi + \eta\dot{\phi} = -4\lambda\phi^3 + m(T)^2\phi + h$$
$$m^2(T) = \frac{m_\sigma^2}{2}(1 - \frac{T^2}{T_c^2}). \tag{8.1}$$

Here Φ is taken to be along σ direction only which we represent by ϕ and h is the

explicit chiral symmetry breaking term. The chiral limit corresponds to $h = 0$. In the above equation,the time derivatives are w.r.t the proper time τ. η is taken to be $1/\tau$ for Bjorken 1-d expansion of the plasma [29] . In ref. [25] constant value of η as well as an additional thermal dissipation term with $\eta' \propto T^2$ was also considered [30] . Here, we will establish the correspondence between the above field equation and RD equation by neglecting the explicit chiral symmetry breaking term, i.e. we take $h = 0$. (In ref. [24–26] we have also presented the case with non-zero h.) Let us also consider high dissipation case where $\ddot{\phi}$ is negligible w.r.t $\eta\dot{\phi}$. After rescaling the variables as $\vec{x} \to m(T)\vec{x}$, $\tau \to \frac{m(T)^2}{\eta}\tau$ and $\phi \to 2\frac{\sqrt{\lambda}}{m(T)}\phi$, the resulting equation is,

$$\dot{\phi} = \bigtriangledown^2\phi - \phi^3 + \phi. \tag{8.2}$$

In 1-D the above equation becomes,

$$\dot{\phi} = \frac{d^2\phi}{dx^2} - \phi^3 + \phi, \tag{8.3}$$

which is exactly same as the reaction diffusion equation known as Newell-Whitehead equation [22–26] . The term $d^2\phi/dx^2$ can be identified as the *diffusion term* while the other terms on the right hand side of the above equation are called *reaction term* (representing reaction of members of biological species for the biological systems). Newell-Whitehead equation has non-trivial traveling front solutions with suitable boundary conditions, namely $\phi = 0$ and 1 at $x \to \pm\infty$. The analytical solution with these boundary conditions has the form,

$$\phi(z) = [1 + exp(z/\sqrt{2})]^{-1}, \tag{8.4}$$

where $z = x - v\tau$. v is the velocity of the front and has the value $v = 3/\sqrt{2}$ for this solution. In our field domain picture, the center of the domain ($z = 0$) will correspond to one of the boundary values of ϕ, namely $\phi \simeq 0$, while $\phi(|z|) \to 1, z \to \pm\infty$. To achieve the value of the field at domain center to be close to the boundary condition, $\phi(z = 0) \simeq 0$ we need to have large size of the domain with the following profile of the field

$$\phi(z) = 1 - exp((|z| - R_0)/\sqrt{2})^{-1}, \tag{8.5}$$

In the figure 8.1 , we have shown this field profile (with $R_0 = 20$), and the propagation of the front near the boundary of the domain [24] . (We mention that in this particular figure in ref. [24] , the labels showed various quantities in dimensionful units. This is incorrect as the plots in the corresponding figure in that reference were for the above equation including domain size R_0, which is written in a dimensionless form.) Note that the front has a shape very similar to an interface for a first order transition and the shape is retained as the front propagates. RD equations have several solutions, each with different propagating speed e.g. Newell-Whitehead equation also has a static solution of the form $tanh(z)$, for details, see [24–26]) . It is important to note the general feature of RD equation, that is, the existence of travel front solution of reaction-diffusion equation depends crucially on the shape of the underlying potential. If the potential allows for a non-zero order parameter in the vacuum state, along with a local maximum of the potential, then traveling front solution exists. The corresponding values of the order parameter provide the required boundary conditions for the propagating front solution. In ref. [24] , some of us have demonstrated how the dynamics of chiral phase transition and confinement-deconfinement phase transition can be dramatically changed due to these propagating solutions of the RD equation, mimicking a first order transition even when the transition is actually a crossover (or a second order transition). In fact, the physics of RD equation implies that RD propagating front should exist whenever the potential admits a local maximum and a minimum, with the corresponding field values providing the required boundary conditions for the front solution. For example, see the discussion of DCC formation discussed in ref. [25] .

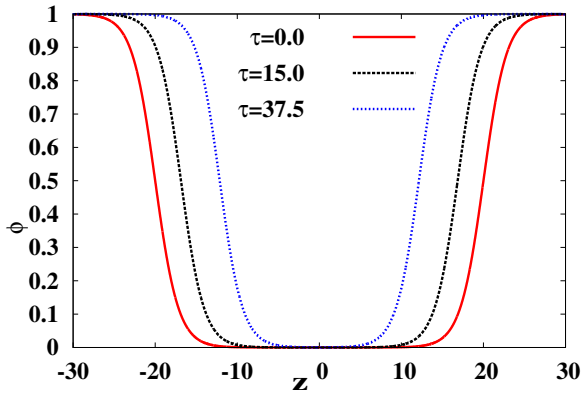

Figure 8.1: Plot of the numerical solution for the travelling front of Newell-Whitehead equation at different times. Note that in this case symmetric initial field profile w.r.t the center is considered [24]

.

8.3.1 Expanding high potential energy chiral field domains in heavy-ion collisions

In ref. [25] we have extended the application of reaction-diffusion dynamics for the case of formation of the so called domains of disoriented chiral condensate (DCC) in the context of chiral phase transition. We briefly recall that discussion here because the discussion of RD equation in the context of DCC formation will have a direct analogy with inflation. The expanding DCC domain will be exactly analogous to the inflating *field domain*. Further, the chiral sigma model potential has exactly the same features as the natural inflation model.

DCC is an extended region where the chiral field is misaligned from the true vacuum, hence has high potential energy. This topic has been extensively discussed in the literature in the context of explaining the anomalous result in Centauro events in cosmic ray experiments [31] . A large DCC domain can give rise to the coherent emission of pions when the chiral field rolls down to the true vacuum (quite like the roll down of the inflaton field at the end of inflation) [32] . In the context of heavy-ion collisions, it was believed, that chiral symmetry restoration in the transient quark-gluon plasma (QGP) state, and subsequent spontaneous breaking of chiral symmetry,

will eventually give rise to DCC domains. However, due to large volume of the QGP region in heavy-ion collisions, and expected DCC domains being much smaller, the coherent pions signal got washed out.

Formation of DCC domains in high energy hadron collisions was also investigated, but the major difficulty here was small DCC domain (leading to very few coherent pions which could not be distinguished from the background) as well as the uncertainty of achieving intermediate stage of chiral symmetry restoration at those energies. The main problem here was that even if one could achieve chiral symmetry restoration in hadronic collisions, DCC domains would have been very small due to rapid roll down of the chiral field to the true vacuum. (Note that this is like the problem of the inflaton field rolling down fast making it difficult for the relevant Hubble region to enter inflation.) This is the problem where RD equation solutions become relevant. Some of us have shown in [25] that initially small DCC domains can have correct profile as needed for slowly moving propagating fronts of RD equations, thereby strongly delaying the roll down of the chiral field to the true vacuum (again, despite the fact that there is no metastable vacuum). Expanding plasma then stretches this domain where the chiral field is still stuck near the top of the potential (strongly disoriented) leading to a large DCC domain. It is now clear that this is exactly the situation one would like to achieve for the inflaton field inside a Hubble volume, and as we will see below this indeed can be achieved. Below we will provide a brief summary of DCC formation via RD equation from ref. [25] .

The formalism of DCC formation is discussed in the framework of linear sigma model. Physics of chiral symmetry breaking is an important ingredient of chiral sigma model. When the temperature of the system drops below the critical temperature, the chiral field ($\Phi = (\sigma, \vec{\pi})$ as discussed for Eq.8.1) picks up random directions in the vacuum manifold in different regions in the physical space. Lagrangian density of this model is given by,

$$L = \frac{1}{2}\partial_\mu \Phi \partial^\mu \Phi - V(\Phi, T), \tag{8.6}$$

where the finite temperature effective potential $V(\Phi, T)$ at one loop order is given by,

$$V = \frac{m_\sigma^2}{4}\left(\frac{T^2}{T_c^2} - 1\right)|\Phi|^2 + \lambda|\Phi|^4. - h\sigma \tag{8.7}$$

We take parameter values as in ref. [25] . In the absence of explicit chiral symmetry breaking (i.e. $h = 0$), the vacuum manifold is S^3 where all the points on vacuum manifold are equally likely. But in the presence of explicit chiral symmetry breaking term ($h \neq 0$), there is a unique vacuum state. Shape of the chiral effective potential in the presence of explicit symmetry breaking is shown in the figure 8.2 .

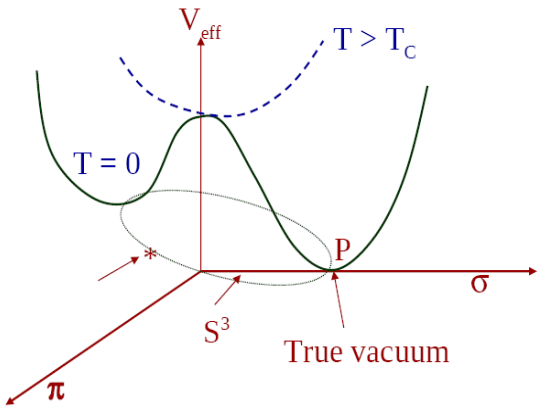

Figure 8.2: Effective potential for the chiral field Φ. P denotes the true vacuum on the (approximately degenerate) vacuum manifold while $\star$ marks the value of the chiral field inside a DCC domain which is disoriented from the true vacuum direction [25] .

In a rapidly cooling system, one expects that the chiral field will take some arbitrary value in the vacuum manifold within a correlation domain. If this value differs from the true vacuum then one gets DCC domains. Subsequently, the field will roll down to the true vacuum, leading to coherent pion emission. To study the roll down of the chiral field we have used field equations from Lagrangian in Eqn. 8.6 (which, as we have argued above, leads to reaction-diffusion dynamics). Note that, as we mentioned above, we use a second time derivative term as well, and still the propagating front solution exists (apart from some oscillations arising from the second

time derivative term). We have considered the case of maximal disorientation where field value at the center of the domain is opposite to the true vacuum on the vacuum manifold. (We also considered field value slightly away from the saddle point, and our results remain almost unchanged, see [25] for a discussion of this point.) Outside the domain, field takes true vacuum value. With this initial condition, we used field equation appropriate for the chiral phase transition. It is important to note that this boundary condition does not guarantee the propagating front solution. For RD equations, the corresponding boundary conditions are set for the local maximum of the potential. But in the case of DCC, the boundary condition is set for the saddle point. Interestingly saddle point boundary condition also works because the requirement of local maximum of the potential is satisfied at that point in the angular direction. Thus boundary conditions with saddle point and the true vacuum seem appropriate, and indeed these give rise to traveling front solution. If one starts with the field configuration such that at boundary the field value is close to the saddle point, then in that case the field starts rolling down slowly towards the true vacuum, though slowly propagating front still exists [25] .

Here we highlight the major achievements of using RD equation. Normally one would expect roll down of the field from the saddle point to the true vacuum in a timescale of the order of fm. However, because of the reaction-diffusion dynamics, front solution delays this roll down. The field retains its value close to the saddle point in a significant region for long duration of time. During the slow rolling of the field due to the reaction-diffusion dynamics, plasma continues to expand, therefore the region where the chiral field was initially disoriented stretches to a larger region. This results in a DCC domain which is expanding and getting bigger without the chiral field in the interior rolling down towards the true vacuum. Extra potential energy coming from the kinetic energy of plasma expansion (just like the situation of negative pressure where expansion requires input of energy). As an example, if one starts with DCC domain of size of order 2-3 fm initially, then due to RD equation solution, the size of the DCC domain can grow to several times larger than the original one, and within this large domain the field value will still remain close to the saddle

point. This is shown in figure 8.3 where one sees the stretching of the profile of σ without any significant roll down of the field towards the true vacuum. Also, one sees that the π_3 component stretches appropriately indicating that the field profile traces the same path in the valley of the chiral potential (Fig. 8.2) between the saddle point and the true vacuum.

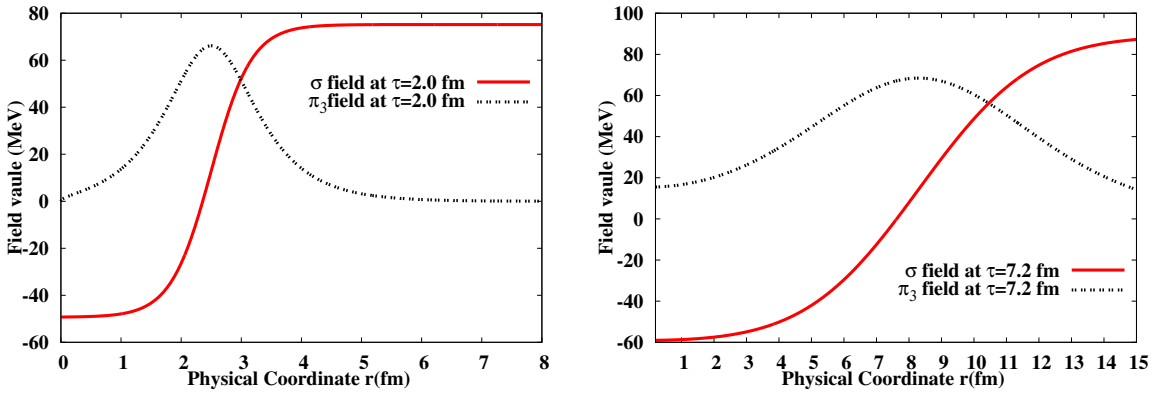

Figure 8.3: Plot in the top panel shows the initial profile of the chiral field. Solid (red) curve shows the profile of the σ field which interpolates between the true vacuum value and the saddle point opposite to the true vacuum. Corresponding variation of π_3 is shown by the dashed (black) curve showing that the chiral field traces a path along the valley of the chiral potential between the saddle point and the true vacuum. Plot in the bottom panel shows the σ and π_3 field profiles at a later time, showing the stretching of the domain due to plasma expansion [25].

Stretching of the field domain shown in Fig. 8.3 is exactly what we need for the inflation case. The shape of the potential for natural inflation is exactly similar to the linear sigma model case for the chiral field rolling down the valley of the potential. Only difference between the two potentials is the relevant energy scales. We now turn to the discussion for the case of inflation.

8.4 Reaction-Diffusion Equation For Natural Inflation

In this section, we will use propagating front solutions of the RD equation, as used above for DCC formation, to address the issue of initial condition in case of Natural inflation model. We will not discuss the issue of the viability of the inflation model in this chapter. Any model of inflation has to address the issue of initial conditions for the field. Also, our model can be extended to other models of inflation. We take the PNGB potential of the form,

$$V(\phi) = \Lambda^4(1 + cos(\phi/f)) \tag{8.8}$$

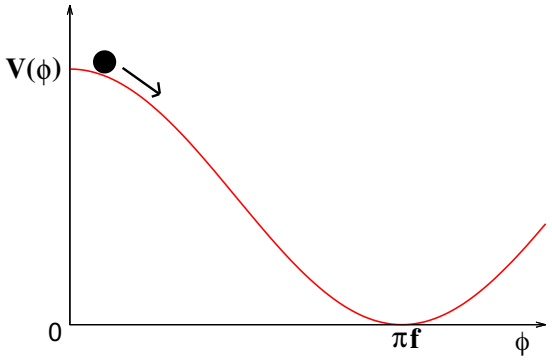

Figure 8.4: Plot of the potential for natural inflation. Note, ϕ here corresponds to the angular variable in Fig. 8.2 while the top of the potential corresponds to the height of the saddle point opposite to the true vacuum (P).

The shape of this is given in Fig. 8.4. To relate to the chiral model case of figure 8.2 , ϕ corresponds to the angular variable in Fig. 8.2, and Λ is related to the explicit symmetry breaking term $h\sigma$ in Eq.8.7. The height of the potential in Eq. 8.8 is $2\Lambda^4$. The potential has a unique minimum at $\phi = \pi f$ (which corresponds to the true vacuum for the chiral potential in Fig. 8.2). $\phi = 0$ is the local maximum of the potential and corresponds to the saddle point in Fig. 8.2. The periodicity of ϕ is $2\pi f$. We have taken $f = m_{pl}$ and $\Lambda = 10^{15}$ GeV which satisfies the constraints

coming from slow roll condition, the requirement of enough inflation and observational constraint on the density contrast at the surface of the last scattering [9] . Though it is important to realize that these constraints were derived for a homogeneous field configuration which has value close to $\phi = 0$ over several Hubble volumes. Thus, in the field evolution $\bigtriangledown^2\phi$ term was ignored. For our case this term plays crucial role in stabilizing the non-trivial profile of the propagating front. So, appropriate constraints in our case will arise by comparing vacuum energy to the kinetic energy as well as the gradient energy of the field configuration. However, now all these three contributions depend on the exact field profile in the domain, as well as exact dynamics of the field. So, kinetic energy does not arise only from the roll down of the field from near the top of the potential, but also from the motion of the propagating front which is well inside the Hubble volume (the entire field domain being much smaller than the initial Hubble volume at the GUT scale). Further, there is gradient energy contribution which changes as the front evolves. So, no analytic expressions can be written down for these different contributions unless one finds an exact solution for the propagating front for the field equation in expanding universe. It certainly will be very interesting to find such exact solutions of these *generalized* RD equations. We only use the parameter values for the natural inflation as in the literature for the conventional case, and show that inflation is possible via RD equation fronts. It is quite possible that quite different parameter choices may also provide inflation (with correct fluctuations) when RD equation solutions are used.

Since the potential is symmetric about its minimum, we assume that inflation begins with the value of the field inside a domain, $\phi = \phi_1$, $0 < \phi_1/f < \pi$. For sufficient inflation, ϕ should satisfy the condition $0 \leq \phi_1 \leq \phi_1^{max}$, e.g if one takes $f = m_{pl}$ then ϕ_1^{max}/f is about 0.2π. We assume that the Hubble volume at the GUT scale is filled with radiation energy (with typical number of degrees of freedom as appropriate for GUT scale, we take it to be 100), in addition to that Hubble volume contains several field domains where field profile takes non-trivial shape. As the potential energy for the inflaton field (in this natural inflation model with PNGB field) arises at the GUT scale, it is reasonable to assume that inside these domains

the field can have high potential energy, while outside the domain the field lies in the true vacuum. Thus typical profile in each field domain will be the field rising up towards the top of the potential inside the domains, while smoothly changing to the true vacuum value outside the domains, as was discussed above. In different correlation domains ϕ_1 will be expected to be randomly distributed between 0 and πf. In all the domains where the field inside the field domain is not very close to zero, the field will very quickly roll down to the true vacuum.

We consider a single domain where ϕ_1 is very close to zero inside the domain (changing smoothly to vev at the boundary of the domain), and this is the only domain which will survive with nontrivial field profile as the Universe evolves. In the standard picture if we do not invoke reaction-diffusion dynamics then one expects that in the time scale given by the shape of the potential, the field ϕ should rapidly roll down to the true vacuum with zero potential energy. But in the presence of reaction-diffusion dynamics situation is very different. We will show that traveling front solution of reaction-diffusion equation delays the roll-down of ϕ. The field rolls down very slowly in the interior of the domain, and the size of the domain also shrinks extremely slowly (in comoving coordinates). End result is that vacuum energy starts dominating the average energy density in that Hubble volume. The Hubble region then enters inflationary stage. Eventually one will achieve homogeneous field configuration over the entire Hubble volume starting from a very general inhomogeneous initial condition. This will be the stage of beginning of proper inflationary stage of the Universe. Duration of inflation will depend on the roll down of the field at the center of the domain, which will depend on the exact profile of the field in that domain. Important thing to note here is that we do not take the field to be homogeneous over several Hubble volumes (or even one Hubble volume). Rather, we take the field to be roughly uniform over a much smaller region. This is the most important difference between the traditional models of inflation and our model.

Once the initial conditions are fixed, now we can focus on the dynamics of the inflaton field. With the above choice of potential, the equations governing the dynamics of inflaton field become,

$$\ddot{\phi} - \frac{\nabla^2\phi}{a^2} + 3H\dot{\phi} - \frac{\Lambda^4}{f}sin(\phi/f) = 0 \tag{8.9}$$

$$H^2 = \left(\frac{\dot{a}}{a}\right)^2 = \frac{8\pi}{3m_p^2}(\rho_\phi + \rho_{rad}) \tag{8.10}$$

$$\rho_\phi = \frac{1}{2}\dot{\phi}^2 + \frac{(\nabla\phi)^2}{2a^2} + \Lambda^4(1 + cos(\phi/f)) \tag{8.11}$$

$$\rho_{rad} \propto a^{-4} \tag{8.12}$$

where Eq. 8.9 is the classical equation of motion of the inflaton field in FRW background. Eq. 8.10 gives the evolution of the scale factor a. ρ_ϕ in Eq. 8.11 is the energy density associated with the scalar field and Eq. 8.12 gives the standard evolution of the radiation energy density. We rescale the variables as follows, $\vec{x}\Lambda \to \vec{x}$, $t\Lambda \to t$, $\phi/f \to \phi$, $H/\Lambda \to H$. The resulting equations are,

$$\ddot{\phi} + 3H\dot{\phi} + \frac{\Lambda^2}{f^2}sin(\phi) - \frac{(\nabla^2\phi)}{a^2} = 0 \tag{8.13}$$

$$H^2 = \left(\frac{\dot{a}}{a}\right)^2 = \frac{8\pi}{3}\frac{f^2}{m_{pl}^2}\left(\frac{1}{2}\dot{\phi}^2 + \frac{1}{2}\left(\frac{\nabla\phi}{a}\right)^2 + \frac{\Lambda^2}{f^2}\left(1 + cos(\phi)\right) + \frac{\rho_{rad,0}}{f^2\Lambda^2}\left(\frac{a_0}{a(t)}\right)^4\right) \tag{8.14}$$

where we have taken the value of $\rho_{rad,0} = g^*\Lambda^4$ i.e. radiation energy density at GUT scale with number of degrees of freedom $g^* = 100$. Recall, in our model we have taken $\Lambda = 10^{15}$GeV, and $f = m_{pl}$. If we neglect the $\ddot{\phi}$ term in Eq. 8.13 and take H to be constant then Eq. 8.13 becomes a reaction-diffusion equation (with time dependent diffusion constant). The potential term here (the reaction term for the RD equation) is new and we have not seen any standard RD equation with this form of the reaction term. From the general analysis of RD equations, we expect this equation also to have well defined propagating front solutions for appropriate boundary conditions. Again, as for the chiral field case, we expect approximate solutions to survive even in

the presence of second time derivative term, as well as with time dependent H, as in Eq. 8.13 .

To solve this set of differential equations we need the initial field profile which satisfies proper boundary condition. We have taken *tanh* profile of the field interpolating between minimum of the potential at $\phi = \pi f$ and the maximum of the potential at $\phi = 0$. We have taken this profile for 1-D (planar propagating front) as well for 3D case (spherically symmetric propagating front). In our earlier works [24–26] when we have investigated reaction-diffusion dynamics, we have also taken exact solution of the corresponding RD equation as initial profile which has zero velocity. In the present case we take *tanh* profile as an example (which has sufficiently rapid fall off behavior which helps us in doing simulation with limited size of lattice). Exact solutions for this *generalized* RD equation are not known. Further, it is very important to mention that even if one starts with a different profile interpolating between correct boundary values, very quickly the profile changes to the appropriate profile corresponding to the RD equation under consideration (see, discussion in ref. [24–26]) . So our results for the propagating front are not sensitive to the initial profile. However, the choice of the profile also determines the value of the field at the center of the domain, which eventually will determine the full duration of inflation. The issue of dependence of duration of inflation on the exact profile of the field requires long time simulations, and will be addressed in a future publication. As we mentioned above, it is not easy to determine the roll down of the field at the center of the domain simply from field equations by neglecting the space dependence of field as $\nabla^2\phi$ terms plays most crucial role in the motion of the propagating front (hence roll down of the field).

As we mentioned earlier, $\dot{\phi}$ term plays crucial role in the propagating front solutions of the RD equations. For this purpose we have also considered a thermal dissipation term in Eq. 8.13 along with the $H\dot{\phi}$ term. With this, the equation of motion for ϕ becomes

$$\ddot{\phi} + (3H + \eta)\dot{\phi} + \frac{\Lambda^2}{f^2} sin(\phi) - \frac{(\nabla^2\phi)}{a^2} = 0 \tag{8.15}$$

We have taken thermal dissipation term to be proportional to T. In the literature different models for thermal dissipation have been discussed leading to T as well as T^2 dependence [30, 33] . We take T dependence for the following reason. First this leads to a large contribution from thermal dissipation compared to Hubble term which gives better results for RD equation fronts. Though we will also present results without any thermal dissipation term, i.e. with only $3H\dot{\phi}$ term as in Eq. 8.13, but that requires larger domain size (still much smaller than the GUT Hubble size). One can justify $\eta \sim T$ dependence compared to T^2 dependence as with T^2 dependence the $H\dot{\phi}$ term and $\eta\dot{\phi}$ term will always have the same relative strengths in a radiation dominated universe (with both H and $T^2 \sim 1/t$). This is not reasonable as thermal dissipation arises from particle interactions and we expect Hubble expansion effects to become less relevant for later times for micro physics of particle interactions. Thus, we take η to be of same magnitude as $3H$ at the Planck stage. (Corresponding to the case when the Universe is in thermal Equilibrium at the Planck stage. Note, this is only for estimate of η, we never use this equilibrium Planck stage in our model). Subsequently we take η to decrease as proportional to T. In scaled coordinates η is given by

$$\eta(T) = \frac{T}{T_{Pl}} 3H_{Pl} = 3\frac{T_{Pl}}{T_{GUT}} \frac{H(T_{GUT})}{a} \tag{8.16}$$

with the scale factor a taken to be 1 at the GUT scale. Thus at the GUT scale of 10^{15} GeV, η becomes about 10^4 times larger than the GUT scale Hubble constant. However, effective Hubble constant for our case is much larger due to large contribution of field gradient energy. With that large value of H, thermal dissipation is found to be larger than $3H$ by a factor of about 500 at the GUT scale. Subsequently, thermal dissipation becomes much larger as temperature decreases. This thermal dissipation term is important for us only until the Hubble volume enters inflation (more conservatively when the domain exits the Hubble volume). We find that by that time temperature only decreases by about 4-5 orders of magnitude (from the GUT value), so it is reasonable to take the standard picture of thermal dissipation. Subsequently,

when inflation is established then even if thermal dissipation becomes ineffective, it is of no consequence.

8.5 Numerical Results

We will consider the domain to be spherically symmetric such that the field in the interior of the domain takes the value near the top of the potential, while it smoothly changes to the true vacuum value at the boundary of the domain. In this sense, this domain is something like an *inverted* bubble profile for a first order transition (as the interior of the domain has high potential energy, note though that the potential here corresponds to a second order transition). For the evolution of the profile of the field in this domain, first we will consider a 1-D solution, where $\nabla^2\phi = \frac{d^2\phi}{dz^2}$. For large domains this should be a good approximation as the domain boundary will be approximately planar. 1-D profile is used primarily due to boundary conditions for the numerical solution as we will discuss below. We will later also give solutions of 3-D equation. We also include thermal dissipation as discussed above. Later we will present results also for the case without any thermal dissipation. All the length and time scales are expressed in the units of Λ^{-1} and ϕ is in the units of f.

8.5.1 1-D field profile

We take the propagating front to be planar, so that the resulting spatial derivative becomes one-dimensional. The field equation Eq. 8.15 becomes:

$$\ddot{\phi} + (3H + \eta)\dot{\phi} + \frac{\Lambda^2}{f^2} sin(\phi) - \frac{1}{a^2}\frac{d^2\phi}{dz^2} = 0. \tag{8.17}$$

For large domains this should be a good approximation. For 1-D equation we have taken symmetric initial profile w.r.t to the center of the domain which is taken to be $z = 0$. The field profile from the center in positive z direction is taken as

$$\phi(z) = \frac{\pi}{2}[1 + tanh((z - z_0)/d)]. \tag{8.18}$$

Here, z_0 characterizes the size of the domain where field is very close to 0, and d gives initial thickness of the region in which field changes to the true vacuum value (π) (recall, ϕ is in units of f in Eq. 8.15). The reason we evolve ϕ in the full domain, even though the field is symmetric about the domain center, is because for numerical evolution we need to fix boundary conditions. If we fix ϕ in the domain center to be at the top of the potential ($\phi = 0$) then it will raise concern whether the evolution of the front, and any possible roll down of the field, is crucially affected due to this fixed boundary condition (even though for large value of z_0, ϕ at domain center should not matter). To avoid such concerns we fix the field at the two ends of the domain to lie at the true vacuum value, so that the field is free to roll down in the center. This is also the reason we work with 1-D solution first. For 3-D case, with the radial profile of ϕ, there is no option but to fix $\phi = 0$ at $r = 0$. However, as we have already found slowly propagating well defined fronts for the 1-D case, we are confident that the fixed boundary condition at $r = 0$ for the 3-D case has insignificant effect on the evolution of the field profile. (This is for the time scale for which we have carried out the simulation. Eventually the field will roll down depending on the relative size of the domain and the Hubble size, and at that stage the role of fixed boundary condition at $r = 0$ will become important.)

The field profile at the initial stage (GUT scale) is shown in Fig. 8.5. The diameter of this *field domain* is about 30 (everywhere, time and lengths are in units of Λ^{-1}). This is also the physical size of the domain as the scale factor a is taken to be 1 initially at the GUT scale. $H_{GUT}^{-1} \simeq 723$ for GUT scale of 10^{15} GeV. This entire H_{GUT}^{-1} region is shown in Fig. 8.5 to illustrate that this field domain is much smaller initially than the causal horizon. However, the energy of the field domain has very large contributions from the gradient of the field due to non-trivial spatial profile of ϕ. Including this contribution for the region containing the field domain, the actual value of $H^{-1} \simeq 33$, which is still larger than the size of the field domain we have taken. We again mention that we are working with a strong assumption of using FRW metric with such highly inhomogeneous energy density distribution. We expect that a complete solution of the problem will still not affect the roll down of the field

being governed by (possibly a generalized) RD equation front, though it will certainly affect the local expansion rate.

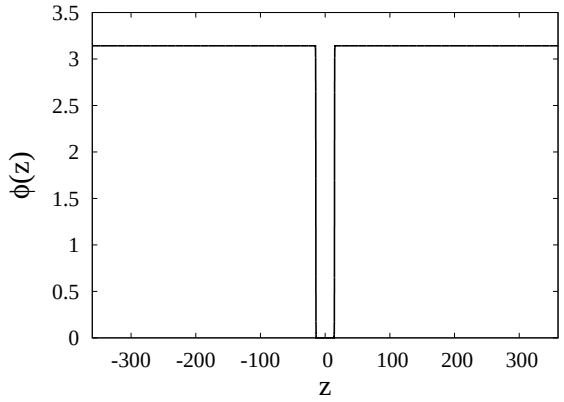

Figure 8.5: Profile of ϕ for the initial field domain. The diameter of the domain is about 30 (everywhere, time and lengths are in units of Λ^{-1}). This is also the physical size of the domain as the scale factor a is taken to be 1 initially at the GUT scale. Note that $H_{GUT}^{-1} \simeq 723$ for GUT scale of 10^{15} GeV. This entire H_{GUT}^{-1} region is shown in the figure to illustrate that the field domain is much smaller initially than the causal horizon. However, the field domain has very large contributions from the gradient of the field due to non-trivial spatial profile of ϕ. Including this contribution for the region containing the field domain, the actual value of $H^{-1} \simeq 33$, which is still larger than the size of the field domain.

We carry out the simulation by simultaneously solving Eqn. 8.14 (for 1-D) and Eqn. 8.17 . So, for the initial field profile of Fig. 8.5 , we calculate total field energy, and by taking the GUT scale Hubble size as the region of interest, we calculate field energy density. We add to this the radiation energy density at the GUT scale ($\sim g^*\Lambda^4$ with $g^* = 100$) and then calculate resulting Hubble constant for this total energy density. Due to very large contribution of field energy, the final Hubble constant is much larger than the GUT scale Hubble constant. We find that the net value of H^{-1} is about 33 which is much smaller than $H_{GUT}^{-1} \sim 723$. With this new value of H the field equation (Eq. 8.17) is solved for the evolution of the field profile. The evolution of field configuration changes relative proportions of vacuum energy contribution, and the gradient and kinetic energy of field, as well as radiation energy, and new Hubble parameter is calculated at each time step with this changed energy density. We have

evolved field configuration up to $t = 110600$ by which time the Hubble parameter becomes almost constant due to complete dominance of the vacuum energy density of the field profile over all other energy contributions.

Fig. 8.6 shows the final profile of ϕ at $t = 110600$ and the initial profile in the comoving coordinates. Note that the shape of the propagating front has changed, primarily to adopt to the correct solution of this generalized RD equation (Eq. 8.17). The shrinking of the domain in comoving coordinates is insignificant and expansion of the Universe leads to stretching of the domain in physical coordinates. The initial size of the actual Hubble region H^{-1}, incorporating field energy contributions, is about 33, which is still larger than the initial domain size.

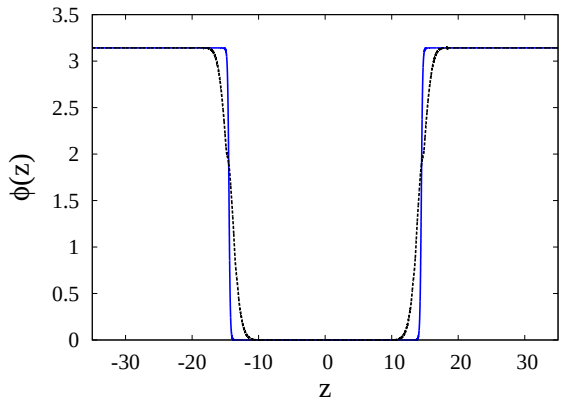

Figure 8.6: Final plot of ϕ in comoving coordinates at $t \simeq 110600$ is shown by the black (dashed) curve. The blue (solid) curve shows the initial profile of the field. The initial size of the actual Hubble region H^{-1}, incorporating field energy contributions, is about 33, which is still larger than the initial domain size.

Fig. 8.7 is the log-log plot of the evolution of energy density as well as of the Hubble parameter. Fig. 8.7 a shows the evolution of different components of the energy density as a function of time. Note, initially, the most dominant component is the kinetic energy + gradient energy part of the field (which actually leads to much larger value of H than what is expected at the GUT scale). With time, all other components decrease except the vacuum energy density which remains essentially constant. Minor changes in vacuum energy density occur due to adjustment of the field configuration

with changed H (through the $\dot{\phi}$ term) during the evolution of the propagating front. We find that the vacuum energy becomes most dominant component at $t \simeq 14923$. Fig. 8.7 b shows the evolution of the Hubble parameter H (Eqn. 8.14) . During early stages H changes non-trivially due to the adjustment of propagating front to correct solution of the RD equation (also note, time is taken as $t = 0$ at the GUT scale, so there is a constant t_{GUT} in writing a relationship between the scale factor a and t). Subsequently, H evolves as a power law, eventually turning over to a constant value of H signaling the beginning of the inflationary phase. In Fig. 8.7 b, this beginning of the inflationary phase happens around at $t \simeq 15000$ which coincides with the stage of the dominance of the vacuum energy in Fig. 8.7 a.

Even though the vacuum energy becomes dominant by $t \simeq 15000$, as shown in Fig. 8.7 , and H almost constant, if the field domain remains within the Hubble size H^{-1} then, in principle, dynamics of field inside the domain can disturb the inflationary phase. To apply the standard techniques of calculations of density fluctuations etc. we need the domain to exit the horizon size so that proper 60 $e-fold$ inflation can occur. We have carried out the simulation until a stage so that the stretching of domain by expansion completely overtakes the increase in H^{-1} (as H becomes almost constant at late stages). This is shown in Fig. 8.8. Solid (black) curve shows the location of the domain wall in physical coordinates, by noting down the position of the wall where $\phi = 0.25$ vev. Dashed (blue) curve shows the value of H^{-1}. During initial stages, field domain stretching due to universe expansion is insignificant compared to the increase in the value of H^{-1} as shown in Fig. 8.8 a. However, towards the end of simulation, H^{-1} becomes practically constant while physical size of the domain (due to expansion of the Universe) keeps increasing. By the end of simulation here, at $t \simeq 110600$, as shown in Fig. 8.8 b, one can see that the domain exits the horizon, marking beginning of proper inflationary stage.

The duration of inflation will be decided by the roll down of the field at the center of the domain. With the profile of ϕ as given above for Eq. 8.18 , ϕ is very close to zero at $z = 0$. However, it gets pulled down during evolution due to non-zero slope of the potential as well as due to the non-trivial profile of ϕ. Fig. 8.9 shows the

evolution of $\phi(z=0)$. (We show plot on linear scale here to focus on late part of the evolution.) From this, one can estimate the time after which the field will become significantly non-zero, causing it to rapidly roll down, thereby ending the period of inflation. A rough estimate, assuming linear shape for the final stages in Fig. 8.9 , will suggest that after time of order 10^{36}, $\phi(z=0)$ will become of order 1. (This may be a serious overestimate given the shape of the plot. It may appear that the roll down is exponential in nature. However, the roll down of the field at center here is governed by complex factors depending on the gradient of the field and potential shape. It is thus not clear that the nature of roll down remains same at later stages. Thus we do not attempt to fit any specific function to this plot for determining the duration of inflation.) This period of inflation crucially depends on the size z_0 in the ϕ profile in Eq. 8.18 . For a larger value of z_0 duration of inflation will be larger, though at the same time it will become harder to justify a very large value of z_0.

8.5.2 3-D field profile

As we mentioned above, due to requirements of fixed boundary conditions for the numerical evolution of field equations, 1-D case has advantage as one can properly study the evolution of field at the center of the domain which is crucially important for the total duration of inflation. Having done that in the previous section, we should now study the 3-D case. This is particularly important as the nature of propagating front solution of RD equations crucially depend on the form of the equation. For the 3-D case, for spherically symmetric field profile, the field equation, Eq.8.15 becomes:

$$\ddot{\phi} + (3H + \eta)\dot{\phi} + \frac{\Lambda^2}{f^2} sin(\phi) - \frac{1}{a^2}(\frac{d^2\phi}{dr^2} + \frac{2}{r}\frac{d\phi}{dr}) = 0. \tag{8.19}$$

Solutions of this 3-D RD equation can have very different propagating fronts. For example, in flat space one does not expect any static solution of 3-D RD equation (with standard kinetic terms, due to the well known Derrick's theorem). Indeed, we find that the profile of the propagating front is wider for the 3-D case as compared to the 1-D case (with the same parameter values). Due to this one needs to have a

larger domain size. The radial field profile at the initial stage (GUT scale) is shown by the solid (black) curve in Fig. 8.10 (plotting the region near the boundary of the domain). Here also we take a *tanh* profile of the same form as in 1-D case with z_0 giving the size of the region where ϕ is close to zero. The diameter of the *field domain* in this case is taken to be about 87. Again, as for the 1-D case, $H_{GUT}^{-1} \simeq 723$ for GUT scale of 10^{15} GeV, but incorporating field energy contributions, the actual value of $H^{-1} \simeq 11$. So, in this case the domain size is much larger than the actual H^{-1}, though still smaller than H_{GUT}^{-1}. We again mention that the domain sizes used here should be taken as examples where inflation is shown to occur. It is quite possible that much smaller domain sizes (here as well as for the 1-D profile case) may still lead to inflationary phase (especially if larger dissipation terms are chosen). The dashed (red) curve in Fig. 8.10 shows the final profile of ϕ at the end of simulation. We have run this simulation only until the stage when the vacuum energy starts dominating over the other contributions. Fig. 8.11 shows plots of various components of energy density, as well as the plot of the Hubble constant. Following the case of 1-D profile, it is clear that the region will enter inflationary phase. Note, in this case we are not able to study the roll down of the field at the center of the domain as field at $r = 0$ is fixed to be $\phi = 0$.

8.5.3 Field evolution in the absence of any thermal dissipation

We have argued above that it is perfectly reasonable to take thermal dissipation term in field equations. However, it is important to see whether in our model, inflationary phase can occur even in the absence of such a thermal dissipation. For this, we take a 1-D field profile given by Eq. 8.18 and evolve it with field equations without any thermal dissipation. So the field equation is:

$$\ddot{\phi} + 3H\dot{\phi} + \frac{\Lambda^2}{f^2} sin(\phi) - \frac{1}{a^2}\frac{d^2\phi}{dz^2} = 0 \tag{8.20}$$

As the dissipation term is much smaller here, field evolution develops strong oscillations, which is very different from the steadily moving propagating fronts of RD equation. However, as was discussed in ref. [24–26] , rough structure of propagating front still remains. In fact, apart from some oscillations of the field at the front position, remaining evolution is again by slow motion of the front position. Thus one will expect that one should again be able to get inflationary phase, though in this case the vacuum energy needs to dominate over a much larger contributions from the gradient and kinetic energy contributions resulting from oscillations.

Due to smaller dissipation, we need to take larger domain in this case (compared to the 1-D case with thermal dissipation). The diameter of the *field domain* in this case is taken to be about 73, which is 1/10 of $H_{GUT}^{-1} \simeq 723$, but much larger than actual $H^{-1} \simeq 13$ when field energy contributions are incorporated. Solid (black) curve in Fig. 8.12 shows this initial field profile and the dashed (red) curve shows the final profile of ϕ at the end of simulation. The final shape of the profile is almost stable and changes very little subsequently. In this case the kinetic energy and gradient energy of the field change much more slowly. In fact the kinetic energy and gradient energy contributions are almost the same here (while in other cases the final kinetic energy was much smaller than the gradient energy). We have run this simulation until the stage when the kinetic energy + gradient energy becomes close to the vacuum energy. It is clear from the plots that the vacuum energy part will become completely dominant as in Fig. 8.7 a, leading to the inflationary phase. Fig. 8.13 shows plots of various components of energy density, as well as evolution of H. Following the case of 1-D profile, it is clear that the region will enter inflationary phase.

8.6 Discussion and Conclusions

We have studied evolution of a highly inhomogeneous field configuration, forming a sub-horizon domain like structure, as one may expect to arise after a phase transition, and have shown that in the presence of thermal dissipation a single such domain can lead to inflation. This happens due to very special nature of propagating front

solutions of RD equations which slows down field roll down sufficiently, allowing domain structure to survive for long time. With this, the expansion of the Universe is able to stretch the domain so that the vacuum energy starts dominating over other forms of energy densities signaling beginning of inflation. The domain we take is still larger than the thermal correlation length, but much smaller than H_{GUT}^{-1}, and even smaller than the Hubble parameter incorporating field energy contributions (for the 1-D profile case, and with thermal dissipation). In the absence of thermal dissipation, (as well as for a 3-D field profile) we needed to take larger domains, but still one is able to achieve the stage of dominance of vacuum energy.

One of the most important limitations of our analysis is that we have not accounted for self gravity of these domains which will obviously affect the evolution of these domains. We take FRW metric even in the presence of strongly inhomogeneous energy density. To take care of this one needs to have a more rigorous simulation with full Einstein's equations as was done in ref. [19]. It is quite likely that even with such evolution the special feature of these propagating front solutions of RD equations will survive so that one may be able to achieve inflation with a more realistic field profile than the conventional assumption of restricted field variation over super Hubble scales which is hard to justify in view of small sizes of field correlation domains.

The requirement of strong dissipation in our model brings to attention the warm inflation scenario [11]. There is strong dissipation present in the warm inflation case which is responsible for the constant presence of thermal bath. Study of RD equation solutions in warm inflation will certainly be very interesting and may provide new possibilities. At the same time, it also points to another limitation of our analysis, that is the neglect of fluctuation terms. Certainly, fluctuations will affect these propagating fronts, as we had also noted in ref. [24–26]. We hope to incorporate these effects in a future work.

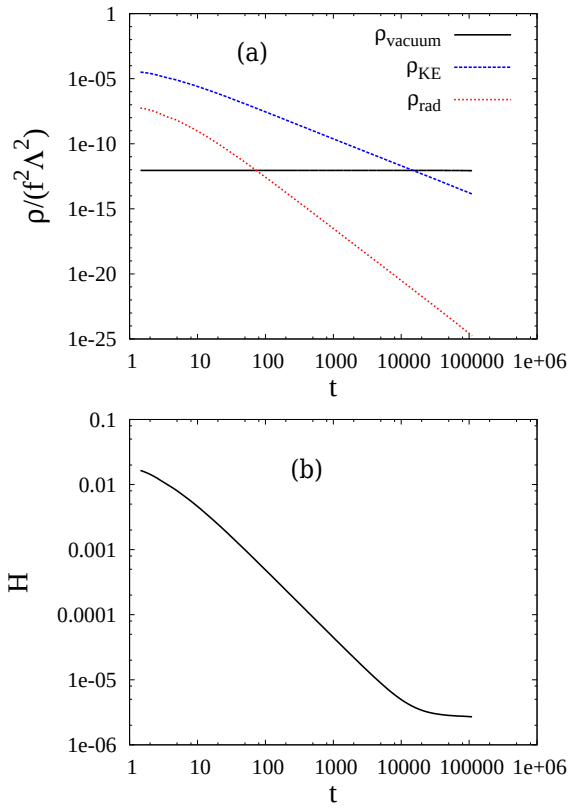

Figure 8.7: (a) Log-Log plot of the evolution of different components of the energy density as a function of time. Solid (black), dotted (red), dashed (blue) curves show the contributions of the field vacuum energy, the field kinetic energy + gradient energy (denoted by ρ_{KE}), and the radiation energy density respectively. The vacuum energy becomes most dominant component at $t \simeq 14923$. (b) Log-Log plot of the evolution of the Hubble parameter H. During early stages H changes non-trivially, subsequently, H evolves as a power law, eventually turning over to a constant value of H signaling the beginning of the inflationary phase. In (b), this happens around at $t \simeq 15000$ which coincides with the stage of the dominance of the vacuum energy in (a).

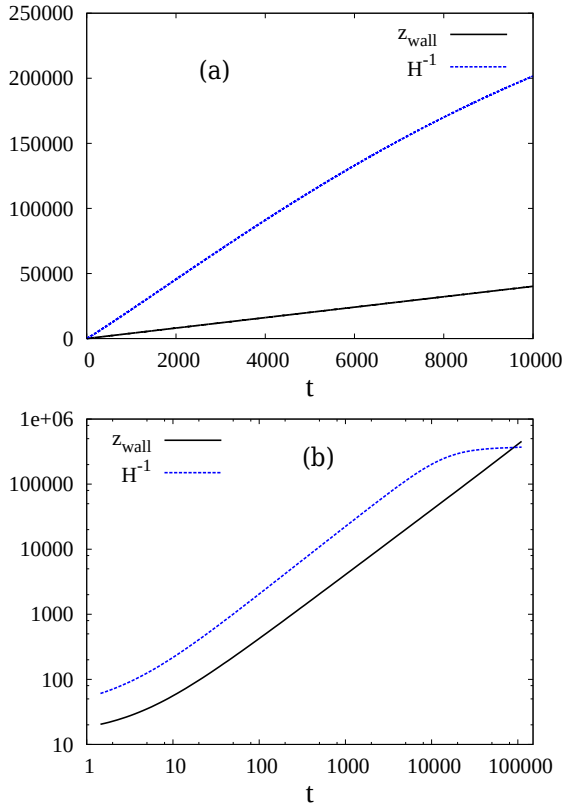

Figure 8.8: Solid (black) curve shows the location of the domain wall in physical coordinates, by noting down the position of the wall where $\phi = 0.25vev$. Dashed (blue) curve shows the value of H^{-1}. (a) During initial stages, field domain expansion is insignificant compared to the increase in the value of H^{-1}. (b) Towards the end of simulation, H^{-1} is practically constant while physical size of the domain (due to expansion of the Universe) keeps increasing. By the end of simulation here, at $t \simeq 110600$, one can see that the domain exits the horizon, marking beginning of proper inflationary stage.

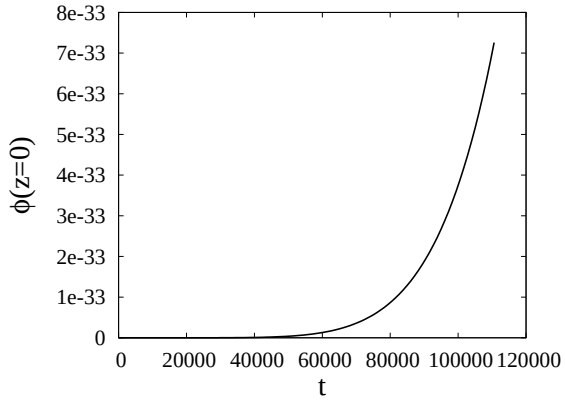

Figure 8.9: The evolution of $\phi(z=0)$. From this plot, one can make a rough estimate of time after which the field will become significantly non-zero, ending the period of inflation. A rough estimate (assuming linear shape for the final stages in this plot, which may be a serious overestimate given the shape of the curve, which may very well be exponential) will suggest that after time of order $t \sim 10^{36}$, $\phi(z=0)$ will become of order 1. This period of inflation crucially depends on the size z_0 in the ϕ profile in Eq. 8.18. For a larger value of z_0 duration of inflation will be larger, though at the same time it will become harder to justify a very large value of z_0.

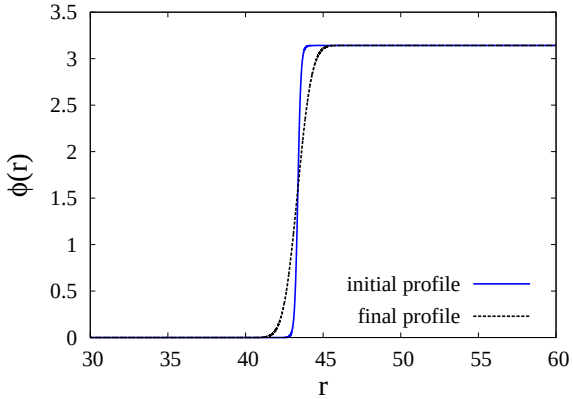

Figure 8.10: The solid (blue) curve shows the initial radial profile of the field for the 3-D field profile case. Final plot of ϕ (in comoving coordinates) at $t = 9348$ is shown by the dashed (black) curve.

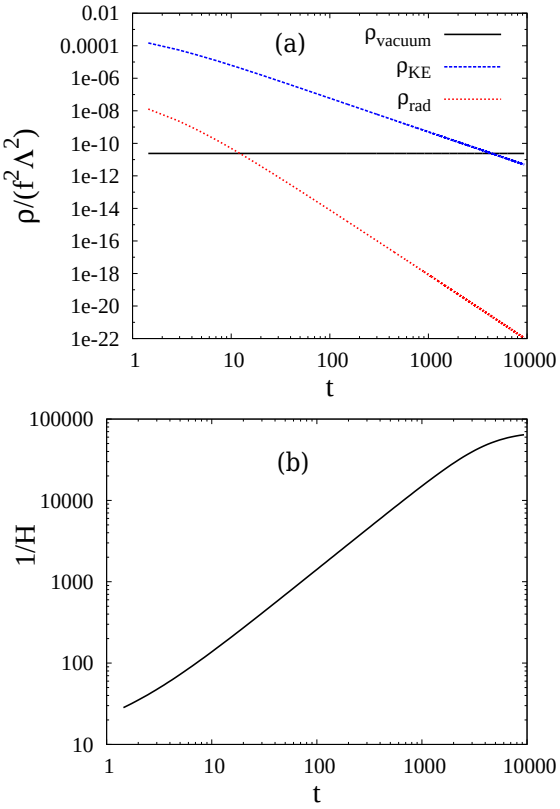

Figure 8.11: (a)Evolution of different components of the energy density for the 3-D field profile case. Solid (black), dotted (red), dashed (blue) curves show the contributions of the field vacuum energy, the field kinetic energy + gradient energy (denoted by ρ_{KE}), and the radiation energy density respectively. The simulation is run until the vacuum energy becomes most dominant component indicating the beginning of inflationary phase. (b) Evolution of the Hubble size H^{-1}. Again, note the turning of the curve from linear shape when vacuum energy starts dominating indicating the beginning of inflationary phase.

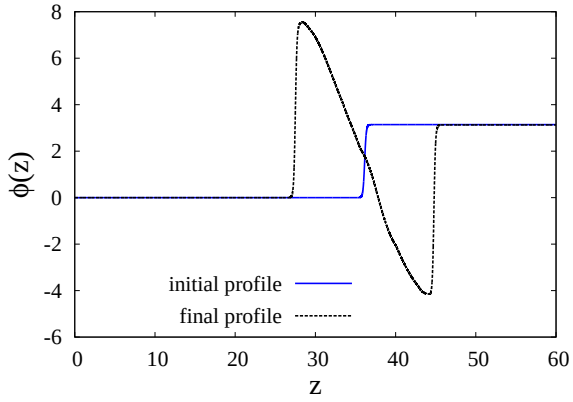

Figure 8.12: Evolution of 1-D field profile for the case without any thermal dissipation. We only show plot for $z \geq 0$, the profile being symmetric about $z = 0$. The solid (blue) curve shows the initial radial profile of the field. Final plot of ϕ (in comoving coordinates) at $t = 14430$ is shown by the dashed (black) curve.

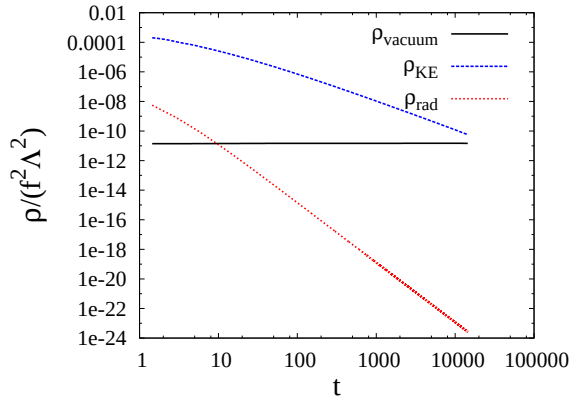

Figure 8.13: Evolution of different components of the energy density for the case without any thermal dissipation. Solid (black), dotted (red), dashed (blue) curves show the contributions of the field vacuum energy, the field kinetic energy + gradient energy (denoted by ρ_{KE}), and the radiation energy density respectively. The simulation is run until the kinetic energy + gradient energy becomes close to the vacuum energy part.

Bibliography

[1] "Gravitation and cosmology: principles and applications of the general theory of relativity", S. Weinberg, Wiley Publication, 1972.

[2] A. Riotto, arXiv:hep-ph/0210162.

[3] A. H. Guth, Phys. Rev.**D 23**, 347 (1981).

[4] A. Linde, Phys. Lett.**B 108**, 389 (1982).

[5] A. Albrecht and P. Steinhardt, Phys. Rev. Lett. **48**, 1220 (1982).

[6] R. H. Brandenberger, arXiv:hep-ph/9702217.

[7] A. D. Linde, Phys.Lett. **B 129**, 177, 1983.

[8] A. A. Starobinsky, in Field Theory, Quantum Gravity and Strings, ed. H. J. de Vega and N. Sanchez (Springer, Berlin 1986); S. J. Rey, Nucl. Phys. **B 284**, 706 (1987); J. M. Bardeen and G. J. Bublik, Class. Quan. Grav. **4**, 473 (1987); M. Morikawa, Phys. Rev. **D 42**, 1027 (1990); H. E. Kandrup, Phys. Rev. **39**, 2245 (1989).

[9] K. Freese, J. A. Frieman and A. V. Olinto, Phys. Rev. Lett. **65**, 3233 (1990); K. Freese, arXiv:astro-ph/9310012; K. Freese, W. H. Kinney, Phys.Rev. **D 70**, 083512 (2004); K. Freese, W. H. Kinney, arXiv:1403.5277.

[10] A. A. Starobinsky, Phys. Lett. **B 91**, 99 (1980).

[11] A. Berera, Phys. Rev. Lett. **75**, 3218 (1995); A. Berera, Contemporary Physics **47**, 33 (2006); A. Berera, I. G. Moss, R. O. Ramos, Rept.Prog.Phys.**72**, 026901 (2009).

[12] A. Linde, JCAP **02**, 006 (2017).

[13] G. F. Mazenko, R. M. Wald and W. G. Unruh, Phys. Rev. **D 31**, 273 (1985).

[14] M. Bucher, A Goldhaber and N. Turok, Phys. Rev. **D 52**, 3314 (1995)

[15] A. Berera and C. Gordon, Phys.Rev. **D 63**, 063505 (2001).

[16] M. Bastero-Gil, A. Berera, R. Brandenberger, I. G. Moss, R. O. Ramos and J. G. Rosa, arXiv:1612.04726.

[17] A. Albrecht, R. H. Brandenberger and R. Matzner, Phys.Rev. **D 35**, 429 (1987); *ibid* Phys.Rev. **D 32**, 1280 (1985).

[18] R. Brandenberger, Int. J. Mod. Phys. **D 26**, 1740002 (2016).

[19] W. E. East, M. Kleban, A. Linde and L. Senatore, JCAP 1609, 010 (2016).

[20] J. H. Kung and R. Brandenberger, Phys. Rev. **D 42**, 1008 (1990); D. S. Goldwirth and T. Piran, Phys. Rept. **214**, 223 (1992).

[21] R. Rangarajan, arxiv 1506.07433.

[22] J.D.Murray, "Mathematical Biology, I : An Introduction", Third Edition, (Springer), 2002; J.D.Murray, "Lectures on Nonlinear-Differential-Equation Mod- els in Biology", (Clarendon Press), 1977; B.Bradshaw-Hajek, "Reaction-diffusion Equations for Population Genetics", (Ph.D. thesis, School of Mathematics and Applied Statistics, University of Wollongong), 2004, (http://ro.uow.edu.au/thesis/201); B.H.Gilding and R.Kersner, "Travelling Waves in Nonlinear Diffusion Convection Reaction", (Springer Basel AG, Switzerland), 2004.

[23] R. Peschanski, Phys. Rev. **D 81**, 054014 (2010); S. Munier and R. Peschanski, Phys. Rev. Lett. **91**, 232001 (2003); D. Ghoshal, JHEP, **1112**, 015 (2011); D. Ghoshal and P. Patcharamaneepakorn, JHEP, **1403**, 015 (2014).

[24] P. Bagchi, A. Das, S. Sengupta and A. M. Srivastava, Phys.Rev. **C 92**, 034902 (2015) [arXiv:1507.01015], and references therein.

[25] P. Bagchi, A. Das, S. Sengupta and A. M. Srivastava, Phys.Rev. **C 93**, 024914 (2016) [arXiv:1508.07752].

[26] S. Sengupta,“ Aspects of QCD Phase Transition with Reaction-Diffusion Equations’, (Ph.D. thesis, Homi Bhabha National Institute, India, 2015).

[27] “The Early Universe”, E.W. Kolb and M.S. Turner, Addison-Wesley Publishing Company, (1990).

[28] S. Das, G. Goswami, J. Prasad and R. Rangarajan, JCAP **06**, 001 (2015).

[29] J.D. Bjorken, Phys. Rev. **D27**, 140 (1983).

[30] T. S. Biro and C. Greiner, Phys. Rev. Lett. **79**, 3138 (1997); C. Greiner, Z. Xu and T. S. Biro, arXiv:hep-ph/9809461.

[31] C. M. G. Lattes, Y. Fujimoto and S. Hasegawa, Phys. Rep. **65**, 151 (1980); L. T. Baradzei et al., Nucl. Phys. **B 370**, 365 (1992), and references therein.

[32] J.D. Bjorken, K.L. Kowalski and C.C. Taylor, in Results and Perspectives in Particle Physics 1993; Proceedings of the 7th Rencontres de Physique de la Vallee dAoste, La Thuile, Italy, 1993, edited by M. Greco (Editions Frontieres, Gif-sur-Yvette, France, 1993).

[33] C. Greiner and B. Muller, Phys. Rev. **D 55**, 1026 (1997).

Chapter 9

Summary

Here we summarize the work presented in this thesis. After a general introduction given in chapter 1, we have presented a brief review of QCD and the physics of QGP in chapter 2. In chapter 2 we have discussed first order and second order phase transition using simple field theory models. In the case of first order phase transition we have also introduced the notion of false vacuum decay. We then discussed different aspects of QCD phase transitions, specifically, the chiral transition and the confinement-deconfinement (C-D) transition. We discussed the effective Lagrangians for these transitions. For the C-D transition, we used the effective Lagrangian for the thermal expectation value of the Polyakov loop which acts as an order parameter for the C-D transition. For the chiral transition we used the linear sigma model written in terms of the order parameter field $\Phi = (\sigma, \vec{\pi})$, which is an $O(4)$ vector. Earlier it used to be believed that the quark-hadron transition is of first order even at low chemical potential (as in the early universe). However lattice results show that quark-hadron transition is a cross-over for zero chemical potential and high temperature situation. Variation of Polyakov Loop, chiral order parameter and their associated susceptibility as a function of gauge coupling shows that the confinement-deconfinement transitions and chiral transition happen almost simultaneously. In this chapter we have also discussed topological defects which emerge as a consequence of symmetry breaking phase transitions. Whenever there is a phase transition based on spontaneous symmetry breaking, topological defects are produced if they are allowed by the structure of the

vacuum manifold. We have discussed the formation of domain walls in a simple field theory model with a single real scalar field having double well potential. We have also given the classification of different topological defects depending upon the homotopy groups of the vacuum manifold. In the pure QCD gauge theory, $Z(3)$ symmetry is spontaneously broken. Thus the vacuum manifold has disconnected pieces. In this case, domain walls appear as topological defects.

In the chapter 3 after a general introduction to neutron stars we have given a comprehensive introduction to the the structure of neutron stars e.g., its mass and radius, different phases inside the core of the neutron stars etc. Neutron superfluidity exists in the core of the neutron stars at very high density. Superfluid vortex creep model and two fluid model is very successful in explaining the pulsar glitch phenomena which exploits the presence of neutron superfluidity. However recent observation of anti-glitch cannot be explained by the vortex creep model. Apart from the nuclear superfluidity, deconfined QCD phase e.g, QGP, 2SC phase, CFL phase etc. can exists in the core of the neutron stars.

Chapter 4 and 5 present our research work where we have presented a unified framework which can explain glitch as well as anti-glitch. Our approach is based on the fact that phase transitions are typically associated with density change as well as density fluctuation. Density fluctuation in the core of a stars will in general lead to transient changes in its moment of inertia (MI), along with a permanent change in MI due to phase transition. It affects the rotation of the neutron star and hence the pulsar timings. Sensitive experiments ($\frac{\delta I}{I} \sim 10^{-9}$) might be able to detect it. It may provide sensitive probe for phase transitions in these compact objects. Non zero off-diagonal components of MI arising from density fluctuations imply wobbling of rotating neutron stars, which leads to modulation of peak intensity of pulses. Density fluctuations will lead to rapidly changing quadrupole moment which can be a new source for gravitational wave emission. We have considered net change in the moment of inertia for a strong first order phase transition from hadronic phase to QGP phase. Apart from the net change in moment of inertia we have also considered transient change in moment of inertia coming from density fluctuations.

We have also considered density fluctuations coming from topological defects. We find that moment of inertia can increase or decrease, which gives the possibility of accounting for the phenomenon of glitches and anti-glitches in a unified framework. Density fluctuations arising during phase transitions crucially depend on the nature of phase transition. Identification of these density fluctuations via pulsar timings (and gravitational waves) can pin down the specific transition occurring inside the pulsar core.

In chapter 6 we gave a general introduction to the physics of inflation. In early universe cosmology inflation was introduced to resolve some issues of hot big bang cosmology. Hot big bang cosmology suffers from the horizon problem, flatness problem and monopole problem. In chapter 6 we have discussed these problems and also discussed how an accelerating phase in the early universe can resolve these issues. This accelerating phase is also known as inflation. In this chapter we have discussed old and new inflation models. In the context of new inflation model where inflaton field start at $\phi = 0$ and rolls towards the true vacuum, we have discussed the issue of initial conditions. In the standard models of inflation, certain average value of the inflaton field is assumed over entire Hubble volume. He have argued on the basis of correlation domains that assumption of uniform field value over entire Hubble volume is not generic rather it is highly fine tuned. For a concrete discussion we have taken Natural inflation model where Pseudo Nambu Goldstone boson plays the role of inflaton field. In the case of Natural inflation we have reemphasized the issue of initial conditions.

In chapter 7 we have taken a detour to discuss reaction-diffusion(RD) equation. RD equation has very interesting traveling front solutions under proper boundary conditions. propagating interfaces routinely arise in the context of RD equation even when the underlying transition is a continuous transition or a cross-over. We provided a brief review of reaction-diffusion equations in Chapter 7. The only difference between the field equations in relativistic field theory case and the reaction-diffusion case is the absence of a second order time derivative in the latter case. The correspondence between the two cases was, thus, established in the presence of a strong

dissipation term leading to a dominant first order time derivative term. Basic feature of RD equation is that, if the underlying potential of the field theory system has local maxima and true minima then rolldown of the field from local maxima to true minima will be slowed down. In the diffusion driven dynamics rolldown of the field is very slow. On top of this if the system is expanding then a large region of space can be disoriented from the true vacuum. We demonstrated the existence of propagating front solutions for chiral phase transition in QCD even when the underlying transition is a cross-over or a continuous transition. As an example of RD equation for expanding system we have demonstrated the formation of disoriented chiral condensate (DCC) domains. DCC corresponds to formation of an extended region, where the chiral field is misaligned from the true vacuum. Rapid roll down of the chiral field to true vacuum is avoided due to a rapid three dimensional expansion of the system which makes reaction-diffusion equation applicable for governing the dynamics of the chiral field for this system. The discussion related to DCC is directly applicable to the case of inflation.

In chapter 8 we have presented our work on the issue of initial conditions in inflation and how to resolve it using reaction-diffusion equation. We have discussed the issue of setting appropriate initial conditions for inflation. Specifically, we consider natural inflation model and discuss the fine tuning required for setting almost homogeneous initial conditions over a region of order several times the Hubble size which is orders of magnitude larger than any relevant correlation length for field fluctuations. We then propose to use the special propagating front solutions of reaction-diffusion equations for localized field domains of much smaller sizes. Due to very small velocities of these propagating fronts we find that the inflaton field in such a field domain changes very slowly, contrary to naive expectation of rapid roll down to the true vacuum. Continued expansion leads to the energy density in the Hubble region being dominated by the vacuum energy, thereby beginning the inflationary phase. Our results show that inflation can occur even with a single localized field domain of size much smaller than the Hubble size. We discuss possible extensions of our results for different inflationary models, as well as various limitations of our analysis (e.g.

neglecting self gravity of the localized field domain).